Multimodal Imaging of Hypoxia

in Breast Cancer

Multimodal Imaging of Hypoxia

in Breast Cancer

Een multimodale moleculaire imaging studie naar hypoxie in borstkanker

(met een samenvatting in het Nederlands)

Proefschrift

ter verkrijging van de graad van doctor aan de Universiteit Utrecht
op gezag van de rector magnificus, prof.dr. G.J. van der Zwaan, ingevolge het
besluit van het college voor promoties in het openbaar te verdedigen op
maandag 5 november 2012 des middags te 2.30 uur

door

Kamila Chughtai

geboren op 13 februari 1981

te Lublin, Polen

To my lovely grandmother
Stanislawa

Contents

Chapter 1
Introduction

1. Introduction

Visualization and analysis of the tumor metabolome, lipidome and proteome are crucial for understanding tumor growth, angiogenesis, hypoxia, metastasis, drug- and radio-resistance, apoptosis and necrosis. All these processes contribute to tumor aggressiveness and challenge our understanding of tumor expansion and treatment strategies. In this study, we integrated multimodal imaging of tumor tissue, which provided multiple metabolite, lipid and peptide distributions with state of the art quantitative proteomics for detailed and comprehensive information about hypoxia-induced proteome changes in breast cancer. A combination of optical imaging techniques such as bright field/fluorescence microscopy and histochemical staining methods together with mass spectrometric imaging (MSI) were employed for *ex vivo* visualization of multiple biomolecules in normoxic, hypoxic and necrotic tumor regions. This approach allowed us to image breast tumors at the molecular level and better understand their biochemical composition.

1.1 Incorporation of MSI into multimodal imaging

Multimodal imaging combines two or more imaging techniques. Its palette contains a variety of specialized visualization methods for imaging different structures, microenvironments, biomolecules and probes present in the studied sample under investigation. Multimodal imaging fuses two or more imaging modalities of ultrasonography, positron emission tomography (PET) imaging, magnetic resonance imaging (MRI), computed tomography (CT), optical imaging and most recently MSI, and is gaining importance in more and more imaging centers worldwide. Such an approach provides deep insight into processes occurring inside organisms, healthy organs or diseased tissue and helps to unravel mechanisms of physiological as well as pathological processes. For instance, combining *in vivo* and *ex vivo* imaging methods provides anatomical as well as biochemical information about the system under investigation. *In vivo* imaging performed by ultrasonography, MRI, PET or CT provides detailed three-dimensional (3D) visualization of anatomy. The drawback of these methods is in some cases that they are limited to imaging only certain types of structures, may require injection of external probes or lack biomolecular specificity. Magnetic resonance spectroscopy imaging (MRSI) can obtain 3D metabolic information with 'biomolecular specificity' *in vivo* without injection of external probes, but the drawback of this technique is that it is relatively insensitive, e.g. it gives relatively low spectral and spatial resolution *in vivo*. On the other hand, *ex vivo* imaging methods such as immunohistochemistry (IHC), MSI

or optical microscopy are capable of localizing molecules of interest at higher spatial resolution and high biomolecular specificity, but only after tissue removal and sectioning, whereby the native tissue state is disturbed and all three-dimensional tissue information is lost. By combining the strengths of *in vivo* and *ex vivo* imaging methods it is possible to obtain both a general anatomical overview of an organ under investigation as well as more detailed biochemical information of selected regions. Figure 1.1 presents results of *in vivo* MRSI and *ex vivo* optical imaging of a breast tumor xenograft model. MRSI provides information about the morphology of the tumor by means of imaging the water signal as well as the distribution of choline and lipid-related signals, while optical fluorescence microscopy visualizes the localization of a red fluorescent protein expressed in the hypoxic regions of this genetically modified tumor models.
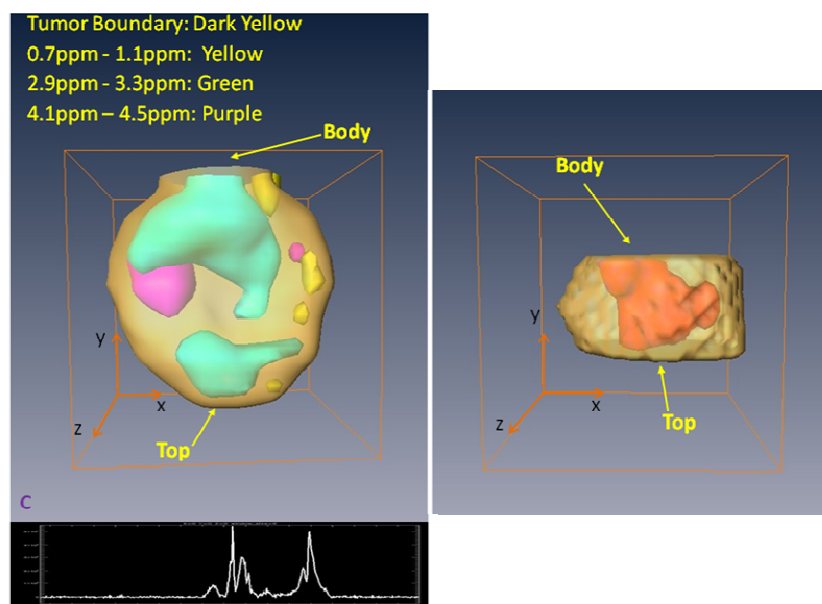
Figure 1.1 Multimodal imaging of a breast tumor xenograft model. Left: 3D image of the lipid signal (yellow), choline (green) and residual water (purple) acquired in vivo by MRSI from a breast tumor xenograft. Right: 3D reconstruction of the tumor boundary and the volume of the hypoxic region acquired ex vivo from the same tumor by bright field and fluorescence microscopy.

MSI with a broad spectrum of different ionization sources, mass analyzers, detectors and software tools covers multiple scientific areas. Its interdisciplinary applicability makes it suitable for *ex vivo* imaging of samples of microbial, plant or animal origin with sample sizes ranging from single cells up to whole body sections of rodents.[1] Its detected mass range starts at elements and has theoretically no upper limit, practically ending at intact proteins of up to

100 kDa. Additionally, a variety of existing sample preparation techniques adjust and enhance the detection of specific classes of molecules. MSI also has one unique feature not present in any other imaging method; its capability of identifying multiple imaged molecules in a massively parallel manner. It can not only perform the visualization of a broad range of unknown molecules and substances, but also very specifically characterize their composition, which helps to gather an enormous knowledge about the system under investigation. Each successful MSI experiment generates an illustrated encyclopedia, where every molecule's localization is printed on a separate page and aligned with all other detected molecules. Such an encyclopedia can be expanded into a whole library by performing MSI on a 3D stack generated from the same sample or samples prepared under different experimental conditions. Such a MSI library can be converted into an easily accessible bookstore open for searching by multiple readers from various locations.

1.2 Application of MSI in breast cancer studies

In this study, MSI has been incorporated into multimodal imaging of breast tumor xenograft models, which were developed for studying tumor hypoxia. Hypoxia, a state of low oxygen tension, plays a central role during embryonic vascularization and development as well as postnatal life in both physiological and pathophysiological processes such as tissue repair, stroke, cardiovascular diseases, pulmonary hypertension, pre-eclampsia, tissue transplantation and tumor growth.[2-6] Cells growing under hypoxic conditions sense low oxygen tension and trigger responses resulting in rapid metabolic changes, a decrease in the proliferation rate and an expansion of the existing vasculature bed. Cancer cells growing inside a tumor face hypoxia mostly when they are located too far away from oxygen-supplying capillaries to be within the effective oxygen distance.[7] Cancer cells have adopted hypoxia-response mechanisms as a survival strategy, which often results in their resistance to chemo- and radio-therapy as well as a metastatic tumor phenotype. In the tumor model used in this study, the imaging of hypoxic regions was possible due to a red fluorescent protein exclusively expressed under hypoxic conditions and typically visualized by fluorescence microscopy. However, due to the multifaceted nature of mass spectrometry, for the first time we detected and imaged this fluorescent protein also by classical proteomics as well as MSI approaches. State of the art mass spectrometry combined with bottom-up proteomics and peptides labeling enabled us to quantify hypoxia-induced proteome changes and highlighted pathways that were up- and down-regulated under oxygen deprivation in breast cancer cells.

1.3 Scope of the thesis

In this thesis, the challenge of analyzing complex and heterogeneous breast tumor xenograft models is addressed. The focus is on exploring the composition of different tumor microenvironments. In order to study such a challenging and multifaceted phenomenon, we employed a broad selection of methods and techniques. Multimodal imaging combined with genetically engineered tumor models allowed us to visualize biomolecules present inside different microenvironments of breast tumors.

Chapter two describes the general principle of mass spectrometry and explains how non-imaging mass spectrometry was transformed into an imaging technique. This chapter is a tool box containing information required for successful biological tissue preparation, the correct choice of the most appropriate ionization method as well as the selection of the most effective instrumentation. It is supplemented with examples of MSI used for biomedical tissue analysis.

Chapter three describes a novel co-registration method developed for multimodal imaging incorporating MSI. This newly developed co-registration technique uses fiducial markers such as cresyl violet, Ponceau S, and bromophenol blue. Those compounds possess a combination of optical and molecular properties that result in a clear mass spectrometric signature. Fiducial markers were optimized for accurate 2-dimensional co-registration of images obtained by different modalities and 3-dimensional reconstruction of serial histological, fluorescence microscopic and MSI images from breast tumor models.

Chapter four presents an approach used for identification and MSI visualization of a red fluorescent protein exclusively expressed in the hypoxic regions of a breast tumor xenograft model. For the first time, a fluorescent protein has been visualized by both optical microscopy and MSI. Visualization of this fluorescent protein by MSI directly from breast tumor tissue sections will allow simultaneous detection of multiple molecules present in hypoxic regions of this breast tumor xenograft model.

Chapter five shows how the developed multimodal imaging approach that incorporates MSI enabled the identification and localization of multiple phospholipids as well as metabolites directly from different microenvironments of breast tumor xenograft models. Some of the most abundant lipid species were localized in viable tumor regions, while less abundant lipids were detected from necrotic tumor regions. A sphingomyelin and two acylcarnitines were

localized in hypoxic tumor regions and identified by using ion mobility separation. This chapter demonstrates the first visualization of phospholipids in a human breast tumor xenograft model and sheds more light on processes occurring during tumor growth.

Chapter six presents the results of classical mass spectrometry, state of the art quantitative proteomics and multimodal imaging of beast tumor xenograft tissue, all of which were combined for investigating hypoxia-induced proteome changes in breast cancer. This approach allowed us to detect local protein signaling in normoxic, hypoxic and necrotic tumor microenvironments, up-regulation of pathways involved in metastasis and down-regulation of molecules responsible for cell attachment.

Chapter 2

Mass Spectrometric Imaging for Biomedical Tissue Analysis

2. Mass spectrometric imaging for biomedical tissue analysis[*]

This chapter provides an introduction to MSI covering most aspects of this novel technique. It describes the general principle of mass spectrometry and explains how non-imaging mass spectrometry was transformed into an imaging technique. We also briefly discussed the main advantages and limitations of MSI and presented a detailed overview of sample preparation methods and tips for a successful MSI experiment. Different types of mass analyzers and software used for MSI have been listed, which can help match the most suitable instrument and visualization method to the type of MSI experiment performed. We have also added some additional topics, such as ion mobility separation, microscope mode of acquisition, profiling and tags, which may proof helpful in solving problems with sample complexity, spatial resolution, molecule identification and visualization. The last part of this chapter covers descriptions of several biomedical applications of MSI in disease pathology, biological sciences, proteomics/peptidomics, metabolomics, lipidomics, pharmacokinetic studies and 3D volume reconstruction. This chapter gathers all necessary knowledge in the field of MSI and its applications needed for performing experiments and interpreting the acquired data presented in the following chapters of my thesis.

---

[*] Based on: K. Chughtai and R.M.A. Heeren. Mass spectrometric imaging for biomedical tissue analysis. Chem. Rev. 110, 3237–3277 (2010).

2.1 Introduction

2.1.1 Mass spectrometry

A mass spectrometer is described as the smallest weighing scale in the world ever used.[8] Mass spectrometry (MS) is a unique technique that has an interdisciplinary nature, which freely crosses the borders of physics, chemistry and biology. Mass spectrometry makes a great scientific tool due to its capabilities to determine the mass of large biomolecular complexes, individual biomolecules, small organic molecules as well as single atoms and their isotopes. Right from the time of its invention in the first decade of the 20th century, mass spectrometry has undergone tremendous improvements in terms of its sensitivity, resolution and mass range. It currently finds applications in all scientific disciplines such as chemistry, physics, biology, pharmacology, medicine, biochemistry and bio-agro-based industry.

Introduction of "soft" ionization sources such as electrospray ionization (ESI) by J.B. Fenn et al.[9] and matrix-assisted laser desorption/ionization (MALDI) by M. Karas et al.[10] in 1980s revolutionized mass spectrometry as it offered the capability to analyze large intact biomolecules. As such MS became an irreplaceable tool for the biological sciences. The development of both ESI and MALDI made possible the ionization of smaller biomolecules such as drugs and metabolites as well larger biomolecules such as lipids, peptides and even proteins.[9, 11] The molecular weight (M_w) ranges we use in this chapter are defined as follows. The low M_w range includes elements and molecules from 1 to 500 Da. Molecules with M_w between 500 and 2000 Da fall in the medium M_w range. All molecules with $M_w > 2000$ Da are considered to be part of the high molecular weight class. It goes beyond the scope of this chapter to cover all developments in MS. Rather this chapter focuses on one of the latest, rapidly developing innovations in MS namely MSI. This young technique takes benefit from all methodological and technological developments in general MS implemented over the last decades. Over the last twenty years MSI has transformed from an esoteric, specialist technology studied by few researchers only to a technique that now finds itself at the center stage of mainstream MS. Over the last years the technology has matured to find applications in many different areas, with instrument developments taken up by all MS instrument manufacturers resulting in a rapid rise of the number of research groups active in this area. In this chapter we describe and review approximately 20 years of MSI development from the perspective of its application to biomedical imaging. We will emphasize the key research

steps and pitfalls that determine the outcome of this relatively new *label free* biomolecular imaging technique in life sciences.

2.1.2 Mass spectrometric imaging

MSI allows the rapid detection, localization and identification of many molecules from the most complex, biological sample surfaces. It emerged as a response to demand of spatial information of biomolecules detected by conventional mass spectrometry. The MSI instrumentation, methods and protocols have been developed to study the spatial distribution of endogenous compounds such as lipids or proteins, and exogenous compounds such as polymers or pharmaceutical compounds on complex surfaces. It is a *label free* technique that can deliver detailed understanding of biological processes on different length scales, from sub-cellular to multi-cellular level and from organs to whole biological systems. Although MSI takes advantage of all modern developments in MS the concept already existed before the development period reviewed here. In particular in the field of Physics secondary ion mass spectrometry (SIMS) was used extensively to study semiconductor surfaces and the like. It was not until the introduction of MALDI-MSI in 1997 by R. Caprioli et al.[12] that the current rapid developments of methodologies, instrumentation and software used for imaging of biological samples started. Now, peptide and protein profiling directly from biological tissue samples is almost routine already, while the first images of whole tissue sections were shown only in 2001, illustrating the speed of application development.[13]

SIMS has also seen limited application for imaging biological samples.[14,15] The development of liquid metal ion guns (LMIG) as a primary ion source for SIMS experiments in the 1990s revolutionized SIMS imaging. It realized a much wider scope of applications of high spatial resolution MSI of biological surfaces.[16]

The third ionization method used for MSI evolved recently in the form of desorption electrospray ionization (DESI). This relatively new technique has emerged from the lab of G. Cooks and co-workers in 2004.[17]

These three desorption and ionization methods, MALDI, SIMS and DESI lay at the heart of modern MSI developments. In the next section we will review the basic principles of MSI and its desorption and ionization techniques in more detail to provide a thorough basic understanding before discussing their many different applications in section 2.3 of this thesis.

2.1.3 MSI – Basic principles and ionization techniques

Mass spectrometric imaging is essentially a four step process. It involves sample preparation, desorption and ionization, mass analysis and image registration. All four elements need to be carefully controlled and monitored to generate meaningful images. Sample preparation is a key to any analytical technique. Its special requirements for MSI will be extensively discussed in section 2.2 of this thesis. After introduction of the samples into an MSI instrument the biomolecules first are desorbed and ionized from the surface. This is achieved through exposure of the surface to a laser beam (LDI/MALDI), a primary ion beam (SIMS) or a charged droplet flux (DESI). The ionized molecules are subsequently mass separated inside the mass analyzer. This can be a time of flight (TOF), Fourier transform ion cyclotron resonance (FTICR), linear quadrupole (Q) or Orbitrap or any of the available mass spectrometric systems that can be interfaced with these desorption and ionization sources. The different nature of these instruments renders different mass spectral quality and information, which will be discussed in detail in the section 2.2 of this thesis. The whole surface of the sample is examined during a MSI experiment to collect mass spectral information about the molecular composition and distribution of the analyzed molecules at every point. The resulting molecular ion distributions are presented in the form of ion images.

In life sciences there is a growing demand for a technique or tool capable to visualize macromolecular distributions directly from biological samples. So far, MSI is the only technique that generates high resolution bio-macromolecular images directly from tissue sections and without the need of labels.[16]

2.1.3.1 Matrix assisted laser desorption/ionization

MALDI-MS is a dramatic improvement of laser desorption/ionization mass spectrometry (LDI-MS). It is a powerful method that allows the analysis and detection of a wide range of biomolecules directly from tissue sections. MALDI is an ionization technique that is capable of producing intact higher M_w ions through the use of a pulsed laser beam combined with energy absorbing matrix molecules. In non-imaging MALDI analysis, the analyte is mixed with an excess of chemical matrix, usually a small organic acid at molar matrix to analyte ratio 10^3-10^5:1.[18] The role of the matrix is to absorb the majority of the laser energy leading to explosive desorption of the matrix crystals together with incorporated analyte into the gas phase without degradation of the analyte. The matrix also aids the ionization of analyte molecules in the gas phase due to presence of protons from added acids such as trifluoroacetic

acid (TFA). The first reported LDI-MS experiments were performed using a fine powder of cobalt metal in glycerol as the matrix for the observation of ions with the mass over charge ratio (*m/z*) of 34 000.[19] Soon afterward MALDI-MS results of serum albumin (67 000 Da) were reported using nicotinic acid as the matrix.[20] MALDI-MS has low femtomole to attomole sensitivity, a mass range up to 100 kDa and is routinely used for the analysis of metabolites, lipids, peptides and proteins.[8,18]

Molecular imaging of tissue sections with MALDI-MSI requires the tissue surface to be covered by a solution of a low M_w organic compound (matrix). On tissue application of this matrix solution results in *in situ* extraction of biomolecules from the biological sample. The subsequent evaporation of the solvent from the matrix solution causes the crystallization of the matrix and incorporation of the analyte molecules into growing crystals. The matrix is always applied in concentrations well above the surface analyte concentrations. The resulting crystal surface is irradiated with pulsed laser light of sufficient fluence leading to desorption and ionization of matrix and analyte molecules as schematically indicated in figure 2.1. The incorporation of the analyte into the matrix crystals ultimately prevents fragmentation of larger analyte molecules during desorption through the reduction of the direct interaction of the analyte molecules with the laser light. The matrix molecules absorb the laser energy and facilitate the explosive desorption and ionization process. Fragmentation of the acidic matrix molecules typically leads to an excess of protons above the surface that in turn result in gas-phase ion-molecule reactions producing pseudomolecular ions.
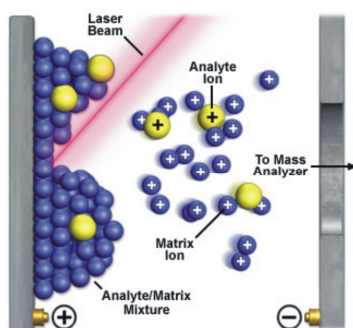
Figure 2.1 Schematic representation of MALDI desorption and ionization process. Adapted with permission from www.magnet.fsu.edu. Copyright 2008 National High Magnetic Field Laboratory.

During a MALDI-MSI experiment the laser beam is rastered across the surface of the matrix covered tissue, which allows desorption and ionization of biomolecules. The ablation crater is estimated to have a depth of 1 µm or more, depending on laser fluence.[16] The position of the

laser beam on the surface is usually varied by moving the target plate while the laser beam remains fixed in an optimized position with respect to the inlet of the mass spectrometer. The introduction of N_2 (337 nm) or neodymium-doped yttrium aluminum garnet (Nd:YAG) (355 nm) lasers with repetition rates of 200-1000 Hz and typical pulse lengths of 3 ns or less shortened the time needed for sufficient data acquisition.[21] To make MALDI-MSI a practical application the laser spot size was reduced from 100-150 μm to 20 μm.[22] Further laser spot size reduction and micrometric spatial resolution was achieved by a MALDI instrument equipped with a highly focused laser.[23] Focusing of the laser beam to the diameter of a single cell (~7 μm) has been also reported by A. Holle et al. in 2006.[24] Unfortunately, the improvement in resolution decreased sensitivity. Laser intensity modulation within the laser spot, such as implemented in the SmartBeam technology, is used to enhance the signal to noise ratio in a MALDI-MSI experiment. The use of an acousto optic modulator or a programmable liquid crystal phase modulator can create random patterns of hotspots in solid state lasers, similar to those naturally found in a plasma based laser such as a nitrogen laser.[25] It combines the sensitivity, resolution, ease of a nitrogen laser use, focusing ability, variable beam diameter and the high repetition rate of common solid state lasers.

The time needed to obtain images from the sample depends on the number of analyzed spots, the repetition rate of the laser (Hz) and data collecting and processing speed of computers. On modern state of the art MALDI mass spectrometers equipped with lasers operating at 1 kHz, a whole-body mouse or rat section would take less than 4 h to image.[26]

MALDI-MSI is a leading method for recording intact peptide and protein distributions because it can detect hundreds of peptides and proteins directly from tissue sections due to its high sensitivity, large tolerance for salts and other contaminants, a wide mass range, little fragmentation, *label free* detection method and easy data interpretation because the majority of ions are singly protonated $[M+H]^+$.

2.1.3.2 Secondary ion mass spectrometry

SIMS is a desorption and ionization technique used for MSI which utilizes a primary ion beam (e.g. metal ions) to produce secondary ions from the surface of the sample as schematically shown in figure 2.2. For this purpose an ion column is used that produces, accelerates, conditions, focuses and steers a primary ion beam. This primary ion beam can be focused as sharply as 50 nm, depending on the primary ion beam current, the M_w and the charge state of the primary ions. The energy of the primary ions deposited into the surface is substantially higher than the energy deposited into the surface by a laser beam during a LDI

or MALDI experiments. SIMS therefore often yields extensive fragmentation of surface molecules. However, as ion beams can be focused with much higher precision than a laser beam, SIMS is a unique tool for high spatial resolution MSI of elements and small organic molecules in different organelles in the cell.[16,27]
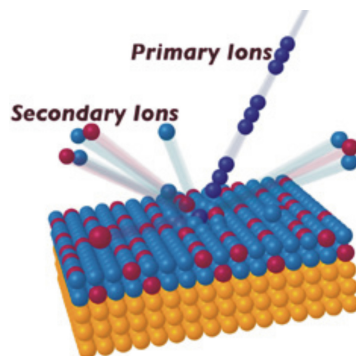
Figure 2.2 Schematic representation of SIMS desorption and ionization process. Reprinted with permission from www.nb.engr.washington.edu. Copyright 2010 NESAC/BIO and University of Washington.

SIMS imaging of biological materials was principally developed by Winograd et al. and by Todd et al.[22,28] This ionization method yields chemical information on lower M_w species at very high spatial resolution (less than 10 nm has been reported).[29] A collision cascade transfers the energy of the primary ions to the sample surface. Typical energies of the primary ions are in the range of 5-25 keV, which are much higher compared to bond energies of surface molecules. This results in extensive fragmentation of molecules and bond breaking near the collision site, producing essentially only the emission of atomic particles. When moving away from the primary collision site less fragmentation occurs. A small fraction of intact molecules is subsequently ejected from the first layers of the surface if the surface binding energy is overcome. In most cases, the molecules are found to desorb from within 5–10 nm of the impact point. Most molecules are emitted as neutrals and only approximately 1% of them are charged. Depending on the electron configuration of the surface molecules both positive and negative ions can be generated. An important parameter in SIMS is the damage cross-section: this is a measure of the surface area affected by the impact of a single primary ion. The impact of a primary ion damages the molecules close to the point of impact. Re-sampling the damaged areas would provide chemical information about the damaged areas, and not the surface. In order to ensure that the chemical information corresponds to the pristine surface, very low primary ion doses (< 10^{13} ions cm^{-2}) are used. Within this regime less than 1% of the top surface layer of atoms (or small molecules) receives a primary ion

impact. Statistically it is unlikely that the same area is sampled twice; consequently the mass spectrum provides chemical information about the unchanged (static) surface. This type of SIMS is known as static SIMS and the ion dose limit constitutes the static SIMS limit. Above this limit the technique is referred to as dynamic SIMS. This review will concentrate on static SIMS, unless otherwise stated SIMS refers to static SIMS.

The current developments in primary ion guns used for MSI predominantly employ monoatomic primary ions (Ar^+, Ga^+, In^+, Au^+, Xe^+, Bi^+). The development of softer primary ion beams such as C_{60}^+, SF_5^+, Bi_3^+, Au_n^+, Cs_n^+ [30, 31] extend the applicability of SIMS for larger M_w species. These polyatomic primary beams are able to desorb secondary ions from the sample surface without extensive fragmentation. As a result they are more suitable for the analysis of intact biomolecules from tissue surfaces.[21,29] The secondary ions are introduced into a mass analyzer after acceleration using a high voltage acceleration system. The polarity of the accelerator is employed to select if positive or negative ions are analyzed. A TOF system is most commonly used for mass determination in SIMS, although alternative approaches, such as those based on a magnetic sector mass analyzer are also employed. The primary ion source must provide short pulse widths (subnanosecond) to yield secondary ions with minimal time dispersion for TOF analysis. The energy and angular dispersion of the secondary ions that originate with the emission process can be compensated using focusing elements such as an ion mirror or reflectron. The reflectron focuses the secondary ions through a retarding electric field in the middle of the flight path, resulting in improved mass resolution. After mass separation, the secondary ions are focused onto a detector. The detector consists of a microchannel plate for ion-to-electron conversion, a scintillator for electron-to-photon conversion, and a photomultiplier, which is placed outside the vacuum chamber.

A wide range of samples can be analyzed by this surface specific technique which is extremely sensitive to any sample preparation treatment. Sample preparation protocol for SIMS imaging experiment requires only mounting of the tissue section on an indium tin oxide (ITO)-coated glass slide without any further washing steps. The sample must be stable under ultra high vacuum (UHV) conditions which ensure that both the primary and secondary ions travel from their origin to their final destination without undergoing collisions. The surface morphology of the sample can affect the generation of secondary ions. Samples with surfaces as flat as possible are desired in order to avoid possible shadow effects.

Several surface modification methods have been developed that can enhance the production of intact secondary ions in a SIMS experiment. The application of a thin metal coating for metal assisted-SIMS (MetA-SIMS) or the application of an energy moderating matrix for

matrix enhanced-SIMS (ME-SIMS) prevent fragmentation of surface molecules by primary ion beam impact.[32,33] Both techniques will be discussed in the following paragraphs as they enable the use of SIMS for the analysis of intact biomolecules such as lipids and peptides.

MetA-SIMS employs metallization of (organic) samples with a thin layer of silver, gold or platinum and it has been shown to increase secondary ion yields of intact molecular ions in SIMS.[34,35] It provides increased sensitivities for larger analytes (<5 kDa) as diverse as fatty acids, lipids and peptides. In addition, the thin metal layer provides a conductive contact thus effectively converting insulating samples into conducting samples, thereby removing the need for charge compensation.[16] A complication of using sample metallization is that the ions observed are frequently adducts with the metal and metal clusters.

ME-SIMS can be considered as a combination of MALDI and SIMS. The organic acid is applied on the surface which enhances the ionization efficiency of larger molecules in a very similar manner as MALDI.[16,36] Standard MALDI matrixes can be used for ME-SIMS such as 2,5-dihydroxy-benzoic acid (DHB) which results in signal intensity enhancement for a wide range of molecular species. One of the advantages of ME-SIMS is that it is both easy and cheap to implement. In ME-SIMS standard SIMS instrumentation and MALDI sample preparations protocols can be used.[33]

The apparent limitations of SIMS are the lack of sensitivity on the mass range over 1000 m/z, due to in-source fragmentation of complex molecules and/or decreased ionization yield and very few or no information on hydrophilic metabolites. Mass spectra obtained by SIMS can be more complicated for interpretation than that from MALDI due to extensive fragmentation of molecules, and SIMS instruments do not operate in MS/MS mode which limits identification of molecules.[37] Given the current state of the technique it does not seem possible to liberate, ionize and detect intact, low abundance proteins with SIMS or ME-SIMS.[16] However, new developments in instrumentation may lead to an increase in SIMS mass range. One such example is a new system for MSI which used MeV ion beams, termed MeV-SIMS.[38] MeV-SIMS demonstrated a more than 1000-fold increase in molecular ion yield from a peptide sample (1154 Da), compared to keV ion irradiation.

The rapid development of SIMS imaging offered new possibilities in biotechnology and biological research with applications in medicine and pathology.[39] SIMS found numerous applications such as imaging of unicellular organisms[27,40,41] and single cells,[14,42,43,44,45,46] chromosomes,[47] embryos,[48] different organs such as kidney,[49,50,51] brain,[52,53,54, 55, 56] prostate,[22] adipose tissue,[39,57,58] cockroach and snail tissue[33] and distribution of herbicide on leaf.[59] There are also medical applications of SIMS such as analysis of biomaterial implants,[60] a mouse

model of Duchenne muscular dystrophy,[61,62] retinopathy,[63] the cornea and conjunctiva,[64] cardiovascular diseases,[65,66] human breast cancer cell lines,[67] 3D imaging of tumors and oocytes.[68,69]

Pharmacokinetic studies of accumulation of pharmaceuticals in cancer cells[70,71] or molecular imaging of vitamins in neurons[72] were also performed using SIMS. In addition, archeological studies of thousand year-old Peruvian mummies[73] or art[74] can benefit from this technique. Two recent reviews presented SIMS as an imaging technique.[39,75]

2.1.3.3 Desorption electrospray ionization

DESI, an ionization method developed by R.G. Cooks in 2004,[17] can be used for MSI analysis in ambient environment.[76] Contrary to MALDI and SIMS, which operate under high vacuum (HV) or UHV conditions, DESI is employed under atmospheric pressure (AP). DESI is a combination of two MS ionization methods: electrospray ionization (ESI) and desorption ionization (DI). Instead of a laser beam or a primary ion beam, DESI uses energetic, charged electrosprayed solvent droplets to desorb the molecules from the sample surface. Figure 2.3 illustrates the operational principle of DESI and its implementation on a linear trap quadrupole (LTQ)-based mass spectrometer. The formation of molecular ions from secondary droplets occurs either by ion emission (ion evaporation model)[77] or by evaporation of neutral solvent molecules (charged residue model).[78] As a result gaseous ions are produced in a process similar to ESI. So the solid samples analyzed by DESI produce multiply charged ions in the form of $[M + nH]^{n+}$ or $[M-nH]^{n-}$ which is a characteristic feature of the ESI method.
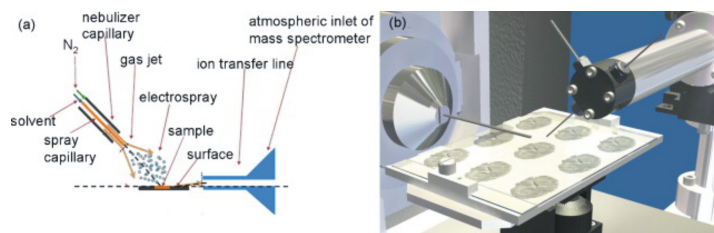
Figure 2.3 Desorption electrospray ionization. (A) Schematic representation of DESI desorption and ionization process; (B) brain tissue imaging analysis using DESI. Reprinted with permission from ref[79]. Copyright 2008 Elsevier.

For DESI imaging, the sample is either placed onto a target (e.g. microscope glass slide) or analyzed *in situ*.[79,80,81] The most common DESI probe design allows a lateral resolution of better than 400 μm on rat brain tissue.[76] A recent spray design theoretically predicts an improvement in achievable lateral resolution of 40 μm.[82] MALDI routinely provides a higher

spatial resolution but requires more complicated sample preparation. The first MSI experiments used DESI to profile plant tissue for alkaloid distributions using a line scan.[17] These experiments were followed by line profiles of thin sections of liver tissue.[76] Although there are still damage, sensitivity and resolution issues to address, the technique holds the promise of soft, local, liquid atmospheric desorption and ionization. This could resolve one of the problems often forwarded by biologists, namely the desire to perform imaging experiments away from the harsh vacuum environment of the mass spectrometer.[16]

DESI was applied to study lipids,[79] endogenous and drug metabolites,[83] alkaloid content in plant tissue,[17] natural products in algae[84] and antifungal molecules in seaweed.[85] DESI was also combined with an ion mobility TOF mass spectrometer to probe the conformations of proteins desorbed from an insulating surface.[86]

2.1.3.4 Other desorption and ionization techniques for MSI

Several other desorption and ionization methods are described in the literature that find their application in MSI, such as laser desorption ionization (LDI),[23,87] surface enhanced laser desorption (SELDI)[88], nano-particle-assisted laser desorption/ionization (nano-PALDI),[89] matrix-enhanced surface-assisted laser desorption/ionization (ME-SALDI),[90] and nanostructure initiator mass spectrometry (NIMS).[91]

One of the desorption and ionization techniques that is gaining popularity for MSI is laser ablation inductively coupled plasma MS (LA-ICP-MS). This technique is capable of quantitative imaging of elemental distributions generated from surfaces. A comprehensive review of this methodology has been published recently to which the interested reader is referred.[92]

Combinations of different desorption and ionization technologies are being developed to enable local desorption and ionization in the ambient environment. Although these techniques, such as matrix assisted laser desorption electrospray ionization (MALDESI),[93] laser ablation electrospray ionization (LAESI)[94] and infrared MALDI (IR-MALDI)[95] have great potential but they have not yet resulted in routine MSI applications.

2.1.4 The advantages of MSI

MSI offers a unique tool box for sample surface analysis. Several methods offer high spatial resolution biomolecular analysis. The achievable spatial resolution depends on the ionization technique used, e.g. typically MALDI allows probing spots as small as 25 μm in diameter,[13] while nanoSIMS ion beam can be focused to the size of 50 nm in diameter.[27] With a typical

mammalian cell size of 10 μm, MALDI collects spectra covering approximately 4 cells per image point while SIMS can probe subcellular structures.[96] Special approaches such as the utilization of a high resolution 1 μm coaxial objective or 600 nm microscope mode[23] can be used to overcome some of these spatial resolution limitations. However, these instruments are not widely available yet and the experiments at extreme high spatial resolution can suffer from the lack of sensitivity.

Modern mass spectrometers are capable of separating and detecting ions with very high mass resolution. Resolving power $(m/\Delta m)_{50\%}$ in excess of 10^5 is routinely available on commercial instruments. High mass resolving power can be used to reveal spatial features that remain hidden with low resolution technologies.[97] Ion mobility separation (IMS) combined with mass spectrometry allows the gas-phase separation of isobaric ions or molecules with similar nominal mass during an MSI experiment.[98]

MSI takes full advantage of high sensitivity MS instrumentation to image molecules present at very low concentrations inside the cells. At present the instruments are capable of detecting molecules present in concentrations as low as 500 amol, which facilitates detection of components from a single cell.[99] The sensitivity of MS instruments was estimated by spotting protein (insulin) on brain tissue which resulted in detection of a minimal signal at a concentration of 12 fmol/mm^2 obtained from a spot of insulin.[100] With the laser spot diameter of 50 μm this resulted in an absolute detection level of 25 amol per image point. This sensitivity is in a range where it can be used to detect biomolecules present in tissue sections.

In order to visualize different classes of biomolecules present inside the cells the instruments must be able to detect a broad range of ions, from very low M_w ions such as drugs and metabolites to large M_w ions of intact proteins. In theory TOF mass analyzers can separate all ions without lower or upper size limits.

MS instruments can be also used for imaging unknown compounds present in the biological sample without any *a priori* knowledge or labels. This is a key advantage of MSI as unknown molecules can be then identified using tandem mass spectrometry. For this purpose an ion of interest (parent ion) is fragmented and its fragments (daughter ions) are mass analyzed. This type of analysis is also known as tandem MS, MS^n or MS/MS because it involves two or more mass spectrometers: the first one is used for the selection of the ion of interest, prior to fragmentation in the collision cell, and the second one is used to separate the fragments according to their *m/z* ratio. Tandem MS can be also utilized for MSI analysis.

Another advantage of MSI is that molecules are detected directly from the biological sample without complicated preparation steps. Normally the protocol for MSI requires a short tissue

wash followed by matrix application for MALDI and ME-SIMS.[29] While conventional SIMS typically uses no sample preparation whatsoever.

The time of sample analysis is also a crucial aspect of any imaging technique. In the case of MSI, the time of image acquisition depends on the selected spatial resolution, the repetition rate of the MALDI laser and the sampled area. The data acquisition of an average imaging experiment lasts from minutes to several hours depending on the instrumentation utilized. The process is fully automated and normally does not require any supervision.

2.1.5 The limitations of MSI

The sensitive nature of MSI instruments requires that the samples remain stable at room temperature (RT) as well as in HV. Unfortunately some molecules degrade at RT within a couple of minutes.[96] The sample preparation process must be carried out as fast as possible without exposing the samples to the air, moisture or high temperature. Also all types of sample treatment including cutting, washing, digestion or matrix application possess the risk of sample contamination and molecular diffusion, which can affect the reproducibility of the data, complicate their analysis or affect the quality of the image. The spatial resolution of a MALDI image can also be affected by the matrix crystal size which typically is above 10 μm.[101,102] The image quality can be compromised by the presence of matrix clusters and their alkali metal ion adducts which complicate detection of compounds in the 500-1500 Da range.[103] SIMS does not require matrix or any sample washing steps but its extensive in-source molecule fragmentation limits the detected ions size to 1000 *m/z*.[21,104]

Biological tissue represents an extremely complex and challenging sample for direct analysis by MSI. The multiple molecules present in a tissue section (e.g. proteins, lipids, oligonucleotides, carbohydrates, small organic molecules, matrix ions and salts) can negatively influence each other's desorption and ionization efficiency and prevent optimal detection. This phenomenon is called ion suppression and was reported by a number of authors.[105,106] The presence of ion-suppressing phenomena differentially attenuate the ionization process and can limit the number of detected molecules.[107] Ionization suppression occurs when one analyte is present in great excess over another or ionizes more easily than others. For example components such as lipids, carbohydrates and salts can promote adduct formation and affect co-crystallization of biomolecules with matrix, which affects the quality of the mass spectra and number of biomolecules detected by MS.[101] Some other examples show that MS spectra can also be dominated by easily ionizing hemoglobin chains desorbed from highly vascularized tissues such as heart.[102] Such signals can significantly compromise

other protein signals in the spectrum. This phenomenon can be minimized by careful tissue removal during the surgical process to avoid tissue contact with blood, washing of the tissue surface to remove hemoglobin or in the case of profiling (see **Profiling vs. imaging**), avoiding the analysis of the highly vascularized regions of the tissue.[102] On the other hand, the presence of low level ion signals from hemoglobin chains can be used as an internal calibrant.[102]

Ion suppression and adduct formation can decrease the quality of MSI analyses. However, the efforts to remove non-protein components may affect integrity of the surface and cause diffusion of analytes.[29] A great care has to be taken that proper control experiments are conducted before drawing any conclusion from a given MSI experiment.

The theoretically unlimited mass range of TOF mass analyzers starts in practice at 600 Da with an upper limit around 25-30 kDa, because the lower mass region is partially obscured by ions from the matrix while the sensitivity drops rapidly for bigger molecules.[96] This can be ameliorated through the utilization of smart matrices such as meso-tetrakis (pentafluorophenyl) porphyrin (F20TPP) that have no low M_w peaks nor does it lead to cluster formation.[108]

2.1.6 MSI – applications

MSI has a broad scope of applications and is being successfully applied in biology, pathology, medicine and pharmacology.[109,110] Key features that make MSI a practical tool in these different domains of the life sciences are the *label free* nature of molecular imaging, high sensitivity, high resolution and its capability to visualize in parallel the distribution of many molecules of interest.

The popularity of MSI augmented quickly as a result of its almost unlimited range of applications. Sample for MSI can be obtained from any type of organism, ranging from bacteria and plants to animal and human tissues. This technique has been used to examine samples of different biological origins, from single cells[14,42,43,111] to whole animal body sections,[26,98,112,113] from both normal[114,115,116] as well as pathological specimens,[117,118,119] from organisms on different developmental stage such as fertilized oocytes,[120] embryos[48] to adult animals.[121] A detailed review of MSI applications in different fields of life science is presented in section 2.3.

2.2 Methodological description and current improvements

2.2.1 Biological sample preparation

In this section we present the key practical aspect of MSI, the preparation of biological samples. Several crucial preparation steps such as sample handling, washing, matrix application and on-tissue digestion will be discussed. This will be followed by an in-depth description of mass spectrometric instruments and software used for imaging. New instrumental developments that challenge the boundaries of MSI such as IMS, microscope and microprobe modes of image acquisition and their application in MSI are briefly discussed. In this section, we will also explore and explain the difference between profiling and imaging modes of MSI.

2.2.1.1 Biological sample handling

The MSI sample handling protocols must maintain the integrity and spatial organization of the molecules in biological samples. Collection and treatment procedure need to be sufficiently fast to prevent rapid tissue degradation. The samples for MSI come from a variety of biological sources. They can originate from the resection of an organ or tissue, a whole animal body dosed with a pharmaceutical compound, individual cells or clusters of cells isolated by laser capture microdissection (LCM) or contact blotting of a tissue on a target membrane. The sample degradation process starts immediately after the blood/oxygen flow to an organ has ceased, even prior to tissue removal (see **Sample degradation**). This implies that samples must be properly and timely collected, processed and stored before MSI analysis.

Types of the samples

All kinds of biological samples can be subjected to MSI, ranging from single cells,[27,122] bacterial colonies,[40,123,124] animal embryos,[48] tissues from different plants[84,85,125,126] or animal organs,[121,127] as well as rodent whole body sections.[26,75,98,105,113] Different fresh, snap-frozen,[128,129] alcohol preserved[130] or formaldehyde fixed and paraffin embedded (FFPE)[131, 132,133,134,135,136,137] samples were used for MSI. To date, the most imaged tissue type is a rodent brain. This is due to its small size, characteristic internal structure and the ease with which it can be sectioned.[138] Additionally, the symmetrical nature of the brain provides a very good internal control of the imaging process. Other types of animal organs were also subjected to MSI analysis. The sample list shows the imagination of the researchers involved. It consists of a large variety of biological tissue types, from the more difficult to section, air filled lungs,[83]

heart,[139] kidney,[49] tumor samples of different origin (glioma,[140,141] breast cancer,[135,142] prostate cancer,[119] ovarian cancer,[143] lung tumor[129]), human biopsies and resected tissue from surgery,[57,144] to cells from cell culture[44,145] or LCM.[146]

Sample storage

The most common first step used in any MSI protocol is tissue storage utilizing snap-freezing of the material and storage at -80°C. Tissue biopsies, organs or whole organisms e.g. zebra fish, should be frozen immediately after collection in order to preserve the sample's morphology, minimize protein degradation through endogenous enzymatic proteolysis, oxidation of biomolecules or changes in the metabolome of the cells.[107,147] However, the freezing process can lead to sample cracking and fragmentation as different parts of the tissue cool down at different rates and ice crystals may form. To avoid sample damage the tissue may be loosely wrapped in aluminum foil and frozen in liquid nitrogen, ethanol or isopropanol at temperatures below -70°C by gently lowering the tissue into the liquid over a period of 30–60 s. This preserves the shape of the tissue and also protects the biological tissue components from degradation.[102] It is also important to avoid tissue deformation during storage which usually occurs due to wrapping of the tissue in plastic film or keeping it in a tube.[107] Whole tissues may remain frozen in a freezer at -80°C for at least a year with no significant degradation.[102] After one year of storage, even at -80°C, it is difficult to obtain good peptide/protein spectra from tissues.[102,148] This phenomenon of tissue aging is especially important for samples collected and stored over a long time period in medical centralized tissue repositories. It is very important to optimize and standardize the protocols for medical applications of MSI. Especially when it is not always possible to analyze freshly prepared samples.[148] A number of innovative protocols for MSI of fresh and aged biomedical samples have been recently developed.[130] The second most common form of tissue preservation found in medical tissue banks are FFPE tissue blocks. They are usually kept at RT, which leads to degradation of nucleic acids, metabolites and many biomolecules other than proteins cross-linked by formaldehyde. The cross-linking in turn hampers easy desorption and ionization. These samples require special protocols ensuring removal of MS incompatible paraffin, digestion of cross-linked proteins and correct identification of imaged molecules.[135]

Sample degradation

In MSI the quality of biological samples is of great importance. Unfortunately many molecules present in functional tissue undergo rapid degradation just after tissue dissection or

even during agonal states of animals. Several factors, including pre- and post-mortem factors, can affect tissue quality.[149] Pre-mortem factors include prolonged agonal states, perfusions, use of drugs, infections, tumors, hypoxia and seizures. Post-mortem factors that influence tissue quality include post-mortem interval (PMI), which is the period from death to freezing of the tissue for long-term storage at -80°C,[149] storage temperature and duration of the storage as well as tissue processing and handling.

Molecular degradation studies show that endogenous proteolytic degradation carried out by enzymes including calpains, cathepsins and those of the proteasome complex is already extensive at 3 min post-mortem.[150,151] It has been also demonstrated that the levels of several post-translational modifications (PTMs) in brain tissue are significantly changed within minutes post-mortem.[152,153] Post-mortem degradation of glycerophospholipids (GPLs) was observed within 15 min by MSI in a series of mouse brains extracted at different times, presumably because of stimulation of phospholipases A (PLAs) under ischemic (restricted blood supply) conditions.[114] Most studies concentrated on protein degradation have been conducted on animal (mouse, rat) brains, due to their availability. In these studies, either specific proteins were targeted, such as phosphorylated signal proteins, pre- and postsynaptic proteins, G-proteins, synaptophysin, microtubule-associated proteins, calpain or samples were analyzed in a more holistic proteomics approach.[154,155,156]

The study of endogenous degradation processes in human prefrontal cortex showed that most human brain proteins are quite stable with respect to post-mortem factors, such as PMI and storage temperature. Nevertheless, the storage temperature seemed to significantly influence certain protein levels. Raising the storage temperature from 4°C to RT increased the number of degrading proteins from 17 degraded proteins at 4°C to 54 degraded proteins at RT.[149] This is indicative of the effect of temperature on naturally occurring post-mortem protein degradation. The majority of the identified proteins belonged to the functional classes of structural or metabolic proteins, which appear to degrade very easily during post-mortem delay.[149]

Figure 2.4A shows the time dependent loss of signals detected by MSI of rodent brains.[96,157] To prevent/minimize the molecular degradation process some strategies such as *in vivo* fixation through focused microwave irradiation have been applied in MSI. However, the application area of the focused microwave instrument is limited to the size of small rodents and optimized for the brain tissue samples.[158,159,160]

Recently a novel tissue stabilization system (Stabilizor T1, Denator AB, www.denator.com) was developed by Denator Biotechnology and can be used for MSI samples.[161] Figure 2.4B

illustrates the stabilizing effect of thermal treatment of biological tissue using this instrument. Substantial degradation is observed without this treatment. The instrument handles any type of tissue sample, both fresh and frozen and utilizes a combination of heat and pressure, which prevents sample deformation while thermally inactivating/denaturing the enzymes responsible for rapid degradation of biomolecules in the tissue. The temperature of the sample is rapidly raised up to 90°C but does not exceed 95°C in any part of the sample.

Some other specific protocols need to be developed to meet the requirements of certain samples. For example some tissues collected for MSI can contain drugs that are light-sensitive. To prevent the photodegradation of these components before analysis the section should be kept in the dark.[102]
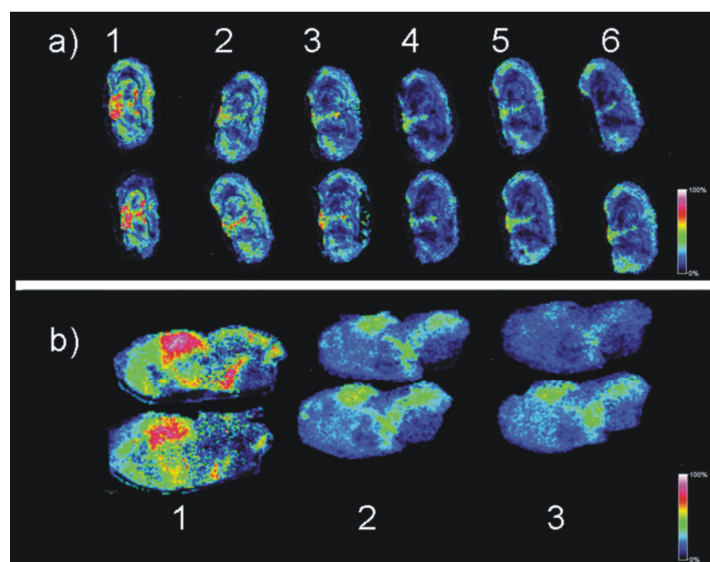
Figure 2.4 Degradation of molecular species during a time course of incubation of the tissue at room temperature visualized by MALDI-MSI. (A) Coronal sections of mouse brain warmed on the target slide for 0, 0.5, 1, 1.75, 2.75 and 5.25 min. Upper and lower series are from two separate technical replicates. (B) Parasagittal sections of mouse brain incubated for 5 min. Sample 1 was heat treated (Denator system) to denature proteins immediately after tissue collection. Sample 2 is the corresponding untreated tissue and sample 3 was heat treated on the slide after sectioning and thaw mounting. Reprinted with permission from ref[96]. Copyright 2008 Wiley Interscience.

2.2.1.2 Tissue preparation

Fixation

The majority of samples used for MSI are fresh, snap-frozen, chemically unmodified tissue sections. Unfortunately, it is not always possible to obtain fresh tissue for imaging

experiments because many, especially medical samples, are routinely formaldehyde or alcohol fixed just after dissection and before any analysis. Due to protein cross-linking introduced by formalin fixation the MSI analysis of FFPE tissues is difficult. The development of protocols useful for imaging and a recovery of polypeptides from FFPE samples allowed access to the different tissue banks, which store the samples in form of paraffin blocks.[131,132,133,134,135] A successful example of the application of such a protocol employing on-tissue proteolytic digestion for biomedical imaging of FFPE brain sections is shown in figure 2.5. The protocols must include a paraffin removal step followed by tissue digestion. The sample's analysis and data interpretation must consider the oxidation and degradation processes as well as effects of fixation and removal of paraffin on molecular structures.[135] All these aspects must be taken into account when old samples, large sample sets or patient cohorts are going to be compared. This also implies that the profiling results of a 100-year-old FFPE tissue biopsy obtained from a patient with amyloidosis, presented by E.H. Seeley et al. in 2008 has to be dealt with great caution.[141] This puts constraints on the analysis of large existing sample collections using MSI as in many cases the history of these samples is not well known. If it is unknown how long the sample was kept at RT and under ambient conditions, it is impossible to compare the MSI results from such samples with the MSI results from comparable fresh samples, which typically display well-defined states of the proteome.
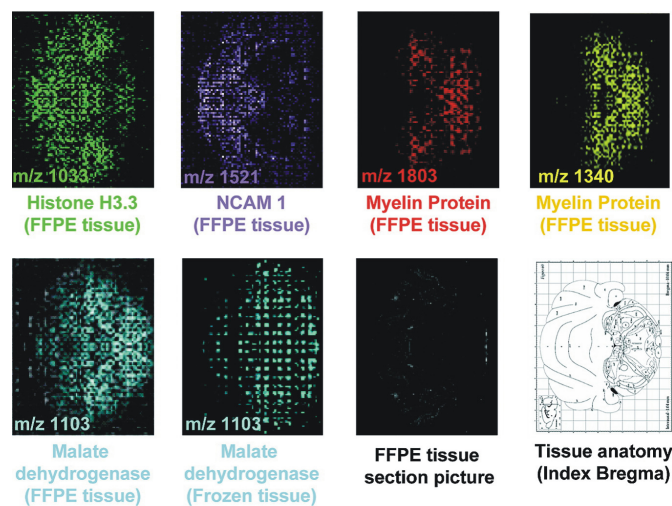
Figure 2.5 MALDI molecular images obtained from 2 years old FFPE rat brain tissue section subjected to on-tissue trypsin digestion. Reprinted with permission from ref[134]. Copyright 2007 American Chemical Society.

Alternative fixing methods rely on heat stabilization of tissues, which cause favorable protein denaturation (see **Sample degradation**) or the preservation of samples in an alcohol bath. Figure 2.6 illustrates a comparison of MSI results between fresh frozen and ethanol-preserved brain tissue.[130]

A new method of tissue fixation using RCL2/CS100 which is a non-cross-linking, non-toxic, and non-volatile organic fixative suitable for shotgun proteomic analyses and tissue imaging has been published by A. Mange et al. in 2009.[162]
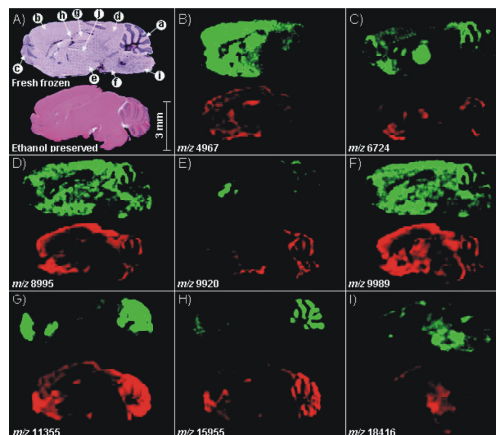
Figure 2.6 MALDI-MSI analysis of fresh-frozen and ethanol-preserved sagittal mouse brain sections. (A) Photomicrographs of the sections after H&E staining; (a) cerebellum, (b) cerebral cortex, (c) main olfactory bulb, (d) midbrain, (e) hypothalamus, (f) pons, (g) hippocampal formation, (h) corpus callosum, (i) medulla, (j) thalamus. (B-I) Corresponding ion density maps from a subset of proteins observed in common from both sections. Reprinted with permission from ref[130]. Copyright 2008 American Chemical Society.

Embedding

The embedding of the tissue in a supporting material allows easy handling and precise microtoming of sections. For histological applications tissues cut on cryostat microtomes are usually embedded in the optimal cutting temperature (OCT) polymer. However materials such as OCT, agar, sucrose, 2% (wt/vol) carboxymethylcellulose (CMC) and other polymer-based embedding media typically used for histological applications, ionize easily during MS analysis and act as significant ion suppressors as shown in figure 2.7.[102,138] To minimize tissue tearing the use of gelatin as embedding material is recommended. Gelatin provides much cleaner signal background compared with OCT.[163]

A large number of FFPE biological samples has been collected and stored in many tissue banks worldwide. Paraffin present in the samples suppresses ionization and must be removed

before tissue analysis using a xylene wash. An MSI protocol employing dewaxing and hydration steps of such samples has been published by Lemaire et al. in 2007.[134]
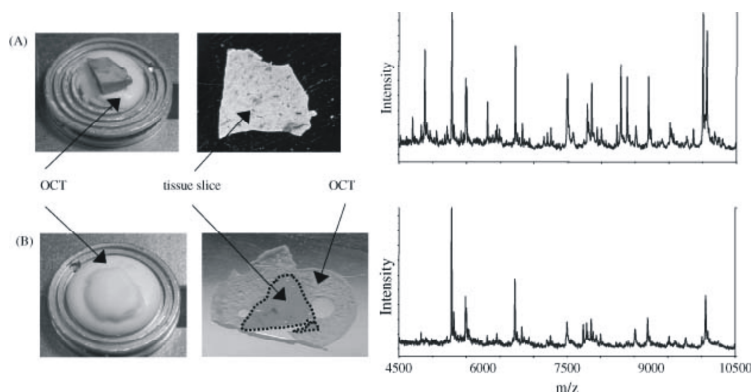
Figure 2.7 Analysis of effect of OCT on MALDI signal from rat liver. (A) Procedure where OCT is used to adhere the tissue to the sample stage but does not come into contact with the sliced tissue. The resulting spectrum shows many intense signals between m/z 4500 and 10500. (B) The tissue was embedded in OCT and attached to the sample stage. The resulting spectrum contains only about half of the signals as that in (A). Reprinted with permission from ref[102]. Copyright 2003 Wiley Interscience.

Sectioning

For MSI the tissue sections are usually 5-20 μm thick. Thinner sections tear easily, while thicker sections although easier to manipulate, may not be electrically conductive and take longer to dry, which can cause cracking and warping of the sections.[102] Thus tissues are usually sliced to a thickness of the diameter of a mammalian cell (10–20 μm), so that the majority of the cells in the slice are cut open, exposing the intracellular contents for analysis.[102] However the thinner tissue sections, cut at 2-5 μm, have been recommended for analyzing molecules in the larger size range of 3 to 21 kDa.[96,164] Tissue blocks are mounted to the cryo-microtome's cutting stage and sliced with a stainless steel microtome blade. The disposable blades used for sectioning are often packaged with a very thin film of oil between each blade which potentially can be a source of sample contamination. To avoid contamination from this oil, it is recommended to rinse the blades with methanol and acetone prior to tissue sectioning.[107] The sample stage temperature is typically maintained between -5°C and -25°C, depending on the tissue type. Tissues with high fat content e.g. brain, require lower temperatures to achieve high quality sections.[165] For example samples such as breast tissue or visceral fat tissue can coagulate during sectioning at warmer cryo-microtome temperatures.[102]

Tissue attachment

In order to perform MSI analysis, the tissue sections must be attached to an electrically conductive steel plate or glass slide. Conductive substrates are used to properly define the electric extraction field that will accelerate the ions produced from the surface.

In the past tissue sections were thaw-mounted on flat metallic target plates such as aluminum, stainless steel, and gold-coated plates, with the last offering a fairly nice contrast for visualization of major histological features from the sections. However, opaque target plates were not suitable for microscopic visualization of the section. These plates have been replaced by conductive ITO-coated glass slides, coated with 130 Å film of indium-tin oxide for electrical conductivity.[166] The transparent glass slides provide the possibility of microscopic observation of the MALDI samples.

There are two approaches for tissue attachment to these substrates: the use of an adhesive double-sided conductive tape or thaw mounting. The tape binds the section to the target while thaw mounting attaches the tissue by warming the reverse of the target to produce a localized warm patch. The first method requires special care to avoid trapping air bubbles which can affect the image acquisition. The latter method reduces the risk of sample contamination and tissue loss during the washing step. However the thaw mounting method can cause significant variation in mass profiles due to rapid degradation of molecules during the tissue attachment process. Thaw mounting may be not good enough for additional procedures involving polar solvents (see **Washing of tissue**).

Transfer of the tissue slice to a target plate or glass slide can be accomplished in several ways. One of the methods recommends cooling the plate by placing it in the cryo-microtome chamber at -15°C before sectioning.[102] The tissue section is picked up using forceps for thicker sections or an artist's brush for thinner sections and transferred on the cold plate. The plate and tissue section are then quickly warmed together. This method prevents loss of water-soluble proteins since all ice crystals remain on the tissue section surface and not on the cryo-microtome cutting stage. The second method uses a plate held at RT that is placed over the frozen section. In this case the ice crystals remain on the cutting surface. Sections transferred with this method may give poorer mass spectra, especially in the case of imaging water-soluble molecules.

Properly performed thawing does not cause any significant delocalization of the proteins proved by traditional biochemical assays such as immunohistochemistry and autoradiography.[102] Regardless of the tissue transfer and attachment method used, the section must be transferred to the plate with great care without introducing any scratches, tears or

rolled-up edges. The mounted section should be immediately dried in a vacuum desiccator for 30 min to avoid moisture condensation that could cause delocalization of proteins.

Results of MSI often are compared to the histopathological information of the imaged tissue. During sectioning of the sample an adjacent tissue section is collected on a regular microscopic slide for histological staining in order to correlate morphological information with the mass spectrometric images. In order to visualize tissue histology prior to MSI, protocols utilize optically transparent ITO-coated glass slides together with MSI friendly tissue staining protocols (e.g. methylene blue, cresyl violet).[167] This enables the microscopic evaluation of a tissue section by a pathologist followed by the molecular imaging of the same section by MSI. Another approach involves removal of the matrix from the tissue section followed by hematoxylin and eosin (H&E) staining of the same sample on an ITO-coated slide in order to visualize the morphology of tissue.[107,138] In this case, the visualization of microscopic structures may not be easy and depends strongly on the quality of the sample surface after completion of the MSI experiment. Samples used for SIMS or examined with the MALDI approach usually can be successfully stained and subjected to microscopic examination.

Washing of tissue

Washing is required to remove unwanted molecules and salts from the surface of the tissue. Salts are released from ruptured cells or interstitial fluids during sectioning and suppress ionization through direct ionization or adduct formation with the lipids, proteins and peptides.[96] The standard washing steps usually employ a brief 70% ethanol wash to remove salts and debris followed by a 90-100% ethanol wash to dehydrate and temporarily fix the tissue.[101,102,167] The ethanol wash does not cause any significant delocalization of proteins due to its fixative properties.[102] For many tissue types that have a high lipid content a wash with an organic solvent such as chloroform or xylene is recommended.[96,148] Lipid removal simplifies mass spectra in the 500-1000 *m/z* mass range, thus allowing the identification of low mass peptides that are usually masked by the high abundance of lipid peaks.[148] Washing protocols using organic solvents are acclaimed not to cause any delocalization or extraction of peptides or proteins but also to not reduce salt adducts.[148]

The washing method must be optimized for the specific MSI application since different classes of molecules require different treatment. For example peptide analysis may require an additional step of tissue treatment which includes 30 seconds of washing in 90% ethanol, 9% glacial acetic acid and 1% deionized water.[168,169] Tissue samples washed in ethanol can be

stored in a closed container at RT for up to 6 h without noticeable degradation observed in the MALDI spectra.[101] Some molecules can be detected only if washing has not been performed. In order to visualize all possible molecules a combination of different tactics can be tested.

The washing method is an important aspect in sample preparation. Usually either the slide, with tissue sample mounted on it, is immersed in the washing solution or the solution is applied on the tissue by pipette.[102] In case of immersion of the slide in the washing solution, there is a risk of tissue loss especially if the section was not properly mounted on the slide.

On-tissue digestion

The current practical upper limit of TOF-mass analyzers is 30 kDa (the theoretical limit is much larger for singly charged species), which limits the detection to approximately half of all proteins present in tissue.[170] With approximately 2000 proteins expressed in a typical mammalian cell,[171] 1000 additional proteins could potentially be imaged if TOF-mass analyzers were able to detect an unlimited mass range that potentially could be imaged. In order to bring these proteins into the MS range on-tissue digestion must be performed. This requires the local application of a proteolytic enzyme on the surface of the tissue section. Optimal enzyme activity requires the sample to remain moist at temperatures ranging from RT to 37°C for an incubation period of 1 hour up to overnight depending on the research target and protocol used. Excess liquid applied in conjunction with the enzyme can lead to analyte diffusion during the incubation process. In order to prevent diffusion of peptides two methods of enzyme application were optimized: spray-coating or spotting. During spray-coating the entire surface of the sample is covered with the solution of the enzyme. In this case, the spatial resolution is limited by a combination of diffusion and the diameter of the laser spot. The spotting of the enzyme prevents analyte diffusion and can be used if no extremely high spatial resolution is required.[168] In this case small solution volumes e.g. 100 pL are deposited on an area of 100 µm diameter on the surface of the tissue. The digestion process and diffusion of analytes occurs exclusively within the spotted area. The distribution of enzyme spots limits the spatial resolution of the MS image. The protocol for on-tissue digestion for both frozen as well as FFPE samples was published by M.C. Djidja et al.[135]

Other methods of protein digestion involve tissue blotting through a polyvinylidene fluoride (PVDF) membrane with trypsin immobilized on the surface followed by capture of the resulting peptides onto a second PVDF membrane, which maintains some degree of spatial resolution.[168,172] This procedure is referred to as the molecular scanner.[173] The lack of

sensitivity and spatial resolution resulting from the blotting process in this approach results in limited practical applicability.

Protein digestion typically yields peptides in the range of 400-3500 Da, a range where instrumental sensitivity is higher than that for intact proteins.[174] The mass spectrum of trypsin digested tissue is more complicated in the medium mass region due to simultaneous detection of peptides and overlapping signals from ionized lipids, matrix clusters and smaller biomolecules.

On-tissue digestion results in the detection of multiple peptides derived from a number of proteins present in the tissue section. Protein identification can be performed using tandem MS instruments which have capabilities for efficient fragmentation of selected peptides allowing identification of the original protein. However, the chemical and molecular complexity of tissue may deliver multiple peptides at each nominal mass. As a consequence, except for highly abundant peptides, identification by MS/MS may prove difficult due to fragments originating from different peptides. Tandem MS analysis of peptides may also be complicated by overlapping isobaric lipid ions. The recently developed IMS-MSI technique proved to be useful in the separation of isobaric ions that cannot be separated by conventional MS instruments (see **Application of ion mobility separation for MSI**).[98]

2.2.1.3 Matrix application

Matrix solution must be applied on the surface of the tissue before MALDI and ME-SIMS analysis. The matrix solution consists of three components a) an organic solvent such as methanol or acetonitrile, b) an organic acid (the matrix) such as sinapinic acid (SA) and c) TFA. The organic solvent extracts the molecules from the tissue and quickly evaporates allowing matrix crystal formation from the weak organic acid.[29] The extracted molecules are incorporated into growing matrix crystals. The addition of TFA increases the amount of available protons for ionization and augments the number of intact pseudomolecular ions formed from the surface. During MSI analysis the surface of the sample is probed with an appropriate laser beam or primary ion beam. The energy of the beam is absorbed by the matrix crystals which evaporate quickly releasing the trapped molecules. The matrix plays an active role in the ionization of the analytes.[175] The ionized molecules are typically singly charged $[M+H]^+$.

The choice of matrix (organic acid) applied on the tissue section depends on the mass range analyzed and chemical properties of analytes. Many different types of matrices are used for MALDI-MSI. An overview of the matrices used for MSI can be found in a number of

MALDI and sample preparation reviews.[29,106,176] They commonly include derivatives of benzoic acid, cinnamic acid and picolinic acid.[177,178,179,180] SA (3,5-dimethoxy-4-hydroxycinnamic acid) is routinely used for higher M_w proteins while alpha-cyano-4-hydroxycinnamic acid (CHCA) is more common for lower M_w molecules such as peptides.[102,181] For phospholipids and drug analysis matrices such as 2,6-dihydroxyacetophenone (DHA)[18] or DHB are used.[181,182]

The matrices can be also used in combination, such as SA in combination with 20% DHB, which provided good crystallization and a relatively homogeneous matrix layer across all organ tissues and resulted in detection of hundreds of protein signals from analyzed tissues.[26]

More effective matrix systems for MSI experiments are being developed. For example, a new class of ionic solid and ionic liquid matrices for MALDI-MSI has been developed.[183] Solid ionic matrices are obtained from the equimolar reaction mixture of acidic crystalline matrices such as CHCA, SA or DHB with different bases such as aniline or N,N-dimethylaniline. Lemaire et al.[184] performed MALDI imaging on rat brain sections comparing the ionic matrix CHCA/aniline with regular CHCA. The application of ionic matrix resulted in higher signal intensity and sensitivity, better image quality and peptide localization, reproducibility, and higher resistance to laser ablation.

The organic matrices absorb the energy of the laser beam in the UV-range resulting in efficient desorption and ionization of the matrix material.[185] The ionization of the matrix and related clustering processes create strong background signals in the low mass region of the spectrum, which complicates the MALDI-MSI analysis of low M_w compounds. In order to lower the chemical noise at low mass ranges, high molecular weight porphyrin based matrices (in the mass range from 566.70 Da to 1531.96 Da) have been used for MALDI analysis of vitamins and drugs.[186,187] Gold nanoparticles (AuNPs) with a size range of 2-10 nm, can also be used as new generation matrices for high resolution imaging. They do not ionize easily but allow desorption and ionization of analytes with minimum background signal coming from the matrix itself.[188] C.L. Su et al. compared bare and functionalized AuNPs with DHB, and showed the successful detection of small carbohydrates of up to *m/z* 500 with AuNPs.[189] The background interference from matrices occurs as a result of their high concentration in comparison to analyte concentrations and the fact that clusters of matrix molecules also ionize and are detected together with analytes.

Recently a new matrix, containing the coumarin moiety (7-mercapto-4-methylcoumarin), was used for MSI analysis of small molecular compounds such as choline alkaloids from the areca nut with decreased background interference in the mass range below *m/z* 600.[190]

The concentration of the matrix in solution must be carefully considered before matrix application. If the concentration is too low, the analyte may diffuse from its original position before crystallization or there will not be a sufficient amount of organic acid to form proper crystals. Too high matrix concentration could result in rapid crystal formation and a limited time for analyte extraction and incorporation. Depending on the specific application, the matrix concentration range is 10-30 mg/mL SA for protein analysis and 10-20 mg/mL CHCA for peptide analysis.[181] The results from a comparison between three different SA matrix concentrations, presented in figure 2.8, showed that a saturated matrix solution (>30 mg/mL) yielded the highest number of ion signals with the best mass spectral appearance.[102]

In the same study a series of saturated SA solutions with varying organic solvent/water combinations were deposited on a mouse liver section and analyzed by MALDI-MS in order to show the effect of solvent composition on the resulting mass spectra. Solvent combinations consisted of acetonitrile, ethanol, methanol, isopropanol and acetone in different solvent/water proportions. Two solvent solutions: 50:50 acetonitrile/water and 50:50 ethanol/water were recommended as good general solvents for different types of tissue samples.[102] More non-polar solvents such as methanol or isopropanol can be used for analyzing more hydrophobic analytes.[181] As this study showed, the TFA concentration also affects the MS signals and corresponding results of direct tissue analysis. This study found that a concentration range of 0.3–1.0% TFA maximizes the total number of proteins analyzed.[102] However, in most current MSI protocols for analyzing different classes of biomolecules TFA is used at lower concentration of 0.1%.[11,191]

Hydrophobic proteins, such as membrane-bound or transmembrane proteins, are generally not easily extracted and cannot be detected during MSI analysis. Methods for dissolving molecules in organic/water solutions are ineffective for this class of molecules. For tissue imaging and profiling the application of MS-compatible detergents (such as octyl β-D-glucopyranoside (n-octyl glucoside) or 3-[3-(1,1-bisalkyloxyethyl)pyridin-1-yl]propane-1-sulfonate (PPS) to the tissue surface significantly enhanced detection of membrane/lipophilic proteins.[135,192]

The size of the crystals can influence the sensitivity of MSI detection. Usually too small crystals lead to lower sensitivity for detecting intact biomolecules in MALDI-MSI. In ME-SIMS small crystals assist in obtaining higher spatial resolution. ME-SIMS only samples the top 50 nm of the matrix surface and sputters less than 1% of the surface area in the static SIMS mode (see section 2.1.3.2 for the explanation of static vs. dynamic SIMS) whereas MALDI typically ablates much more material both in depth and in surface area. Ultimately,

the choice of matrix crystal size is determined by a combination of desorption and ionization technique used, required spatial resolution and required sensitivity.
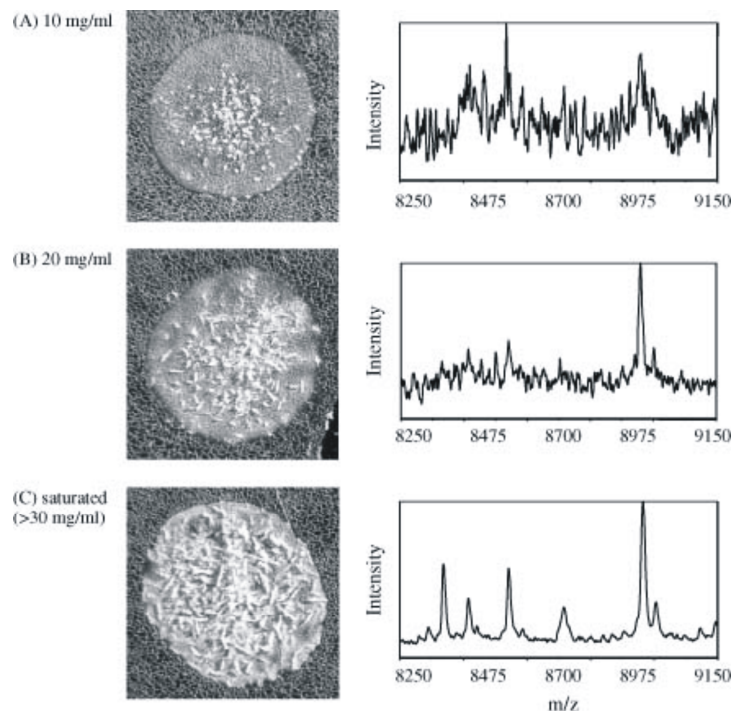
Figure 2.8 Analysis of matrix crystallization from solutions of different matrix concentration. Solutions of sinapinic acid in 50:50 acetonitrile/0.1% TFA in water at concentrations of (A) 10 mg/mL, (B) 20 mg/mL, and (C) saturated (>30 mg/mL). The spectra obtained from solutions spotted on mouse liver tissue section showed that the greater the concentration of matrix, the greater the crystal coverage, and the better the resulting mass spectrum. Reprinted with permission from ref[102]. Copyright 2003 Wiley Interscience.

In order to obtain bigger crystals, a sufficiently long incubation time is required. Longer incubation allows the solvent to extract the biomolecules of interest from the tissue surface into the droplet prior to crystal formation. There are two parameters that influence the formation of matrix crystals: the speed of solvent evaporation and the time of matrix incubation. Slower solvent evaporation leads to bigger crystals.[16] This process depends on the solvent to water ratio, the higher the concentration of the solvent the faster its evaporation. Slow crystallization can be also achieved by keeping the sample after matrix deposition at 4°C for 1 h. This process results in lower noise mass spectra, as already pointed out by Stoeckli et al.[193] The time of matrix incubation should be sufficient for effective solvent evaporation after each round of its application; too fast matrix application leads to analyte diffusion due to an excess of solvent solution present on the surface of the tissue. The amount

of solvent applied on the tissue should allow efficient extraction of biomolecules without diffusion of analytes. On the other hand, too big crystals (> 100 μm) cover a large area of the tissue extracting the molecules from many cells at a time and affecting the resolution of the MS image. For example, a 100 nL droplet dries to form a 900 μm diameter crystalline spot and extracts proteins from about 1000 individual cells.[102] Smaller matrix spots are necessary for increasing the spatial resolution of the image since it is limited by two key parameters, spot size and laser beam diameter. Larger spots require larger sample step sizes between laser shots, while smaller spots allow decreased sample step sizes. With spot diameters smaller than the laser beam, the imaging resolution is generally limited to the laser beam diameter (50–150 μm).

Smaller matrix spots and better coverage of the tissue with the matrix material were obtained by applying a thin layer of mechanically ground SA particles on the surface of the tissue section.[101] The seeded matrix produced more homogeneous ion signals throughout each matrix spot and reduced the number of droplets required to obtain matrix spots with good crystal coverage.

The crystallization process is heavily influenced by the presence of salts and surface-active compounds such as carbohydrates, lipids or excessive amounts of hemoglobin.[101,183] The local concentration of these interfering substances may lead to differences in the crystallization process, crystal heterogeneity, decreased signal quality and formation of analyte-rich matrix crystals called "sweet spots" or "hot spots" as well as crystals formed exclusively by matrix and containing no or very little analytes.[183] Rinsing of the tissue section with ethanol prior to matrix application removes salts from the sample's surface and improves the crystallization process. It has been demonstrated that different salt/matrix compositions locally lead to the formation of different pseudomolecular ion types and different degree of fragmentation.[194] Another important aspect of effective matrix crystallization is the choice of matrix since different matrices give different crystal patterns. Evaluation of the three most common matrices, SA, CHCA, and DHB, presented in figure 2.9 showed that the pattern of SA crystallization is the most uniform, giving an even layer of crystals over the spotted area.[102] In comparison, DHB formed crystals on the rim of the drying droplet which may compromise the quality of the image. With high repetition rate lasers (typically 200 Hz or more) the fast and accurate generation of averaged molecular profiles for each spot on the tissue surface became possible.
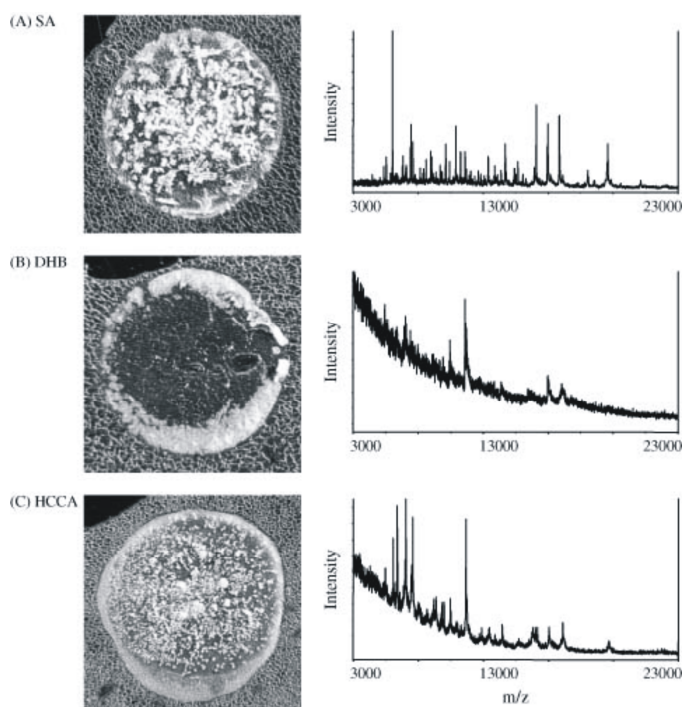
Figure 2.9 Analysis of matrix crystallization on tissue. Comparison of three different matrices, (A) SA, (B) DHB, and (C) CHCA at concentration 20 mg/mL (in 50:50 acetonitrile:water/0.1% TFA). SA and CHCA form dense crystals on the tissue, while DHB crystallizes on the rim of the spot. Reprinted with permission from ref[102]. Copyright 2003 Wiley Interscience.

Matrix application methods

The matrix solution can be deposited on the tissue section as individual droplets (spotted) or as a homogeneous layer (coated). The method of matrix deposition depends on the spatial resolution required for the analysis. Both methods are focused on homogenous crystallization of the smallest possible crystals trapping the largest amount of analytes without any diffusion of molecules. Both methods, spotting and spraying, can be performed either manually or automatically. Automated devices offer better reproducibility and control over extraction processes, which allows comparison between different samples. Both spotting and spraying parameters must be experimentally optimized for every tissue type since the quality of MSI depends on matrix coverage, wetness of the surface during matrix application and thickness of the crystal layer with all of these parameters being surface dependant. In both cases, multiple passes of matrix application are necessary to coat the entire tissue, but excess amount of matrix (over-coating) can suppress analyte signal.[181] The matrix layer can be monitored under a microscope until an even coating with small crystals is achieved. To check the homogeneity

of the matrix coating and to correct for uneven matrix distributions, an internal calibrant, typically a peptide in the same mass range as the analyte of interest, can be added to the matrix solution.[172]

Matrix deposition methods developed at the FOM-Institute for Atomic and Molecular Physics (AMOLF) for different matrix deposition devices and high-resolution MSI were reviewed by A.F.M. Altelaar and R.M.A. Heeren in 2009.[195] Here, the most popular spotting and spraying devices currently available for MSI are presented.

Spotting

The spotting of the matrix solution onto the tissue section limits diffusion of the analytes to the spot size. Manual spotting can be done using a micropipette that delivers microliter (μL) droplets generating spots of approximately millimeter size. Robotic spotting deposits picoliter (pL) droplets and provides a spot size of around 100-200 μm, which allows MSI at a spatial resolution of approximately 200 μm.[96,196]

Two popular automated spotting devices utilize two different types of droplet ejectors: inkjet-style piezo nozzles and focused acoustic dispensers. General matrix deposition guidelines for both types of spotting devices have been described.[101,168] Both ejectors can release 100 pL droplets that dry on the tissue to a 100-200 μm diameter spot. The resolution of MSI analysis is in this case limited by the matrix spots which is generally larger than the focused laser spots.[197] Smaller, closely spaced droplets are best for high resolution images and effectively limit analyte migration to the area covered by the droplets but are harder to generate and evenly sample with the desorption laser. Larger droplets spread on the sample surface, increase the possibility of analyte diffusion within the matrix spot and are better suited to profiling rather than imaging.[101] Spotting devices allow multiple rounds of droplet deposition, which can be performed onto the same location to increase analyte extraction from the tissue. A number of devices are available for generating and accurately depositing droplets onto a surface. Matrix spotting devices such as CHIP (Shimadzu Corporation, Kyoto, Japan) are equipped with inkjet-style piezo nozzles which were first applied to the fabrication of microarrays of DNA, proteins and other bioactive molecules.[183] Another automated method for matrix deposition, a desktop inkjet printer with a six-channel piezoelectric head that delivered 3 pL droplets, was presented by D.L. Baluya et al. in 2007.[198] The comparison of different matrix deposition methods such as electrospray, airbrush and inkjet showed that the mass spectral images gathered from inkjet-printed tissue specimens were of better quality and more reproducible than from specimens prepared by the electrospray and airbrush methods.

The significant limitation of inkjet dispensers is the clogging of the capillary when spotting highly concentrated matrix solutions.

Focused acoustic dispensers utilize acoustic energy to generate very small droplets of matrix on tissue sections. Matrix solution is kept in a reservoir which is constructed from an acoustically transparent membrane that is coupled to a piezo transponder by way of a column of water. The sound wave produced by the transponder reaches the surface of the matrix solution in the reservoir which ejects droplets of matrix with a volume of approximately 120 pL. These droplets are then collected on the tissue section held inverted over the matrix reservoir. Since the droplets are ejected from a large surface reservoir, there is no possible clogging.[101,107] A robot capable of acoustic droplet ejection (RapidSpotter, Picoliter Inc., Sunnyvale, CA, USA) is being used to eject picoliter-sized matrix droplets onto the surface of the tissue, effectively coating the section. This technique results in a crystal surface similar to electrosprayed surfaces, but it allows multiple rounds of precise droplet deposition. This matrix application method deposits droplets which can remain wet longer and minimizes molecule delocalization to the area of droplet. Another spotting device, Acoustic Reagent Multispotter (Labcyte Inc., Sunnyvale, CA, USA), consists of an acoustic ejector, translational stage with lateral precision of 3 μm, and video telescopes integrated under software control.[101]

The matrix spotters can be also divided into contact and noncontact deposition devices. Contact deposition methods require a pin or capillary to physically contact the sample for droplet deposition, which can introduce cross-contamination. The reproducibility of spotting small amounts of liquid using pins or microcapillaries can be low.

Noncontact printing devices such as piezoelectric, thermal inkjet, solenoid valves, and pulsed field ejectors do not have these limitations. Microdroplets are ejected from small capillaries onto the tissue by applying pressure pulses without any contact between capillary and the sample.[101]

Spraying

Spray coating is employed to cover the surface of the sample with a fine distribution of small droplets of matrix solution. After drying of these droplets a homogenous thin film of solid matrix crystals is formed. Spraying devices deposit a matrix mist on the tissue surface which results in much smaller droplets than those generated by spotting devices. This approach provides smaller crystal sizes (<< 100 μm) and allows higher image resolution.[16] Both manual (pneumatic sprayer, airbrush or thin-layer chromatography (TLC) sprayer) and automated

(robotic pneumatic sprayer, vibrational sprayer, electrospray) spray coating methods have been developed. Automated methods yield more reproducible results and provide more uniform application conditions. Currently one fully automated vibrational sprayer system (ImagePrep, Bruker Daltonics GmbH, Bremen, Germany) is commercially available.

The spray coating delivers smaller crystal sizes but less reproducible matrix deposition and higher chance of analyte diffusion in comparison to spotting application methods if the surface is wetted too much. The advantage of spray coating is the size of the crystals formed which are typically around 20 μm, not larger than the diameter of the focused laser beam. A more even coating can be obtained when the final spray consists of only solvent allowing pre-deposited matrix crystals to re-dissolve and re-crystallize, which increases the incorporation of analytes in the final crystals.[165] The smallest crystal size, <<5 μm, can be obtained using electrospray deposition which has been shown to yield subcellular resolution in ME-SIMS experiments.[34]

Both spotting and spraying of the matrix take place at RT, but spotting needs more time than spraying which can cause degradation of some molecules during the matrix application process. Additionally, matrix application by coating covers the whole surface of the tissue section with a layer of matrix solution and requires a more careful application protocol than spotting.

Alternative matrix application, solvent-free and matrix-free methods

Some other matrix application methods for MSI have been tested. One of them is sublimation which was successfully used for matrix application and resulted in the formation of very small crystals. A protocol using sublimation for matrix deposition was reported in 2007 and provided a homogeneous coating of matrix for obtaining high resolution phospholipid images from tissue.[199] The sublimation apparatus is relatively simple and became commercially available. The key advantage of sublimation deposition in comparison to other matrix application techniques is the elimination of diffusion of the analyte molecules because no solvent is used during the matrix deposition step. Another advantage is the increased purity of the matrix and the reduction of the crystal size.[200] Sublimation of matrix for imaging of peptides and proteins requires re-wetting of the surface to enable surface extraction of these analytes.

Another alternative matrix application method optimized for detection of proteins involved co-crystallization of matrix with analyte acquired through placing a tissue section upon a drop of SA matrix dissolved in 90% ethanol and 0.5% Triton X-100.[11] After solvent evaporation a

seed layer of sinapinic crystals was added as dispersion in xylene, followed by application of additional layers of SA added as solutions in 90% ethanol followed by 50% acetonitrile. An increased mass range between 25 kDa to 50 kDa of proteins was obtained from tissue sections such as kidney, heart, lung and brain of different rodent species.

Some variants of matrix application methods such as covering the complete area with a large matrix volume at 4°C followed by a drying step at RT or complete immersion of the sample in a matrix solution followed by a drying step were tested but both caused extensive protein diffusion.[100] However, the first method yielded very strong ion signals while the second provided a very thin layer of crystals and modest signal intensity.

Desorption-ionization on silicon (DIOS) was implemented in MSI.[201,202] This matrix free approach was introduced in 1999 by the G. Siuzdak group[203] predominantly for the analysis of small M_w compounds by using silicon surfaces prepared via a galvanostatic etching procedure on a Si wafer. The physical properties of the silicon material (high area surface, UV absorption) are crucial for desorption/ionization process. A DIOS based MSI experiment requires the transfer of analytes to the DIOS surface by direct contact with the tissue of interest. After removal of the tissue a mass spectral image can be acquired.

Colloidal graphite-assisted laser desorption/ionization (GALDI) MS has been demonstrated to work in MSI.[204] The method requires spraying of graphite nanoparticles onto the surface of the tissue. The sensitivity, suppression of ionization and optimum distribution of the particles must be improved in order to apply this method on a broader scale.

Carbon nanotubes (CNTs) are another desorption and ionization method with potential application for MSI.[205,206] They are generated *in situ* by chemical vapor deposition. This method gives minimal interference, but this has not been shown to work on proteins or peptides.

NIMS employed clathrates.[99] Clathrate nanostructures provided a spatial resolution comparable to MALDI-MSI, while maintaining the soft nature of MALDI. In this method 'initiator' molecules trapped in nanostructured surfaces (clathrates) release and ionize intact molecules adsorbed on the surface. This surface can be used together with both ion and laser beam irradiation.

Finely ground matrix particles which were filtered directly onto the tissue through a 20 μm stainless steel sieve is another variant of a dry-coating, solvent-free matrix deposition employed in MSI.[182] The analysis of phospholipids from mouse brain sections revealed that the results from dry matrix deposition shown in figure 2.10 were identical to results from TLC spray-coated sections. However, dry matrix deposition resulted in simpler and faster sample

preparation with virtually no analyte delocalization. This approach provided highly reproducible results and eliminated the variation caused by operator differences.
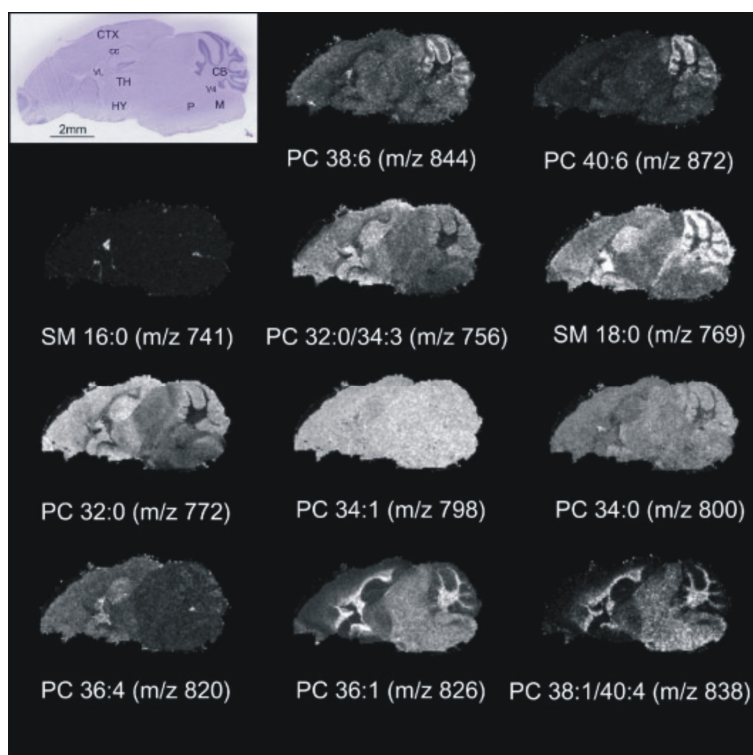
Figure 2.10 The optical image of H&E-stained sagittal mouse brain section showing the anatomy of the brain and selected ion images from a dry-coated serial sagittal section showing the phospholipid patterns in the brain. CB, cerebellum; CC, corpus callosum; CTX, cerebral cortex; HY, hypothalamus; M, medulla; P, pons; TH, thalamus; V4, fourth ventricle; VL, lateral ventricle; PC, phosphatidylcholine; SM, sphingomyelin. Reprinted with permission from ref[182]. Copyright 2009 Elsevier.

Another method of solvent-free matrix deposition involved coating of the tissue section with a thin layer of seed matrix but in that case a painter's brush was used to distribute the ground matrix such as SA on the tissue surface.[101] Excess material was removed using a gentle blow of compressed air in a laboratory hood. Observation of the tissue under a microscope indicated a high density dispersion of 0.3-3.0 μm particles across the section. Figure 2.11 presents the experiment comparing dry coating and regular coating using airbrush which showed that the solvent free matrix application technique was more beneficial for MALDI imaging of lipids since solvent was necessary for extracting peptides from tissue samples.[163]
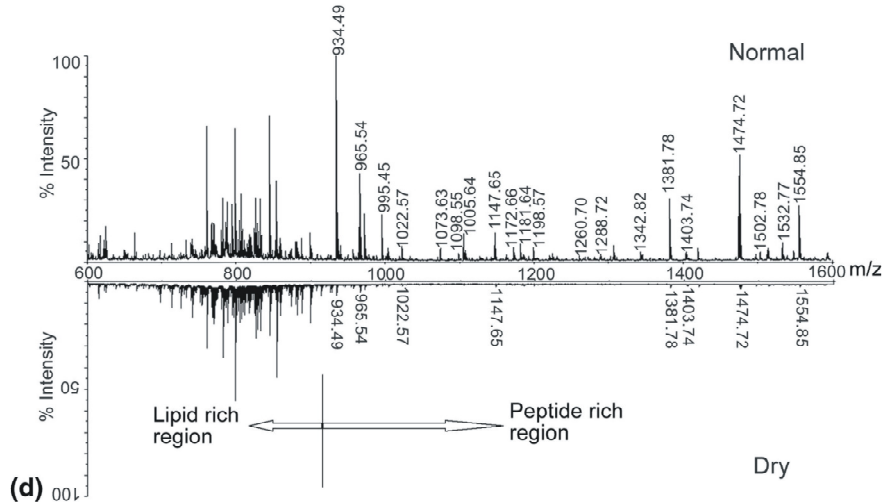
Figure 2.11 Comparison of dry matrix spraying and regular matrix spraying for lipid and neuropeptide detection from C. borealis brain. Reprinted with permission from ref[163]. Copyright 2007 Nature Publishing Group.

2.2.1.4 Staining

Staining of MSI tissue sections helps to correlate the data obtained from imaging experiments with tissue histology. Staining can be done either before or after an MSI experiment. If staining is performed before MS measurements the protocol must contain MS friendly histological dyes such as cresyl violet or methylene blue.[165,167] H&E staining protocols, which are the most commonly used staining protocols in clinical pathology, cannot be used prior to MSI analysis since these dyes affect the quality of the mass spectra.[165] H&E staining can be performed after MSI measurements following matrix removal from the surface of the sections. Matrix removal can be achieved by immersing the glass slide in a 70% ethanol solution for approximately 1 min followed by dehydration of the section in a graded ethanol series before H&E staining.[107]

The morphology of the sample must be also visualized before tissue profiling experiments since only specific regions of the heterogeneous sample are subject to analysis (see **Profiling vs. imaging**). When staining cannot be performed, e.g. the tissue section was mounted on a steel plate, correlation of the MSI data with the morphology of the sample can be accomplished by using two adjacent sections, one for histology (on a glass slide) and one for MSI analysis. An example resulting from this approach is shown in figure 2.12. However, visual co-registration between both sections can be complicated due to differences in the structure of adjacent tissue sections. Morphologically and functionally distinct regions of

heterogeneous tumor samples are interesting objects for MSI analysis for medical diagnostics. Studies of different regions of lung and breast tumor sections resulted in the detection of many differences on the biomolecular level.[129,142] In both cases, the adjacent H&E stained tissue sections were used to select the regions of interest (ROIs) prior to profiling.
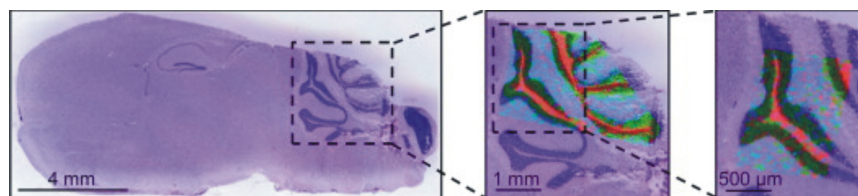
Figure 2.12 High-resolution MALDI images of a mouse cerebellum. The left panel shows the H&E-stained optical image of a mouse brain section. The overlaid phospholipid images show the localization of PC 40:6 (m/z 872 in light blue) to the cerebellar cortex, PC 36:1 and PC 38:4 (m/z 826 in the middle and m/z 810 on the left in red) to the cerebellar nucleus, and PC 38:6 (m/z 844 in green) to the granule cell layer. Reprinted with permission from ref[182]. Copyright 2008 Elsevier.

2.2.1.5 Contaminants

After successful tissue preparation the sample is introduced and analyzed in a mass spectrometer which results in detection of hundreds of different ions. The correct identification of detected peaks is the next biggest challenge. The increasing sensitivity of MSI instruments allows detection of molecules from the tissue present at very low concentration. Along with the biomolecules many contaminants introduced during sample preparation steps will be ionized and detected as well. Among the most often detected contaminants of biological samples are the impurities present in the solvents used for tissue washing and matrix deposition, salt adducts, keratin or polymers such as OCT or polyethylene glycol (PEG). A recently published review of common MS contaminants contains a broad list of unwanted ions of different origin.[207] The contaminants are classified into two groups. The first group contains proteinaceous interferences or contaminants which include e.g. enzymes used in sample preparations, keratins and other abundant, involuntarily introduced proteins or instrument-induced peptide fragment interferences. Non-proteinaceous interferences or contaminants such as matrix clusters in MALDI-MS, adducts, solvents and polymeric interferences, plasticizers and additives have been grouped in a second category of contaminants.

Ion mobility MS, high-field asymmetric waveform ion mobility spectrometry (FAIMS), matrix-free laser desorption/ionization techniques including DIOS, DESI, or direct analysis in

real time (DART) are some techniques that are helpful in minimization or elimination of certain background interferences.[207] In addition to that all steps of tissue preparation should be carefully performed, which includes the use of gloves and clean lab glass ware. Every MS analysis should also include blank tests such as system-, solvent-, method-, matrix- and equipment blanks.[207]

2.2.2 MSI instrumentation and processing tools

2.2.2.1 Mass analyzers

Technological improvements in mass spectrometric instrumentation have enabled various high throughput peptide and protein screening applications in a large variety of samples. Proteomics as a scientific field that has emerged over the last decade has been a major driving force. Approaches such as shot-gun proteomics, quantitative proteomics, top-down proteomics and chemical proteomics[208] have all developed out of mass spectrometric innovations. MSI is taking the same advantage of these innovative technological developments. In this section we will discuss some of these innovations from a more instrumental perspective, highlighting their respective benefits in MALDI or SIMS analysis of tissue. Table 2.1 provides an overview of the most commonly used mass spectrometers for MSI together with their characteristic performance indicators.

Time of flight mass spectrometry

The majority of MSI experiments are performed on TOF systems. Stephens and co-workers introduced the TOF-MS in 1946[209] and since then the TOF analyzer has been combined with SIMS ion sources in the 80's and with MALDI sources since it's conception. TOF-MS offers good transmission ratio (50-100%), sensitivity, dynamic mass range, and repetition rate. The first high mass resolving power imaging experiment with a SIMS-TOF in a scanning microprobe mode was published in 1991.[210] The reported secondary ion images were obtained from a polymer surface with an average M_w of 1400 *m/z*. TOF analyzers allow the separation of ionized accelerated molecules according to their molecular masses. Generated by the ionization beam in the source, ions characteristic of the surface species are accelerated by an electric field between the conductive support (and sample) and the extraction grid (10-25 kV) to the same kinetic energy. Therefore, the ions arrive at the detector with different speeds, which are inversely proportional to their mass over charge values. Three main TOF analyzer geometries are defined in order to increase the sensitivity, mass accuracy and mass resolving

power. These entry geometries are linear, reflectron and orthogonal. The linear geometry is commonly used in TOF imaging mass spectrometry and provides the highest sensitivity and mass range. The reflectron geometry utilizes an electrostatic mirror that compensates velocity differences obtained during desorption and ionization processes in the source. This compensation results in a substantial improvement of the mass resolving power as high as 60000 FWHM (full width at half maximum).

Table 2.1 Characteristic performances of different mass analyzers for imaging MS

Mass analyzer	Mass resolving power	*m/z* range		Transmission (%)	Detection	Pixel acquisition frequency
		low	high			
Time-of-flight[a]	10^3-10^4	0	150k	50-100	Parallel	>10 Hz
FTICR[b]	10^4-10^6	20	5-10k	20-90	Parallel	> 1 Hz
(Linear) Ion Traps[c]	10^2-10^3	50	4.5k	1-80	Sequential	<10 Hz
Triple-Quad[d]	10^2-10^3	0	1-5k	1-80	SRM/MRM/ Sequential	>100 Hz
Magnetic sector[e]	10^2-10^3	0	5k	<2	Single ion/ array detection	<1 Hz

Notes: Generally, the type of desorption and ionization technique will impact upon the performance of a mass spectrometer. The numbers in this table are to be considered to provide a general impression of what the analyzer is minimally capable of in a standard MALDI-MSI. [a] The mass range of a TOF system is limited by detection efficiency only. Using special high mass detectors the high mass limit can be extended to several MDa. [b] The mass limits in FTICR-MS are determined by magnetic field strength numbers and are provided for a 7 Tesla system. [c] Ion traps usually have a low mass cut-off depending on the radiofrequencies and mass analysis methods used. Linear ion traps are often hybridized with a second mass analyzer for multiplexed parallel tandem MS analysis. [d] Triple Quadrupoles have the same limitations as single quadrupoles but in multiple reaction monitoring (MRM) the analytical quadrupoles are fixed so that the transmission for that specific reaction channel is substantially higher and the analysis is faster as no sequential scanning is needed. [e] Magnetic sector instruments are not used for MALDI but mainly for dynamic SIMS. In that case one or more selected ions are continuously imaged at high sensitivity. In the scanning

mode a sector instrument is impractical for MSI. As a result most ions are discarded and transmission is low.

The use of a reflectron typically limits the mass range and in imaging studies it is predominantly used to analyze singly charged ions with a M_w in the range of 15-20 kDa. Although a highly sensitive and rapid molecular weight profiling technique, MALDI-TOF has limited mass measurement accuracy (MMA) and resolving power and lacks the capability to perform effective tandem mass spectrometry experiments for peptide sequencing.[211] This changed with the introduction of an alternative TOF geometry, using orthogonal acceleration, by the group of Guilhaus.[212] The orthogonal acceleration-TOF (oa-TOF) approach allowed the decoupling of the ion source from the mass analyzer and led to the introduction of hybrid analyzers that combine a quadrupole mass analyzer with a TOF-MS the so-called qTOF geometry. These oa-TOF or qTOF systems revolutionized the usefulness of TOF-MS systems for structural analysis with tandem mass spectrometry. Combined with the improved mass accuracy this geometry is extremely useful for imaging mass spectrometry. The most recent development in this field is the introduction of IMS (see **Application of ion mobility separation for MSI**).

An alternative approach for structural analysis with a TOF-MS system is the combination of two TOF-MS mass spectrometers coupled together in a so-called TOF-TOF configuration. The first TOF system is used to select a precursor ion for fragmentation and the second TOF system is employed for rapid, parallel fragment analysis.

Fourier transform ion cyclotron resonance mass spectrometry (FTICR MS)

The FTICR MS technique is based on the determination of the ion cyclotron frequencies of ions trapped in a Penning trap. The mass to charge ratio of the ions is determined from this frequency in first approximation by the equation $\omega_c=qB/m$. In FTICR MS experiments, the ions can be generated directly inside the ion trap or the ions can be generated externally and transported to the ion trap. The latter approach has the advantage that a multitude of ion sources can be used. The ion trap or ion cyclotron resonance (ICR) cell generally consists of two trap electrodes, two excitation electrodes and two detection electrodes. The trap electrodes define a parabolic trapping potential that confines the ions axially. Typical trapping potentials are of the order of ±1 V. Radially, the ions are confined by the magnetic field in which the ICR cell is positioned. After ions have been trapped and stored for a variable time (which can be as short as a few milliseconds and as long as a few hours) the ion cyclotron motion is excited by the application of a radio frequency (RF) excitation pulse on the

excitation electrodes. As a result of this time-varying electric field the ions experience a net outward force which causes the ions to increase their cyclotron radius. More important, at the same time the ion motion also becomes coherent. The coherently orbiting ions induce image charge in the detection electrodes. The ICR signal is measured by digitizing the voltage difference between the two detection electrodes as a function of time. This signal is often referred to as the ICR transient. Fourier transformation of the time-domain transient results in the cyclotron frequency spectra, which can subsequently be converted into mass spectra.

Fourier transform mass spectrometers (FTMSs) offer several unique advantages including high mass resolving power, high MMA, and multistage MS/MS capabilities. Furthermore, the ability to trap and store ions while allowing additional ions to be introduced into the ICR cell makes it possible to accumulate ions from multiple MALDI ionization events in the FTICR cell prior to detection. Such in-cell ion accumulation (ICA) methods produce a significant signal to noise improvement over the more commonly used signal averaging methods.[211]

Sub-ppm MMA and mass resolutions greater than 100,000 allow, in theory, the detection and identification of a greater number of metabolites.[213] Recently it was shown by researchers from the AMOLF for the first time that direct identification capabilities required for biomolecular imaging studies can be realized by the implementation of FTICR MS at 7 Tesla for molecular imaging.[97] FTICR MS delivers a unique combination of high mass spectral resolution and tandem mass spectrometric capabilities.[97] This combination allows the mass spectral separation of different species from complex systems while tandem mass spectrometry is employed to dissociate selected molecular ions for structural determination. The extreme resolution offered by FTICR MS allows the visualization of spatial details that remain hidden under lower mass spectral resolution conditions.

Other groups have since utilized the high mass resolving power capabilities of FTMS and FT-Orbitrap technology to analyze a variety of systems, ranging from the study of Crab neuropeptides by MALDI-FT profiling[211] to human tissue sections.[214]

Linear ion traps

Modern linear ion traps (LIT) are improving throughput and sensitivity for the identification of tryptic peptides in shotgun proteomics.[215] Their operating principle, a linear quadrupole ion trap in combination with a high performance mass spectrometer such as FTICR MS or FT-Orbitrap provides the capabilities to multiplex mass spectral analysis. This approach has several advantages for MSI and has been described for example by the groups of R.G. Cooks[216] and R.A. Yost.[217] A new intermediate-pressure MALDI LIT mass spectrometer and

its capabilities for imaging mass spectrometry are described by Garret et al.[218] The instrument design is described and is characterized in terms of four performance issues (1) MALDI performance at intermediate pressure; (2) analysis of samples on non-conductive and conductive glass slides; (3) critical importance of tandem mass spectrometry (both MS^2 and MS^3) for identification of analyte species and imaging of isobaric species; (4) capability for repeated analysis of the same tissue section. Application of the new instrument to imaging phospholipids in rat brain sections is described in detail.[218]

Triple quadrupole mass analyzers

Triple quadrupole mass analyzers have long been thought not to be useful for imaging mass spectrometry. The rationale behind this was the lack of speed and the low duty cycle if the objective of the surface analysis targets the whole mass range. A quadrupole is a mass filter, transmitting only ions in a certain mass window and obtaining a mass spectrum requires scanning the filter characteristics. This mode of operation is not compatible with a pulsed ionization technique such as MALDI as most of the ions produced at the surface are not analyzed. The triple-quadrupole system is for that reason mainly used with continuous ionization sources for small, low molecular weight analysis such as ESI or atmospheric pressure chemical ionization (APCI). A new method was introduced that allows the useful combination of a pulsed MALDI source with a triple quadrupole linear ion trap (MALDI-QqQLIT) instrument for high throughput quantitative analysis of low M_w molecules.[219] This method allows rapid single or multiple reaction monitoring (SRM/MRM) of small molecules at surfaces and is as a result very useful for targeted pharmaceutical compound and metabolite imaging. The SRM/MRM involves the selection of one or more (but sequential) structure specific fragmentation channels. A SRM experiment involves the selection of a precursor mass (by the first quadrupole), a fragmentation step (in the second quadrupole) and the selection of a specific fragment mass (by the third quadrupole). The quadrupole settings are fixed and provide high ion transmission of the system resulting in a sensitive analysis. In this mode the triple quad becomes a selective mass filter for a specific precursor molecule combined with a specific fragment of that precursor molecule. In MRM mode several SRM channels are automatically examined sequentially. The group of G. Hopfgartner has elegantly demonstrated how this approach can be used for rapid, quantitative imaging of selected compounds in whole body tissue sections.[112]

Magnetic sector mass analyzers

Magnetic sectors are also used for imaging mass spectrometry. They are employed mainly for high resolution elemental analysis using dynamic SIMS. In that case one or more selected ions are continuously imaged at high sensitivity. As a result most other ions are discarded and the overall transmission is low. In particular, the Cameca NanoSIMS 50[220] shows an instrumental configuration for high spatial resolution SIMS: the primary ions and secondary ions in this instrument are controlled by the same ion-optical elements near the sample. This allows perpendicular sample analysis with small spot sizes and high secondary-ion collection efficiency. The magnetic sector and several moveable detectors allow simultaneous detection of several elements or small molecules (within a narrow mass range) with high detection sensitivity.

2.2.2.2 Software for MSI

Data collected from MSI yield high resolution molecular profiles across the tissue with data files of up to few gigabytes which require complex visualization software. MSI software controls data acquisition and processing in order to generate ion images. A comparison of several recently developed MSI software was presented by O. Jardin-Mathé et al. in 2008.[221] Here, we will present a couple of examples of imaging software.

BioMap

BioMap (Novartis, Basel, Switzerland, www.maldi-msi.org) is an image processing application. BioMap was originally developed by M. Rausch for the evaluation of MRI data in biomedical research and due to multiple modifications it can now support many more imaging data formats, including optical, PET, CT, near-infrared fluorescence (NIRF) and MSI.[100] BioMap was written in IDL™ (Research Systems, Boulder, CO). Visualization is based on multi-planar reconstruction allowing extraction of arbitrary slices from a 3D-volume. Other features linked to visualization are overlaying of two individual data sets or displaying the ROIs. It allows displaying the mass spectrum from selected single points or ROIs on the generated image. Another mode is to select on the mass spectrum the analyte of interest and to calculate by integration over the corresponding peak its distribution on the scanned area.[172] Routines for baseline correction of spectra, spatial filtering and averaging of spectra enhance the information obtainable from a data set.[100] The software provides visualization and a storage platform, which can be easily extended by various software packages, individually designed for the analysis of specific data sets.

FlexImaging

FlexImaging™ 2.0 (Bruker Daltonics GmbH, Bremen, Germany, www.bdal.com) software is used for acquisition and evaluation of MALDI-TOF and TOF/TOF imaging data. This software allows color-coded visualization of the distribution of any ion detected during MSI and overlaying of the optical and MS images. Integrating statistical classifications such as principal component analysis (PCA) or variance ranking, the software provides "Class Imaging" which allows the classification of tissue types and determination of the class membership of comparable tissue samples.

MALDI Imaging Team Imaging Computing System (MITICS)

MITICS is new software compatible with many types of instruments developed for MALDI imaging.[221] MITICS is divided in two parts: MITICS control for data acquisition and MITICS Image for data processing and image reconstruction. MITICS control is used for setting the acquisition parameters for the imaging sequence, such as creating the raster of acquisition and controlling post acquisition data processing. MITICS control is available for Applied BioSystems MALDI-TOF instruments and MITICS Image for both Applied BioSystems and Bruker Daltonics ones.[221]

Datacube Explorer

The Datacube Explorer (DCE, www.imzml.org>Software Tools), developed at the AMOLF, is a lightweight visualization tool for analyzing imaging mass spectrometry datasets. It offers both an image-based as well as a spectrum-based view of the data, with an easy way to dynamically scroll through the masses in a dataset. The DCE includes features such as on-the-fly spectral binning, ROI spectral analysis and image smoothing. It also includes a self-organizing map feature for image classification. The DCE is able to read and write the AMOLF datacube dataset format, and read imzML. The lightweight nature of the application makes it possible to easily share the application among several partners in scientific collaborations.

The Volume Explorer, also developed at the AMOLF, is a software tool to create 3D volumes out of a set of several 'image slices' for any *m/z* value. It uses the Visualisation Toolkit (VTK, www.vtk.org) for the 3D visualization part.

Imaging and database searching

Mascot (www.matrixscience.com) is a powerful search engine, which uses mass spectrometry data to identify proteins from primary sequence databases.[222] To identify an unknown protein from the sample, the protein of interest must be first purified usually by 2-dimensional polyacrylamide gel electrophoresis (2D-PAGE) or liquid chromatography (LC) and digested with a proteolytic enzyme, such as trypsin. The resulting digest mixture containing peptides obtained after digestion is analyzed by mass spectrometry. For MS/MS analysis of individual peptides, the digest mixture is separated by chromatography prior to analysis. The experimental mass values are then compared with calculated peptide mass or fragment ion mass values, obtained by applying cleavage rules to the entries in a comprehensive primary sequence database. By using an appropriate scoring algorithm, the closest match or matches can be identified. If the sequence database does not contain the unknown protein, then the aim is to pull out those entries which exhibit the closest homology, often equivalent proteins from related species. The sequence databases that can be searched on the Mascot server are MSDB, NCBInr, SwissProt and dbEST.

imzML

In order to ensure flexible and fast handling of the MSI data two separate files are used: a small (ini or XML) file for the metadata and a larger (binary) file for the mass spectral data (biomap, DCE, udp). The metadata file is based on the mass spectrometry standard mzML developed by the Human Proteome Organization-Proteomics Standards Initiative (HUPO-PSI). The MS data are stored in one of two binary formats in order to ensure the most efficient storage of these large data sets. A new controlled vocabulary was compiled for imzML to include parameters that are specific for imaging experiments. These parameters are stored in the imagingMS.obo file.

Digital staining algorithms

MSI is at present one of many techniques used to visualize the spatial distribution of specific biomolecules from tissue sections. The main advantage of MSI over other techniques is its capability to monitor the distribution of a large number of different molecules in a broad mass range and at the same time. With thousands of mass spectra containing hundreds of peaks collected from one sample, the automated and reliable computational analysis of MSI data becomes indispensable.[223] These algorithms could in the future potentially constitute a

valuable tool for pathologists or medical doctors that have to analyze large numbers of tissue samples. In that case, reliable classifiers can help minimize the risk of underdiagnosis.

Some applications of digital staining, namely hierarchical clustering and PCA were used to analyze data collected from tissue sections of gastric cancer and non-neoplastic mucosa.[224] A PCA approach was also applied to the analysis of metabolites in starvation-induced fatty liver tissue sections.[225] A conceptual overview of PCA for MSI along with a demonstration of this approach on an MSI data set collected from a transversal section of the spinal cord of a standard control rat was published by R. Van de Plas et al. in 2007.[226]

2.2.3 Application of ion mobility separation for MSI

Since its development in 1970's, IMS, known also as plasma chromatography or ion chromatography, has mainly been applied to the analysis of volatile organic compounds and used as a tool to probe the electronic states of ions.[227] IMS is a gas phase separation method that adds new dimensions to mass spectrometry due to its capabilities to separate isobaric ions that cannot be separated by conventional TOF mass spectrometry.[98,228] Figure 2.13 shows an example of the separation of two spatially structured isobaric species, a peptide and a lipid, resolved in an imaging MALDI ion mobility mass spectrometric experiment. IMS separates ions based on their collision cross-section and can be coupled with TOF mass spectrometry to yield a powerful tool used in the identification and characterization of biomolecules.[227] IMS adds an additional separation dimension which improves the resolution of imaging instruments and allows better characterization of detected biomolecules. IMS does not enhance the sensitivity of the instruments since it does not modify the ionization conditions and both ESI and MALDI ionization sources can be coupled to IMS instruments.
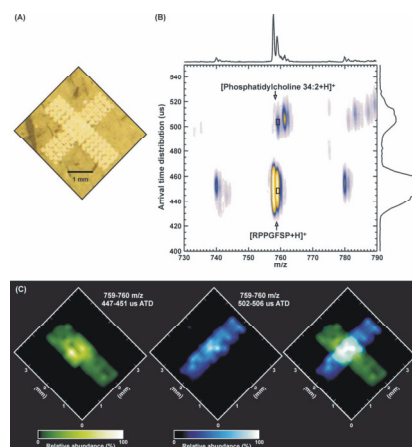

Figure 2.13 MSI in IMS mode of a nominally isobaric peptide (RPPGFSP) and lipid (PC 34:2) deposited onto a mouse liver thin tissue section in the pattern of an X. (A) An optical

image of the patterned matrix/analyte spots deposited on the tissue section. (B) A zoomed view in the region of PC 34:2 and RPPGFSP for a representative IMS of a mixture of the two analytes. (C) Extracted ion intensity maps for the peptide (left, green), the lipid (center, blue), and an overlay of the two maps at 50% transparency. Reprinted with permission from ref[229]. Copyright 2007 Wiley Interscience.

IMS has been applied to protein conformer differentiation, top-down protein sequencing, non-covalent protein complexes, isobaric compound identification and mass spectrometry imaging.[228,230,231] It is necessary to develop the tools to interpret the additional dimension of IMS data and gather valuable conformational information.

A fundamental introduction to ion mobility as it applies to macromolecules illustrated by a spectrum of a tryptic digest of bovine hemoglobin has been presented by G. Verbeck et al.[227] SYNAPT[TM] HDMS (Waters Corporation, Milford, MA) is at present the only commercially available instrument with IMS which can be used as a powerful tool for the identification and characterization of a variety of biomolecules.[232] This instrument has a quadrupole orthogonal acceleration TOF geometry and is equipped with an IMS device located between the quadrupole and the TOF analyzer. The ion mobility separator used consists of three consecutive traveling wave regions. The first traveling wave (trap) is used to store ions when an IMS is performed, to maximize the duty cycle of the IMS. Next is an actual IMS part of the T-wave. The final traveling wave device (transfer) is used to transfer ions from the ion mobility separator to the TOF mass analyzer maintaining the ions' separation. Collision induced dissociation (CID) can be achieved in either the trap or transfer T-wave or in both. The instrument is equipped with an interchangeable MALDI source, which can be replaced with AP ionization sources, such as ESI or APCI. MALDI is performed in an intermediate-pressure environment (9×10^{-2} mbar) using a frequency-tripled Nd:YAG laser (355 nm). Imaging data are obtained by moving the tissue sections in a raster pattern on an x/y stage relative to the laser beam position, which remains fixed.

MALDI-IMS-MSI has the ability to improve the imaging of some drugs, metabolites, lipids and peptides by separating such ions from endogenous or matrix-related isobaric ions as shown in figure 2.14. One such application is whole body imaging of rats dosed at 6 mg/kg with an anticancer drug, vinblastine.[98] The distribution of the precursor ion at *m/z* 811.4 and several product ions including *m/z* 793, 751, 733, 719, 691, 649, 524, and 355 have been investigated. Clearly demonstrated in these data is the removal of interfering isobaric ions within the images of *m/z* 811.4 and also of the fragment ion of *m/z* 751, resulting in a higher

confidence in the imaging data. Within this work, IMS has shown to be advantageous in both MS and MS/MS imaging experiments by separating vinblastine from an endogenous isobaric lipid.[98] The same combination of MALDI-IMS-MSI for improving the detection of low-abundance proteins that are difficult to detect by direct MALDI-MSI analysis was described by M.C. Djidja et al.[135] Both frozen as well as FFPE breast tumor tissue sections were subjected to a modified trypsin digestion followed by protein imaging and profiling. The advantages of imaging using IMS prior to MS analysis were also demonstrated for profiling of human glioma and selective lipid imaging from rat brain.[229] Also the distribution of phosphatidylcholine and cerebroside species was mapped from coronal rat brain sections using MALDI-IMS-MSI.[228] And most recently, the use of IMS coupled with MALDI-MSI enabled both the localization and *in situ* identification of a tumor biomarker, glucose regulated protein 78 kDa (Grp78), within FFPE pancreatic tumor tissue sections.[136]
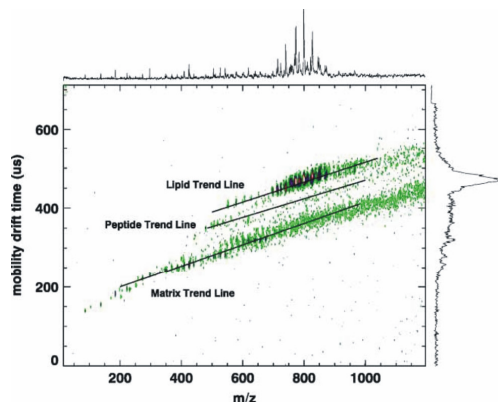
Figure 2.14 IMS diagram of ions detected from a rat brain tissue section covered with DHB. Ions of different drift time but overlapping m/z can be separated from each other. Reprinted with permission from ref[228]. Copyright 2007 Wiley Interscience.

2.2.4 Microscope vs. microprobe mode of image acquisition

Microprobe and microscope modes of MS image acquisition are two different approaches of ion detection implemented in imaging instruments.[16] Figure 2.15 schematically illustrates the two different imaging approaches. Microprobe mode is the more widely used form of MSI data acquisition. The sample is rastered with a laser beam or primary ion beam and the analyte ions are detected from each point separately. The laser beam or primary ion beam is highly focused in order to achieve maximum image resolution. In microscope mode the spatial relationship of ions desorbed from within the area irradiated by the defocused laser beam or primary ion beam is maintained from the moment of ions desorption until detection on a 2D-detector.[16,233] This instrument is capable of resolving spatial features within the area

irradiated by a laser beam to produce an effective spatial resolution of 4 μm.[233] The principle of position correlated ion detection instead of position correlated ion generation removes the need for a tightly focused microprobe for high lateral resolution imaging MS.[16] The speed of analysis is no longer limited by the large amounts of spots that need to be analyzed in a microprobe mode imaging experiment, and images can be generated at a speed limited by the repetition rate of the laser.[16]
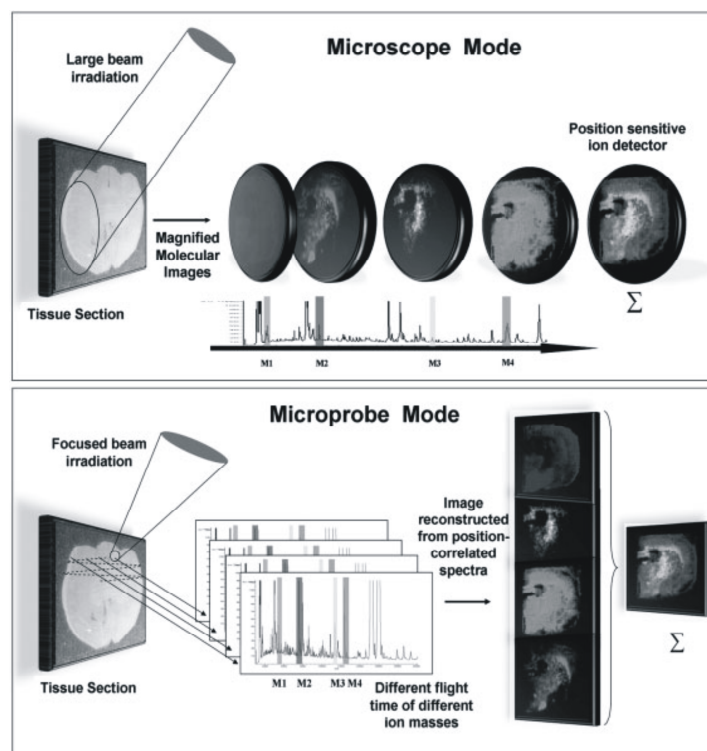
Figure 2.15 Schematic representation of MSI acquisition process performed in (A) microscope mode and (B) microprobe mode. Reprinted with permission from ref[106]. Copyright 2007 Wiley Interscience.

2.2.5 Profiling vs. imaging

MSI experiments fall into two major groups: profiling (low spatial resolution) or imaging (high spatial resolution).[165] Profiling involves sampling of discrete areas of the tissue sections and subjecting the resulting protein profiles to statistical analysis. In a typical profiling experiment from the whole tissue section only for example 5–20 spots (approximately 1 mm in diameter) are analyzed. These experiments are designed to make comparisons between different types of tissue, such as normal versus tumor or control versus treated. Large numbers of samples are used to achieve statistical significance, and sophisticated data algorithms are required for meaningful data mining and classifications. Alternatively, imaging

of a tissue requires an entire tissue section to be analyzed through an ordered array of spots, in which spectra are acquired at every 50-100 μm in both the x and the y directions. 2D ion intensity maps or images can then be created by plotting the intensities of any signal obtained as a function of its x,y coordinates. This array may contain several thousands to tens of thousands of pixels.[165] The resulting images allow comparison of molecule distributions between different regions of the sample as well as between the samples.[110] The size of the data files generated in imaging mode and the time required for data acquisition is much larger than that for profiling experiments. The sample preparation procedures for profiling and imaging experiments have been automated and allow correlation of matrix application with MS acquisition. The sample preparation methods are very similar for both types of experiments and the current matrix spotting instruments can print the matrix spots directly on tissue section either as individual spots on selected sample features for profiling or as dense spot arrays over the entire tissue or as large ROI for imaging.[101]

LCM is a specific cell isolation method used for tissue profiling experiments. In LCM a narrow infrared laser beam (7–10 μm diameter) is focused onto heat sensitive, ethylene vinyl acetate (EVA) thermoplastic film. The laser light heats and locally deforms the polymer, enabling contact to the cell(s) of interest. The cell binds the polymer and is lifted from the tissue section when the polymer is removed. The polymer film containing the specific cells can be transferred to a MALDI-MS target plate using double-sided conductive tape. The "captured cells" are then spotted with matrix solution, and protein profiles are acquired by MALDI-MS. Several reports described the combination of LCM and MS technologies for the analysis of several types of cells, including normal breast stroma cells, normal breast epithelial cells, malignant invasive breast carcinoma cells, and malignant metastatic breast carcinoma cells from radical mastectomies.[234,235] Protein profiling showed unique protein patterns from these different disease subsets.

2.2.6 Tags

Photocleavable molecular tags have also been designed to enhance the specificity of MALDI-MSI analyses. In this strategy the sample section is incubated with the tagging reagent and image analysis is performed on the low M_w tag compound instead of the target molecule.[236] The tag-mass strategy is based on the indirect MALDI imaging of mRNA or proteins using a probe labeled with a photocleavable linker, which is cleaved by the MALDI UV laser, releasing a tag molecule. The tag is a known molecule with a characteristic mass that can be detected efficiently during MSI thus allowing for molecular images to be obtained more

accurately and efficiently. Using this approach proteins that are normally below the detection threshold of direct MALDI-MSI such as synaptophysin in neuroendocrine cells in healthy human pancreatic tissue or the cancer markers PS100 and HMB45 from liver invaded by metastatic melanoma can be visualized.[237]

2.3 Applications of mass spectrometric imaging

After almost two decades of MSI developments the technology is finding more and more applications in the life sciences. This is a marked difference from the initial development stages where the images were taken from standard surfaces and well-known, well-defined substrates. More and more, applied MSI research is crossing the barriers between scientific disciplines. This can be seen by the great variety in applications found in the current literature, ranging from disease pathology to molecular biology. In this section we have chosen to elaborate on a number of these different life-science oriented application domains of MSI. We realize that this list is not complete, but does provide an overview of the MSI application domains that are receiving most attention throughout the scientific disciplines.

2.3.1 Application of MSI in disease pathology

MSI has been applied in a vast spectrum of disease pathology. A number of diseases such as Parkinson's disease,[117,238] Alzheimer's disease,[172,239] Fabry's disease,[144,240] muscular dystrophy,[241] kidney diseases,[181,242,243] nonalcoholic fatty liver disease (NAFLD),[244] Tay-Sachs/Sandhoff's disease[245] and cardiovascular disease[66] have been investigated by MSI technique.

Similarly many cancer types such as breast cancer,[135,142,246] prostate cancer,[119,247] ovarian cancer,[143] lung cancer,[129] glioma[44,140] and colon cancer liver metastasis[248] were analyzed using MSI. As the demand to understand cancer biology is constantly increasing, the number of projects being carried out in this field and the spectrum of applied techniques is also dramatically expanding. In this regard MSI becomes a practical tool to study cancer biology. The availability of tumor tissue samples (biopsies, resected tumors and xenograft models) increases the practicability of MSI in cancer biology as they make good samples for MSI analysis.

Many molecular complexities such as the transformation of cells from normal to malignant as well as the involved pathways are very important scientific questions at present. A number of MSI studies were carried out to compare the protein or lipid profiles obtained from normal

and tumor tissue.[249,250,251,252] The objective of this comparative analysis is to distinguish cancer from normal tissue as well as classify different grades or subtypes of cancer on a molecular level.[110]

In this section we present the application of MSI in current medical research. In the first of the presented applications, a large series of quantitative element maps (such as Fe, Cu, Zn and Mn) were produced in native brain sections of mice subchronically intoxicated with 1-methyl-4-phenyl-1,2,3,6-tetrahydropyridin (MPTP) as a model of Parkinson's disease by a newly developed LA-ICP-MS imaging technique.[253] Significant decreases of Cu concentrations in the periventricular zone and the fascia dentata at 2 hours and 7 days and a recovery or overcompensation at 28 day, most pronounced in the rostral periventricular zone (+40%) were observed. In the cortex Cu decreased slightly to -10%. Fe increased in the interpeduncular nucleus (+40%) but not in the substantia nigra. Some other model of neurodegenerative disease was recently investigated using MSI.[254] The analysis of the Scrapper-knockout (SCR-KO) mouse brain showed two types of neurodegenerative pathologies, spongiform neurodegeneration and shrinkage of neuronal cells. PCA revealed numerous alterations and their position in the KO mouse brain. In another study, SIMS-TOF was used to image the distribution of biochemical compounds on tissue sections of steatotic liver.[255] Fatty liver or steatosis is a frequent histopathological change, which is a precursor for steatohepatitis that may progress to cirrhosis and in some cases to hepatocellular carcinoma. The analysis of steatotic vesicles disclosed a selective enrichment in cholesterol as well as in diacylglycerol (DAG) species carrying long alkyl chains and demonstrated that DAG species C30, C32, C34 and C36 carrying at least one unsaturated alkyl chain were selectively concentrated in the steatotic vesicles. Moreover, investigations performed on the non-steatotic part of the fatty livers despite exhibiting normal histological aspects revealed small lipid droplets corresponding most likely to the first steps of lipid accretion. Similar experiments were performed using SIMS-TOF with a bismuth cluster ion source to map lipids *in situ* at the micrometer scale and to simultaneously characterize their molecular distribution on liver sections obtained from patients suffering from NAFLD.[244] Accumulation of triacylglycerols (TAG), DAGs, monoacylglycerols, fatty acids, with the apparition of myristic acid, together with a dramatic depletion of vitamin E and a selective macrovacuolar localization of cholesterol were observed in steatosis areas of fatty livers compared to control livers. Finally, the analysis revealed lipid zonation in normal human liver and accumulation of very similar lipids to those detected in areas of fatty livers, which were not characterized as steatotic ones by the histological control performed on serial tissue sections. MSI potentially could be

employed in early detection of steatosis, even before the pathological changes are detectable by histological examination.

In another example, MALDI-MSI was involved in studying the specific molecular profiles of ovarian cancer interface zones (IZ), which are the regions between tumors and normal tissues.[251] Unique profiles were identified for the tumors, the normal zone, and the IZ. Analysis identified two interface-specific proteins: plastin 2 and peroxiredoxin 1 (PRDX 1), which were differentially regulated between zones. The results were confirmed by fluorescence microscopy which revealed high expression levels of plastin 2 and PRDX 1 along the IZ of ovarian tumors. This comparative proteomics study suggested that the IZ is different from the adjacent tumor and normal zones, and that plastin 2 and PRDX 1 may be interface markers specific to ovarian tumors.

Cancer biology was also investigated by DESI-MSI used to image differential expression and distribution of different classes of lipids in thin tissue sections of canine spontaneous invasive transitional cell carcinoma of the urinary bladder (a model of human invasive bladder cancer) as well as adjacent normal tissue from different dogs.[252] The tumor and adjacent normal tissue showed differences in the relative distributions of the lipid species. Increased absolute and relative intensities for at least five different GPLs and three free fatty acids in the negative ion mode and at least four different lipid species in the positive ion mode were seen in the tumor region of the samples in all four dogs. In addition, one sphingolipid species exhibited increased signal intensity in the positive ion mode in normal tissue relative to the diseased tissue.

The same imaging technique was also used for the profiling and imaging of arterial plaques.[256] Sodium (in positive ion mode) and chloride (in negative ion mode) adducts of diacyl glycerophosphocholines (GPChos), sphingomyelins (SMs), and hydrolyzed GPChos were detected. Additionally, cholesteryl esters were detected via adduct formation with ammonium cations. Finally, cholesterol was imaged in the atheroma by doping the charge labeling reagent betaine aldehyde directly into the DESI solvent spray, leading to *in situ* chemical derivatization of the otherwise nonionic cholesterol. The results revealed lipid rich regions of two different lipid profiles within the arterial walls. These lipid rich regions likely correspond to the areas of the tissue where lipoprotein particles accumulated. It is also possible that the different lipid distributions may correlate with the stability or vulnerability of that particular region of the plaque.

MS profiling technique has been applied to detect the highly expressed proteins in human oral squamous cell carcinoma of tongue biopsy. In this study two distinct molecules at

approximately 4500 Da and approximately 8360 Da were detected in cancer tissue.[257] To study pancreas pathology, different regions of the pancreas of both control and obese mice were imaged by MALDI-MSI and peptide-specific profiling was performed.[118] The distribution of C-peptide of insulin and glicentin-related polypeptide displayed a striking resemblance with Langerhans islet's histology.

Recently a new strategy in MSI was developed to use more than 9 years old rat brain tissues of Parkinson's disease animal model stored in FFPE blocks.[133] The method employed MALDI tissue profiling combining the use of automatic spotting of the MALDI matrix with *in situ* tissue enzymatic digestion. The analyses confirmed that ubiquitin, trans_elongation factor 1_ (eEF1), hexokinase, and the Neurofilament M were down-regulated as previously shown in human or animal models of Parkinson's disease. In contrast, peroxidoredoxin 6, F1 ATPase, and alpha-enolase were up-regulated. In addition, three novel putative biomarkers were uncovered from protein libraries: eEF1 and collapsin response mediator 1 and 2. Finally, the identity of CRMP-2 protein was validated using immunocytochemistry and MALDI imaging based on the different ions from tryptic digestion of the protein.

SIMS-TOF was used to obtain high-resolution ion images in ischemic retinal tissues.[258] Marked changes in Ca^+ distribution, compared with other fundamental ions, such as Na^+, K^+, and Mg^+, were detected during the progression of ischemia. Furthermore, the Ca^+ redistribution pattern correlated closely with TUNEL-positive (positive for terminal deoxynucleotidyl transferase-mediated 2'-deoxyuridine 5'-triphosphate nick end-labeling) cell death in ischemic retinas. After treatment with a calcium chelator, Ca^+ ion redistribution was delayed, resulting in a decrease in TUNEL-positive cells. Results showed that ischemia-induced Ca^+ redistribution within retinal tissues was associated with the degree of apoptotic cell death, which possibly explains the different susceptibility of various types of retinal cells to ischemia.

MSI quickly became a very important tool for molecular histology. Pathologists have already recognized its potential and started exploring biological material collected from patients and stored in hospital tissue banks. Since these banks usually contain a large number of different samples, it became clear that MSI analysis of such material must be automated. The development of an automated set-up for high throughput molecular histology MSI has been recently presented by L.A. McDonnell et al.[259] This device consists of a controlled environment sample storage chamber, a sample loading robot, and a MALDI TOF/TOF mass spectrometer, all controlled by a single user interface. The automated set up has the positional stability and experimental reproducibility necessary for its clinical application.

Figure 2.16 illustrates the use of MSI to image proteins from an ethanol-preserved and paraffin embedded (EPPE) tumor bearing mouse lung section.[130] A clear distinction between tumorous tissue and healthy tissue is observed indicating the applicability of MSI as a medical diagnostic imaging tool. An additional example in tumor biology is provided in figure 2.17 where MSI is employed to study a MCF-7 xenograft breast cancer model.[135] Both of these examples employ MSI to provide detailed molecular insight in tumor biology.
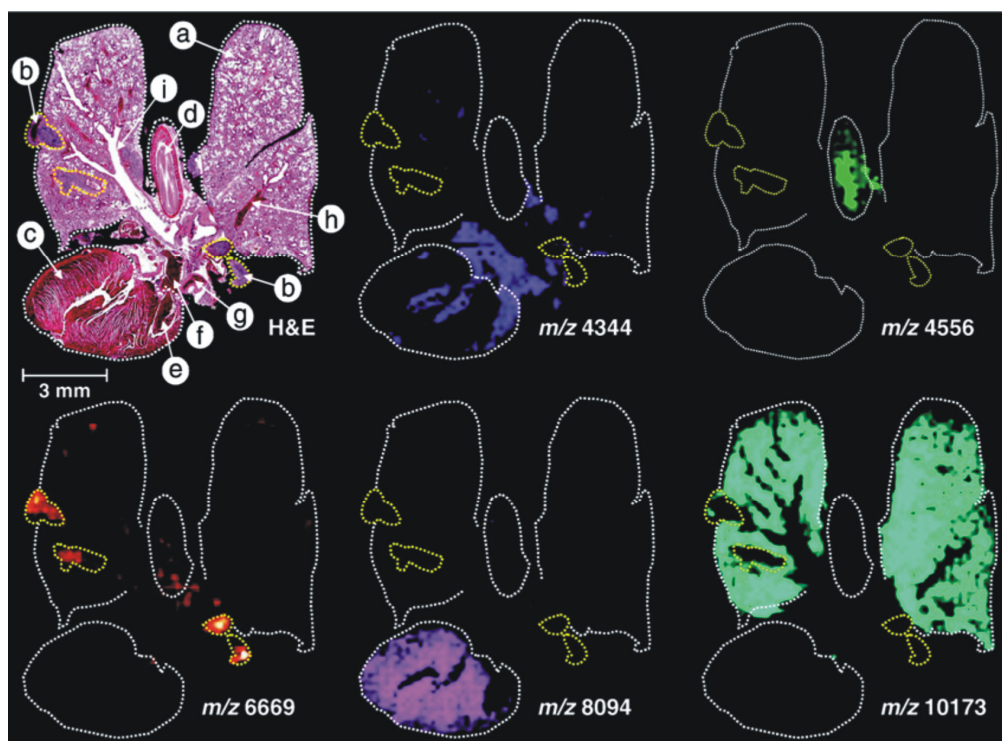
Figure 2.16 Analysis of a tissue section from an EPPE tumor bearing mouse lung specimen. The photomicrograph of the section H&E stained after MSI acquisition and matrix removal presents several different histologies: (a) lung, (b) lung tumors (areas in yellow dotted lines), (c) heart, (d) upper respiratory pathways, (e) left heart ventricle, (f) aorta, (g) right pulmonary artery, (h) artery, (i) bronchus. Five distinct ion density maps from proteins which distinctively localize in different areas of the section are displayed. Reprinted with permission from ref[130]. Copyright 2009 Wiley Interscience.

Along with advances in instrumentation, MSI became well recognized in the medical community. There is a number of MSI reviews dedicated to the application of MSI in disease and pathology.[100,260,261,262,263,264]
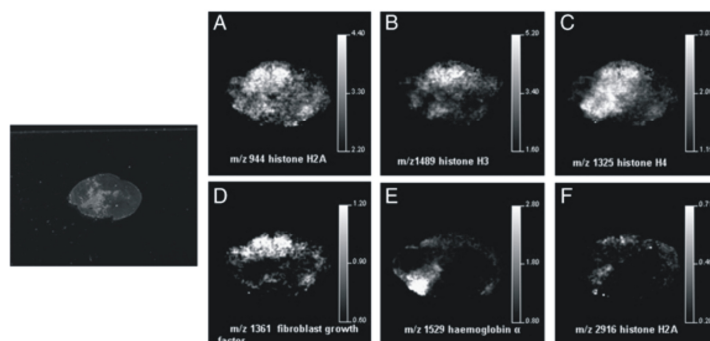
Figure 2.17 MALDI MS images of peptides distribution within an MCF-7 xenograft tissue section. Reprinted with permission from ref[135]. Copyright 2008 American Chemical Society.

2.3.2 Application of MSI in biological sciences

MSI has numerous applications in the field of biological sciences. Direct tissue analysis from any type of biological material made this technique a powerful tool for life sciences. Here, we present some examples of MSI being applied to investigate biological samples of different origin.

An MSI technique was applied to investigate a novel family of antimicrobial peptides, named raniseptins present in the dorsal skin of a frog (*Hypsiboas raniceps*).[265] These studies demonstrated that the mature raniseptin peptides are in fact secreted as intact molecules within a defined glandular domain of the dorsal skin. *De novo* MS/MS sequencing and direct MALDI imaging experiments of the skin from another frog (*Phyllomedusa hypochondrialis*), identified eighteen bradykinin related peptides (BRPs) along with their PTMs.[266]

Calf and mature bovine lenses were imaged by MALDI-MSI methods to obtain the distribution of lens alpha-crystallins and their modified forms.[267] The results from this study shed light on the physiological significance of the modified forms of the two alpha-crystallin subunits. Another study, involved MSI to investigate the distribution of the age-related changes of human lens alpha-crystallin including a novel L52F alphaA-crystallin mutation in a cataractous lens.[268] Application of this technique to lens biology enhanced the understanding of alpha-crystallin protein processing in aging and diseased human lenses. Ocular lens and retinal tissues were used as model samples for developing new MALDI-MSI tissue preparation protocol for integral membrane proteins.[269] Molecular images of full-length Aquaporin-0 (AQP0) and its most abundant truncation products were obtained from bovine and human lens sections. This tissue preparation protocol was also successfully applied to image the distribution of the G-protein coupled receptor, opsin, in the rabbit retina. In

addition, both fresh or formaldehyde fixed mammalian lenses were analyzed by direct profiling of two relevant phospholipid classes, phosphatidylcholines (PCs) and SMs.[270] Neuropeptides are another class of biomolecules which can be investigated using an MSI technique. Neuropeptide distributions directly from rat, mouse and human pituitary tissue sections were obtained using MALDI-MSI in microscope mode,[233] from crustacean neuronal tissues by MALDI-FTMS instrument[271] and from a wide variety of invertebrate samples such as tissues and ganglia, single neurons or single vesicles by MALDI-MSI.[272] Distributions of peptide isoforms belonging to ten neuropeptide families were investigated in the brain of the Jonah crab (*Cancer borealis*).[273] This study revealed the spatial relationships between multiple neuropeptide isoforms of the same family as well as the relative distributions of neuropeptide families. In addition, a MALDI ion trap was used to visualize neuropeptides from dissected tissue of the house cricket (*Acheta domesticus*).[274] Tissue imaging together with tandem MS allowed successful identification of neuropeptides present in the corpora cardiaca and allata of the insect.

MSI was applied to obtain distributions of ganglioside molecular species in the mouse hippocampus.[275] In this study, the location of age-dependent C20-GD1 accumulation was successfully characterized. Another study of the gangliosides inside mouse brain tissue sections demonstrated that the N-fatty acyl chains of gangliosides were differentially distributed in mouse hippocampal regions, whereby the gangliosides with N-C18 acyl chain were enriched in the CA1 region, while gangliosides with N-C20 acyl chain were enriched in the dentate gyrus.[276] In this study, ionic liquid matrix was used for MSI of gangliosides which provided excellent sensitivity for ganglioside detection without significant loss of sialic acid residues.

Another class of lipids detected from rat brains was mapped by MSI to study the normal functioning of the brain. The differential distribution of PCs such as PC(32:0), PC(34:1), and PC(36:1) in different parts of the rat brain was successfully investigated by S. Mikawa et al. by using MALDI-MSI.[121] PC(32:0) and PC(34:1) were more abundantly observed in the gray matter areas than in the white matter areas, while PC(36:1) was evenly distributed throughout the central nervous system. In addition, PC(32:0) and PC(34:1) were mostly detected in the granular layer of the olfactory bulb, piriform cortex, insular cortex, and molecular layer of the cerebellum, regions known for high neuronal plasticity. In another study, the cell-selective distributions of poly-unsaturated fatty acid-containing glycerol phospholipids in the mouse brain were presented.[114] The results showed that arachidonic acid- and docosahexaenoic acid-

containing PCs were seen in the hippocampal neurons and cerebellar Purkinje cells, respectively.

Plant tissues of different origin can be also subject for MSI. The first paper describing MALDI-MSI analysis of oligosaccharides in plant system was published by S. Robinson et al.[277] Endogenous water-soluble oligosaccharides found in the stems of wheat (*Triticum aestivum*) were investigated as a potential indicator of grain yield. Water-soluble oligosaccharides up to 11 hexose residues were ionized as potassiated molecules, and found to be located in the stem pith that is retained predominantly around the inner stem wall.

MALDI-MSI was applied by A.K. Mullen et al. in 2005 for imaging of the herbicide (mesotrione) and the fungicide (azoxystrobin) on the surface of the soya leaf and inside the stem of the soya plant.[278] This study demonstrated the applicability of MALDI imaging to the detection and imaging of small organic compounds in plant tissue. The same imaging technique provided new insights into the distribution of the pesticide nicosulfuron in sunflower plant tissue using direct tissue imaging following root and foliar uptake.[279] Images of fragment ions and alkali metal adducts were obtained which showed the distribution of the parent compound and a phase 1 metabolite in the plant. MALDI-MSI also enabled to look at the distribution of metabolites within plant tissues such as wheat seeds.[280] Results showed the localization of metabolites such as amino acids, glucose-6-phosphate and sucrose within seeds. Not only MALDI-TOF but also SIMS-TOF was used for imaging of biomolecules inside plant tissues. The movement of herbicide formulation components into and across plant cuticles was monitored at high spatial resolution by SIMS-TOF.[59] The studied components included the oligomeric ethoxylate surfactants Synperonic A7 and A20 and the active ingredient Sulfosate (trimesium glyphosate). Clear differences in penetration/diffusion behavior of these molecules into the surface of *Prunus laurocerasus* leaves and across the isolated plant cuticle were identified. Colloidal silver LDI mass spectrometry was employed to directly profile and image epicuticular wax metabolites on leaves and flowers of a model organism *Arabidopsis thaliana*.[281] Silver adducts of major cuticular wax compounds, such as very long-chain fatty acids, alcohols, alkanes, and ketones, were successfully detected. For the first time the surface metabolites of different flower organs (carpels, petals, and sepals) were profiled at a spatial resolution of approximately 100 μm. Mass spectral profiles and images were collected from wild type and a mutant strain, which carried alleles affecting its surface constituents. Obtained data provided new insights into the complexity of epicuticular wax deposition in plants. In addition, colloidal GALDI MSI was employed to map the location and the degree of light-induced accumulation of flavonoids in stem sections of

Arabidopsis thaliana.[126] The main targeted metabolites were flavonoids and cuticular waxes. The mass spectral profiles revealed tissue-specific accumulation of flavonoids in flowers and petals. Conventional MALDI-MSI was employed to localize the major allergen present in peach in the outer part of the fruits.[282] The structure of this allergen, the lipid transfer protein (LTP), Pru p 3, was identified by ESI, coupled to single stage (quadrupole) or advanced (FT-MS) analyzers. The results showed the full potential of mass spectrometry for obtaining high quality structural data of relevant food proteins. MALDI-MSI was also used to study the spatial distribution of metabolites from the cyanobacteria *Lyngbya majuscula* 3L and JHB, *Oscillatoria nigro-viridis*, *Lyngbya bouillonii*, and a *Phormidium* species as well as the sponge *Dysidea herbacea*.[125]

The same ionization technique was employed for detecting high concentrations of the marine alkaloid, norzoanthamine, present in the epidermal tissue in the colonial zoanthid *Zoanthus sp*.[283] The first examples of DESI imaging of metabolites on biological surfaces illustrated the potential of DESI-MS in understanding chemically-mediated biological processes.[85] DESI-MSI was employed to investigate the concentrations of natural algal antifungal products such as bromophycolides from the red macroalga *Callophycus serratus*.[85] The analysis of the images shown in figure 2.18 revealed that surface-associated bromophycolides were found exclusively in association with distinct surface patches at concentrations sufficient for fungal inhibition. A short review describing the application of DESI-MSI in probing marine natural product defenses was published by E. Esquenazi et al. in 2009.[84] DESI-MSI was also applied for *in situ* detection of alkaloids in the tissue of poison hemlock (*Conium maculatum*), jimsonweed (*Datura stramonium*) and deadly nightshade (*Atropa belladonna*).[81] Different types of plant material were analyzed including seeds, stems, leaves, roots and flowers.

MSI was used to investigate the biological processes occurring in the reproductive system of small rodents. For example, MALDI-MSI provided global and time-correlated information on the local proteomic composition of the sexually mature mouse epididymis.[127] Tissue sections, cells collected by LCM and secretory products were analyzed which resulted in detection of over 400 different proteins. In another study, MALDI-MSI technology was used to characterize the spatial and temporal distribution of phospholipid species associated with mouse embryo implantation.[284] The ion images showed that linoleate- and docosahexaenoate-containing phospholipids localized to regions destined to undergo cell death, whereas oleate-containing phospholipids localized to angiogenic regions. Molecular images revealed the dynamic complexity of lipid distributions in early pregnancy and shed light on the complex interplay of lipid molecules in uterine biology and implantation. Also molecular composition,

relative abundance, and spatial distribution of a large number of proteins expressed during the peri-implantation period were investigated by MALDI-MSI.[120] For the first time, *in situ* proteome profiles of implantation and interimplantation sites in mice in a region- and stage-specific manner with the progression of implantation were obtained. Cytosolic phospholipase A (2 alpha) null females that show implantation defects were also investigated, which provided new insights regarding uterine biology. SIMS-TOF equipped with a gold ion gun was used to image mouse embryo sections and analyze tissue types such as brain, spinal cord, skull, rib, heart and liver.[48] PCA was used to reduce the spectral data generated by SIMS-TOF. MALDI-MSI was also used to study the temporal diffusion of honeybee venom in envenomed tissue.[285]
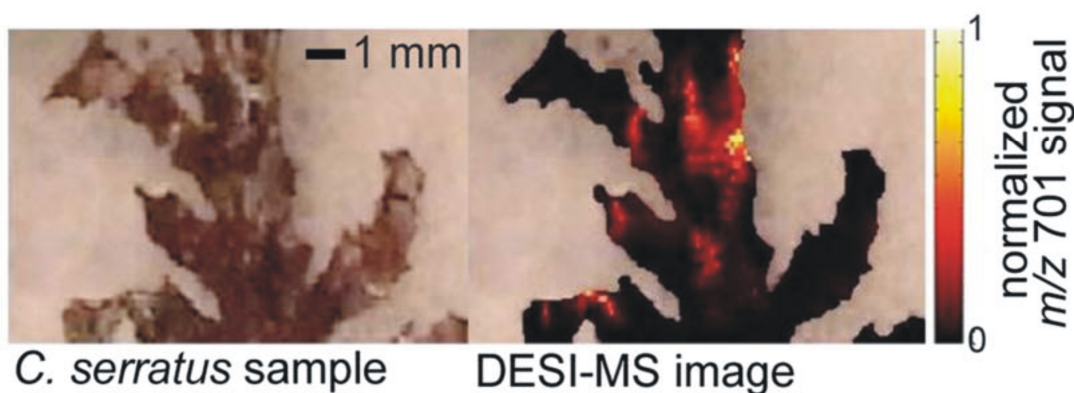
Figure 2.18 Negative-ion DESI mass spectra of bromophycolides. DESI-MS image (200 μm resolution) of bromophycolide A/B chloride adduct ion m/z 701 on C.serratus surface, indicating that bromophycolide ''hot spots'' correspond to pale patches. Reprinted with permission from ref[85]. Copyright 2009 Wiley Interscience.

2.3.3 Application of MSI in proteomics/peptidomics

Here, we briefly discuss the issue of peptide and protein detection directly from tissue sections. Topics such as bottom-up and top-down on-tissue proteomics, on-tissue protein digestion and single-cell MALDI-MS profiling will be discussed.

Mass spectrometry evolved into an indispensable tool for proteomics research.[286] The demand for spatial information of detected proteins and peptides pushed the boundary of mass spectrometry capabilities and started a new era of MSI. Three strategies for protein identification and characterization are currently employed in proteomics: bottom-up proteomics, which analyzes proteolytic peptide mixtures, middle-proteomics, which analyzes longer peptides and top-down strategies, which analyze intact proteins.[287] It became clear that rapidly developing MSI instrumentation should allow detection, identification and

characterization of proteins directly from biological tissue also in terms of their interactions with other molecules, PTMs and different isoforms expressed inside the cells.

In terms of the bottom-up approach, the proteins present in biological tissue must be first subjected to *in situ* digestion by proteolytic enzyme. The protocol designed for MSI was published by M.R. Groseclose et al. in 2007.[168] The method for on-tissue protein digestion involved a tissue washing step with organic solvents capable of removing lipids. Otherwise the strong lipid signals in the same mass range as the obtained peptides interfere with peptide detection and identification. After removal of lipids, tissue section should be sprayed or spotted with the solution of proteolytic enzyme, most commonly trypsin and after the incubation time covered with matrix (usually DHB or CHCA).

The top-down approach allows detection of intact proteins directly from tissue sections. The upper mass range of the instruments used for MSI is the detection limiting factor. Therefore, efficient detection and identification of proteins with M_w > 30 kDa needs to be improved. MALDI also suffers from mass dependent sensitivity drop-off, which means that bigger proteins must be present at sufficient concentration in order to be detected and analyzed. One of the solutions for the sensitivity issue could be tag-mass (see **Tags**). The complexity of the sample and high M_w of the analyzed proteins, which very often limits detection of biomolecules directly from tissue sections, can be reduced by simultaneous extraction, separation and digestion of proteins from the tissue section while preserving their relative location. To reduce the complexity of the sample contact blotting of fresh cut tissue sections on a surface of C18-coated resin beads[12] or on a polymeric conductive membrane[288] can be performed. The chemical properties of the blotting surface determine which analytes are detected during MSI. Typically hydrophobic surfaces are used because they can be washed with water in order to remove salts before matrix application. More complex surfaces such as teflon plates or antibodies bound to surfaces were also tested for extraction of specific proteins or a class of proteins from the tissue.[100] While the concept of blotting is quite straightforward, the process involves transfer of the proteins from the tissue into the methanol sprayed MALDI target which requires diffusion of molecules which can lead to loss of spatial resolution in the imaging experiment.[100] The molecular scanner approach, introduced by Hochstrasser and co-workers, combined both a blotting step with enzymatic digestion.[173,289,290] The molecular scanner was initially developed for 2D gels. It allows protein separation using 2D-PAGE with parallel digestion of the separated proteins and transfer of obtained peptides onto a membrane while keeping their relative positions. The membrane is then sprayed with a matrix solution and analyzed in a mass spectrometer.[291]

One of the interesting applications of MALDI-MSI for analyzing intact proteins directly from tissue sections was presented by F.R. Dani et al. in 2008.[292] MSI was applied to study *Anopheles gambiae* antennae, with the aim of analyzing the expression of soluble proteins involved in olfaction perireceptor events. Profiling of the proteins on the antennae surface, shown in figure 2.19, revealed distinct protein profiles between male and female antennae and imaging experiments showed differences in the localization of some of the detected proteins. High resolution measurement and top-down MS/MS experiments resulted in the identification of two proteins, a 8 kDa protein which matched with an unannotated sequence of the *A. gambiae* genome and <u>o</u>dorant <u>b</u>inding <u>p</u>rotein 9 (OBP-9). This work showed that MALDI-MS profiling is a technique suitable for the analysis and comparison studies of small and medium proteins in insect appendices.
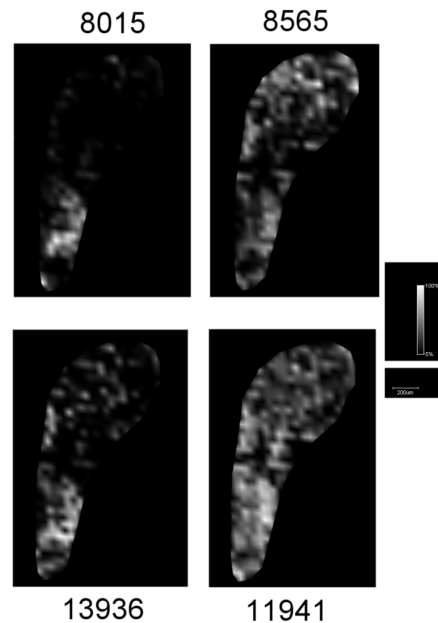
Figure 2.19 MALDI imaging of proteins from an Anopheles gambiae male antenna. Ion images of four proteins are reported: 8015 m/z, 8565 m/z, 11941 m/z and 13936 m/z respectively, showing a different distribution across the antenna. Reprinted with permission from ref[292]. Copyright 2009 PNAS.

A similar approach was used for comparison of the peptide profiles of the sea slug (*Aplysia californica*) neurons using MALDI-MSI which revealed distinct peptide profiles for each neuronal subtype analyzed and identification of previously unknown peptides.[293] In this study, individual F cells were isolated based on their position, size, and pigmentation and Tungsten

needles were used to transfer each cell onto a MALDI target plate containing 0.5 mL DHB solution.

Single-cell MALDI-MS profiling

A review presenting single-cell MALDI-MS peptide profiling from individual cells and other mass-limited tissue samples was published by L. Li et al. in 2000.[294] The most recent review presents the history of single-cell mass spectrometry with the emphasis on live single-cell MS.[295] Single-cell MALDI-MS has multiple advantages such as: (1) compatibility with crude mixtures; (2) minimal sample clean up; (3) no need for tagging or pre-selecting the peptide of interest; (4) simple instrumentation; (5) high sensitivity; (6) complementary information to immunochemical methods; and (7) compatibility with PTMs.[294] One important characteristic of single-cell MALDI-MS is its ability to directly profile intact cell and tissue samples without any purification of peptides or proteins. Simplified sample preparation preserves spatial and biomolecular information within the cells, reduces degradation processes, dilution of biomolecules or contamination from adjacent cells which can have different sets of peptides or proteins. Among the disadvantages would be: (1) too low sensitivity of instruments to probe the entire content of a single cell and (2) too small size of the cell making it hard to probe with a laser.[295]

The first MALDI-MS profiling analyses of peptides in single neurons were done by P.A. van Veelen et al. in 1993,[296] C.R. Jiménez et al. in 1994[297] and S. Hsieh et al. in 1998.[298] Neuropeptides were directly detected in single neurons and the neurohemal area of peptidergic (neuroendocrine) systems in the *Lymnaea* brain.[297] The study of neuroendocrine systems revealed that processing of the complex prohormone expressed in this system occurred entirely in the soma. In addition, novel as well as previously identified peptides were detected. These experiments demonstrated that MALDI-MS was promising and a valuable approach to study the synthesis and expression of bioactive peptides, with potential application to single-cell studies in vertebrates, including humans. Since then a number of single-cell MALDI-MS experiments were performed on cells of different origin such as crayfish,[299] insects,[300] red blood cells,[301] single neurons,[297] mouse bone marrow-derived mast cells[302] and individual rat pituitary cells.[303] The review article published by C.R. Jiménez and A.L. Burlingame provided an overview of MALDI as a tool for direct analysis of peptide profiles contained in single cells from invertebrate (the pond snail), vertebrate species (*Xenopus* and rat) and tissue biopsies with a special emphasis on the sample handling required for each application.[304] MALDI-MS was successfully applied for profiling the proteome of

single cells but imaging is still not possible due to currently available laser spot sizes, which at present can be focused to a minimal diameter of 20 μm. Development of lasers capable to probe single cells, together with improved matrix application methods, delivering small crystals containing highly concentrated analytes, will open the gate for MALDI-MSI of single cells.

Obviously single cells are routinely analyzed by SIMS-TOF but the detection limit (upper mass <1000 Da), extensive in source fragmentation of secondary ions and lack of MS/MS capabilities of SIMS-TOF instruments limits at present its application in proteomic studies.

The first application of MALDI-MSI to proteomics was presented by R.M. Caprioli et al. in 1997.[12] The analysis of regions of rat splenic pancreas and rat pituitary revealed many peptides and proteins detected from the C-18 blotted target.[12] The next paper showed direct profiling of proteins present in tissue sections for several organs of the mouse where over 100 peptide/protein signals in the 2000-30,000 Da range were observed after blotting of the tissue sections on a conductive polyethylene membrane and coating with SA.[288] Later, MALDI-MSI was used to determine peptide distributions directly from rat, mouse and human pituitary tissue sections with high-resolution MSI which allowed localization of neuropeptide distributions within different cell clusters of a pituitary tissue section.[233] MALDI-MS was also employed to detect and structurally characterize small cardioactive peptides in two functionally related neurons, which form a network involved in the modulation of heartbeat in freshwater snails *Lymnaea*.[298] MALDI-MS was also used to study the intricate processing pattern of a preprohormone expressed in neurons of this gastropod mollusk.[305] Isolated cells and tissues, including egg-laying hormone-releasing cells, from the central nervous systems of the model marine mollusks *Aplysia californica* and *Pleurobranchaea californica* were used to demonstrate the salt removal method and detect several neuroactive peptides previously characterized by conventional biochemical methods.[306] MALDI-MSI was applied to the study of amyloid β peptide distribution in brain sections from a mouse model of Alzheimer's disease.[193] A combination of MS profiling and LCM of normal breast stroma, normal ductal epithelium, ductal carcinoma *in situ*, and invasive ductal carcinoma microdissected from a single frozen section was presented by D.E. Palmer-Toy et al. in 2000.[235] Each tissue type when analyzed separately revealed characteristic peaks. Several prominent peaks in the 4500–7000 Da range distinguished the breast stroma from ductal epithelium while high-mass peaks in the mass range of 45 to 60 kDa were characteristic only for the invasive carcinoma.[235] A recent review focused on four state of the art proteomic technologies applied in the discovery of potential tumor markers, namely 2D difference gel electrophoresis, MALDI-MSI, electron

transfer dissociation mass spectrometry and reverse-phase protein array, presented progress in proteomic technologies from 1997 to 2008.[307]

2.3.4 Application of MSI in metabolomics

The functional levels of biological cells or organisms can be separated into the genome, transcriptome, proteome and metabolome. Here, we concentrate on applications of MSI for metabolomics. The term, metabolism, is derived from the Greek word μεταβολή (*metabolé*), meaning change. Metabolome is defined as the total quantitative collection of low M_w compounds (metabolites) present in cells or organisms which participate in metabolic reactions required for growth, maintenance and normal function.[308] The metabolome is composed of small M_w organic and inorganic species, generally of a mass less than 1500 Da. The number of metabolites is generally ten-fold smaller compared to that of genes, for example, the yeast *S. cerevisiae* has a genome encoding more than 6600 genes and contains 584 identified metabolites.[213,309] But the number of metabolite molecules present within one cell can vary from just a few (signaling molecules) to millions (glucose). The concentration of metabolites depends on the metabolic state of the investigated cell. Metabolites can be of endogenous origin (synthesized or catabolized within the cell or organism) or of exogenous derivation (pharmaceuticals or food nutrients).[213]

Metabolomics is currently rapidly developing discipline for the study of microbial, plant and mammalian metabolomes. A recent review focused on the collection of analytical data for metabolomic studies was published by W.B. Dunn in 2008.[213] A review, presenting the capabilities of current MSI techniques for imaging metabolite molecules and a summary of representative MSI studies of both endogenous and exogenous metabolites was recently published by Y. Sugiura and M. Setou.[310]

Here, some of the MSI applications for metabolomic studies of animals, plants, sponges and cyanobacteria are presented. MSI has been recently employed for detection and identification of 13 primary metabolites such as adenosine monophosphate (AMP), adenosine diphosphate (ADP), adenosine triphosphate (ATP), uridine diphosphate (UDP) or N-acetyl-D-glucosamine (GlcNAc) directly from rat brain sections using 9-aminoacridine matrix (9-AA).[311] The mass spectral images of the metabolites in figure 2.20 clearly illustrate the usefulness of MSI in disease metabolomic studies. The combination of MALDI and SALDI known as ME-SALDI-MS, enabled successful MSI of low mass species from mouse heart and brain tissues with improved detection sensitivity.[139] Two imaging instruments (MALDI-TOF and MALDI-FTICR) were used to image two human immunodeficiency virus (HIV) protease inhibitors,

saquinavir and nelfinavir, in Mono Mac 6 cells.[200] MALDI-TOF and cluster-SIMS-TOF imaging approaches were used to study the localization of lipids (cholesterol, cholesterol sulfate, vitamin E, glycosphingolipids) on skin and kidney sections of patients affected by the Fabry disease.[240] A number of plant metabolites such as amino acids, sugars, and phosphorylated metabolites in wheat seeds were imaged by using a combination of two matrices CHCA and 9-AA.[280] MALDI-MSI was also used to image the distribution of the pesticide nicosulfuron (parent compound and a phase 1 metabolite) in plant tissue following root and foliar uptake.[279] The spatial distributions of natural products with potential therapeutic applications were characterized by a MALDI-MSI approach.[125] In this study, a number of metabolites from the cyanobacteria *Lyngbya majuscula*, *Oscillatoria nigro-viridis*, *Lyngbya bouillonii*, and a *Phormidium* species were identified. In addition to known natural products such as curacin A and curazole, a large number of unknown ions co-localized with the different cyanobacteria. MSI proved to be useful as a strategy for *de novo* drug discovery. The same technique was used to observe the secondary metabolites found within the sponge *Dysidea herbacea*. These data demonstrated the potential of MSI for providing spatial distribution of natural products, from single strands of cyanobacteria to the very complex marine assemblage of a sponge.[125]
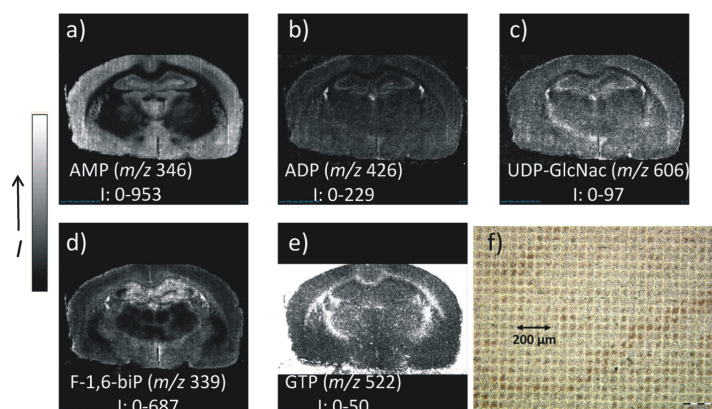
Figure 2.20 MALDI images of (A) AMP, (B) ADP, (C) UDP-GlcNac, (D) F-1,6-biP, and (E) GTP acquired in the negative ion mode from a rat brain section coated with 9-AA matrix. (F) Optical image of a brain tissue section after 9-AA deposition and analysis by MALDI imaging with a 50 μm pixel size. Reprinted with permission from ref[311]. Copyright 2009 American Chemical Society.

2.3.5 Application of MSI in lipidomics

Lipids, important components of the cells, serve as the building blocks of cellular membranes (phospholipids, cholesterol), participate in many signaling pathways (diacylglycerol,

ceramide, glycolipids, steroids or prostaglandins)[312] and are stored as an energy source (triacylglycerols).[313] Various different types of lipids such as GPLs, sphingolipids, sterol lipids, prenol lipids, saccharolipids, waxes and fat-soluble vitamins are found in biological systems. Some examples of common lipid structures are presented in figure 2.21. GPLs, the key components of the cellular membranes and also important constituents of serum lipoproteins and pulmonary surfactant,[314] are the most abundant lipids in the brain[315] and play the role in metabolism and cell signaling. In GPLs, two hydroxyl groups of the glycerol are esterified by two different fatty acid chains. The third hydroxyl group of glycerol backbone is esterified by phosphate. The phosphate group can be further esterified by inositol, glycerol, choline, serine or ethanolamine. In the case of phosphatidic acid, phosphate remains in its unesterified form. Different subclasses of GPLs contain different types of bonds between glycerol backbone and fatty acid chain, e.g. acyl, alkyl or alk-1´-enyl. The fatty acid chains in biomembranes usually contain an even number of carbon atoms, which can be saturated (e.g. 16:0, 18:0) or unsaturated (e.g. 16:1, 18:1, 18:2).[313]
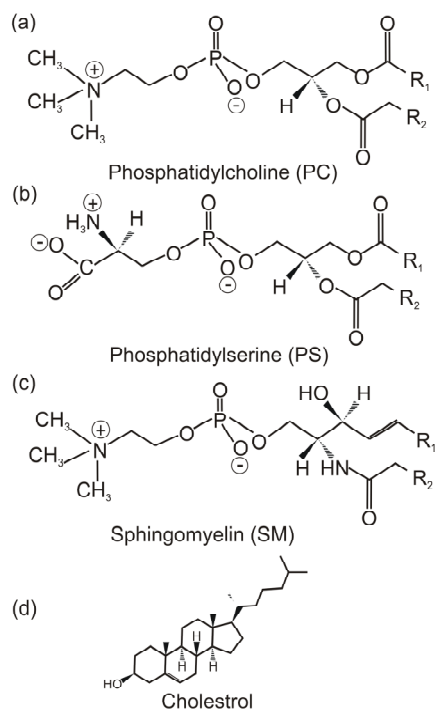

Figure 2.21 Most common (A,B) GPLs, (C) sphingolipid, and (D) sterol lipid structures. Reprinted with permission from ref[350]. Copyright 2010 American Chemical Society.

Sterols are another important lipid constituent of biological membranes. For example, cholesterol is part of cellular membranes in animals, where it regulates the cellular membrane

fluidity but also serves as a secondary messenger in developmental signaling.[316,317] Researchers interested in lipid biology may visit a comprehensive Lipid MAPS (<u>M</u>etabolites <u>a</u>nd <u>P</u>athways <u>S</u>trategy) database website (www.lipidmaps.org) for more information about different classes of lipids and most recent discoveries in this field of science.[318]

Almost all types of ionization sources used for MSI have been successfully applied in the field of lipid imaging.[319] Lipids were imaged using MALDI,[121] DESI,[320] SIMS[57] and also the recently developed nano-PALDI[89] ionization method. In general, most lipids present in tissues ionize easily due to their polar head groups[321] (e.g. phosphocholine [M+H]$^+$ m/z 184,[322] phosphoinositol [M-H]$^-$ m/z 241,[323] phosphoethanolamine [M-H]$^-$ m/z 140[324]). Phosphatidylcholines, sphingomyelins and cholesterol ionize in positive ion mode, while phosphatidylinositols, phosphatidylserines, and sulfatides ionize in negative ion mode.[18] <u>P</u>hosphatidyl<u>e</u>tha<u>n</u>olamine (PE) can be analyzed in both positive and negative ion mode.

Most biological samples subjected to MSI have a rich lipid content which manifests in a strong ion signal around m/z 800.[148] A commonly observed phospholipid in tissues is phosphatidylcholine PC(16:0/18:1) with an ion [M+H]$^+$ at m/z 760.5 having the elemental composition of $C_{42}H_{83}NO_8P$.[115] Phosphatidylcholines are at present the most commonly detected and imaged lipid class.[57,62,65,68,256] They dominate mass spectra due to the presence of the positively charged quaternary ammonium group in the choline head.[18] Collisional activation and fragmentation of all phosphatidylcholines yield a major product of phosphocholine at m/z 184. However when a phosphatidylcholine molecular species is cationized with either Na$^+$ or K$^+$, closely related but structurally quite different ions at m/z 147 and 163, respectively are observed.[115] In fact these product ions became very characteristic MS features by which cationized PC can be easily identified.

Lipids can also generate abundant negative ions. For phospholipids, such as PE, <u>p</u>hosphatidyl<u>s</u>erine (PS), <u>p</u>hosphatidic <u>a</u>cid (PA), <u>p</u>hosphatidyl<u>g</u>lycerol (PG) and <u>p</u>hosphatidyl<u>i</u>nositol (PI), this is due to the presence of the phosphodiester moiety which can exist as a very stable gas phase anion.[115] Other lipids, such as SM (phosphodiester), sulfatides (sulfuric acid ester) and bacterial lipids related to lipid A (phosphate esters), also yield quite abundant [M-H]$^-$ molecular anions. For some polyphosphate esters, doubly charged ions [M-2H]$^{2-}$ can also be observed.[115] Phosphatidylinositol and <u>l</u>yso<u>p</u>hosphatidyl<u>i</u>nositol (LPI) yield a specific fragment ion at m/z 241, while <u>pla</u>smenyl<u>etha</u>nolamine (PlsEtn) and PE at m/z 196.[148] The MS analysis of cellular membranes results in the detection of signal from hundreds of different phospholipid molecular species. In contrast, cholesterol is present in the plasma membrane as a single molecular species. During the MALDI desorption/ionization process

cholesterol undergoes dehydration which results in detection of the $[M+H-H_2O]^+$ ion at m/z 369.3, instead of $[M+H]^+$ at m/z 387.3, $[H+NH_4]^+$ at m/z 404 or $[M+Na]^+$ at 409.3.[115]

A review of matrices used for the analysis of cellular phospholipids has been recently published by Y. Kim et al.[325] Matrices such as 30 mg/mL DHA in 50:50 ethanol/water,[18] 5 mg/mL CHCA in 50:50 acetonitrile/0.1% TFAaq[121] and 40 mg/mL DHB in 20 mM potassium acetate, 70:30 methanol/0.1% TFAaq[114] were used for imaging of lipids. The lipid spectra can be simplified by addition of potassium acetate[114] or LiCl[326] to the matrix solution, which results in the formation of only potassium or lithium adducts of lipids, respectively. By changing the concentration of alkali metal salts in the matrix solution it is also possible to selectively ionize either polar or nonpolar lipids. The presence of alkali metal salts in the matrix solution enhanced the detection of polar lipids, while a salt-free matrix solution was suitable for the detection of nonpolar lipids.[327]

The selection of matrix must be tailored to the type of tissue examined and class of lipids being analyzed. For MSI analysis of lipids in lens, PNA (p-nitroaniline) at a concentration of 20 mg/mL resulted in improved sensitivity as compared to DHB.[270] The ionic liquid matrix offered excellent sensitivity for detection of gangliosides without significant loss of sialic acid residues.[276] The matrix application method should be carefully selected as well. The optimal matrix application should not cause any diffusion of lipids from their original position in the tissue section. Various matrix application methods have been examined for MSI of lipids. Among them are a spray-droplet method,[328] inkjet printing,[198] sublimation,[199] airbrush application,[248] and most recently, an oscillating capillary nebulizer system[245] or a dry-coating technique.[182] Matrix application by direct sublimation of an organic matrix described by J.A. Hankin et al., provides multiple advantages.[115,199] Such a matrix deposition method prevents diffusion of the lipids, delivers extremely small matrix crystal sizes and results in a substantial increase in sensitivity. Because no solvent is needed, this method provides enhanced purity of matrix applied to the sample and uniformity of deposition.[182,199] In terms of the tissue sample preparation method the use of OCT is not recommended before lipid imaging due to a significant reduction in the quality of mass spectra.[18]

Current, non-mass spectrometric approaches for phospholipid analysis include an extraction step and subsequent identification of the main phospholipid classes by either ^{31}P NMR (<u>n</u>uclear <u>m</u>agnetic <u>r</u>esonance) spectroscopy or chromatographic separation followed by mass spectrometric detection.[270] In comparison to these techniques MSI offers a quick and easy method of lipid analysis. The summary of different analytical techniques used for the differentiation and quantification of phospholipids in biological samples was presented by J.J.

Jones et al.[313] A review presenting MALDI-TOF MS as a technique suitable for all known lipid classes together with its advantages and disadvantages in comparison to other established lipid analysis methods was discussed by J. Schiller et al. in 2004.[319] A review presenting mass spectrometry-based strategies for lipid analysis including imaging was published in 2007 by G. Isaac et al.[329]

Here, we will present some MSI applications for lipid analysis. Detection and imaging of lipid molecules was mostly studied using rodents' brains. For example, whole normal rat brain sections were investigated by imaging technology to observe the distribution of three types of PCs such as PC(32:0), PC(34:1) and PC(36:1).[121] Age-dependent changes in the distribution and amount of PCs molecular species in a rat brain were also evaluated.[114] A number of other scientific questions such as the distribution of gangliosides in different regions of mouse brain,[275] shown in figure 2.22, sulfatide in different layers of rat hippocampus,[89] the distribution of phosphatidylcholine and cerebroside species in rat brain sections,[228] the cell-selective distribution of polyunsaturated fatty acid (PUFA)-containing glycerol phospholipids in a mouse brain section[114] have been addressed. Atlases of lipid distributions in rat brain[216] and mouse brain[114] have been constructed. MSI was also successfully applied to rodent brain sections analyzed by intermediate-pressure MALDI on a LIT instrument[218] and by gold cluster focused ion beam SIMS-TOF.[54] Specific examples in the detection of phospholipids, sphingolipids and glycerolipids were presented with images of mouse brain and kidney tissue slices.[115] In addition to this some other samples such as mouse heart and liver,[313] retina,[330] leg muscle[61,241] and embryo[284] have also been studied for the spatial and temporal distribution of phospholipid species. The localization of specific lipids and osmium oxide (OsO_4), a stain commonly used for unsaturated lipids in electron and optical microscopy of cells and tissues, was independently monitored in mouse adipose tissue by using SIMS-TOF with Bi cluster primary ions.[58] SIMS-TOF was also utilized to address the issue of localization of lipids and inorganic ions in healthy rat aorta and human atherosclerotic plaque.[65] Several frozen vessels bearing atherosclerotic lesion were analyzed by cluster SIMS-TOF to map lipid content at micrometric resolution.[66] D. Debois et al. performed the first *in situ* lipidomic analysis of human liver using SIMS-TOF imaging directly on tissue sections.[244]

In situ detection and structural analysis of phosphatidylcholine species in rat brain tissue was performed using a MALDI TOF/TOF mass spectrometer.[326] Initial profiling of lipids in tissue was conducted by MALDI-TOF and allowed for the assignment of phosphatidylcholine species. To confirm the structure, lithium adducts of phosphatidylcholine species were analyzed by MALDI-MS/MS and yielded fragments that allowed for the identification and

positional assignment of acyl groups in phosphatidylcholine species.[326] The *in situ* analysis of two relevant phospholipid classes, phosphatidylcholines and sphingomyelins, in slices of fresh or fixed bovine lenses was also performed.[270] The methodologies for localization of phospholipids in flat-mounted eye segments from rhesus monkey using MSI has been recently described by T.J. Garrett and W.W. Dawson.[331] DESI-MS was also used to image a variety of tissue samples including human liver adenocarcinoma, rat brain, human breast tissue and canine abdominal tumor tissue.[320]
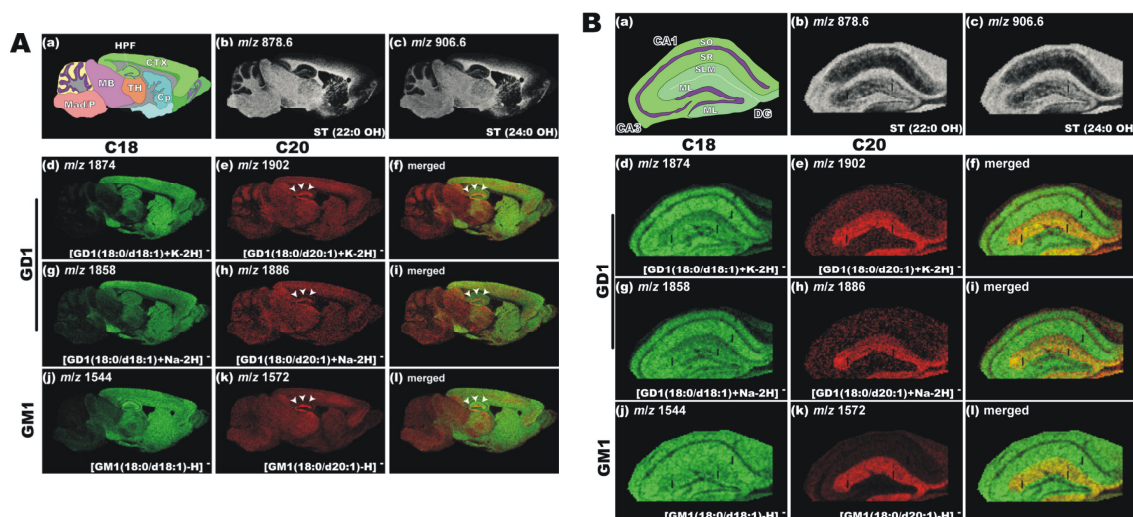
Figure 2.22 Imaging of ganglioside distribution in different brain regions. (A) An overview of ganglioside distribution in different brain regions. (B) The distribution pattern of gangliosides in the hippocampus. Reprinted with permission from ref[275]. Copyright 2008 Sugiura et al.

A new technical variation of NIMS has been recently presented by G.J. Patti et al. for analysis of carbohydrates and steroids, which can be challenging to detect with traditional mass spectrometric approaches.[332] The cation-enhanced NIMS was used to image the distribution of sucrose in a *Gerbera jamesonii* flower stem and the distribution of cholesterol in a mouse brain. The advantages of imaging using IMS prior to MS analysis were demonstrated for profiling of human glioma and selective lipid imaging from rat brain.[229]

Lipids have been implicated in a number of human disease states, including cancer and cardiovascular diseases. Different MSI ionization sources and mass analyzers offer a variety of possibilities for lipid analysis and practical tools to study lipidomics.

2.3.6 Application of MSI in pharmacokinetic study

Pharmacokinetic studies are performed to examine the absorption, distribution, metabolism and excretion of drugs in laboratory animals or humans. This procedure is mandatory for drug approval by the Food and Drug Administration (FDA). Pharmacokinetic studies employ many methods such as whole-body autoradiography (WBA), tissue homogenization and analysis by high performance liquid chromatography tandem mass spectrometry (HPLC MS/MS) and in the last decade also MSI.[105,333] WBA requires the compound of interest to be radioactively labeled. The compound is then administered to animals, which are sacrificed after different post-dose time points. Whole-body sections of these animals are then exposed to a radioactivity detector or film which allows visualizing the spatial radioactivity distribution. The WBA technique is used during early-stage drug development which provides many benefits including parallel sample processing, standardized procedures, high sensitivity and applicable quantification. However, this method has two major limitations such as the expensive, time consuming synthesis of radiolabeled drugs (labeled with e.g. ^{3}H, ^{14}C) and the incapability to distinguish between a parent drug and its metabolites.[105] While the first leads merely to more complexity and increased cost for each experiment, the last cannot be overcome by this technology and additional analysis of tissue homogenates by HPLC MS is required.[105] At present WBA and MSI are two imaging techniques often used together to obtain the most reliable data for drug distribution in small animals.[333] MALDI imaging itself is an excellent tool for visualizing small molecules in tissue sections. Many biologically or pharmacologically relevant compounds are less than 1 kDa in size and can be easily detected by MS. These include both exogenous and endogenous molecules, such as pharmaceutical compounds and their metabolites, drugs of abuse, environmental toxins and endogenous metabolites.[197] In pharmacokinetics F.J. Troendle et al. were the first to demonstrate the use of MALDI-MSI by employing this technique to detect the anticancer drug paclitaxel in a human ovarian tumor and the antipsychotic drug spiperone in spiked sections of rat liver tissue.[334] The development of new MALDI-MSI methods adapted to animal whole-body sections allowed a specific and simultaneous detection of multiple analytes based on their molecular weights and fragmentation patterns.[105] This technique has potential to reveal data related to the drug's metabolism as well as obtain information on the organism's response to drug treatment.[110] On the other hand, MALDI low-molecular-weight imaging suffers from the interference of the ions derived from the matrix. This problem was overcome by applying tandem MS for imaging of drugs in tissue sections. For example, one study examined a

distribution of a drug (SCH 226374) with a calculated protonated monoisotopic M_w that differed from the M_w of the SA matrix cluster ion by less than 0.2 atomic mass unit (amu).[335] In this case collisionally activated dissociation (CAD) was employed to fragment the drug ion at *m/z* 695 into a dominant fragment ion at *m/z* 228. The SA cluster ion at *m/z* 695 fragmented into non-interfering ions at *m/z* 246 and *m/z* 471. Thus, MS/MS was used to indirectly localize the SCH 226374 compound in a mouse tumor sample. Another example of MALDI-MS/MS used to image drugs in tissue was performed on clozapine (*m/z* 327).[336] The MALDI-MS/MS image of the clozapine fragment ion (*m/z* 192) showed the most intense signal in the ventricle area which was in agreement with autoradiography results. The role of the instrument as well as the method used for sample preparation is crucial with respect to the image quality obtained. MSI sample preparation procedures, including sample collection, the choice of matrix, extraction solvent and matrix application method, must be optimized for each drug individually due to the wide variety of structures, solubilities and physicochemical properties of drug compounds.[110] The matrix solution typically contains one or multiple matrices at different concentrations, organic solvent, water and TFA. Standard matrix coating involves spraying saturated CHCA in 50:50 ACN/0.1% TFAaq with a pneumatic TLC sprayer.[105] Some other matrices such as DHB (40 mg/mL) in 75:25 methanol/water[26] or CHCA (25 mg/mL) in 70:30 ethanol/0.1% TFAaq[98] were also successfully used for imaging of different drug compounds. To improve the signal intensity in the low mass range, a thin (5 nm) layer of gold can also be sputter-deposited on top of the dried matrix layer.[34] In contrast to MALDI methods, DESI offers pharmacokinetic studies direct, high-throughput measurements of tissue sections at AP without any prior chemical treatment of the sample. This method was used to map the distribution of clozapine directly from rat brain, lung, kidney and testis after an oral dose of 50 mg/kg.[83] Two reviews presenting various applications of MSI for drug imaging, biomarker discovery and mapping were published in 2005 by T.C. Rohner et al.[172] and by S.S. Rubakhin.[337] Here, we present a short overview of the most recent applications of MSI in pharmacokinetic studies. MSI was used by different scientific groups all over the world to image the distribution of a number of pharmaceuticals such as ketoconazole (an active ingredient in Nizoral),[338] the antipsychotic drugs clozapine[336] and olanzapine,[26,214] chlorisondamine and cocaine,[339] clioquinol as a potential drug for Alzheimer's disease,[239] the anticancer drugs banoxatrone,[340] vinblastine,[98] SCH 226374,[335] paclitaxel,[334] imatinib[214] and oxaliplatin[191] or the antiretroviral drugs saquinavir and nelfinavir.[200] The distribution of the anticancer drug SCH 226374 in mouse tumor tissue and rat brain was published by M.L. Reyzer et al. in 2003.[335] MALDI images were obtained by using the tandem mass

spectrometric technique of SRM to specifically monitor the drug under study. The SRM experiment is accomplished by specifying the parent mass of the compound for MS/MS fragmentation and then specifically monitoring for a single fragment ion. Such an approach minimized the potential for ions arising from either endogenous compounds or the interfering matrix ions. In another application of MALDI-MSI, the absorption of an antifungal agent ketoconazole into skin was examined by the use of an indirect tissue blotting approach.[338] This method can be used to study the absorption of a wide range of xenobiotics into skin. Additionally some preliminary data from a combined solvent-assisted transfer/derivatization approach to sample preparation were also described. The distributions of chlorisondamine, a neuronal nicotinic ganglionic blocker, and cocaine into rat brains were examined.[339] Both compounds were detected in the brains via MALDI-MS using CHCA and DHB as the matrices for chlorisondamine and cocaine, respectively. Tandem MS was employed to confirm the identity of the protonated ions.

The use of MALDI-MSI to study drug distribution in a whole-body mouse section was performed for the first time by Rohner et al. in 2005.[172] First results showed a good correlation between WBA and MALDI-MSI data. This approach was extended by protein imaging to produce whole-body images, as illustrated by figure 2.23, showing the location of drug, drug metabolites, and endogenous markers for various organs of the body.[26] In this study, olanzapine (brand name Zyprexa) was subjected to imaging. Zyprexa is generally used to treat mood disorders such as schizophrenia and acute mania in bipolar patients. MSI analysis of tissues from olanzapine dosed rats revealed the temporal distribution of the drug and metabolites which was in agreement with previous quantitative WBA studies. MALDI-MS/MS analyses were performed on the whole-body sections to detect simultaneously olanzapine (m/z 313) and its fragment ion (m/z 256) and two first-pass metabolites, N-desmethyl-olanzapine (m/z 299) together with its fragment ion (m/z 256) and 2-hydroxymethyl-olanzapine (m/z 329) and its fragment ion (m/z 272). Both metabolites were detected in the liver and bladder, which was consistent with previous autoradiographic data and with the known metabolic pathways in rats. Detection of proteins from organs present in a whole-body sagittal tissue section showed the potential of MSI for the analysis of novel therapeutics with subsequent studies of therapeutic and toxicological processes at the molecular level. Some practical aspects of MALDI-MSI for drug and metabolite imaging in whole-body sections were described by M. Stoeckli et al. in 2007.[105] In another study, S.J. Atkinson et al.[340] applied MALDI-MSI to analyze the distribution of the bioreductive anticancer drug banoxatrone (AQ4N) in H460 lung tumor xenografts. In this study, imaging

resulted in localization of the prodrug and its active form as well as ATP and the co-localization of the active reduced form of the drug in the hypoxic region of the tumor. In another MSI application, the anticancer drug vinblastine was imaged in rat whole-body sections by MALDI-MS.[98] Vinblastine is a chemical analogue of vincristine which was first isolated from the Madagascar periwinkle plant. The mechanism of action of these alkaloids is to arrest cell growth during metaphase through binding to tubulin and inhibiting microtubule assembly.[341] The distribution of the vinblastine precursor ion *m/z* 811.4 together with several product ions including *m/z* 793, 751, 733, 719, 691, 649, 524, and 355 was shown. IMS was employed to remove the interfering matrix ions.[98]

FTICR images of the antitumor drug imatinib (*m/z* 494.2664) and its des-methyl metabolite (*m/z* 480.2506) in mouse brain glioma were shown by D.S. Cornett et al. in 2008.[214] The image showed almost none of the presumed imatinib ion distributed outside of the glioma which indicated that this ion did not accumulate in normal brain. In another study, clioquinol (CQ) was administrated to a mouse model of Alzheimer's disease to study its potential therapeutic effect.[239] CQ is known to interfere with brain metal metabolism and ameliorate disease pathology through a mechanism that is not fully understood. The MSI results showed that CQ was mainly localized within the cortex and the hippocampus, which are brain areas primarily involved in cognitive functions. Recently, imaging of the HIV protease inhibitors saquinavir and nelfinavir in Mono Mac 6 cells by two types of mass spectrometry techniques MALDI-TOF and MALDI-FTICR was performed by L.J. Dekker et al. in 2009.[200] A sublimation/deposition device for homogeneous matrix deposition was constructed which allowed imaging of these HIV protease inhibitors at clinically relevant concentrations. MALDI-MSI has been also applied to assess the distribution of a novel potential therapeutic compound (beta-peptide) in whole-body sections of mice.[113] Beta-peptides display potent biological activity such as somatostatin mimetics and are resistant to the digestion by proteases and peptidases. Finally, a platinum anticancer drug, oxaliplatin, which is mainly used in the treatment of advanced colorectal cancer, was imaged by A. Bouslimani et al. in 2010.[191] In this study, the penetration of oxaliplatin in tissues from treated animals was investigated. Imaging experiments allowed the detection and localization of the drug and its metabolites, the monocysteine and monomethionine complexes, in kidney sections, where they localized exclusively in the cortex, suggesting that the drug did not penetrate deeply into the organ.

MALDI-MSI technology provides molecular images of resected organs or whole-body sections from small animals. It has attracted great interest of scientists interested in drug

delivery and metabolism monitoring.[310] It provides *label free* tracking of both endogenous and exogenous compounds with spatial resolution and molecular specificity. In combination with WBA, this technology significantly improves the analysis of novel therapeutics. MSI is a powerful technique which provides deeper insight into therapeutic and toxicological processes such as metabolic changes or side effects often associated with drug administration.
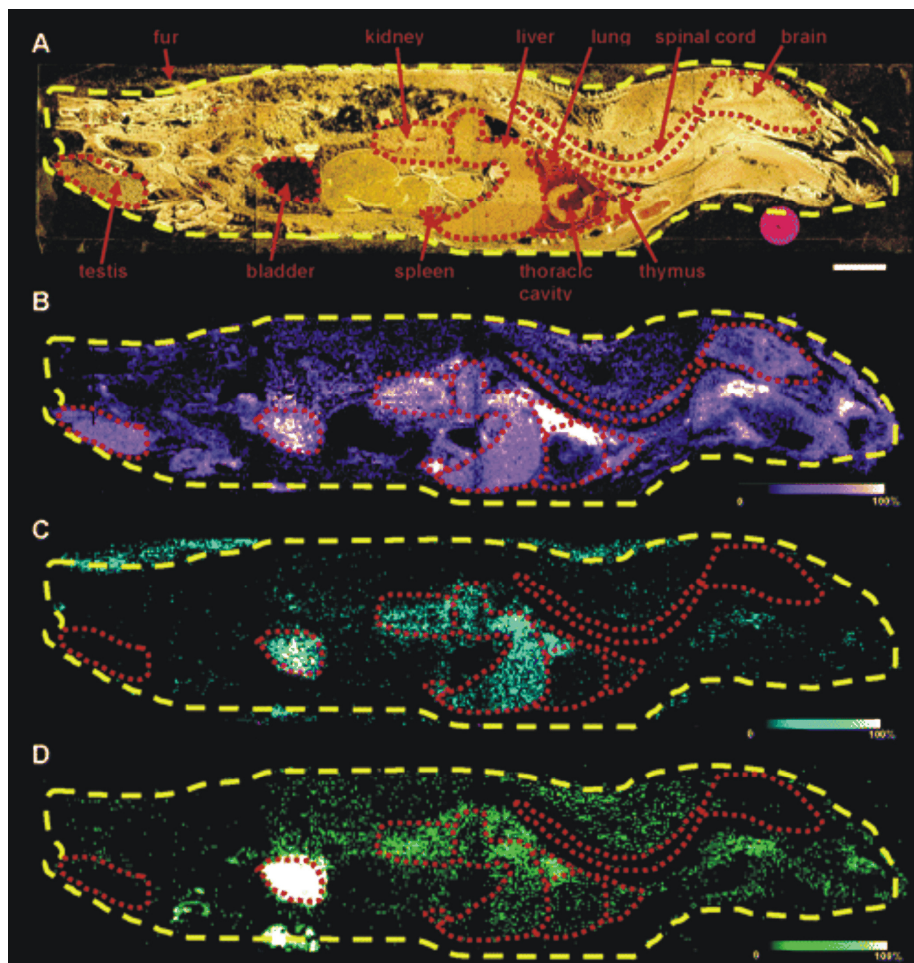
Figure 2.23 Detection of drug and metabolite distribution in a whole rat sagittal tissue section. (A) Optical image of a 2 h post OLZ dosed rat tissue section mounted on a gold MALDI target plate. (B) MS/MS ion image of OLZ (m/z 256). (C) MS/MS ion image of N-desmethyl metabolite (m/z 256). (D) MS/MS ion image of 2-hydroxymethyl metabolite (m/z 272). Scale bar, 1 cm. Reprinted with permission from ref[26]. Copyright 2006 American Chemical Society.

2.3.7 MSI 3D imaging

MSI provides two dimensional distributions of multiple ions detected from biological samples. This technique has been recently extended to the third dimension. It provides 3D

distributions of the selected molecules detected by MSI from biological samples. A stack of 2D MS images of a selected ion acquired from the same sample can be stitched together to reconstruct a 3D distribution map of that ion. This extension of a conventional MSI experiment provides more comprehensive information about the spatial distribution of selected molecules inside the whole sample. To perform MSI 3D reconstruction, the sample is cut into serial sections which are processed under identical conditions and analyzed by MSI. The acquired images are stitched together by software such as Image J[342] to obtain the 3D distribution of a particular ion.[163] Here, we present some practical aspects of 3D MSI, its applications and future perspectives of this youngest modification in the MSI family.

In terms of the sample, at the beginning of 3D MSI, the rodent brain was the most commonly chosen organ. This was due to its small size, well defined internal/external structure and an anatomical atlas which was used as reference for the methodology development. So far, 3D reconstructions have been performed for myelin basic protein (MBP) in the corpus callosum of a mouse brain,[138] Substance P and PEP-19 in the rat ventral midbrain,[169] neuropeptide (CabTRP 1a) and lipid PC(38:6) in the brain of the crab *Cancer borealis*[163] and lipids in a mouse brain.[343] Figure 2.24 shows an example of the 3D distribution of a lipid and a peptide in a crab brain. A 3D reconstruction of the distribution of lipids throughout the mouse brain has been recently presented by L.S. Eberlin et al.[343] These results represent the first 3D molecular reconstruction of mouse brain imaged by DESI-MS. Imaging of two lipids, PS(18:0/22:6) and ST(sulfatide)(24:1), allowed a full visualization of the gray-matter region as well as the white-matter region in the total volume of the brain. This allowed a complete view of substructures, such as the corpus callosum and anterior commissure, throughout the brain volume. Cross-sectional views of the 3D models can be used to investigate distributions of many additional molecules detected by MSI. The co-registration of MSI proteomic data from the whole mouse head with *in vivo* MRI data was reported by T.K. Sinha et al. in 2008.[344] A detailed procedure describing how to make 3D volume reconstructions of MALDI-MSI data was published by M. Andersson et al.[169]

On a subcellular scale 3D MSI images of the mitotic spindle from T98G human glioblastoma tumor cells were acquired by SIMS-TOF.[43] This study demonstrated that 3D SIMS imaging was essential for the analysis of mitotic cells, where specialized regions such as the mitotic spindle were hidden beneath the cell surface. Another study applied SIMS-TOF to visualize the 3D distribution of phosphocholine and inorganic ions in single cells.[68]

Unlike *in vivo* tomographic imaging techniques, 3D MALDI-MS images require the specimen to be sliced into thin serial sections. Sectioning can lead to tissue tearing and deformation.

Therefore, correlating consecutive 2D images to obtain a 3D reconstruction must be performed carefully. To properly reconstruct a 3D volume from 2D MSI data the images must be co-registered. The co-registration can involve inter- and/or intra-section registration. The inter-section registration provides alignment of optical images of the tissue sections, while the intra-section registration aligns the MALDI-MSI data to the corresponding optical image. Another co-registration technique involves the use of fiducial markers. The imaging of the sample includes the region containing the markers used as orientation and alignment points during the 3D reconstruction process.

One of the advantages of 3D MSI is the possibility to correlate distributions of the multiple biomolecular ions with physiological and structural information observed by *in vivo* imaging techniques, such as CT, PET, and MRSI. These *in vivo* imaging techniques are limited to a few molecules and cannot show protein distributions. Of the current techniques, MSI can image the widest range of molecules.
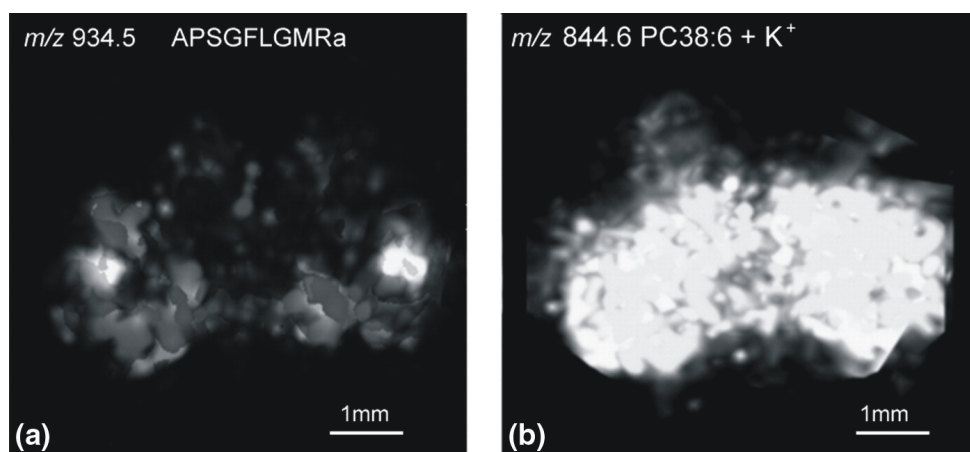
Figure 2.24 3D reconstruction of images of (A) CabTRP 1a and (B) lipid PC 38:6 acquired from the brain of C. borealis. For images shown in (A), tissue sections were prepared using regular matrix coating method. In contrast, images of (B) were obtained from tissue sections prepared using dry matrix spraying technique that favored detection of lipids. Reprinted with permission from ref[163]. Copyright 2009 Elsevier.

2.4 Future perspectives

MSI is becoming an established tool for imaging of the most complex biological samples. Its key applications are foreseen in a biomedical environment, more specifically in molecular histology. This *ex vivo* imaging technique provides a lot of information about the biomolecular composition of the tissue, without the need for labels, complicated sample preparation protocols or staining procedures. No *a priori* knowledge about the sample is

necessary but for correct interpretation of results some MS knowledge is required. The instrumentation used for imaging has reached a degree of maturation with ionization sources performing at high resolution and mass analyzers of a broad mass range and high sensitivity. MSI is rapidly developing into an imaging tool used by pathologists, biologists and biochemists. In the future it has the potential to become a routine tool for imaging of tissues dissected during surgical operations or stored in tissue banks. MSI can help to understand the link between the localization of certain molecules and their function during pathogenesis, disease progression or treatment. It can accelerate our efforts to provide more effective therapeutics for a broad range of diseases such as cancer, neurodegenerative diseases or age-related problems.

Having said this, there are still areas of development needed. To make MSI a routine tool the method needs to be validated on large patient or sample cohorts. This requires a higher degree of automation than currently available. Automation and robotics developments will improve the throughput of the MSI technologies allowing a researcher to analyze more samples. The capability of high-throughput imaging also will drive the developments in sample preparation. The sample preparation protocols need to keep up with the speed of the new instruments. This requires automated sectioning, mounting, washing and surface preparation. These tools are not available today.

High-throughput perspectives drastically increase the amount of data generated in MSI experiments. It will soon become difficult to keep all the raw data from a MSI validation study at high spatial resolution. On-the-fly data reduction and feature extraction protocols have to be developed that address this issue. In addition multimodal imaging approaches will assist in the validation and acceptance of MSI technology in molecular biology. The increased throughput will also induce a larger demand for 3D MSI. The capabilities are existing already, but only a few good examples exist due to the lack of proper processing infrastructure. These prospective improvements in MSI technology put further strain on the data storage and processing resources. As a result they pose new challenges for the bioinformaticians working in this field.

New desorption and ionization techniques in the ambient environment offer new application possibilities. They will migrate the MSI field from *ex-vivo* analysis to *in-vivo* analysis of living systems, such as bacterial colonies and living cells in aqueous environments. Given its current status and all of these high-end developments that lay ahead, MSI is strongly positioned to be an important molecular imaging tool for life sciences in the immediate future and many years to come.

Chapter 3

Fiducial Markers for Combined 3-Dimensional Mass Spectrometric and Optical Tissue Imaging

3. Fiducial Markers for Combined 3-Dimensional Mass Spectrometric and Optical Tissue Imaging[*]

Mass spectrometric imaging has become widely used in the analysis of a variety of biological surfaces. Biological samples are spatially, morphologically, and metabolically complex. As mentioned in the first chapter, multimodal molecular imaging is an emerging approach that is capable of dealing with this complexity. In a multimodal approach, different imaging modalities can provide precise information about the local molecular composition of the surfaces. Images obtained by MSI can be co-registered with images obtained by other molecular imaging techniques such as microscopic images of fluorescent protein expression or histologically stained sections. In order to properly co-register images from different modalities, each tissue section must contain points of reference, which are visible in all data sets. Here, we describe a newly developed co-registration technique using fiducial markers such as cresyl violet, Ponceau S, and bromophenol blue that possess a combination of optical and molecular properties that result in a clear mass spectrometric signature. We describe these fiducial markers and demonstrate an application that allows accurate co-registration and 3-dimensional reconstruction of serial histological and fluorescence microscopic images with MS images of thin tissue sections from a breast tumor model.

3.1 Introduction

Multimodal biomedical imaging that incorporates MSI as one modality is a rapidly evolving discipline.[345,346] MSI offers a detailed insight into the molecular composition of complex biological surfaces such as single cells,[347] small histological sections,[348] and up to large whole rodent sections.[349] MSI does not require any *a priori* knowledge about the analyzed sample, which makes it a unique *label free* discovery technique.[350] MSI is an *ex vivo* technique, optimally suited for the analysis of thin tissue sections obtained with a standard cryo-microtome available in most pathology departments. Data acquisition is typically performed directly from 10 μm thick tissue sections, using a mass spectrometer that is capable of acquiring a complete spectrum of molecular ions from each point within a predefined raster of x- and y-coordinates on the sample surface. Dedicated MSI software is used to generate molecular ion images from the acquired spectra that display the intensity distribution of any selected mass-to-charge ratio (*m/z*) of detected biomolecules over the imaged area. The integration of this molecular imaging approach into a clinical workflow requires the ability to compare and contrast the mass resolved images with conventional histological images. This integration of results obtained by methodologies from different disciplines assists in validating and interpreting normal and pathological molecular patterns as it brings together different pieces of information. Among the conventional histological imaging techniques are H&E staining, which visualizes morphological features of the tissue section, while an IHC staining provides the detailed distribution of a selected protein known to be involved in a pathological cellular process. In biomedical research applications, the use of different fluorescent proteins[351] enables the investigation of protein expression, gene reporter activity, signaling pathways, oncogene activity, or cell tracking at low spatial resolution *in vivo*[352] or at higher spatial resolution in fresh tissue slices *ex vivo*.[353] Mass spectrometric images provide visualization of the distribution of a plethora of molecules that are spatially correlated with a region of interest or with a fluorescent or IHC-stained protein of interest.[345] The validation of this data requires an accurate overlay of the different imaging modalities. The accurate co-registration of MSI and optical (fluorescent, H&E, and IHC) images needs proper alignment and scaling of all modalities. Fiducial markers can assist during processing of 2D datasets obtained from multimodal imaging.

Fiducial markers are also needed for 3D molecular mass spectrometric imaging, which requires accurate alignment of individual molecular images. In this approach 3D molecular volumes of samples are generated by successive 2D MSI experiments of tissue sections that

are cut with well-defined spacing throughout a biological sample (e.g. a tumor or an organ).[354,355] Correct alignment of individual MSI datasets is crucial for the reconstruction of 3D molecular volumes. If clear spatial molecular features are observed in the consecutive MS generated molecular images, they can be used for spatial alignment. In some cases researchers have used blockface optical images taken from the cryo-microtome mounted sample during sectioning, or obtained from target-mounted samples, to enable alignment.[356] In the case of 3D reconstruction of MSI detected distributions in a rodent brain researchers benefited from the availability of an existing anatomical atlas, in which the anatomical structures found in the rodent brain are described in great detail.[350-352] However, in many other cases, samples lack known or visible spatial detail, which makes correct alignment and ion intensity normalization for 3D reconstruction as well as co-registration with histological images impossible without markers.

When combining bright field/fluorescence microscopy, histological staining, and MSI, the selection of suitable fiducial marker(s) is not trivial. Tissue fixation and sectioning can deform and shrink the tissue introducing differences in slice thickness and sectioning angle, which can compromise image co-registration, if markers are not used. Good markers must fulfill a number of requirements, such as intense color for microscopic bright field imaging applications, absorption/emission at selected wavelengths for fluorescence imaging and good ionization for MSI. The fiducial markers should not diffuse during washing and matrix application procedures prior to MSI or histological staining, and allow the co-registration of images acquired by different techniques. In addition, the fiducial markers should have good MALDI-MS properties. MALDI imaging is capable of visualizing molecules with good ionization properties even if they are present in the sample at a relatively low concentration.

Other groups have experimented with fiducial markers for multimodal imaging, but these are incompatible with mass spectrometry. Among them are metallic needles,[357,358] or air-filled Teflon rods for imaging of tumor xenografts in rodents,[359] which can be positioned inside the tissue of interest prior to imaging. Visualized by MRI and PET as well as histology and autoradiography on tissue sections, these rigid markers do not shrink with the surrounding tissue during fixation, and displace and distort the tissue by their insertion. Ink based markers are more flexible and minimally disturb tissue structure during organ resection and sectioning.[360] The Bronze iridescent acrylic paint was found to be an appropriate fiducial marker for MRI at 7 Tesla and for correlation of whole-specimen histopathology with MRI.[361,362] These methods require injection of the marker into living animals, which may affect tissue physiology as well as damage the tissue of interest, making them

disadvantageous for common histological studies as well as making co-registration cumbersome.

We have developed and evaluated a new method that allows easy co-registration of different imaging modalities and 3D reconstruction using fiducial markers added adjacent to the tissue. We tested and optimized three fiducial markers: cresyl violet, Ponceau S, and bromophenol blue, which do not interfere with sample preparation, exhibit good optical and fluorescent properties, are compatible with MS analysis, and serve as docking points for proper 2D/3D image alignment and for normalization of the individual 2D MS image intensities. This novel method is illustrated with an example of 3D multimodal imaging of human breast tumor xenograft models.

3.2 Materials and methods

Chemicals and materials. The matrix CHCA was purchased from Fluka (Switzerland), ethanol, acetic acid, water, ACN, and TFA were purchased from Biosolve (The Netherlands). Modified proteomics grade trypsin was purchased from Sigma (Germany). Cresyl violet acetate and Ponceau S were purchased from Sigma (USA). Bromophenol blue was purchased from BIO-RAD (USA). Gelatin Type A was purchased from Sigma (USA). Mayer's hematoxylin was purchased from Sigma (USA) and aqueous Eosin Y from EMD Chemicals Inc. (USA). The Cytoseal 60 Mounting Medium, Richard-Allan Scientific was purchased from Thermo Scientific (USA).

Fiducial marker analysis. MALDI-MS: Cresyl violet acetate, Ponceau S, and bromophenol blue were prepared at a concentration of 10 mg/mL and dissolved in 100% ethanol (cresyl violet and bromophenol blue) or 1% acetic acid (Ponceau S). Marker solutions were mixed 1:1 with CHCA matrix prepared at a concentration of 10 mg/mL in 1:1 $ACN:H_2O$/0.1% TFA and 1 μL of this solution was spotted on MALDI target for MS analysis by MALDI-Q-TOF (Synapt HDMS, Waters, UK).

Fiducial marker analysis. MALDI-MSI: Gelatin blocks were prepared using 15 mm x 15 mm x 5 mm cryomolds (Sakura Finetek, USA). Cresyl violet acetate, Ponceau S, and bromophenol blue were prepared in 10% warm (37°C) gelatin at a concentration of 10 mg/mL and 0.01 mL volume was injected into 10% gelatin blocks using a 1 mL syringe. Gelatin blocks were frozen at -20°C for 30 minutes and sectioned into 20 µm thick sections using a cryo-microtome (HM525, MICROM, Germany). Two sections were mounted onto one 25 mm x 50 mm x 1.1 mm, Rs=4-8 Ω ITO coated slide (Delta Technologies, USA). CHCA matrix at a concentration of 10 mg/mL in 1:1 $ACN:H_2O$/0.1% TFA was applied on slides

using an ImagePrep (Bruker Daltonics GmbH, Bremen, Germany). Samples were analyzed on a MALDI-Q-TOF (Synapt HDMS, Waters, UK) instrument in TOF mode detecting first positive and subsequently negative ions. The images were acquired at a spatial resolution of 150 μm x 150 μm. Data were visualized using BioMap software (Novartis, Basel, Switzerland).

Breast tumor imaging. The MDA-MB-231 breast cancer cell line was purchased from the American Type Culture Collection (ATCC) and genetically modified to express a red fluorescent protein (tdTomato) under the control of hypoxia response elements as previously described.[363,364] Cells were injected into the upper thoracic mammary fat pad of athymic nude mice ($2x10^6$ cells/injection) and tumor growth was monitored with standard calipers. When tumors reached a volume of approximately 500 mm^3, mice were sacrificed and tumors were removed. Each tumor was embedded into a gelatin block (10% gelatin, cooled to 30°C in order to prevent tissue degradation) and three cresyl violet fiducial markers were injected inside the block next to the tumor. The block was sectioned into serial 2 mm thick fresh tumor sections using an acrylic adjustable tissue slicer (12 mm depth up to 25 mm width; Braintree Scientific, Inc, Braintree, MA) and tissue slicer blades (Braintree Scientific, Inc). These serial fresh tumor xenograft sections were each placed on individual microscope slides (Fisherbrand catalog number 12-550-34; Fisher Scientific, Pittsburgh, PA), and stored in an ice-box containing ice on the bottom, with the slides located on a perforated plate at approximately 1 cm above the ice to minimize tissue degradation. These fresh sections were imaged by bright field and fluorescence microscopy with a 1x objective attached to a Nikon inverted microscope, equipped with a filter set for 528 to 553 nm excitation and 600 to 660 nm emission, and a Nikon Coolpix digital camera (Nikon Instruments, Inc, Melville, NY). Bright field imaging captured the position of the fiducial markers present inside the gelatin block as well as the shape of the tumor tissue. The fluorescence from tdTomato expression in hypoxic regions of these tumor sections was detected by fluorescence microscopy. The GNU Image Manipulation Program (GIMP 2.6) was used for 2D co-registration and overlay of bright field and fluorescence images of 2 mm thick tumor sections.

All 2 mm thick sections were snap-frozen immediately after microscopic imaging. From each 2 mm thick section, 10 µm thick sections were cut at -16°C for MSI using a Microm HM550 cryo-microtome (Microm International GmbH, Walldorf, Germany) along with adjacent 10 µm thick sections for histological staining. Tissue sections for MSI analysis were mounted onto ITO coated slides (Delta Technologies, USA) and for histological staining onto Superfrost Slides (VWR International, Cat. 48311-600).

Before MSI analysis, tissue sections were briefly washed by immersion in 70% and 90% ethanol and dried in a vacuum desiccator for 10 min. Trypsin was resuspended in water at a concentration of 0.05 µg/µL, and 5 nL per spot in a 150 µm x 150 µm raster was deposited by CHIP (Shimadzu, Japan). CHCA matrix was prepared at a concentration of 10 mg/mL in 1:1 ACN:H_2O/0.1% TFA and was applied by an ImagePrep (Bruker Daltonics GmbH, Bremen, Germany) application system. Samples were analyzed on a MALDI-Q-TOF (Synapt HDMS, Waters, UK) instrument in TOF mode detecting the positive ions. The images were acquired with 150 µm x 150 µm spatial resolution. For 2D MSI analysis and overlay of images, data were visualized using BioMap software (Novartis, Basel, Switzerland). 3D multimodal imaging reconstruction and registration was performed using a previously developed software platform,[365] which was written in Matlab (Natick, MS), and using Amira software for 3D visualization and volume rendering (Visage Imaging, Inc.).

H&E staining method. Tissue sections were stained using a modified H&E staining protocol. Briefly, 10 µm sections attached to Superfrost Slides (VWR International, Cat. 48311-600) were washed with phosphate buffered saline (PBS), fixed with 3% paraformaldehyde for 30 min, washed with distilled water (dH_2O), and treated with Mayer's hematoxylin for 30 min at room temperature, followed by 5 washes with dH_2O. Sections were immediately immersed in aqueous Eosin Y for 30 min, followed by 5 washes with dH_2O, mounting with aqueous mounting medium, and attaching of a coverslip. Bright field images of H&E stained sections were acquired using a 1x objective attached to a Nikon microscope, equipped with a Nikon Coolpix digital camera (Nikon Instruments, Inc, Melville, NY).

3.3 Results and discussion

Mass spectrometric analysis of fiducial markers

We investigated MALDI-TOF-compatible fiducial marker compounds compatible with our optical microscopy protocols. Three different compounds were selected as good fiducial markers since they ionized easily during MALDI-MS and exhibited good optical properties. The spectra of these three compounds were obtained in positive ion mode as shown in figure 3.1. Encircled peaks correspond to cresyl violet (CV) [M-CH$_3$COO]$^+$ at *m/z* 262.0 in positive ion mode (figure 3.1A), Ponceau S (PS) did not ionize in positive ion mode (figure 3.1B), and bromophenol blue (BB) [M+H]$^+$ was detected at *m/z* 670.7 in positive ion mode (figure 3.1C).

Figure 3.1 Mass Spectrometric analyses of fiducial markers in positive ion mode. (A) Spectrum of cresyl violet acetate. (B) Spectrum of Ponceau S. (C) Spectrum of bromophenol blue. Peaks of fiducial markers are encircled. Reprinted with permission from ref[366]. Copyright 2012 American Chemical Society.

The spectra of the fiducial markers were also obtained in negative ion mode (figure 3.2). CV (figure 3.2A) did not ionize in negative ion mode, and PS [M-Na]⁻ gave a signal at *m/z* 736.5 in negative ion mode (figure 3.2B). BB [M-H]⁻ was detected at *m/z* 668.4 in negative ion mode (figure 3.2C).
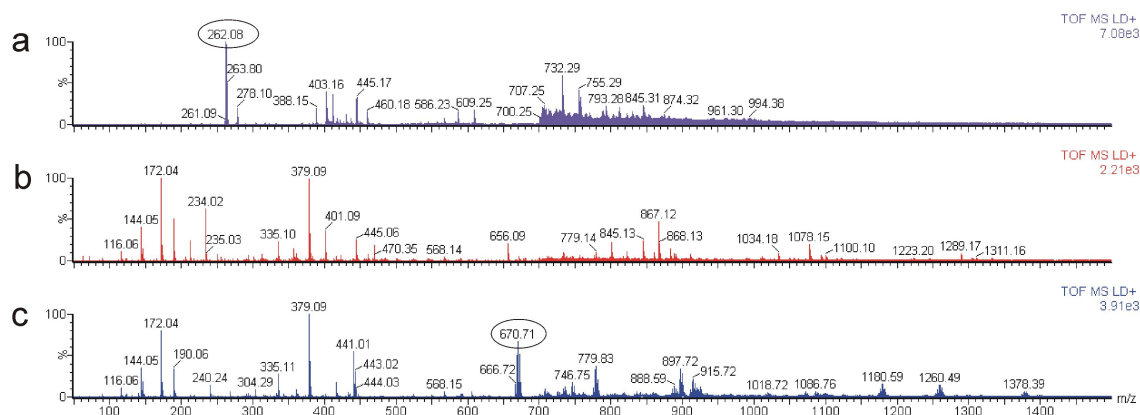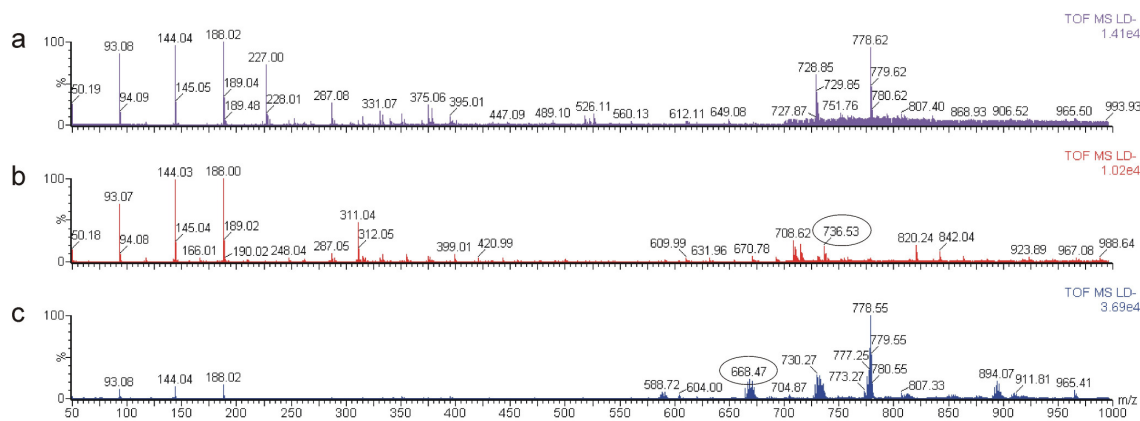

Figure 3.2 Mass Spectrometric analyses of fiducial markers in negative ion mode. (A) Spectrum of cresyl violet acetate. (B) Spectrum of Ponceau S. (C) Spectrum of bromophenol blue. Peaks of fiducial markers are encircled. Reprinted with permission from ref[366]. Copyright 2012 American Chemical Society.

Mass spectrometric imaging of fiducial markers

Three different fiducial markers were selected based on their intense colors for easy detection by microscopic imaging and compatibility with MSI. After resuspending the markers in gelatin and injection into a gelatin block, CV displayed violet color, PS dark red, and BB dark blue as shown in figure 3.3A. After freezing and during cryo-sectioning of the block, the colors of these markers remained unchanged. During matrix application, due to the acidic pH of the matrix solution, BB changed its color to yellow as shown in figure 3.3B.

Two adjacent sections from the gelatin block were subjected to MSI analysis, one in positive and one in negative ion mode. The ion images of different fiducial markers were co-registered with the corresponding optical images of the gelatin block sections (figure 3.3C-H). Following analysis in positive mode, ion images were obtained from the fiducial markers of CV at *m/z* 262.0 and BB at *m/z* 670.7 (figure 3.3C and E). No signal was detected from the PS marker (figure 3.3D).
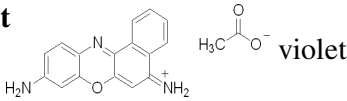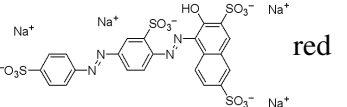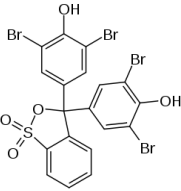
The adjacent section of the gelatin block was analyzed in negative ion mode. No signal was detected from the CV marker (figure 3.3F), while signals from PS at *m/z* 736.5 and BB at *m/z* 668.4 were detected (figure 3.3G and H). The results are summarized in Table 3.1.
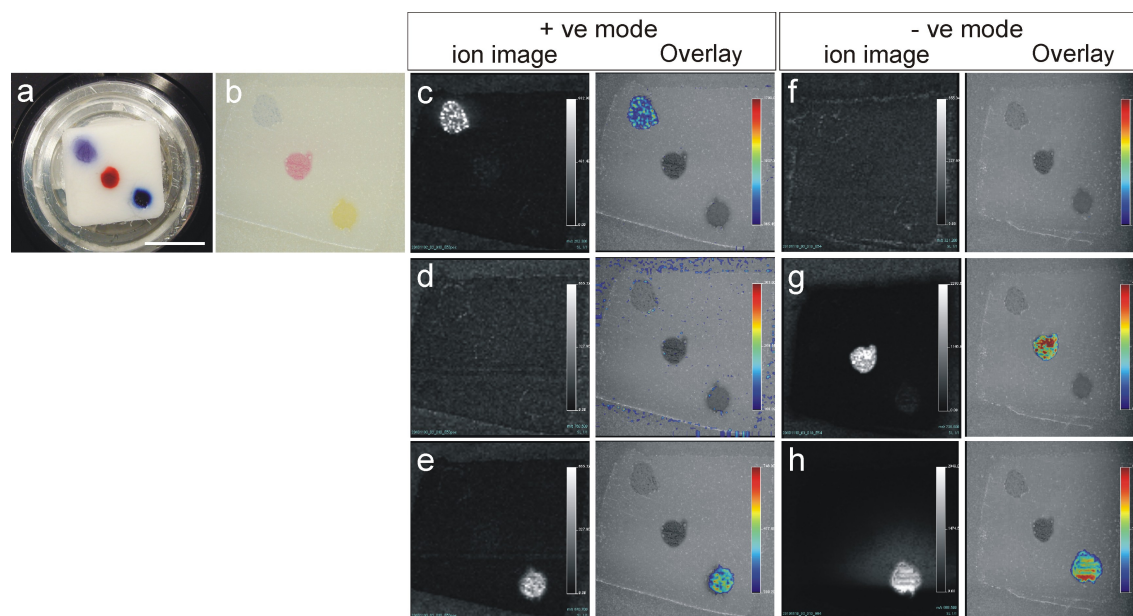
Figure 3.3 MSI of fiducial markers in a gelatin block. (A) Frozen gelatin block with cresyl violet, Ponceau S, and bromophenol blue. (B) An optical image of the section covered with matrix. Ion images together with co-registered optical image of fiducial markers acquired in positive ion mode: (C) cresyl violet at m/z 262.0, (D) Ponceau S (no ion detected), and (E) bromophenol blue at m/z 670.7. Ion images together with the corresponding co-registered optical image of fiducial markers acquired in negative ion mode: (F) cresyl violet (no ion

detected), (G) Ponceau S at m/z 736.5, and (H) bromophenol blue at m/z 668.4. Scale bar, 1 cm. Reprinted with permission from ref[366]. Copyright 2012 American Chemical Society.

Table 3.1 Summary of fiducial markers analysis. Reprinted with permission from ref[366]. Copyright 2012 American Chemical Society.

Name	Chemical structure	Color	Molecular formula and weight (MW)	Positive m/z	Negative m/z
Cresyl violet acetate		violet	$C_{16}H_{12}N_3O\cdot C_2H_3O_2$ MW 321.1	$[M-CH3COO^-]^+$ 262.0	-
Ponceau S		red	$C_{22}H_{12}N_4Na_4O_{13}S_4$ MW 759.9	-	$[M-Na]^-$ 736.5
Bromophenol blue		yellow to purple	$C_{19}H_{10}Br_4O_5S$ MW 669.6	$[M+H]^+$ 670.7	$[M-H]^-$ 668.4

Two fiducial markers, CV and PS, were selected for further analysis because they displayed good visibility in optical imaging and complementary MSI properties. A gelatin block was injected with pure CV, a 1:1 mixture of CV and PS (CVPS), and pure PS. MSI analyses were performed on two adjacent block sections, one in positive and one in negative ion mode as shown in figure 3.4A-F. Ion images were obtained from CV in positive mode (figure 3.4A-C) and PS in negative mode (figure 3.4D-F) and from the mixture of both in both ion modes. The mixture shows clearly visible marker localization in both positive and negative ion modes.

In order to evaluate potential ion suppression effects, solutions of CV and PS were mixed in a 1:1 ratio, spotted on MALDI target with CHCA, and analyzed in positive and in negative ion mode, respectively (figure 3.4G and H). The expected peaks of CV at *m/z* 262.0 in positive ion mode and of PS at *m/z* 736.5 in negative ion mode were detected. From this analysis we concluded that a 1:1 mixture of PS and CV directly resuspended in gelatin is the optimal fiducial marker for MS image co-registration, 3D reconstruction, and normalization if analysis requires detection of both positively and negatively charged ions.
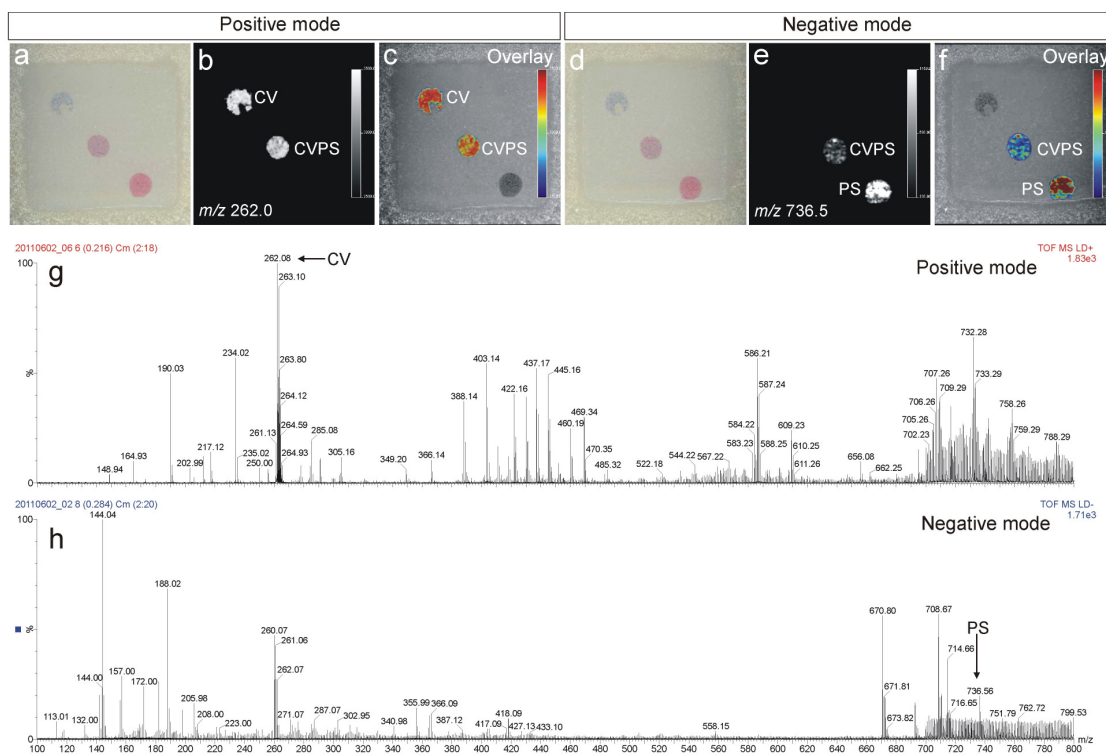
Figure 3.4 Optical images (A) and (D) show two adjacent sections taken from a gelatin block containing the injected fiducial markers: cresyl violet (CV), cresyl violet/Ponceau S (1:1) (CVPS), and Ponceau S (PS). Ion images were obtained in positive and negative ion mode. (B-C) Cresyl violet was detected at m/z 262.0 in positive ion mode. (E-F) Ponceau S was detected at m/z 736.5 in negative ion mode. The mixture of both markers (CVPS) was detected in both modes. (G) Spectrum showing the CV peak at m/z 262.0 detected from the CVPS mixture in positive ion mode. (H) Spectrum showing the PS peak at m/z 736.5 detected from the CVPS mixture in negative ion mode. Reprinted with permission from ref[366]. Copyright 2012 American Chemical Society.

Multimodal MSI of a breast tumor xenograft model

Human breast tumor xenografts that express the tdTomato fluorescent protein in hypoxic regions were orthotopically grown in athymic nude mice, and, following tumor removal, were embedded in gelatin with three CV fiducial markers. Two vertical markers allowed an easy co-registration of the optical and ion images in 2D while the additional diagonal marker was used during 3D volume reconstruction of MSI data. Fresh tumor sections of 2 mm thickness were imaged by bright field and fluorescence microscopy in order to visualize tumor boundary and expression of tdTomato red fluorescent protein present in the hypoxic regions of this tumor model (figure 3.5A and B). The bright field and fluorescence images were co-

registered based on the position of the fiducial markers visible in both images (figure 3.5C). The red color of tdTomato was changed into black for better visualization of hypoxic regions. Positive ion MALDI-TOF images were acquired from subsequently cryo-sectioned 10 μm thick tissue sections, detecting the fiducial markers at *m/z* 262.0 (figure 3.5D) and multiple biomolecular ions. An optical image and the ion images were co-registered in BioMap software based on the position of the fiducial markers (figure 3.5E). Overlays between MSI images, such as the image of *m/z* 1198.7 identified as a tryptic peptide ion of actin (figure 3.5F), and tissue optical images can subsequently be accurately generated (figure 3.5G).
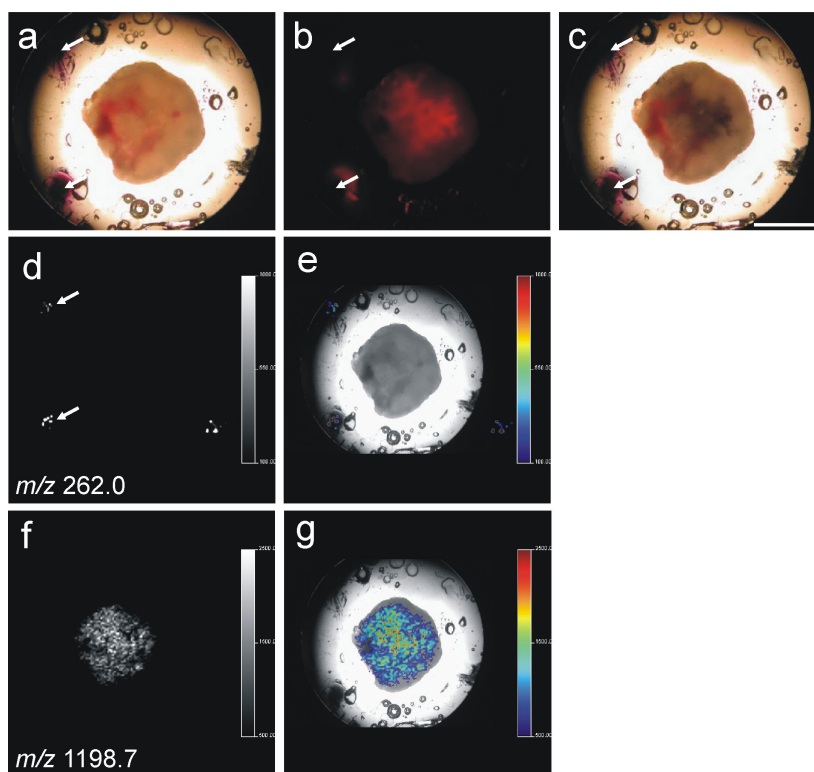
Figure 3.5 Multimodal imaging of MDA-MB-231-HRE-tdTomato-expressing breast tumor xenograft tissue sections. Optical microscopic imaging combined with MSI. (A) Optical image of a representative 2 mm thick tumor section. White arrows indicate the fiducial markers. (B) Fluorescence image of the distribution of tdTomato inside hypoxic tumor regions. (C) Co-registration of optical and fluorescence images based on the position of the fiducial markers. The red color of tdTomato was changed to black for better visualization of the hypoxic region inside tumor tissue. (D) Ion image of the cresyl violet fiducial marker at m/z 262.0. (E) Co-registration of optical image and MSI of the cresyl violet marker. (F) MSI image of the actin tryptic-peptide at m/z 1198.7. (G) Co-registration of optical image and MSI of the actin tryptic-peptide ion image at m/z 1198.7. Scale bar, 500 μm. Reprinted with permission from ref[366]. Copyright 2012 American Chemical Society.

A schematic diagram representing the location of the fiducial markers inside the gelatin block, which allowed proper 3D alignment of multiple ion images acquired by MSI from different sections obtained from the same tumor is shown in figure 3.6A. We took advantage of the abundant presence of actin in all tumor cells for the reconstruction of the total tumor volume. Figure 3.6B shows the 3D reconstructed ion image of the actin tryptic peptide (*m/z* 1198.7, shown in gray) used for the reconstruction of tumor boundaries. The position of fiducial markers was reconstructed based on the signal of CV detected at *m/z* 262.0.
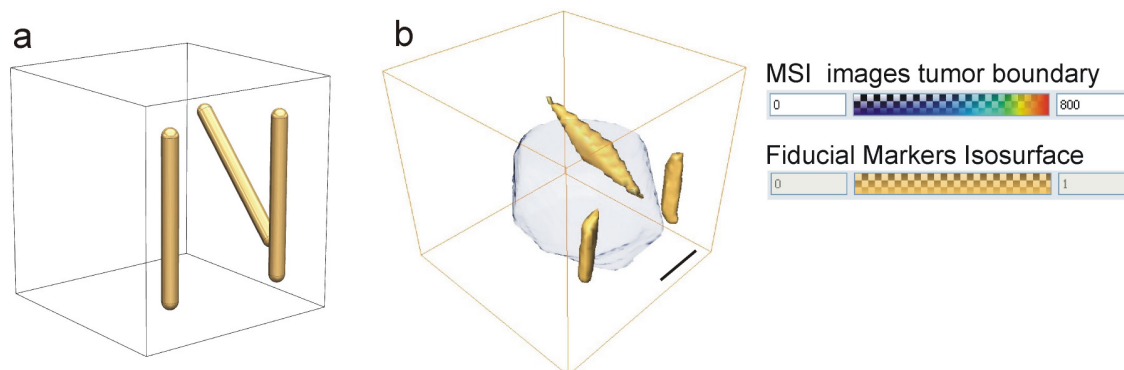
Figure 3.6 Application of fiducial markers for 3D reconstruction of MSI data. (A) Schematic representation of the position of three markers inside the gelatin block. (B) 3D reconstruction of ion images of the actin tryptic-peptide at m/z 1198.7, which was used for 3D reconstruction of the tumor boundary. The cresyl violet ion images were used for alignment of multiple 2D sections of the tumor imaged by MSI. Scale bar, 500 μm. Reprinted with permission from ref[366]. Copyright 2012 American Chemical Society.

The 3D reconstruction of tumor tissue volumes based on the position of the fiducial markers was performed for optical bright field and tdTomato fluorescence microscopic images. Figure 3.7A shows the 3D reconstruction of tumor tissue volumes obtained from three 2 mm tumor sections. The tumor boundary was reconstructed based on the shape of the tumor tissue visualized in bright field as shown in figure 3.5A. The markers were visualized based on their position in the optical bright field images (figure 3.5A). The tdTomato red fluorescent protein signal (shown in figure 3.5B) was used to reconstruct the position and volume of the hypoxic regions present inside the tumor. Figure 3.7B shows the 3D reconstruction performed based on the H&E stained tissue sections of the same tumor. Figure 3.7C presents the 3D reconstruction of the MSI data obtained from the same tumor. The distribution of the hemoglobin tryptic peptide (*m/z* 1529.7, shown in green) was generated to show the localization of hemoglobin inside the tumor, while the distribution of the tdTomato tryptic

peptide (*m/z* 2225.0, shown in red) revealed the position of hypoxic regions inside the tumor. The ion image of the actin tryptic peptide (*m/z* 1198.7, shown in gray) was used to reconstruct the tumor boundary. Fiducial markers (*m/z* 262.0, shown in yellow) were used for alignment of ten MSI 2D data sets.

The ion intensity normalization for 3D reconstruction of the MSI data was performed by using the MSI-detected intensity of the CV marker in each one of the 2D tissue sections. The concentration of each CV marker was constant across the entire gelatin block. The CV ion of each individual sectional 2D MSI image at *m/z* 262.0 was visualized in BioMap software, and the generated MSI image at *m/z* 262.0 was exported as Portable Network Graphics (PNG) file. Each straight marker in each sectional MSI image at *m/z* 262.0 was detected by using an active shape model ('snake' or ASM model) in the Gradient Vector Flow Active Contour Toolbox written in Matlab.[367] An average intensity of all markers within each section and across all sections was calculated using Matlab. The differences between individual and averaged CV intensities across all sections and within each section were corrected in the reconstructed 3D dataset, and the intensities of ions of interest such as actin, tdTomato, or hemoglobin were adjusted accordingly. Normalized 2D images of different ions were intersectionally aligned according to the positions of the corresponding CV markers. Then aligned 2D sectional MSI images were interpolated and rendered into a 3D volume, which was displayed using the Amira software.
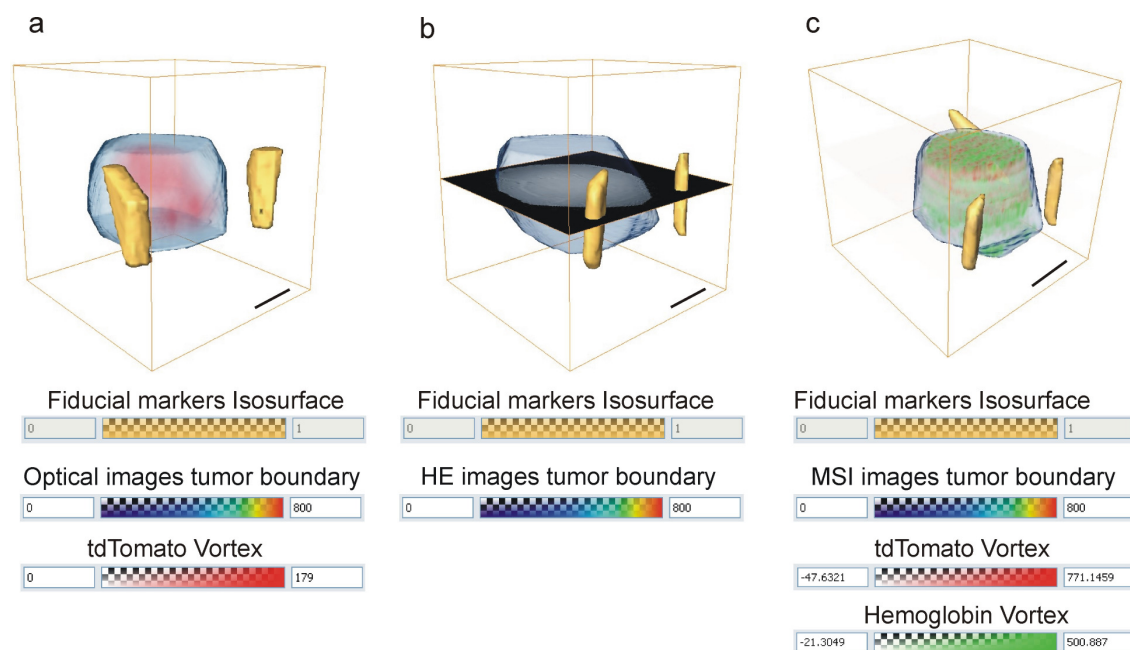
Figure 3.7 Application of fiducial markers for 3D reconstruction of optical imaging and MSI data. (A) 3D reconstruction of the hypoxic region based on optical microscopy images from 2

mm thick tumor sections. The fluorescence signal from tdTomato is shown in red. The tumor boundary was reconstructed based on the tissue shape visualized by optical microscopy. (B) 3D reconstruction of H&E stained tumor sections. The tumor boundary was reconstructed based on the tissue shape obtained from H&E stained images. (C) 3D reconstruction of the tumor imaged by MSI. The actin tryptic-peptide at m/z 1198.7 was used for reconstruction of the tumor boundary. The hemoglobin tryptic-peptide at m/z 1529.7 shown in green was used to visualize the distribution of blood inside the tumor. The tdTomato tryptic-peptide at m/z 2225.0 (in red) was used for reconstruction of the hypoxic region inside the tumor. Scale bars, 500 μm. Reprinted with permission from ref[366]. Copyright 2012 American Chemical Society.

The co-registration of the 3D volumes obtained from bright field/fluorescence microscopy data (figure 3.7A) and MSI data (figure 3.7C) is shown in figure 3.8A, and from the H&E histological staining (figure 3.7B), and MSI data (figure 3.7C) in figure 3.8B. A vertical fiducial marker based rigid registration and a tumor shape based warping was applied to bright field/fluorescence microscopy data in order to perform 3D co-registration of these different modalities.

This example demonstrates the added value of an MS compatible fiducial marker based co-registration in a multimodal molecular imaging experiment. It allows for the accurate reconstruction and registration of 3D tissue volumes without damage to the tissue itself based on the physicochemical properties of the fiducial markers detected in all imaging modalities employed in this study.
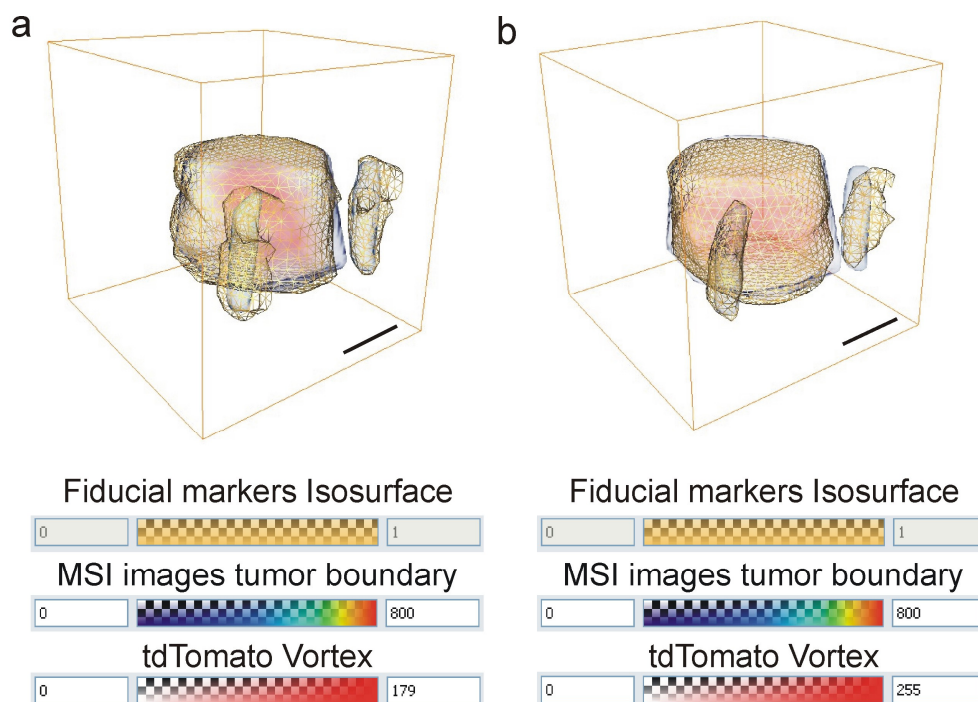
Figure 3.8 Co-registration of 3D images from optical imaging, H&E imaging and MSI based on the position of the fiducial markers. (A) Co-registration of MSI data (gray) and optical imaging data (tumor boundary shown as mesh, hypoxic region in red). (B) Co-registration of MSI data (actin in gray, tdTomato in red) and H&E imaging data (mesh). Scale bars 500 µm. Reprinted with permission from ref[366]. Copyright 2012 American Chemical Society.

Multimodal molecular imaging including bright field/fluorescence imaging, MSI, and histological imaging of the same tissue requires the presence of clear fiducial markers for co-registration, ion intensity normalization, and 3D reconstruction of these different modalities. PS provided an intense red color, no diffusion after ethanol treatment, and exhibited good ionization properties in negative ion mode, but due to its chemical structure did not produce any signal in positive ion mode. CV had an intense violet color, good fluorescence properties, and ionized well in positive ion mode, but dissolved slightly in ethanol during tissue washing, and did not ionize in negative ion mode. The 1:1 mixture of CV and PS fulfilled all requirements for a multimodal marker for imaging in both positive and negative ion modes, showed adequate stability during washing, and had excellent optical properties. The fluorescence properties of CV can be used for co-registering fluorescence images, such as for example images of tdTomato fluorescent protein, which is expressed under hypoxic conditions in the studied tumor model.

BB ionized in both positive and negative ion modes and could be used as a fiducial marker. However, its pH dependent color change to yellow color reduced its practicability due to poor

contrast in the optical images taken after matrix deposition. In this case ion images can be co-registered with optical images of the tissue obtained before matrix deposition.

In the future, co-registration of different imaging modalities may allow an image-based evaluation of disease boundaries based on molecular properties determined by MRI, histology, IHC, or MSI, and can be applied in preclinical studies to measure the effectiveness of new molecular therapies. Moreover, a range of biomedical imaging applications may benefit from multimodal molecular histology, including measuring the effects of laser,[368] radiofrequency,[369] or ultrasound[370] thermal ablation therapies. Their successful application and interpretation will be crucially dependent on accurate co-registration. The fiducial markers and their application described in this manuscript will be key in the automated generation of high-throughput molecular volumes.

3.4 Conclusions

Fiducial markers such as cresyl violet, Ponceau S, and bromophenol blue proved useful for multimodal image co-registration, 3D image alignment, MSI ion intensity normalization, and 3D reconstruction. Our data demonstrate that a 1:1 mixture of cresyl violet and Ponceau S is optimal for combining bright field, fluorescence, and histological imaging with positive and negative ion MSI, resulting in co-registered, 3D-reconstructed, fused multimodal image data sets.

Chapter 4

Mass Spectrometric Imaging of Red Fluorescent Protein in Breast Tumor Xenografts

4. Mass Spectrometric Imaging of Red Fluorescent Protein in Breast Tumor Xenografts[*]

MSI in combination with electrospray ionization mass spectrometry (ESI-MS) is a powerful technique for visualization and identification of a variety of different biomolecules directly from thin tissue sections. As commonly used tools for molecular reporting, fluorescent proteins are molecular reporter tools that have enabled the elucidation of a multitude of biological pathways and processes. To combine these two approaches, we have performed targeted MS analysis and MALDI-MSI visualization of a tdTomato red fluorescent protein, which was expressed exclusively in the hypoxic regions of a breast tumor xenograft model. For the first time, a fluorescent protein has been visualized by both optical microscopy and MALDI-MSI. Visualization of tdTomato by MALDI-MSI directly from breast tumor tissue sections will allow us to simultaneously detect and subsequently identify novel molecules present in hypoxic regions of the tumor. MS and MALDI-MSI of fluorescent proteins, as exemplified in our study, is useful for studies, in which the advantages of MS and MSI will benefit from the combination with molecular approaches that use fluorescent proteins as reporters.

4.1 Introduction

MSI is nowadays a widely used technique for detection and visualization of a variety of different biomolecules directly from thin tissue sections of different origin.[371] MSI is an excellent molecular discovery tool because of its imaging capabilities that cover a broad range of biomolecules of different chemical composition and biological properties, allowing the exploration of complex biological tissue surfaces. In addition, there is no requirement for labeling procedures or *a priori* knowledge about a sample's biochemical composition when performing MSI. MSI easily combines with other imaging techniques, such as optical microscopy, thereby adding additional molecular imaging information to the biological processes under investigation.

The tdTomato protein belongs to the family of fluorescent proteins, which are often used as genetically encoded fusion tags in biomedical applications that utilize cell cultures and animal models.[372] tdTomato is a <u>t</u>andem <u>d</u>imer (td) generated by linking together, via a short random coil sequence, two mutated 28 kDa monomer units of the tetrameric DsRed fluorescent protein.[373,374] The monomer unit of tdTomato was specifically selected based on its low propensity to aggregate and because it is nontoxic. The generation of the dimer gives the protein an exceptional brightness.[372,375] Thus, the combination of a high quantum yield of 0.69 with an extinction coefficient per chain of 138,000 $M^{-1}cm^{-1}$, makes tdTomato the brightest of the currently available fluorescent proteins.[351] Additionally, tdTomato retains desirable physical characteristics observed in many of the smaller monomeric fluorescent proteins, such as a relatively short maturation half-time of one hour at 37°C and excellent photostability, all of which make it useful for *in vivo* optical imaging studies.[351] It has been widely used in biomedical studies for the detection of proteins of interest fused to tdTomato as a fluorescent reporter,[376] as well as in studies of noninvasive optical tracking of cancer cells *in vivo*.[352] In the latter case, it has been established that its emission is readily detectable at or above 620 nm, which is outside the range of absorption and autofluorescence of living tissue.[352] Due to these characteristics, along with its brightness, tdTomato can be detected as deep as 1 cm below the tissue surface. These properties facilitate its use in *in vivo* fluorescence imaging studies in real-time in live animal models.[352,377] Bioimaging that employs tdTomato fluorescent protein as a fluorescent label has multiple benefits over other techniques in which fluorescent dyes or bioluminescence are used.[352]

Here our goal was to detect, identify and visualize the tdTomato protein present in human breast tumor xenograft models by using a multimodal imaging approach that merged optical microscopy and MSI combined with bottom-up proteomics. In our study, tdTomato was used to visualize hypoxic tumor regions, which contribute to tumor aggressiveness, in a genetically engineered tumor xenograft model.[363] The ability to detect tdTomato in the hypoxic regions of this breast tumor model with MSI will enable us to use MSI to map biomolecules that are up- or down-regulated in hypoxic tumor regions. Understanding such hypoxia-induced changes in cancer is crucial for developing novel more effective tumor therapies that can target the often chemo- and radio-resistant hypoxic regions in tumors.

4.2 Materials and methods

Chemicals and materials. The matrix CHCA was purchased from Sigma-Aldrich (Germany), ethanol, acetic acid, water, ACN and TFA were purchased from Biosolve (The Netherlands). Dithiothreitol (DTT), iodoacetamide (IAA) and ammonium bicarbonate (NH_4HCO_3) were purchased from Sigma (Germany). Formic acid for mass spectrometry (98%) was purchased from Fluka (Germany). Modified proteomics grade trypsin was purchased from Sigma (Germany) or Promega (USA). Cresyl violet acetate and gelatin Type A were purchased from Sigma (USA).

Mass spectrometric analysis of cell lysates. MDA-MB-231-EF1α-tdTomato cells[352] were grown under standard cell culture conditions in RPMI medium. MDA-MB-231-EF1α-tdTomato cells were collected and lysed using ProteaPrep Cell Lysis Kit (Protea Biosciences, Inc., USA) according to the manufacturer's protocol. Protein concentrations of lysates were determined using the Bio-Rad Protein Assay (BioRad DC, USA, Cat no 500-0116). NATIVE-PAGE (Bio-Rad, USA) was run in Tris/glycine buffer without SDS added. The 8% gel was loaded with 45 µg of total protein and the red fluorescent band was cut out under a home-built fluorescent lamp equipped with a Gemini 300 high intensity, short arc light source, a 600 to 660 nm emission filter, and a Nikon Coolpix digital camera (Nikon Instruments, Inc, Melville, NY). Gel pieces were frozen at -80ºC until further analysis.

MALDI-MS analysis of gel bands: The fluorescent gel bands were sliced into several gel pieces of 1 mm x 1 mm size and 50 µL of 2:1 ACN:25 mM NH_4HCO_3 was added for 15 min. The supernatant was removed and 50 µL of 25 mM NH_4HCO_3 was added for 10 min. The last two steps were repeated and followed by a final wash in 2:1 ACN:25 mM NH_4HCO_3 for 15 min. The supernatant was removed and the gel pieces were dried in a speed vacuum

centrifuge. Trypsin prepared in 25 mM NH_4HCO_3 at a concentration of 12.5 ng/µL was added to the gel pieces and incubated on ice for 20 min. Following incubation, 25 mM NH_4HCO_3 buffer was added to cover the gel pieces, followed by incubation at 37ºC for 4.5 h. Peptides were extracted by first pooling the supernatant into a second tube and adding 50 µL 2:1 ACN:25 mM NH_4HCO_3 to the gel pieces, followed by 15 min incubation in a shaker at RT. The supernatant was collected and transferred to the tube containing the supernatant from the previous extraction. Then, 100% ACN was added to the gel pieces and the tube was shaken for 20 min at RT. The supernatant was removed and transferred to a tube containing supernatant from the previous extractions. The supernatant was dried down to approximately 10 µL using a speed vacuum microcentrifuge and then mixed with CHCA matrix prepared at a concentration of 10 mg/mL in 1:1 ACN:H_2O/0.1% TFA. This mixture was spotted on a MALDI target plate for MS analysis with a Q-TOF instrument (Synapt, Waters, UK).

LC-ESI-MS analysis of gel bands: The fluorescent gel bands were cut into small pieces and washed with 250 µL milliQ. After removing milliQ, 100% ACN was added, the gel pieces were vortexed, and ACN was removed. The gel pieces were covered with ACN, vortexed and incubated for 15 min at RT. ACN was removed and 100 µL of 10 mM DTT in 50 mM NH_4HCO_3 was added. Gel pieces were incubated in a shaker for 1 h at 60°C. DTT was removed and samples were cooled to RT. One hundred percent ACN was added to cover the gel pieces, vortexed, removed, and a new portion of ACN was added to cover the gel pieces followed by vortexing and incubation for 15 min at RT. ACN was removed and 100 µL of 54 mM fresh IAA was added and incubated at RT in the dark for 30 min. Iodoacetamide was removed and 100% ACN was added to cover the gel pieces, vortexed, and removed. This step was performed once more. The following washing procedure was performed twice: 100 µL of 50 mM NH_4HCO_3 was added, vortexed and incubated for 15 min at RT. After the ammonium bicarbonate was removed, two times 100 µL of 100% ACN was added, vortexed, and removed. Trypsin solution was prepared in 50 mM NH_4HCO_3 at a concentration of 3 ng/µL and 20 µL of this trypsin solution was added to cover the gel pieces, followed by incubation on ice for 90 min. Excess trypsin was removed and 20 µL of 50 mM NH_4HCO_3 was added, followed by overnight incubation at 37°C. Then, the first supernatant was transferred to a new tube and 100 µL of 100% ACN were added to the gel pieces, vortexed and incubated for 15 min at RT. This ACN treatment was repeated three times and each time the supernatants were pooled. The pooled supernatant was dried in a vacuum microcentrifuge and 40 µL of 10%

formic acid was added prior to LC-MS analysis using an LTQ Orbitrap mass spectrometer (Thermo Fisher) equipped with a nanoHPLC system (Agilent).

Breast tumor imaging. The human breast cancer cell line MDA-MB-231 was genetically modified to express tdTomato red fluorescent protein under the control of hypoxia response elements as previously described.[378] Cells in 0.05 mL of Hank's Balanced Salt solution (Sigma) were injected into the upper thoracic mammary fat pad of athymic nude mice ($2x10^6$ cells/injection) and tumor growth was monitored with standard calipers. When tumors reached a volume of approximately 500 mm^3, mice were sacrificed and tumors were removed. Each tumor was embedded into a gelatin block prepared using 15 mm x 15 mm x 5 mm cryomolds (Sakura Finetek, USA), 10% gelatin, cooled to 30°C in order to prevent tissue degradation, and three cresyl violet fiducial markers, which were injected inside the gelatin block next to the tumor as previously described.[379-381] This block was sectioned into serial 2 mm thick fresh tumor sections using an acrylic adjustable tissue slicer (12 mm depth up to 25 mm width; Braintree Scientific, Inc, Braintree, MA) and tissue slicer blades (Braintree Scientific, Inc). These serial fresh tumor xenograft sections were each placed on individual microscope slides (Fisherbrand catalogue number 12-550-34; Fisher Scientific, Pittsburgh, PA), and stored in an ice-box containing ice on the bottom, with the slides located on a perforated plate at approximately 1 cm above the ice to minimize tissue degradation. Fresh sections were imaged by bright field and fluorescence microscopy with a 1x objective attached to a Nikon inverted microscope, equipped with a filter set for 528 to 553 nm excitation and 600 to 660 nm emission, and a Nikon Coolpix digital camera (Nikon Instruments, Inc, Melville, NY). Bright field microscopy captured the position of the fiducial markers inside the gelatin block as well as the shape of the tumor tissue. The fluorescence of tdTomato expression in hypoxic regions of these tumor sections was detected by fluorescence microscopy. All 2 mm thick sections were snap frozen immediately after microscopic imaging. From each 2 mm thick section, 10 µm thick sections were cut at -16°C for MSI using a Microm HM550 cryo-microtome (Microm International GmbH, Walldorf, Germany). A distance of 500 µm was kept between all 10 µm thick sections. Tissue sections for MSI analysis were mounted onto 25 mm x 50 mm x 1.1 mm, Rs=4-8 Ω ITO coated slides (Delta Technologies, USA).

Prior to MSI analysis, tissue sections were briefly washed by immersing them twice in 70% ethanol and dried in a vacuum desiccator for 10 min. Trypsin was resuspended in water at a concentration of 0.05 µg/µL, and 5 nL per spot in a 150 µm x 150 µm raster was deposited by a CHIP-1000 piezo electric spotting robot (Shimadzu, Japan). After trypsin deposition, tissue

sections were incubated in a humid chamber at 37ºC for 12 h. CHCA matrix was prepared at a concentration of 10 mg/mL in 1:1 ACN:H_2O/0.1% TFA and applied by an ImagePrep (Bruker Daltonics GmbH, Bremen, Germany) application system. Samples were analyzed on a MALDI-Q-TOF (Synapt HDMS, Waters, U.K.) instrument in TOF mode detecting positive ions. The images were acquired at a spatial resolution of 150 µm × 150 µm.

Image analysis. Co-localization analysis was performed to quantify the correlation between tdTomato MSI image and the corresponding optical tdTomato fluorescence image. A total of three 10 µm thick cryo-sections, which were used for MSI, were obtained from the corresponding 2 mm thick fresh tissue section, which was scanned by microscopic imaging. Since the thickness of the tissue sections for MSI is much smaller than that of the sections used to obtain optical bright field and fluorescence images, the MSI images were subjected to a projection operation along the thickness direction of the data. This projection operation consisted of the following steps: 1) the three MSI images were aligned by the centroid positions of the external fiducial markers; 2) then those three aligned MSI images were summed up to obtain total ion abundance. Since the spatial resolution of an MSI image is also much lower than that of an optical bright field/fluorescence image and the noise level of an MSI image is much higher than that of an optical bright field/fluorescence image, a nonlinear two-dimensional median filtering method was applied to reduce the noise and preserve the tumor edge in the summed-up MSI image. A combined fiducial marker and tumor boundary based image registration method[380,381] was applied to both the summed-up MSI image and the optical bright field/fluorescence image. The tumor region was masked out by the active shape model in all images.[380,381] The scattering distribution of the registered MSI ion intensity and optical fluorescence signal were plotted against each other, and the resulting Pearson's correlation coefficient was calculated to investigate the linearity between registered MSI ion image and optical fluorescence image.

4.3 Results and discussion

We have for the first time performed MS bottom-up analysis of the tdTomato fluorescent protein, and have subsequently imaged tdTomato with MSI from a tissue containing tdTomato by means of on-tissue digestion and MSI detection of a tdTomato-specific peptide.

tdTomato protein isolation and MS analysis

In order to simplify the search for the tdTomato protein in our MSI experiments, we wanted to obtain a set of reference peptides that can be retraced in the tissue imaging experiments. To

this end, we performed bottom-up MS preceded by LC as a separation step and ESI, which we combined with MALDI-MSI for targeted identification of our molecule of interest (tdTomato). This approach is advantageous when the identification of molecules of interest directly from tissue sections is difficult due to the high complexity of the sample and ion suppression effects.[382] We isolated tdTomato red fluorescent protein from the MDA-MB-231-EF1α-tdTomato breast cancer cell line in which tdTomato was constitutively expressed under the strong elongation factor 1α (EF1α) promoter.[352] After cell lysis and NATIVE-PAGE electrophoresis, the red fluorescent band was cut out and subjected to in-gel trypsin digestion followed by MALDI-MS as well as LC-ESI-MS analysis. LC-ESI-MS identified 10 peptides with different charge states (z) as shown in Table 4.1. Out of those 10 identified peptides of tdTomato protein by LC-ESI-MS, we identified and imaged one peptide at *m/z* of 2225.0 with the amino acid sequence LDITSHNEDYTIVEQYER by MALDI-MS analysis as shown in figure 4.1. This MALDI identified peptide was additionally observed by LC-ESI-MS as both doubly and triply charged ions.
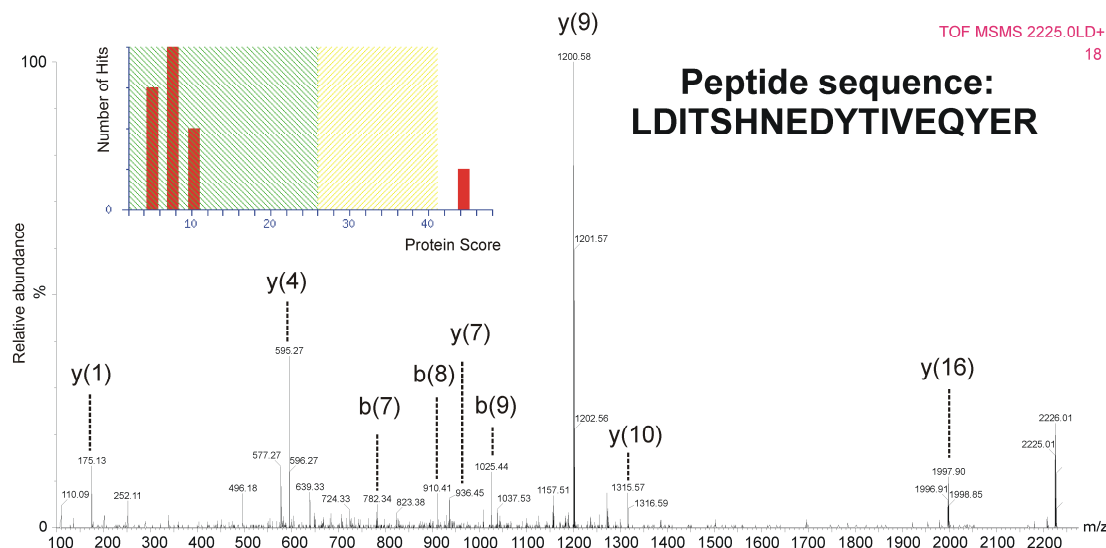

Figure 4.1 MALDI-MS fragmentation of the peptide [M+H]$^+$ at m/z 2225.0 from an in-gel digested 1D native gel band, which was identified as tdTomato peptide with the sequence LDITSHNEDYTIVEQYER.

Table 4.1 LC-ESI-MS and MALDI-MS analyses of tdTomato-containing gel pieces.

IM‡	exp *m/z*[a]	exp Mw[b]	calc Mw[c]	delta[d]	*z*[e]	mc[f]	sequence and modifications
ESI	462.7439	923.4732	923.4753	-0.0020	2	0	LSFPEGFK
ESI	526.7907	1051.567	1051.570	-0.0034	2	1	KLSFPEGFK
ESI	351.5302	1051.569	1051.570	-0.0015	3	1	KLSFPEGFK
ESI	528.2592	1054.504	1054.508	-0.0045	2	0	HPADIPDYK
ESI	582.7858	1163.557	1163.561	-0.0041	2	0	DGGHYLVEFK
ESI	388.8599	1163.558	1163.561	-0.0033	3	0	DGGHYLVEFK
ESI	584.2564	1166.498	1166.503	-0.0043	2	0	TMGWEASTER
ESI	592.2539	1182.493	1182.498	-0.0044	2	0	TMGWEASTER Oxidation (M)[g]
ESI	592.3061	1182.598	1182.603	-0.0057	2	1	HPADIPDYKK
ESI	395.2079	1182.602	1182.603	-0.0015	3	1	HPADIPDYKK
ESI	648.3034	1294.592	1294.598	-0.0053	2	1	KTMGWEASTER
ESI	432.5382	1294.593	1294.598	-0.0048	3	1	KTMGWEASTER
ESI	656.3015	1310.588	1310.593	-0.0041	2	1	KTMGWEASTER Oxidation (M)
ESI	437.8701	1310.588	1310.593	-0.0040	3	1	KTMGWEASTER Oxidation (M)
ESI	465.9047	1394.692	1394.698	-0.0059	3	1	LSFPEGFKWER
ESI	469.2523	1404.735	1404.740	-0.0049	3	1	LKDGGHYLVEFK
ESI	703.3760	1404.738	1404.740	-0.0026	2	1	LKDGGHYLVEFK
ESI	1113.019	2224.023	2224.028	-0.0058	2	0	LDITSHNEDYTIVEQYER
ESI	742.3483	2224.023	2224.028	-0.0054	3	0	LDITSHNEDYTIVEQYER
MALDI	2225.010	2224.010	2224.028	-0.0827	1	0	LDITSHNEDYTIVEQYER

‡IM – ionization method [a]exp *m/z* – experimental *m/z*, [b]exp Mw – experimental molecular weight, [c]calc Mw – calculated molecular weight, [d]delta- difference between exp *m/z* and calc Mw, [e]*z* – charge state, [f]mc – miscleavage, [g]M – methionine

Due to the compactness of the β-barrel structure of fluorescent proteins or non-fluorescent OmpA[383] and α-hemolysin,[384] these proteins are known to display a relatively high resistance to tryptic cleavage.[385,386] In-gel tryptic cleavage of <u>c</u>yan <u>f</u>luorescent <u>p</u>rotein (CFP) protein resulted in a sequence coverage of 50%.[386] Our in-gel digestion method resulted in 26% sequence coverage of the tdTomato protein. ESI ionization enabled the detection of multiple tdTomato peptides with different sequence, length and charge state, while MALDI ionization allowed for the detection of one, singly charged tryptic peptide. We employed this tryptic peptide for the first time to visualize the distribution of a fluorescent protein by MSI.

Microscopic imaging of tdTomato in tumor tissue

A human breast tumor xenograft model expressing tdTomato red fluorescent protein in the hypoxic regions was embedded in a gelatin block containing fiducial markers as previously published.[379-381] The gelatin blocks were sectioned into three 2 mm thick sections for *ex vivo* microscopic visualization of the red fluorescent protein. Figure 4.2 demonstrates multimodal imaging of the 2 mm section obtained from the tumor centre. The corresponding bright field (figure 4.2A) and fluorescence (figure 4.2B) images were co-registered based on the position of the fiducial markers (M), which were visible in both bright field and fluorescence images.

Figure 4.2C presents an overlay of the bright field and fluorescence images. Letters "M" indicate the positions of the fiducial markers used for co-registration of both images. In image overlay (figure 4.2C) the fluorescence image of tdTomato has been changed to black for better visualization of the hypoxic regions. Figure 4.2D shows the false color image of tdTomato fluorescence intensity obtained from the 2 mm tumor section shown in figure 4.2B.
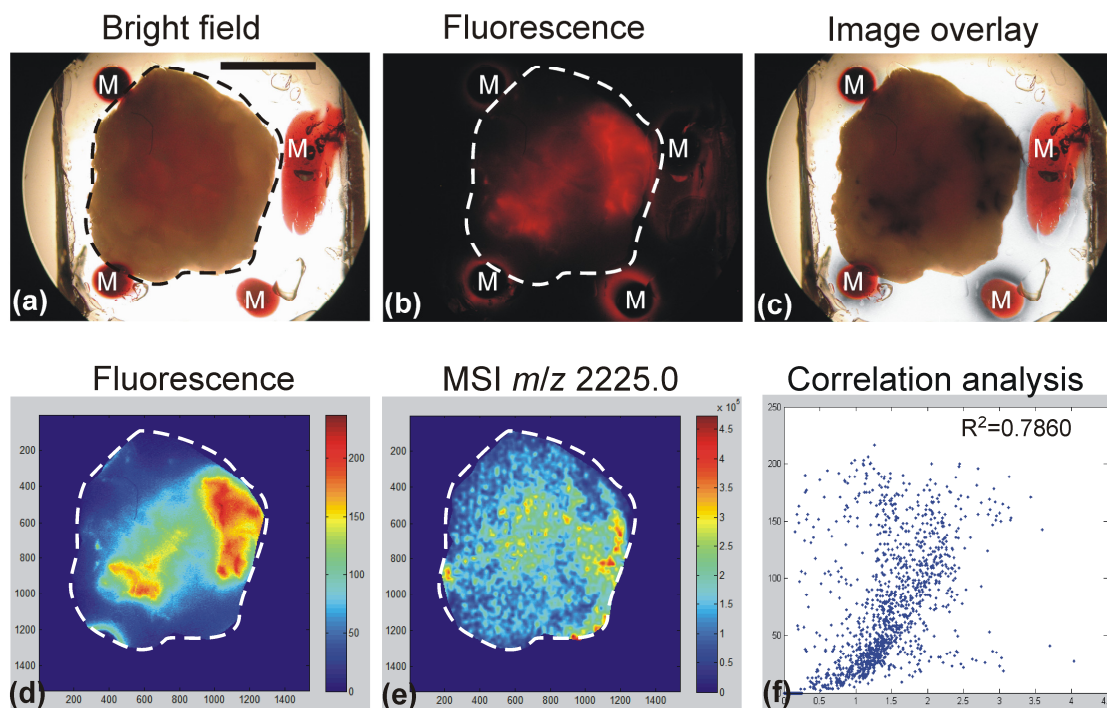
Figure 4.2 Multimodal imaging of tdTomato protein expressed in the hypoxic regions of the MDA-MB-231-HRE-tdTomato breast tumor xenograft. (A) Bright field microscopy of 2 mm tumor section obtained for visualizing tumor boundary. The tissue boundary is outlined by a dashed line. (B) Imaging of the hypoxic tumor regions expressing a red fluorescent protein tdTomato by fluorescence microscopy directly from the 2 mm tumor section. (C) Overlay of images acquired by bright field and fluorescence microscopy. Letters "M" indicate positions of fiducial markers used for co-registration of both images. The fluorescent image of tdTomato has been changed to black for better visualization of the hypoxic regions. (D) False color image of tdTomato expression obtained from the 2 mm tumor section show in (B). (E) False color image of tdTomato peptide [M+H]$^+$ at m/z 2225.0 detected from three 10 μm sections obtained from the 2 mm tumor section shown in (A). (F) Correlation analysis plot resulting from the co-localization analysis of tdTomato images obtained by fluorescence microscopy (D) and MSI (E). The correlation coefficient R^2 was equal to 0.7860. Scale bar, 5 mm.

Mass spectrometric imaging of tdTomato in a tumor

After microscopic imaging, the gelatin-embedded tumor tissue was frozen and further sectioned into 10 µm thick sections for MSI. Three 10 µm thick sections were obtained from the central 2 mm tissue section and used for MSI. The MS-detected fiducial markers were used for alignment of MSI data sets obtained from three 10 µm thick sections. The detection of the tdTomato tryptic-peptide at *m/z* 2225.0 was used to localize by MSI the hypoxic regions, in which the tdTomato fluorescent protein was expressed driven by a <u>h</u>ypoxia <u>r</u>esponse <u>e</u>lement (HRE) containing promoter. Figure 4.2E presents the false color image of the tdTomato tryptic-peptide distribution at *m/z* 2225.0 obtained by MSI from three summed-up 10 µm thick sections. The plot shown in figure 4.2F presents the correlation analysis, which was obtained by co-localization analysis of the tdTomato images obtained by fluorescence microscopy *versus* MSI, and which resulted in a relatively high correlation coefficient R^2 of 0.7860. Figure 4.3 presents a zoomed in spectrum of the region around the ion at *m/z* 2225.0 detected from the hypoxic tissue region as shown in red and the normoxic region as shown in black. The tryptic peptide at *m/z* 2225.0, which was directly detected only from hypoxic, but not from normoxic tumor regions by MSI, was able to distinguish these two regions.
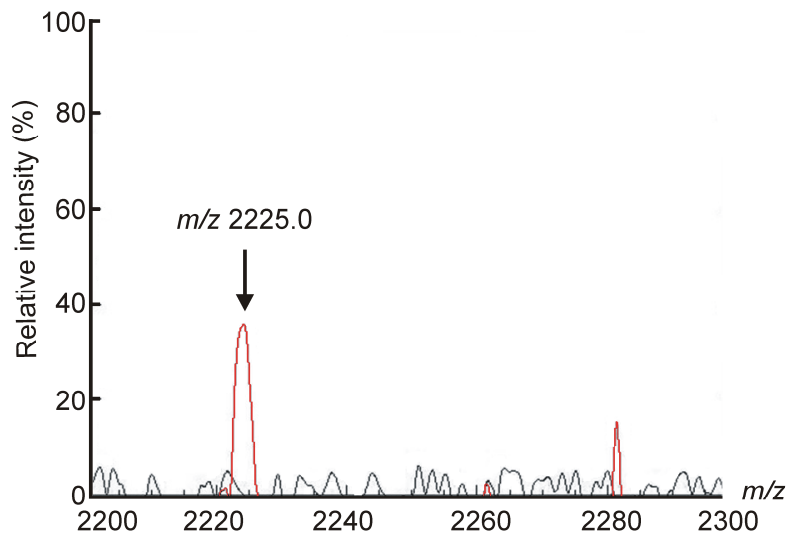

Figure 4.3 Spectrum of ions detected during a ROI analysis of the MSI data from a MDA-MB-231-HRE-tdTomato tumor section. The ROI-spectrum related to a hypoxic tumor region is shown in red with a peak at m/z 2225.0 (tdTomato tryptic peptide) indicated by an arrow. The spectrum recorded from a similarly sized ROI in a normoxic tumor region is shown in black.

In the present study, the normoxic regions of a given tumor tissue section are considered the negative control because they do not express the red fluorescent tdTomato protein. In comparison, the hypoxic regions from the same tumor section express tdTomato. To exclude the possibility of a potential endogenous signal at *m/z* 2225.0, a series of experiments on trypsin-digested tumor sections *versus* non-digested sections was performed. In the case of the non-digested sections, no signal with a signal-to-noise S/N>1 was detected at *m/z* 2225.0. Our proof-of-principle study demonstrated that MSI can be used in molecular studies in which the expression of a fluorescent protein needs to be mapped in tissue sections. MSI visualization of tdTomato directly from breast tumor tissue sections will allow us in the future to simultaneously detect the hypoxic regions and a multitude of different biomolecules in this tumor xenograft model. With this approach, we will be able to identify biomolecules that are up- or down-regulated in these hypoxic tumor regions.

4.4 Conclusions

This study highlights the benefits of multimodal molecular imaging of a breast tumor xenograft model. We have for the first time detected the tdTomato fluorescent protein by bottom-up MS analysis. Subsequently, we have imaged a tryptic peptide from tdTomato by MSI in tumor sections, in which tdTomato was expressed in hypoxic tumor regions of a breast tumor xenograft model genetically modified to express tdTomato under hypoxic conditions. MSI can provide biochemical information about the heterogeneous composition of the tumor tissue. The fusion of MSI with other *in vivo* or *ex vivo* imaging techniques can offer simultaneous detection and identification of multiple biomolecules of interest such as drugs, lipids, peptides and proteins, directly from a specific region of a thin tissue section.

Chapter 5

Mass Spectrometry Images Acylcarnitines, Phosphatidylcholines and Sphingomyelin in MDA-MB-231 Breast Tumor Models

5. Mass Spectrometry Images Acylcarnitines, Phosphatidylcholines and Sphingomyelin in MDA-MB-231 Breast Tumor Models[*]

The lipid compositions of different breast tumor microenvironments are largely unknown due to limitations in lipid imaging techniques. Imaging lipid distributions would enhance our understanding of processes occurring inside growing tumors such as cancer cell proliferation, invasion and metastasis. Recent developments in MALDI-MSI enable rapid and specific detection of lipids directly from thin tissue sections. In this study, we performed multimodal imaging of acylcarnitines, phosphatidylcholines (PC), a lysophosphatidylcholine (LPC) and a sphingomyelin (SM) from different microenvironments of breast tumor xenograft models, which carried tdTomato red fluorescent protein as a hypoxia-response element driven reporter gene. The MSI molecular lipid images revealed spatially heterogeneous lipid distributions within tumor tissue. Four of the most abundant lipid species, namely PC(16:0/16:0), PC(16:0/18:1), PC(18:1/18:1) and PC(18:0/18:1) were localized in viable tumor regions, while LPC(16:0/0:0) was detected in necrotic tumor regions. We identified a heterogeneous distribution of palmitoylcarnitine, stearoylcarnitine, PC(18:0/22:1) and SM(d18:1/16:0) sodium adduct, which mostly co-localized with hypoxic tumor regions. For the first time, we have applied a multimodal imaging approach that has combined optical imaging and MALDI-MSI with ion mobility separation to spatially localize and structurally identify acylcarnitine and a variety of lipid species present in breast tumor xenograft models.

5.1 Introduction

MALDI-MSI can detect, localize and identify multiple biologically relevant molecules directly from thin tissue sections without the necessity for any labeling.[371] The sample preparation of thin tissue sections for MALDI-MSI requires the application of laser absorbing matrix crystals on the tissue surface. During an MSI experiment, the laser beam ablates the matrix coated tissue sample surface while the mass spectrometer acquires a collection of spectra that contain comprehensive information about the local biomolecular composition of the sample. Biomolecules present in the tissue are desorbed and separated by a mass spectrometer according to their *m/z* ratios. Each *m/z* value present in this spectral collection can be converted to an image by using dedicated imaging software. The chemical structure of each ion detected from the tissue surface can be identified after its isolation and fragmentation inside a mass spectrometer.

An additional advantage of MSI is its compatibility with other imaging techniques such as optical bright field and fluorescence microscopy. Such a multimodal approach is particularly useful for analyzing the molecular composition of complex, heterogeneous tumor tissue which comprises of several distinct tumor microenvironments. One example of such heterogeneity is tissue hypoxia, a state of low oxygen tension (pO$_2$ values ≤2.5 mmHg) observed in many solid tumors.[387] Hypoxia increases overall tumor aggressiveness, induces radio- and drug-resistance, triggers resistance to apoptosis, and enhances cellular migration and invasiveness eventually leading to cancer metastasis.[388] On a molecular level, hypoxia triggers many known and unknown metabolome, lipidome and proteome changes, that modulate tumor vascular expansion and provide an overall advantage for malignant growth, causing rapid disease progression.[389] Severe, prolonged hypoxia can lead to cell death and tissue necrosis.[389] Tumor expansion results in the formation of metabolically diverse, viable and necrotic, normoxic and hypoxic, vascularized and avascular tissue regions, which so far have not been imaged in a single experiment or by a single imaging technique. We hypothesize that these different tumor tissue regions have different distributions of metabolites and lipids. MSI has the capability of parallel detection and visualization of biomolecules present in these specific tissue microenvironments, which allows for a more comprehensive analysis of tumor biology.

Unlike cancer cell cultures, human tumor xenograft models in mice provide a three-dimensional, native-like environment for studying different aspects of tumor growth.[390] Additionally, tumor xenograft models allow for genetic modifications such as incorporation

of genes encoding fluorescent proteins for visualizing and monitoring selected processes such as the influence of tissue hypoxia on tumor extracellular matrix[353] or cancer metastasis.[391]

MALDI-MSI is well suited for *ex vivo* detection and localization of different lipid categories and classes from samples of various origin and different sizes. MALDI-MSI has recently been applied in lipidome studies of human skin,[392] veins,[393] ovary,[394] mouse embryo implantation sites,[395] leg muscle,[396] tongue,[397] rat spinal cord,[398] cardiac tissue[399] and liver.[400] Mammalian brain tissue, due to its high lipid content, has also been extensively studied by MSI. Ion images of lipid distributions have been obtained for rat,[400-405] mouse[406,407] and human[408,409] brain sections. Lipid MSI has also been performed for various types of tumor tissue such as human brain tumors,[410] seminoma,[411] ovarian cancer,[412,413] myxoid liposarcomas,[414] human astrocytoma,[415] human prostate cancer tissue,[416] colon cancer liver metastasis[417] and human liver adenocarcinoma.[418]

Lipid-rich tumors have been associated with increased tumor aggressiveness and metastasis.[419-421] To develop effective cancer treatment strategies, it is crucial not only to identify but also to localize the lipid molecules involved in cancer progression. So far, lipid distributions in breast tumors remain largely unknown due to limitations in lipid imaging methods, which often require incorporation of fluorescent tags and provide limited specificity.[422-424] Here, we have adopted a novel multimodal imaging approach, which integrates microscopy and MSI, for a label-free, *ex vivo* visualization of different phospholipids directly from breast tumor xenograft tissue sections. We present spatial distributions of a SM and multiple PC species, which were co-localized either with normoxic, hypoxic or necrotic tumor regions. MSI also localized the distribution of two acylcarnitine molecular ions, which were identified from tumor tissue by ion mobility separation followed by tandem mass spectrometry. We demonstrated that the incorporation of MSI into a multimodal imaging approach revealed the molecular complexity of tumor tissue at an unprecedented level.

5.2 Materials and methods

Chemicals and materials. The matrix CHCA was purchased from Sigma-Aldrich (Germany). Water, ACN and TFA were purchased from Biosolve (The Netherlands). Cresyl violet acetate, Ponceau S and paraformaldehyde powder were purchased from Sigma-Aldrich (USA). Gelatin Type A was purchased from Sigma (USA). Mayer's hematoxylin was purchased from Sigma (USA), and aqueous Eosin Y from EMD Chemicals Inc. (USA).

Cytoseal 60 Mounting Medium, Richard-Allan Scientific was purchased from Thermo Scientific (USA).

Breast tumor xenograft model. The MDA-MB-231 human breast cancer cell line was purchased from the ATCC and used within 6 months of obtaining them from ATCC. This cell line was tested and authenticated by ATCC by two independent methods: the ATCC cytochrome C oxidase I PCR assay and short tandem repeat profiling using multiplex PCR. The MDA-MB-231 cell line was genetically modified to express tdTomato red fluorescent protein under the control of hypoxia response elements (MDA-MB-231-HRE-tdTomato) as previously described.[425] Cells were injected into the upper thoracic mammary fat pad of athymic nude mice ($2x10^6$ cells/injection) and tumor growth was monitored with standard calipers. The research was conducted in conformity with the Public Health Service (PHS) Policy on Humane Care and Use of Laboratory Animals. All experimental animal protocols were approved by the Institutional Animal Care and Use Committee of the Johns Hopkins University School of Medicine.

Tumor dissection and optical imaging. When tumors reached a volume of approximately 500 mm^3, mice were sacrificed and tumors were removed. Three individual tumors were embedded into 10% gelatin blocks prepared using 15 mm x 15 mm x 5 mm cryomolds (Sakura Finetek, USA). Cresyl violet acetate and Ponceau S were prepared in 10% warm (37ºC) gelatin at a concentration of 10 mg/mL, mixed in 1:1 ratio and injected into 10% gelatin blocks next to the tumor tissue. Each block was sectioned into serial 2 mm thick fresh tumor sections using an acrylic adjustable tissue slicer (12 mm depth up to 25 mm width; Braintree Scientific, Inc, Braintree, MA) and tissue slicer blades (Braintree Scientific, Inc) as previously described.[426,427] These serial fresh tumor xenograft sections were each placed on individual microscope slides (Fisherbrand catalog number 12-550-34; Fisher Scientific, Pittsburgh, PA), and stored in an ice-box containing ice on the bottom, with the slides located on a perforated plate at approximately 1 cm above the ice to minimize tissue degradation.[426,427] These fresh sections were imaged by bright field and fluorescence microscopy with a 1x objective attached to a Nikon inverted microscope, equipped with a filter set for 528 to 553 nm excitation and 600 to 660 nm emission, and a Nikon Coolpix digital camera (Nikon Instruments, Inc, Melville, NY). Bright field imaging captured the position of the fiducial markers present inside the gelatin block as well as the shape of the tumor tissue. The fluorescence from tdTomato expression in hypoxic regions of these tumor sections was detected by fluorescence microscopy. The GIMP 2.6 was used for 2D co-registration and overlay of bright field and fluorescence images of 2 mm thick tumor sections.

All 2 mm thick sections were snap-frozen immediately after microscopic imaging and stored at -80 °C until further analysis.

Tumor sectioning. From each 2 mm thick section, 10 µm thick sections were cut at -16°C for MSI using a Microm HM550 cryo-microtome (Microm International GmbH, Walldorf, Germany) along with adjacent 10 µm thick sections for histological staining. Tissue sections for MSI analysis were mounted onto 25 mm x 50 mm x 1.1 mm, R_s=4-8 Ω ITO coated slides (Delta Technologies, USA) and for histological staining onto Superfrost Slides (VWR International, Cat. 48311-600).

H&E staining method. Tissue sections were stained using a modified H&E staining protocol as previously described.[366,426,427] Briefly, 10 µm sections attached to Superfrost Slides (VWR International, Cat. 48311-600) were washed with PBS, fixed with freshly depolymerized 3% paraformaldehyde solution for 30 min, washed with dH_2O, and treated with Mayer's hematoxylin for 30 min at room temperature, followed by 5 washes with dH_2O. Sections were immediately immersed in aqueous Eosin Y for 30 min, followed by 5 washes with dH_2O, mounting with aqueous mounting medium, and attaching of a coverslip. Bright field images of H&E stained sections were acquired using 1x or 20x objectives attached to a Nikon microscope, equipped with a Nikon Coolpix digital camera (Nikon Instruments, Inc, Melville, NY).

MALDI-IMS-MSI. Six tissue sections obtained from three individual tumors were subjected to MSI analysis. Before MSI analysis, tissue sections were placed inside a vacuum desiccator for 30 min. CHCA matrix was prepared at a concentration of 10 mg/mL in 1:1 $ACN:H_2O$/0.1% TFA and was applied by an ImagePrep (Bruker Daltonics GmbH, Bremen, Germany) application system. Tissue sections were analyzed on a MALDI-Q-TOF (Synapt HDMS, Waters, UK) instrument in ion mobility separation mode detecting positive ions. Images were acquired with 150 µm x 150 µm spatial resolution and a 100 µm laser beam spot size. For better detection of masses above *m/z* 700 the instrument was set to suppress all masses below *m/z* 700. For 2D MSI analysis and overlay of images, data were visualized using BioMap software (Novartis, Basel, Switzerland). Ion mobility data analysis and visualization was performed by using DriftScope software (Waters, UK) as well as HDI software (version 31, Waters, UK). The LIPID MAPS (www.lipidmaps.org) was used to search for possible lipid structures.[318,428]

SIMS-MSI. Prior to SIMS analysis slides were placed inside a vacuum desiccator for 30 min, followed by gold-coating using a Quorum Technologies (New Haven, UK) SC7640 sputter coater equipped with a FT7607 quartz crystal microbalance stage and a FT690 film thickness

monitor to deposit a 1 nm thick gold layer. Data was acquired using a Physical Electronics TRIFT II (Physical Electronics, USA) SIMS-TOF equipped with an Au liquid metal ion gun tuned for 22 keV Au^+ primary ions. Images were acquired at a raster size of 101.56 µm over a 13 mm x 13 mm area, 3 seconds/tile. Data was analyzed and visualized using WinCadence software version 4.4.0.17 (Physical Electronics, USA).

Lipid identification by MS/MS analysis. The identification of selected lipid species was performed on-tissue in positive ion mode using a MALDI-Q-TOF instrument (Synapt, Waters, UK) after completing MSI experiments. Lipid ion precursors were selected within a 2 Da selection window and fragmented using 20-30 V collision energy applied in the trap cell (in TOF mode) or 30-40 V applied in the transfer cell (in IMS mode). Spectra were analyzed using MassLynx software (Waters, UK). Ion mobility separated ions were visualized by Driftscope software (Waters, UK) and selected drift time windows were exported to MassLynx for spectral analysis. Fatty acid chains of lipids of interest were identified from a combination of the mass of the lipid and the MS/MS fragmentation pattern obtained with a mass accuracy of 0.1 Da at *m/z* 1000. The LIPID MAPS, Human Metabolome Database version 2.5 (www.hmdb.ca) and the METLIN Metabolite Database (metlin.scripps.edu) were used to search for possible lipid structures and MS/MS fragmentation spectra.

Overlap analysis. We analyzed three MDA-MB-231-HRE-tdTomato breast tumor xenografts that were imaged by the multimodal approach described above. Necrotic tumor regions were outlined in H&E stained 10 µm thick sections. Hypoxic tumor regions were detected from the fluorescence images of tdTomato protein expression in 2 mm thick sections. The remaining tumor regions were normoxic. Ion images of each individual *m/z* were overlaid with the corresponding optical images and co-registered by using the positions of fiducial markers and tumor boundary as previously described.[426,427] The respective normoxic, hypoxic, or necrotic tumor region was masked by applying the active shape model to the registered optical bright field images.[429] The highest 5% of the area under the histogram of each image was automatically thresholded. The volume percentage of an ion's overlap with necrotic, hypoxic and necrotic regions inside tumor was calculated to quantify their co-localizations as previously described.[426,427] Volume percentage of hypoxia was defined as the number of hypoxic voxels that overlap with a given ion normalized to total hypoxic voxels in the tumor. Similarly, volume percentage of ions with normoxic voxels and necrotic voxels was measured. The image registration and co-localiztion analysis program was written in Matlab 2012b (Mathworks Inc., Natick, MA). Mean and standard error of overlap volume percentage

from tumors' centre sections (n=3) were calculated for each *m/z* and tumor region using MS Excel 2003.

5.3 Results

Multimodal imaging approach

We have employed a multimodal imaging approach for investigating the effects of tumor hypoxia and tumor necrosis on the regionally distinct, spatially heterogeneous lipid composition in a breast tumor model. In this approach, we have integrated optical microscopy with MSI. Bright field microscopy visualized the shape of the tumor, fluorescence microscopy outlined the position of hypoxic tumor regions, and histochemical staining revealed the localization of necrotic tumor tissue. MSI employing MALDI-MSI visualized the distribution of intact phospholipid molecular ions. All modalities were combined through the presence of fiducial markers visible in all imaging modalities.[366] Figure 5.1 presents results obtained from a representative breast tumor xenograft using our multimodal imaging approach. Figure 5.1A shows a bright field image of a 2 mm thick tumor section obtained from the tumor centre, which was embedded in a gelatin block containing the fiducial markers as described in materials and methods. Figure 5.1B presents the fluorescence image of tdTomato red fluorescent protein exclusively expressed in the hypoxic tissue regions of this genetically modified tumor model.[425] The co-registration of the bright field image (figure 5.1A) with the tdTomato fluorescence image (figure 5.1B) was performed based on the position of the fiducial markers, which were visible in both images. The red color of the tdTomato signal was changed to black for better visualization of the hypoxic tumor regions and subsequently overlaid on the bright field image of the tumor tissue as shown in figure 5.1C. Figure 5.1D presents the 10 µm thick section obtained from this tumor for MSI. The position of the fiducial markers as visualized by MSI (shown in figure 5.1E) was used for co-registration of the MSI dataset with the fluorescence image of tdTomato as shown in figure 5.1F. Figure 5.1G shows an adjacent 10 µm thick section stained with H&E for visualization of the necrotic tumor regions. Figure 5.1H presents the shape of the necrotic regions inside the tumor, which was outlined by a dotted line. Figure 5.1I shows the co-registration of the necrotic tumor regions obtained from the H&E image (figure 5.1H) with the hypoxic tumor regions from the fluorescence image (figure 5.1B). The fiducial markers were not clearly visible in some H&E images, in which case the co-registration was performed based on the tumor shape by using the ImageJ-TurboReg plug-in (http://rsb.info.nih.gov/ij). Magnified

images of viable and necrotic tumor regions as indicated in figure 5.1G are shown in figures 5.1J and K, respectively.
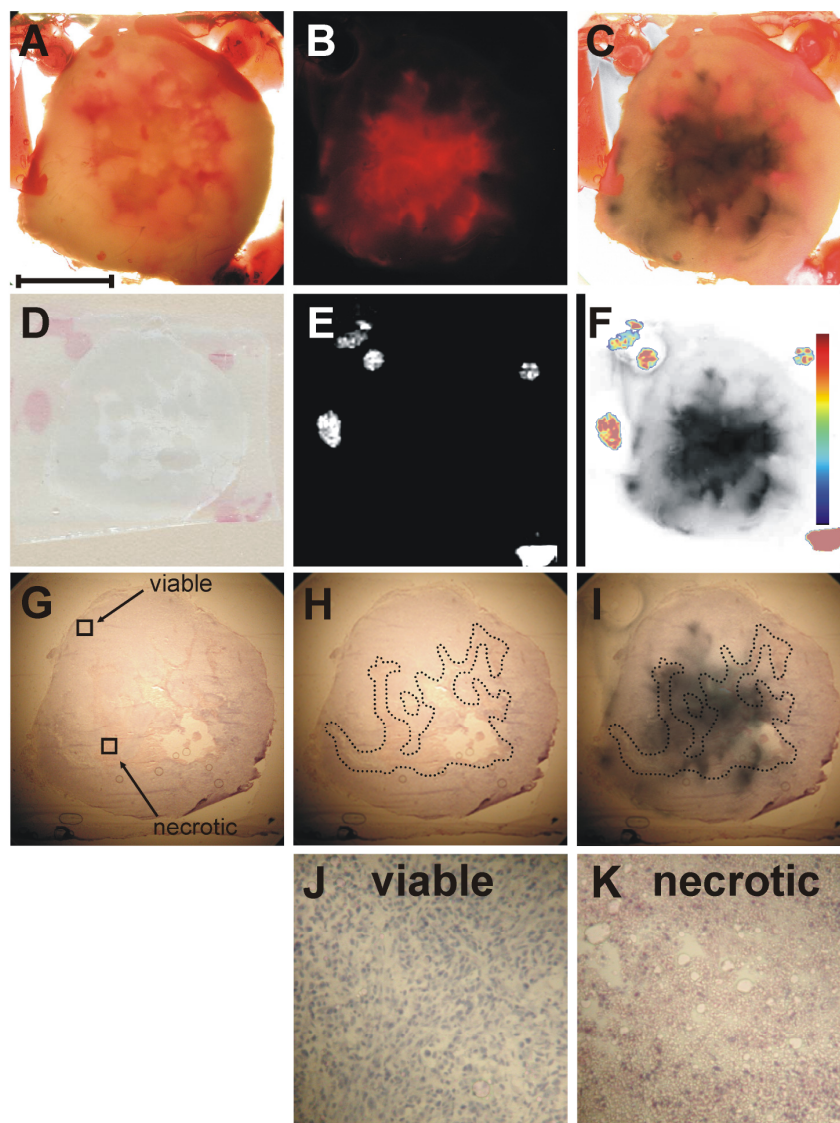
Figure 5.1 Co-registration of optical microscopy and mass spectrometric imaging. (A) Representative bright field image of a 2 mm thick fresh breast tumor tissue section embedded in gelatin containing fiducial markers. (B) Corresponding fluorescence image of tdTomato expression in the hypoxic tumor regions. (C) Co-registration of the bright field image shown in (A) and the fluorescence image shown in (B) based on the position of the fiducial markers present in both images. The red color of the tdTomato signal was changed into black prior to generating this overlay for better visualization of the hypoxic tumor regions. (D) Corresponding optical image of a thin tissue section used for MSI. (E) Corresponding MSI image of the fiducial markers. (F) Co-registration of fiducial markers imaged by MSI and the hypoxic regions imaged by fluorescence microscopy. (G) Image of the adjacent H&E stained

tissue section. (H) Image of the outlined necrotic tissue present inside the tumor. (I) Co-registration of the necrotic region visualized by H&E staining and the hypoxic region imaged by fluorescence microscopy. (J) Magnified image of the viable tumor region as indicated in (G). (K) Magnified image of the necrotic tumor region as indicated in (G). Scale bar, 5 mm A-I; 250 µm J-K.

Mass spectrometric analysis of lipids

Mass spectrometric imaging was employed directly on thin tumor tissue sections for detection, visualization and identification of a number of lipid biomolecules. Figure 5.2 presents selected molecular structures of acylcarnitine and lipids detected by MSI. These all biomolecules have a quaternary amine group, which can attain a positive charge, resulting in good ionization properties.

stearoylcarnitine, *m/z* 428.3
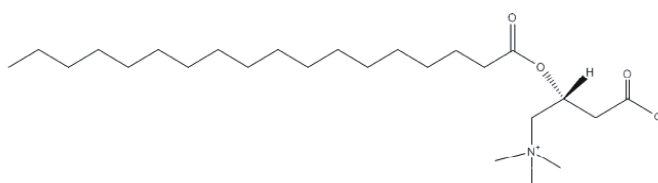
lysophosphatidylcholine, PC(16:0/0:0), *m/z* 496.3
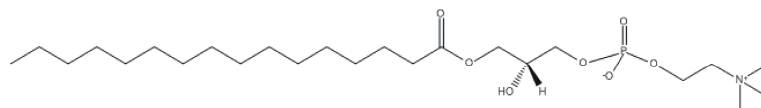
sphingomyelin, SM(d18:1/16:0), *m/z* 703.5
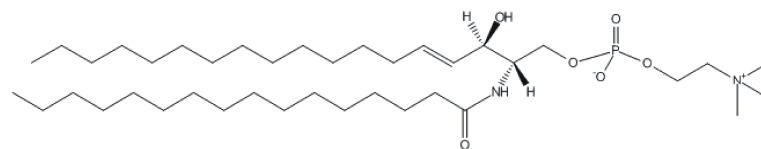
phosphatidylcholine, PC(16:0/18:1), *m/z* 760.5
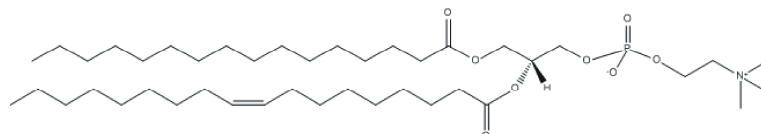
Figure 5.2 Representative examples of acylcarnitine and lipid molecular species such as stearoylcarnitine, LPC, SM and PC detected from tumor tissue by MSI. The molecular structures were obtained from LIPID MAPS (www.lipidmaps.org).

Figure 5.3 shows a representative combined mass spectrum of positively charged ions detected by MALDI-MSI from MDA-MB-231-HRE-tdTomato breast tumor xenograft tissue. In the low mass region, we observed phosphate-related metabolite ions at m/z 125.0 [M+H]$^+$, m/z 146.9 [M+Na]$^+$, and m/z 162.9 [M+K]$^+$, the phosphocholine at m/z 184.0 [M+H]$^+$ as well as a phosphocholine-related ion at m/z 198.0 [M+H]$^+$. Matrix-related ions were detected at m/z 172.0 [M-H$_2$O]$^+$, m/z 190.0 [M+H]$^+$ and m/z 379.0 [2M+H]$^+$. The fiducial marker cresyl violet was observed at m/z 262.0. Two acylcarnitines, palmitoylcarnitine and stearoylcarnitine, were observed at m/z 400.3 [M+H]$^+$ and at m/z 428.3 [M+H]$^+$, respectively. Lysolipid species were detected in the mass range from m/z 450 to m/z 550. Heme was observed at m/z 616.1 [M]$^+$ as a singly charged ion. Intact lipid molecular ions were detected as protonated ions as well as sodium and potassium salt adducts in the mass range from m/z 700 to m/z 860.
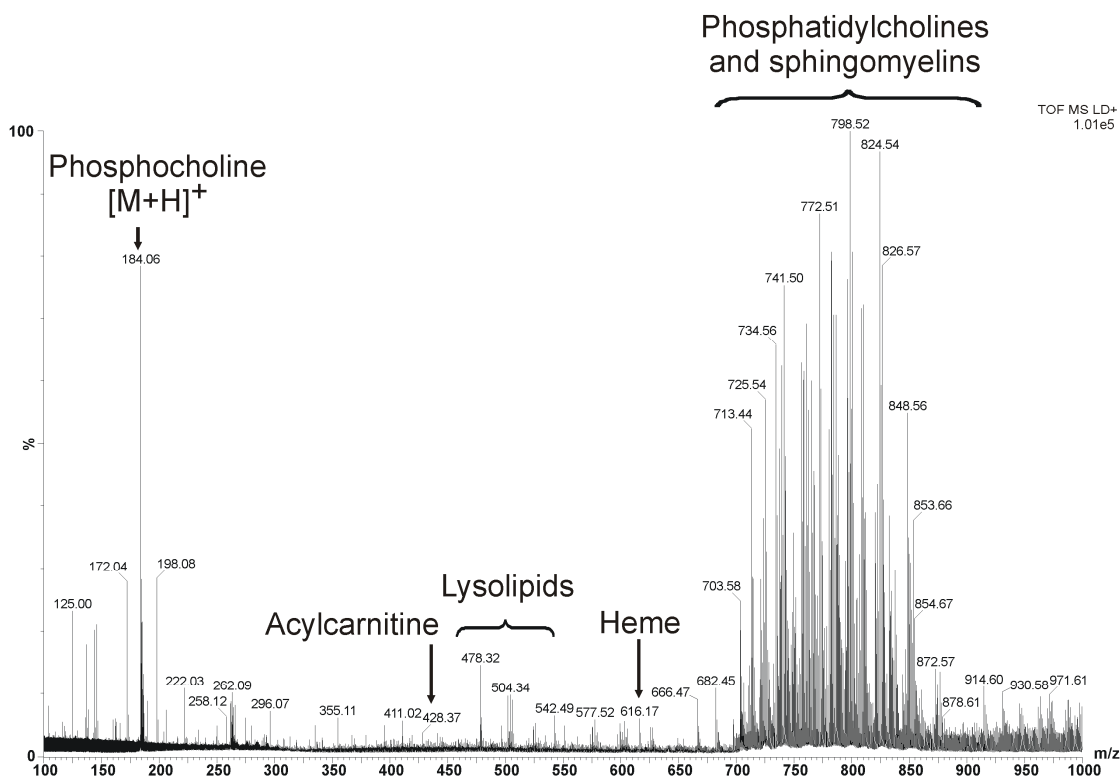
Figure 5.3 Representative combined mass spectrum detected by MALDI-MSI from a MDA-MB-231-HRE-tdTomato breast tumor xenograft. In the low mass range, we detected phosphate-containing ions at m/z 125.0, m/z 146.9 and m/z 162.9, the phosphocholine head group at m/z 184.0 and a related ion at m/z 198.0, matrix-related ions at m/z 172.0, m/z 190.0 and m/z 379.0, as well as the fiducial marker cresyl violet at m/z 262.0. Stearoylcarnitine was observed at m/z 428.3, and lysolipids were detected in the mass range from m/z 450 to m/z

550. The heme ion was present at m/z 616.1. Abundant intact phospholipid molecular ions were observed in the mass range from m/z 700 to m/z 860.

Figure 5.4 presents an expanded view of the spectrum shown in figure 5.3 showing multiple sphingomyelin and phosphatidylcholine species detected as proton, sodium and potassium adducts. We detected and identified protonated species of SM(d18:1/16:0) at *m/z* 703.5, PC(16:0/16:0) at *m/z* 734.5, PC(16:0/18:1) at *m/z* 760.5, PC(18:1/18:1) at *m/z* 786.6 and PC(18:0/18:1) at *m/z* 788.6. The most abundant SM and PC lipid peaks detected from MDA-MB-231-HRE-tdTomato breast tumor xenograft sections by MALDI-MS and MSI acquisitions as sodium and potassium adducts of lipids are listed in Table 5.1.
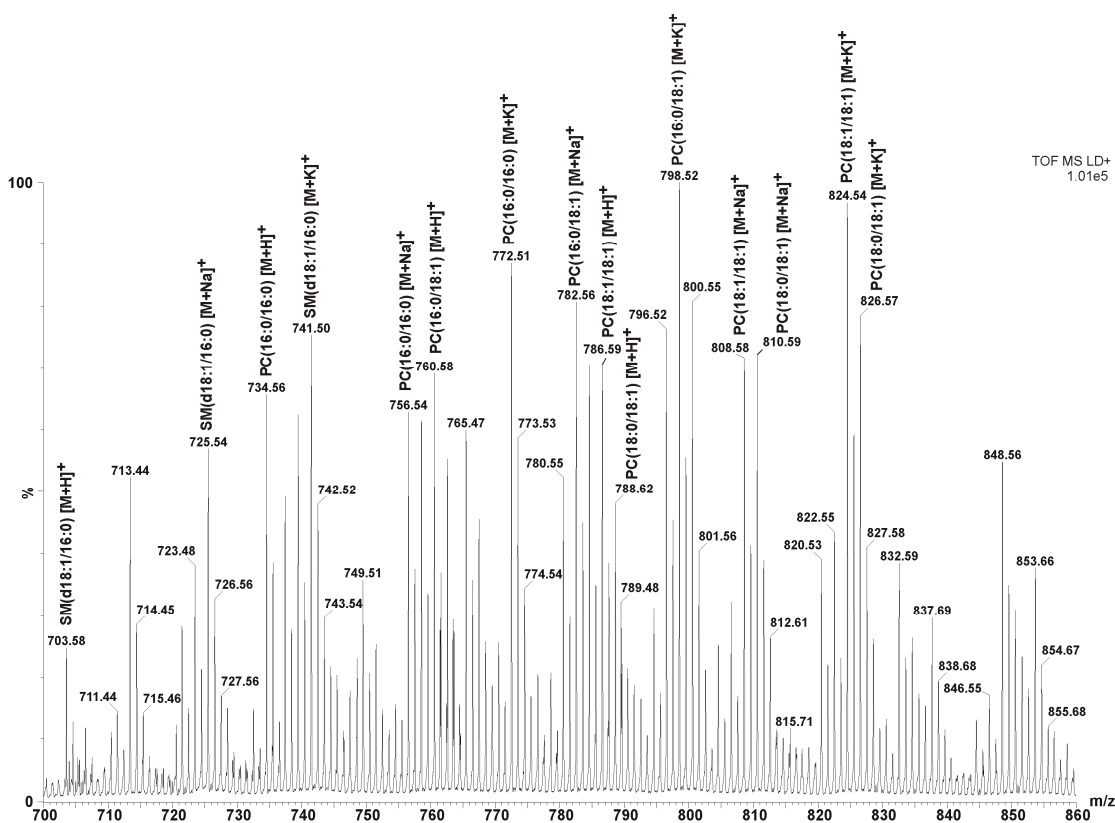
Figure 5.4 Expanded spectrum of proton, sodium and potassium adducts of PC and SM lipid species identified in the mass range from m/z 700 to m/z 860 from a MDA-MB-231-HRE-tdTomato breast tumor xenograft section.

Table 5.1 Most abundant PC and SM species with their observed m/z values, maximum peak intensities per pixel and ion drift times (bins) detected by MSI. Values are listed for protonated ions [M+H]$^+$, sodium adducts [M+Na]$^+$ and potassium adducts [M+K]$^+$ of lipids.

Phospholipid	measured *m/z* values			max peak intensity/pixel			drift time (bins)		
	[M+H]$^+$	[M+Na]$^+$	[M+K]$^+$	[M+H]$^+$	[M+Na]$^+$	[M+K]$^+$	[M+H]$^+$	[M+Na]$^+$	[M+K]$^+$
SM(d18:1/16:0)	703.58	725.54	741.50	81	112	136	89.81	90.74	91.59
PC(16:0/16:0)	734.56	756.54	772.51	131	108	153	90.84	91.70	92.28
PC(16:0/18:1)	760.58	782.56	798.52	140	139	173	92.22	92.55	93.91
PC(18:1/18:1)	786.59	808.58	824.54	121	118	160	94.09	94.68	95.19
PC(18:0/18:1)	788.62	810.59	826.57	95	135	122	95.59	95.99	96.73

The structures of all described lipid species were confirmed by MALDI-MS/MS profiling experiments performed directly on tumor tissue sections. Figure 5.5 shows a typical MS/MS spectrum of protonated PC(16:0/18:1) which has a highly abundant fragment signal at *m/z* 184.0 arising from the protonated phosphocholine ion, a signature peak in the MS/MS of protonated LPC, PC, and SM species. A less abundant signal at *m/z* 86 is characteristic of the choline head group. The loss of trimethylamine from the phosphocholine head group leads to the fragment ion [M+H-59]$^+$ at *m/z* 701.5, while the loss of the entire phosphocholine head group leads to the formation of the fragment ion [M+H-183]$^+$ at *m/z* 577.5. Additionally, the peak at *m/z* 125.0 is a phosphate-related ion, which forms from the protonated phosphocholine head group after neutral loss (NL) of the quaternary amine (NL 59). Other structurally relevant fragment ions are of low abundance. The fragment at *m/z* 478.3 is generated by loss of the 18:1 fatty acyl chain, while the fragment at *m/z* 504.3 forms from loss of the 16:0 fatty acyl chain from the PC precursor. The fragment at *m/z* 496.3 corresponds to the protonated LPC(16:0/0:0). Similarly, the fragment at *m/z* 522.3 corresponds to the protonated LPC(0:0/18:1). These four distinct fragments confirm the identity of *m/z* 760.5 as PC(16:0/18:1).
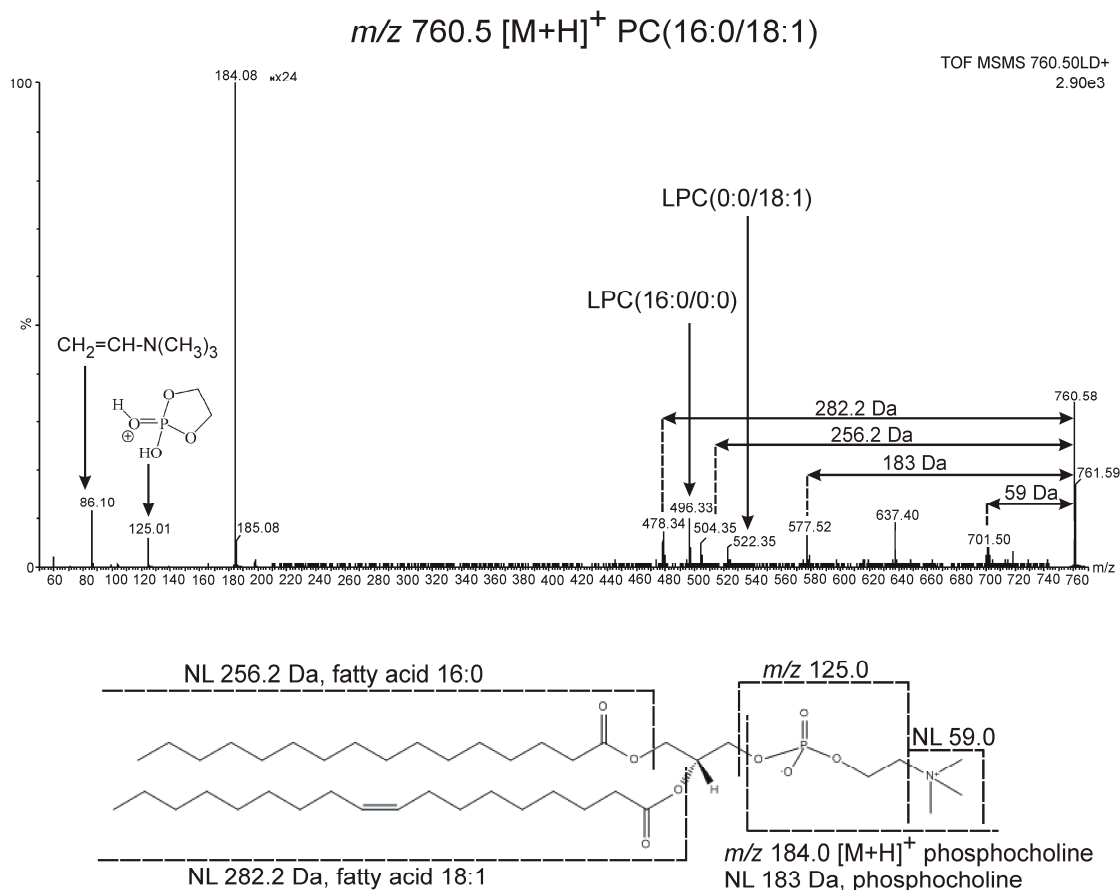
Figure 5.5 MS/MS spectrum and structure of PC(16:0/18:1). The ion at m/z 86 is a characteristic fragment of the choline head group, which ionizes as an intact molecular ion at m/z 184.0. The fragment ion at m/z 478.3 is generated from loss of the 18:1 fatty acyl chain from the intact lipid molecule, while the m/z 504.3 fragment forms from loss of the 16:0 fatty acyl chain from the PC precursor. The protonated LPC(16:0/0:0) is formed as a fragment at m/z 496.3. Similarly, the fragment at m/z 522.3 corresponds to the protonated LPC(0:0/18:1). Neutral loss of the entire phosphocholine head group leads to the formation of the ion [M+H-183]$^+$ at m/z 577.5, while the loss of trimethylamine from the phosphocholine head group generates the fragment ion [M+H-59]$^+$ at m/z 701.5.

Mass spectrometric imaging of lipids

MALDI imaging. Images obtained from optical imaging and MALDI-MSI were co-registered as previously described based on the position of the fiducial markers detected by both optical microscopy as well as MALDI-MSI.[366] During MALDI-MS analysis both PC and SM species ionized as singly charged molecular ions due to the choline head group. Figure

5.6 shows the distributions of protonated [M+H]$^+$ ions derived from PC(16:0/16:0) at *m/z* 734.5, PC(16:0/18:1) at *m/z* 760.5, PC(18:1/18:1) at *m/z* 786.6 and PC(18:0/18:1) at *m/z* 788.6. These highly abundant phospholipid species were detected predominantly from viable (both normoxic as well as hypoxic) tumor regions. We detected the [M+H]$^+$ ion of palmitoylcarnitine at *m/z* 400.3, the [M+H]$^+$ ion of stearoylcarnitine at *m/z* 428.3, the [M+K]$^+$ ion of LPC(16:0/0:0) at *m/z* 534.3, the sodium adduct [M+Na]$^+$ of sphingomyelin SM(d18:1/16:0) at *m/z* 725.5 and the [M+H]$^+$ ion of PC(16:0/22:1) at *m/z* 816.6 mostly in hypoxic and necrotic tumor regions.
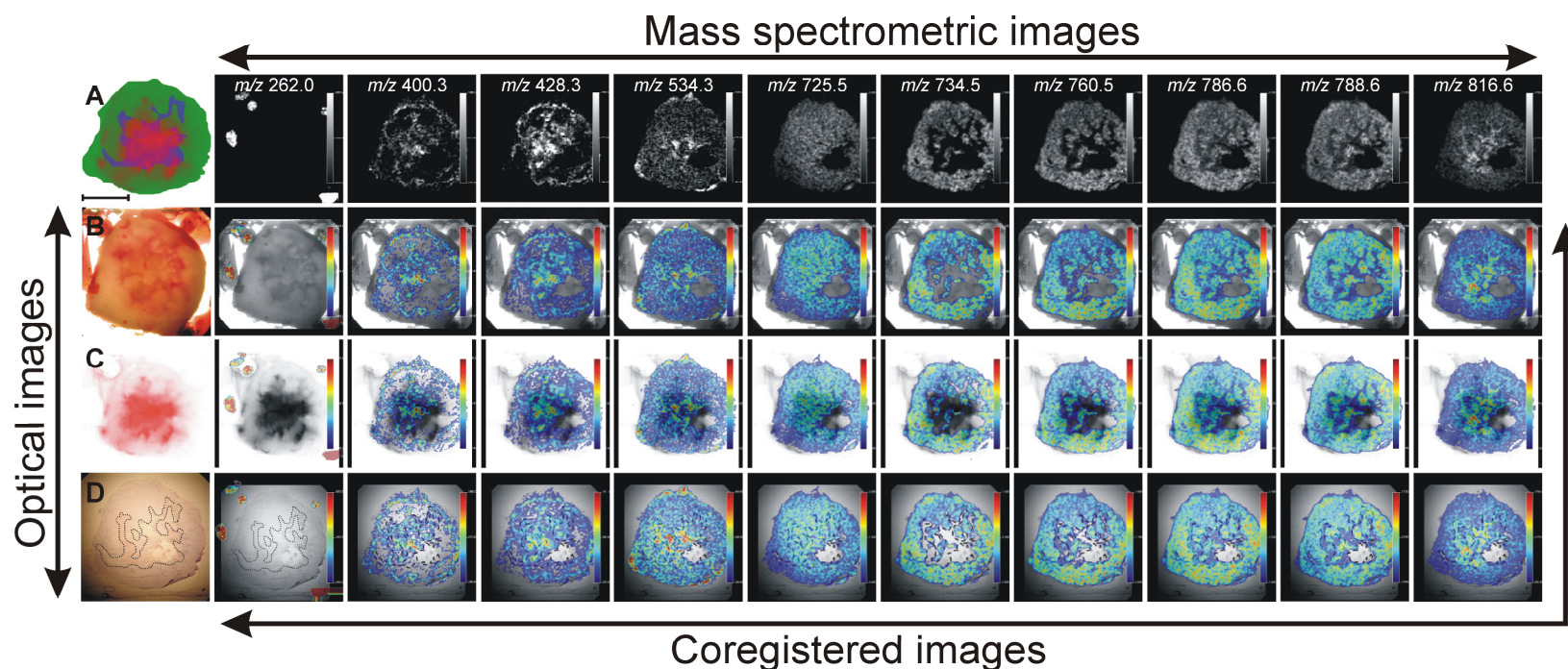
Figure 5.6 Multimodal imaging combining optical microscopy to visualize different tumor microenvironments and mass spectrometric imaging to localize multiple lipid molecular ions. Optical images: (A) Diagram showing the localization of viable (in green), necrotic (in blue) and hypoxic regions (in red) in a representative MDA-MB-231-HRE-tdTomato breast tumor section. (B) Bright field image of the corresponding fresh tumor section and fiducial markers visible as red points. (C) Image of the hypoxic region obtained by fluorescence microscopy of tdTomato. The black background has been removed for better co-registration with MSI. (D) H&E stained image of a tumor section obtained from the section shown in (B). The necrotic region present in the tumor centre has been outlined. The empty hole within this section originated from loss of tissue integrity in a small part of the necrotic tumor region. Mass spectrometric images from left to right: $[M-CH_3COO^-]^+$ of fiducial markers at m/z 262.0, $[M+H]^+$ of palmitoylcarnitine at m/z 400.3, $[M+H]^+$ of stearoylcarnitine at m/z 428.3, $[M+K]^+$ of LPC(16:0/0:0) at m/z 534.3, $[M+Na]^+$ of SM(d18:1/16:0) at m/z 725.5, $[M+H]^+$ of PC(16:0/16:0) at m/z 734.5, $[M+H]^+$ of PC(16:0/18:1) at m/z 760.5, $[M+H]^+$ of PC(18:1/18:1) at m/z 786.6, $[M+H]^+$ of PC(18:0/18:1) at m/z 788.6 and $[M+H]^+$ of PC(16:0/22:1) at m/z 816.6. Co-registered images: The mass spectrometric images in the top row were co-registered with the optical images in the left column based on the position of the fiducial markers. Scale bar, 5 mm.

SIMS imaging. We have integrated high spatial resolution SIMS imaging with our multimodal approach to be able to image the distribution of potassium salts as well as small labile molecules such as phosphocholine and cholesterol. Figure 5.7 presents distributions of the potassium elemental ion (*m/z* 39.0, shown in red) and cholesterol molecular ion (*m/z* 369.3, shown in green), which were detected from viable tumor regions. The phosphocholine ion at *m/z* 184.0 (shown in blue) was specifically detected from the necrotic tumor regions.
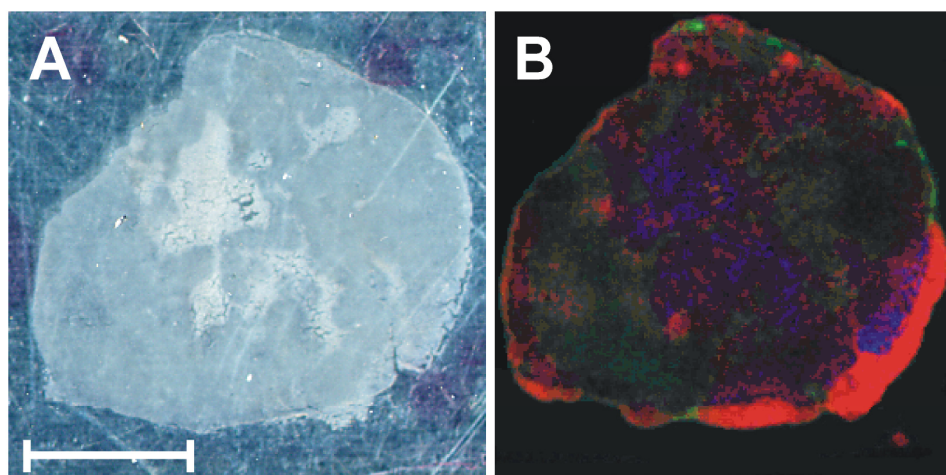
Figure 5.7 SIMS imaging of elements and small molecules. (A) Optical image of a representative MDA-MB-231-HRE-tdTomato breast tumor section. (B) SIMS image of m/z 39.0 shown in red, m/z 184.0 shown in blue and m/z 369.3 shown in green. Scale bar, 5 mm.

To quantify the ion signals in different breast tumor regions, we performed an overlap analysis of each ion distribution with each of the three distinct regions, namely the normoxic, hypoxic, and necrotic tumor region, which were visualized by our multimodal imaging approach from three MDA-MB-231-HRE-tdTomato tumor xenografts. Figure 5.8 presents the results of the overlay analysis. PC(16:0/16:0) overlapped predominantly with normoxic tumor regions, while LPC(16:0/0:0) was highly enriched in necrotic tumor regions. The remaining PCs, SM and acylcarnitines displayed the highest percentage of overlap with hypoxic tumor regions.
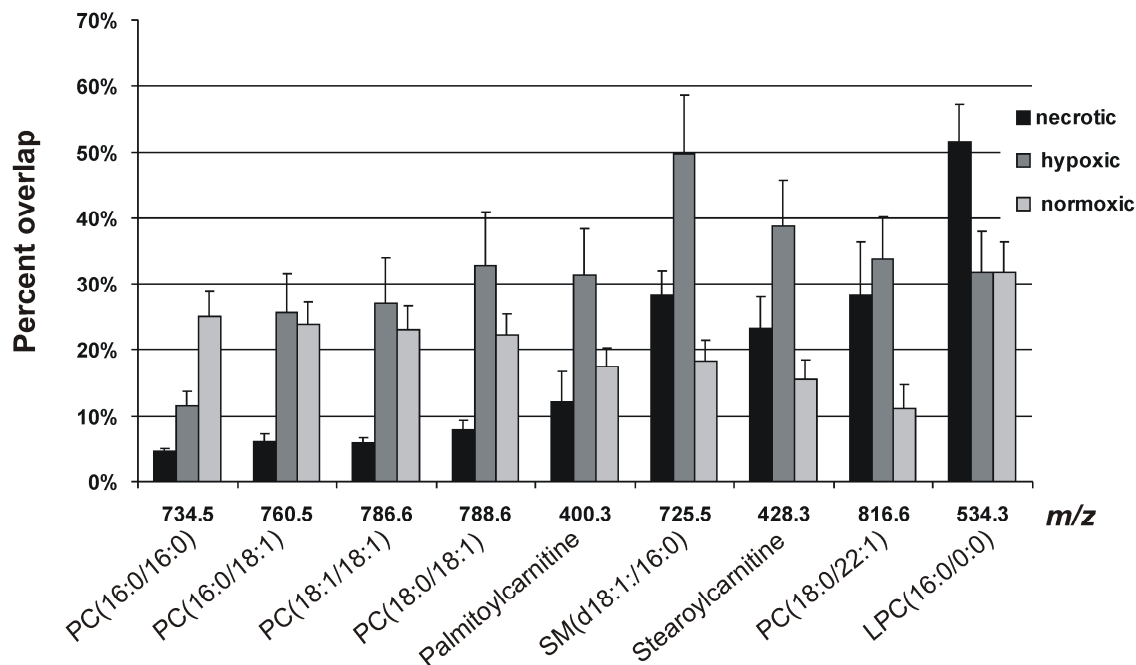
Figure 5.8 Overlap analysis between the MSI detected molecules and different tumor regions. The necrotic region was separated from the viable region by H&E staining, which was further subdivided into hypoxic and normoxic tumor regions by means of fluorescence microscopy of the tdTomato fluorescent protein, which was expressed in hypoxic tumor regions only. The viable region is the sum of the normoxic and the hypoxic regions. PC(16:0/16:0) was mostly detected from normoxic tumor regions, while LPC(16:0/0:0) was characteristic of necrotic tissue. The remaining PCs, SM and acylcarnitines were co-localizing mostly with hypoxic and to a lesser extent with normoxic tumor regions. Data are shown as mean ± standard error.

Imaging of isobaric species in ion mobility separation mode

IMS enables the separation of ions based on their collisional cross-section, which depends on their shape and charge. In our study, IMS separated the background ions (chemical noise, matrix clusters, etc.) from the biomolecular lipid species. Figure 5.9A presents a spectrum of peak-picked data acquired during an IMS imaging experiment, and figure 5.9B shows a drift plot of the separated ions. In figures 5.9A and 5.9B background ions are highlighted in blue, while biomolecular lipid ions are highlighted in red. Ion image 1 in figure 5.9B shows the distribution of a background matrix ion, which was separated from two lipid ions, shown in ion images 2 and 3.
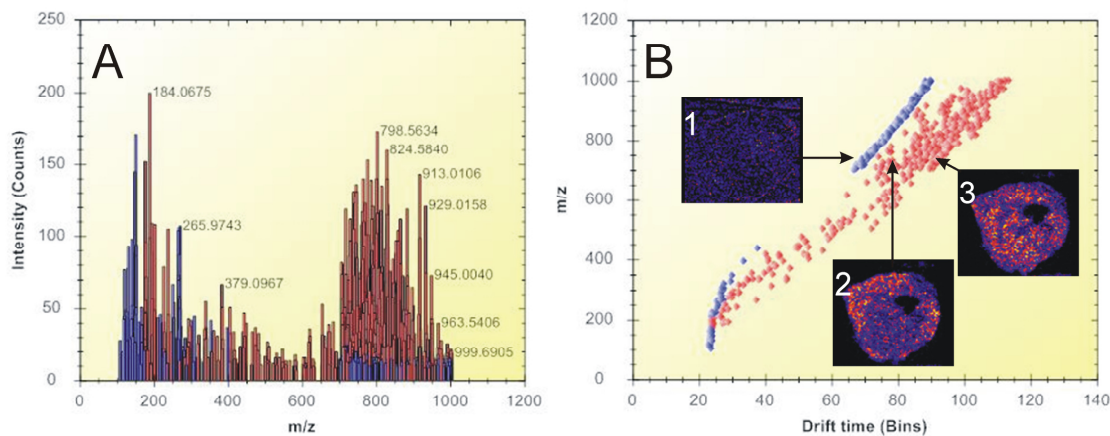
Figure 5.9 Ion mobility separation of biomolecular ions detected from thin tumor tissue sections. (A) Representative spectrum of peak-picked data acquired during an IMS imaging experiment. The lipid peaks are highlighted in red, while matrix-related ions are shown in blue. (B) Drift plot of the separated ions. Ion image 1 shows the distribution of a background matrix ion. Ion images 2 (m/z 746.5) and 3 (m/z 746.6) show the distribution of different lipids in the tumor tissue. Lipid-related ions (highlighted in red) were separated from background ions (blue).

Ion mobility separation not only improved the MSI data obtained from complex tumor tissue, but also enabled the identification of several biomolecules, which otherwise could not have been separated from other ions of similar mass. Figure 5.10 shows an example of two ions at *m/z* 428.25 and *m/z* 428.38, which were analyzed in ion mobility separation mode. Separated precursor ions were fragmented, which resulted in the identification of *m/z* 428.3 as stearoylcarnitine [M+H]$^+$. Figure 5.10A presents the ion mobility graph from two fragmented ions. The left side, circled by the red box, shows the separated faster ion and its fragments, while the green box encircles the slower ion and its fragments. Figure 5.10B presents the corresponding drift time plot showing the intensity of the slow and fast ions and their drift times, which are 1.7 milliseconds and 2.5 milliseconds, respectively. Figure 5.10C presents a full spectrum of detected ions and their fragments, obtained without IMS. Ion mobility separation performed prior to fragmentation resulted in two spectra of fast (figure 5.10D) and slow (figure 5.10E) ions. Subsequent collision-induced dissociation allowed for the identification of the slower ion at *m/z* 428.3 as protonated stearoylcarnitine.
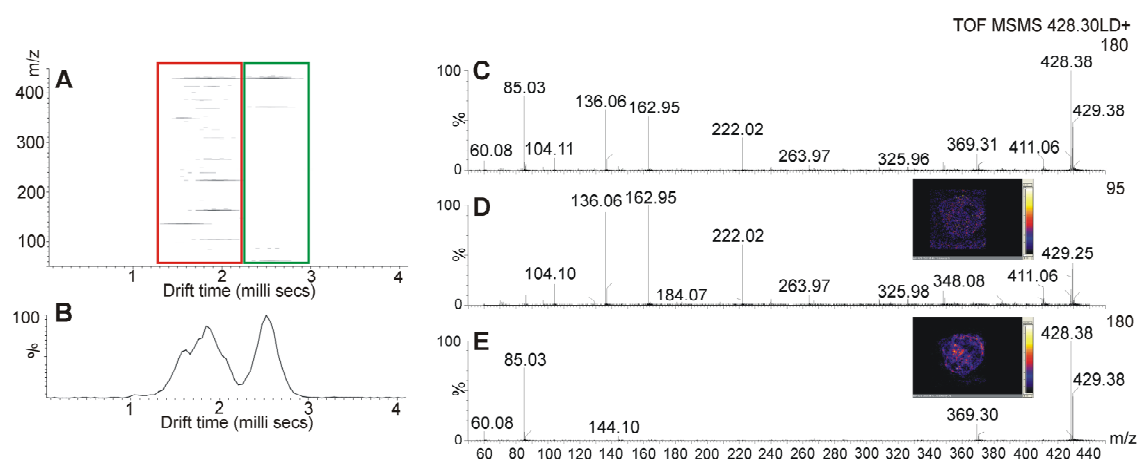
Figure 5.10 Ion mobility separation of molecules present in the MDA-MB-231-HRE-tdTomato breast tumor xenograft model. (A) 2D map (m/z vs drift time) showing ions at m/z 428.2 (red) and m/z 428.3 (green) separated and fragmented during an MS/MS experiment. (B) Drift time plot showing drift times of the two clearly separated ions shown in (A). (C) MS/MS spectrum of fragments detected from both ions without ion mobility separation. (D) MS/MS spectrum of fragments detected only from the ion at m/z 428.2, whose separation was achieved by IMS. (E) MS/MS spectrum of fragments detected only from the stearoylcarnitine ion [M+H]$^+$ at m/z 428.3, whose separation was achieved by IMS.

5.4 Discussion

Advantages of MSI-IMS over other techniques used in lipidomics studies

In the present study, we analyzed human breast tumor xenograft tissue using MSI-IMS, and localized multiple metabolites and phospholipid species in different tumor regions. Unlike classical MALDI mass spectrometry, which is widely used to identify lipids, MSI does not require extraction of the lipids prior to analysis, but rather visualizes their localization directly in the analyzed tissue. MALDI-MSI does not require any labeling of the lipids. Lipid identification is achieved based on their molecular mass and characteristic fragmentation patterns. Such an imaging approach requires very little sample modification prior to imaging, and introduces minimal alterations in lipid localizations and structures. Phospholipid ion formation by MALDI-MSI, when performed directly on a tissue section, generates abundant alkali metal adduct ions, a phenomenon not observed when MALDI is performed on pure lipid extracts. Here, we have employed ion mobility separation, since tissue washing removes certain metabolites and lipids from the tissue or leads to their diffusion. Hence, we decided to follow a sample preparation procedure that introduces minimal changes to the composition of

the tissue. Ion mobility separation provided a separation step for our imaging experiments that is usually performed on lipid extracts by HPLC or TLC prior to mass analysis.[430,431] Ion mobility separation, in which separation occurs in milliseconds, can be easily coupled with MSI and helps obtain ion images of individual lipid species without requiring labor-intense sample preparation procedures or long acquisition times. The development of new HDI software (Waters, UK) incorporating drift plots and ion drift time made our data analysis fast and simple. The effects of acyl chain length, degree of unsaturation, lipid class, head group and cation formation on an ion's collision cross section in the gas phase and on its ionization efficiency have been studied for direct tissue profiling.[432] Such information greatly improves our understanding of ion behaviors detected from a complex tissue sample during MSI-IMS. So far, ion mobility separation has been applied to map the distribution of phosphatidylcholine and cerebroside species from coronal rat brain sections[433] and for imaging of glucosylceramide in spleen sections from a mouse model of Gaucher disease.[434]

Identification of lipids and their biological role

Most of the lipids identified in this study were SM and PC species detected in the mass range from m/z 700 to m/z 850. The presence of a positively charged quaternary ammonium group in both PC and SM species aids in the detection of these two classes of phospholipids in positive ion mode.[432] Previous MALDI-MS studies of phospholipid mixtures have demonstrated that in positive ion mode, PC and SM species can inhibit the detection of other classes of phospholipids, such as PE, present in the tissue at similar concentrations.[435,436] In this study, we focused on identification and imaging of phosphocholine-containing lipids present in MDA-MB-231-HRE-tdTomato breast tumor xenograft models.

Analysis of MALDI mass spectra directly obtained from MDA-MB-231-HRE-tdTomato breast tumor sections revealed multiple PC species with fatty acid chains ranging between 16 and 22 carbons and containing 0 to 2 unsaturated bonds (figure 5.4). These PC species were detected mostly in viable regions of MDA-MB-231-HRE-tdTomato breast tumors, with PC(16:0/16:0) predominantly localized to normoxic tumor regions and all other PC species mostly localized to hypoxic tumor regions (figure 5.8). The identification of all lipid species involved collisional activation (see figure 5.5). The protonated LPCs and PCs yielded a major product ion at m/z 184.0 corresponding to the phosphocholine headgroup as well as phosphate-related ion at m/z 125.0 [M+H]$^+$, while the alkali cationized molecular species instead of m/z 125.0 produced characteristic ions at m/z 146.9 [M+Na]$^+$ and m/z 162.9 [M+K]$^+$.[407]

Our MSI and MS/MS analyses of MDA-MB-231-HRE-tdTomato breast tumor tissue revealed an abundant presence of LPC(16:0/0:0) in necrotic tumor regions, which could be due to breakdown of intact PC species. LPC species are formed during inflammation, in cases of chemical exposure,[437] and following heart[399] and brain[402,438] injury. Multiple different bioactive lysophospholipids exhibit pleomorphic effects on multiple cell lineages including breast and ovarian cancer cells.[439,440] LPC activates the ovarian cancer G protein-coupled receptor 1 (OGR1) family of G protein-coupled receptors (GPCR), known to regulate cellular motility, growth, differentiation, and gene transcription, all of which are factors central to the biology of cancer.[441] The effects of LPC on intracellular signalling in breast cancer cells is translated to functional changes such as increased production of multiple growth factors from breast cancer cells including interleukin 6 and 8, which are potent regulators of neovascularization.[442] The mechanisms regulating the production and degradation of lysophospholipids are just beginning to be elucidated.

MSI analysis of MDA-MB-231-HRE-tdTomato breast tumor tissue also revealed the presence of SM(d18:1/16:0), which was mostly detected in hypoxic tissue regions. SM(d18:1/16:0) is known to be involved in tissue inflammation and acts as a precursor of sphingolipid mediators.[443,444] Sphingolipids such as SM(d18:1/16:0) are detected by MSI in the same mass range as PC species. However, the protonated ions of PC species have even *m/z* values, while those of SM species have odd *m/z* values; therefore, although they occupy similar mass ranges, the peaks do not overlap as evident in figure 5.4.[432] Sphingolipids contribute to the pathogenesis of cancer as well as neurological and autoimmune disorders.[445] Several sphingolipid-regulated functions are implicated in tumor initiation, promotion, progression and response to chemotherapy due to their importance in regulating growth, survival, adhesion, and migration of cancer cells.[446] Sphingolipids have been proposed as cancer markers,[447] and tumors often display alterations in sphingolipid composition.[447] Sphingolipid intermediates may trigger proliferation and impair the ability of damaged cells to undergo apoptosis.[446] Signalling-induced hydrolysis of sphingolipids produces a series of messenger lipids such as ceramides and ceramide-1-phosphate, which, as part of signalling cascades, act by recruiting cytosolic proteins. Sphingosine, sphingosine 1-phosphate, ceramide and ceramide 1-phosphate have pivotal roles in apoptosis, inflammation and arachidonic acid signalling, all of which are pathways that are impaired in many cancers.[448,449]

Carnitine and acylcarnitines are essential compounds in fatty acid metabolism.[450] Carnitine assists with transport of fatty acids into mitochondria, where fatty acids are oxidized by β-oxidation as a major source of energy. We have detected and imaged two acylcarnitines

directly from MDA-MB-231-HRE-tdTomato breast tumor tissue sections by applying MSI together with on-tissue IMS-MS/MS analysis combined with a Human Metabolome Database search for their identification. IMS was successfully employed for removing background ion fragments. We have identified ions at *m/z* 400.3 and *m/z* 428.3 as protonated ions of palmitoylcarnitine and stearoylcarnitine, respectively, which both localized to hypoxic tumor regions. This accumulation of acylcarnitines in hypoxic tumor regions occurred most likely due to a blockage of oxidative processes in these hypoxic tumor regions.[451] The inhibition of β-oxidation during hypoxia leads to an accumulation of acylcarnitines in the cytoplasm of hypoxic cells.[450] The concentration of long-chain acylcarnitines increased rapidly within minutes after the onset of ischemia *in vivo* or hypoxia *in vitro*[452] as shown in plasma and hearts of hypoxic rats,[453-455] a newborn rat model of hypoxia-ischemia,[456] adult canine myocytes,[457] rabbit fetal lungs,[451] and blood samples from neonates.[458] Acylcarnitines are highly polar, zwitterionic molecules and therefore tend to elute together with phospholipids such as phosphatidylcholine in many chromatographic systems. Here, we have demonstrated that due to the presence of their positively charged quaternary ammonium group, acylcarnitines can also be easily detected and localized by MALDI-MSI.

5.5 Conclusions

We detected, identified and visualized several important lipid species in a human breast tumor xenograft model using MALDI-IMS-MSI. The detected lipids belonged to the lipid classes of PC and SM. For the first time, different lipids were visualized in different microenvironmental tumor regions. Most PC species were found in viable normoxic and hypoxic breast tumor regions, while LPC was localized to necrotic regions, which could be attributed to PC breakdown triggered by tissue injury. Two acylcarnitines were localized in hypoxic tumor regions and identified by using ion mobility separation. Their presence in the hypoxic regions suggests blockage of the β-oxidation process of fatty acids inside mitochondria. In addition, SM(d18:1/16:0), known to be involved in cellular signaling processes, was enriched in hypoxic tumor regions. Our study demonstrated the first visualization of phospholipids in a human breast tumor xenograft model and shed more light on processes occurring during tumor growth.

Chapter 6

A Survival Strategy of

Hypoxic Breast Tumors

6. A Survival Strategy of Hypoxic Breast Tumors[*]

Visualization and analysis of the tumor metabolome, lipidome and proteome are crucial for understanding tumor growth, angiogenesis, hypoxia, metastasis, drug- and radio-resistance, apoptosis and necrosis. All these processes contribute to tumor aggressiveness and challenge our understanding of tumor expansion and treatment strategies. In this study, we have integrated state of the art quantitative proteomics which provided global as well as detailed information about hypoxia-induced proteome changes in breast cancer cells. These *in vitro* studies were complemented by multimodal imaging of tumor xenografts grown from the same cell line in mice. A combination of optical imaging techniques such as bright field/fluorescence microscopy and histochemistry combined with MSI were employed for *ex vivo* visualization of tumor tissue vasculature, and regions of normoxia, hypoxia and necrosis. MSI shed light on the spatial distribution of molecules directly involved in tumor response to hypoxia. This approach allowed us to detect local protein signaling, up-regulation of pathways involved in metastasis and down-regulation of molecules responsible for cell attachment. The presented combination of proteomics with a variety of *ex vivo* imaging techniques provided multidimensional information about signaling pathways that occur inside hypoxic regions of breast tumor xenografts.

6.1 Introduction

Hypoxia, a state of reduced O_2 availability, triggers alterations of multiple biological processes. Cancer cells growing under hypoxic conditions experience changes in many different biological pathways, which may ultimately lead to tumor expansion and metastasis.[459] Although the hypoxia inducible factor 1 (HIF-1) and its role in the initiation of response to hypoxia is well established,[460] many proteome changes triggered by HIF-1 remain to be discovered. In order to investigate the effects of hypoxia on protein networks we have employed state of the art MS technology, that provided the wealth of information needed to understand the extreme complexity of cancer biology.

Quantitative proteomics is a powerful tool to explore hypoxia-driven proteome changes in breast cancer cells. It provides a broad overview of the degree of change and helps to understand which proteins/pathways are affected by hypoxia. In the present study, we have investigated breast cancer cell lines exposed to hypoxia compared to control conditions using a dimethyl labeling technique to perform quantitative proteomics. To this end, dimethyl labels containing three different stable isotopes were employed to differentially label peptides in three different samples to allow simultaneous quantitative LC-MS analysis.[461] The combination of regular formaldehyde and cyanoborohydride generated a mass increase of 28 Da per primary amine on a peptide (light label). Using deuterated formaldehyde resulted in a mass increase of 32 Da per primary amine (intermediate label). The third label with a mass increase of 36 Da was achieved through combining deuterated and ^{13}C-labeled formaldehyde with cyanoborodeuteride (heavy label). Since the different isotopes do not affect the behavior of the labeled peptides in LC-MS, the differently labeled samples can be mixed together. During MS analysis the differently labeled peptides can be recognized by the known mass differences between them. Finally, quantification can be performed by comparing the signal intensity of the differently labeled peptides. This state of art quantitative proteomics approach enabled the detection of subtle changes in the cancer cell proteome, while the applied imaging techniques provided information about the spatial distribution of the peptides and proteins detected in tumor tissue. Hypoxic regions in the tumor xenograft tissue were visualized by stable transfection of inoculated human breast cancer cell line with a construct, in which the tdTomato red fluorescent protein is expressed under the control of hypoxia response elements. This approach enabled optical visualization of tumor hypoxia, a phenomenon that strongly depends on fluctuating tumor vascularization and oxygenation. Our

multimodal imaging approach allowed us to detect and visualize signaling biomolecules that are crucial for tumor vascularization and metastasis.

6.2 Materials and methods

In-solution digestion. The lysis buffer was prepared in 50 mM NH_4HCO_3 pH 8-8.5 (Fluka, Germany) and consisted of 8M urea (Merck, Germany), 2M thiourea (Sigma, USA), PhosSTOP Phosphatase Inhibitor Cocktail Tablet (Roche), Complete Protease Inhibitor Cocktail Tablet (Roche). Both 200 mM DTT (Sigma, Canada) and 200 mM iodoacetamide (Sigma, Germany) were prepared in 50 mM NH_4HCO_3, pH 8.5.

On-column labeling reagents. Per sample/label: 4.5 mL of 50 mM sodium phosphate buffer pH 7.5 was mixed with 250 µL of 4% (vol/vol) formaldehyde, either CH_2O (Sigma-Aldrich), CD_2O (SOTEC) or $^{13}CD_2O$ (Aldrich), in water and 250 µL of 0.6 M cyanoborohydride $NaBH_3CN$ (Fluka) or $NaBD_3CN$ (96% D, Isotec) in water. Buffer A, 0.6% acetic acid; buffer B, 80% ACN/0.6% acetic acid and 100% acetonitrile were used during on-column labeling.

HPLC solvents. Reversed phase (RP): solvent A, 0.6% (vol/vol) acetic acid; solvent B, 0.6% (vol/vol) acetic acid and 80% (vol/vol) ACN.

Equipment setup. LC-MS/MS equipment: the Agilent 1100 HPLC system connected to the LTQ-Orbitrap mass spectrometer was equipped with a 100 µm x 20 µm Aqua C18 (Phenomenex) pre-column and a 50 µm x 250 µm Reprosil C18 analytical column according to a vented column setup. Trapping step was performed at 5 µL per min, whereas gradient elution was performed at 100 nL per min.[461]

Chemicals for MSI. The matrix CHCA was purchased from Sigma-Aldrich (Germany). Ethanol, water, ACN, and TFA were purchased from Biosolve (The Netherlands). Modified proteomics grade trypsin was purchased from Sigma (Germany). Ponceau S was purchased from Sigma (USA). Gelatin Type A was purchased from Sigma (USA). Mayer's hematoxylin was purchased from Sigma (USA) and aqueous Eosin Y from EMD Chemicals Inc. (USA). The Cytoseal 60 Mounting Medium, Richard-Allan Scientific was purchased from Thermo Scientific (USA).

Cell culture and hypoxia treatment. Human breast cancer cells MDA-MB-231-HRE-tdTomato,[462] grown in RPMI-1640 media in 10 cm cell culture dishes, were exposed to hypoxic conditions in a commercially available culture chamber (BioSpherix Ltd.). This humidified culture chamber was maintained at 37°C and equilibrated with a mixture of 0.5% O_2 and 5% CO_2 using controlled N_2 and CO_2 gas infusions (BioSpherix Ltd.). For cobalt chloride experiments, hypoxia was mimicked with 200 µmol/L $CoCl_2$. Controls and cobalt

treated samples were placed in a standard cell culture incubator at 37°C in a humidified atmosphere containing 21% O_2 and 5% CO_2. The cells were rinsed with PBS, collected by using cell scrapers and transferred into Eppendorf tubes. The Eppendorf tubes were centrifuged and supernatants were removed. The Eppendorf tubes were frozen at -80ºC until further analysis.

Cell lysis. The lysis buffer (175 µL) was added to the cell pellets, vortexed, incubated on ice for 30 min, spun down for 10 min at 20000 rcf (relative centrifugal force) at 4ºC. Supernatants were transferred into new tubes. Protein concentration in supernatants was estimated using standard Bradford protein assay.[463]

Reduction and alkylation. Two microliters of 200 mM DTT per 100 µL of sample solution were added and the samples were incubated in a shaker for 25 min at 56°C. Subsequently, 4 µL of 200 mM IAA per 100 µL of samples solution were added and the samples were incubated for 30 min at room temperature in the dark.

Enzymatic digestion. Lys-C digestion was performed for 4 h at 37°C using a 1:75 enzyme:substrate ratio. After digestion the samples were diluted in 1:4 ration using 50 mM NH_4HCO_3 to obtain final concentration of urea of 2 M. Subsequently, trypsin digestion was performed overnight at 37°C using a 1:100 enzyme:substrate ratio.

Dimethyl labeling. Labeling was performed on digested samples using Sep-Pak (Sep-Pak, tC18 Catridges, Waters). Before labeling samples were acidified using 10% formic acid to obtain a final concentration of formic acid of 2.5% and a total sample volume of 2 mL. Columns were activated by adding of 1 mL of 100% ACN, followed by column conditioning with 2 x 2 mL of buffer A. Acidified samples were loaded on columns, followed by column washing with 2 x 1 mL of buffer A. Samples were labeled using 5 mL of labeling reagent, followed by column washing with 2 x 1 mL of buffer A. Labeled peptides were eluted using 1 mL of buffer B. Samples were vacuum-dried and frozen at -20ºC until further LC-MS analysis.

Breast tumor imaging. The MDA-MB-231 breast cancer cell line was purchased from ATCC and genetically modified to express the tdTomato red fluorescent protein under the control of hypoxia response elements as previously described.[462] Cells were injected into the upper thoracic mammary fat pad of athymic nude mice (2×10^6 cells/injection), and tumor growth was monitored with standard calipers. When tumors reached a volume of approximately 500 mm^3, mice were sacrificed and tumors were removed. Each tumor was embedded into a gelatin block (10% gelatin) and Ponceau S fiducial markers were injected inside the block next to the tumor. The block was sectioned into serial 2 mm thick fresh tumor

sections using an acrylic adjustable tissue slicer (12 mm depth up to 25 mm width; Braintree Scientific, Inc., Braintree, MA) and tissue slicer blades (Braintree Scientific, Inc.). These serial fresh tumor xenograft sections were each placed on individual microscope slides (Fisherbrand catalog number 12-550-34; Fisher Scientific, Pittsburgh, PA) and stored in an ice-box containing ice on the bottom, with the slides located on a perforated plate at approximately 1 cm above the ice to minimize tissue degradation. These fresh sections were imaged by bright field and fluorescence microscopy with a 1× objective attached to a Nikon inverted microscope, equipped with a filter set for 528 - 553 nm excitation and 600 - 660 nm emission and a Nikon Coolpix digital camera (Nikon Instruments, Inc., Melville, NY). Bright field imaging captured the position of the fiducial markers present inside the gelatin block as well as the shape of the tumor tissue. The fluorescence from tdTomato expression in hypoxic regions of these tumor sections was detected by fluorescence microscopy. The GIMP 2.6 was used for 2D co-registration and overlay of bright field and fluorescence images of 2 mm thick tumor sections. All 2 mm thick sections were snap-frozen immediately after microscopic imaging. From each 2 mm thick section, 10 μm thick sections were cut at -16 °C for MSI using a Microm HM550 cryo-microtome (Microm International GmbH, Walldorf, Germany) along with adjacent 10 μm thick sections for histological staining. Tissue sections for MSI analysis were mounted onto 25 mm × 50 mm × 1.1 mm, Rs = 4−8 Ω ITO coated slides (Delta Technologies, U.S.) and for histological staining onto Superfrost Slides (VWR International, catalog no. 48311-600). Before MSI analysis, tissue sections were briefly washed by immersion in 70% and 90% ethanol and dried in a vacuum desiccator for 10 min. Trypsin was resuspended in water at a concentration of 0.05 μg/μL, and 5 nL per spot in a 150 μm x 150 μm raster was deposited by CHIP (Shimadzu, Japan). CHCA matrix was prepared at a concentration of 10 mg/mL in 1:1 ACN:H_2O/0.1% TFA and was applied by an ImagePrep (Bruker Daltonics GmbH, Bremen, Germany) application system. Samples were analyzed on a MALDI-Q-TOF (Synapt HDMS, Waters, U.K.) instrument in TOF mode detecting the positive ions. The images were acquired with 150 μm x 150 μm spatial resolution. For 2D MSI analysis and overlay of images, data were visualized using BioMap software (Novartis, Basel, Switzerland).

H&E staining method. Tissue sections were stained using a modified H&E staining protocol as previously described.[366,426,427] Briefly, 10 μm sections attached to Superfrost Slides (VWR International, catalog no. 48311-600) were washed with PBS, fixed with 3% paraformaldehyde for 30 min, washed with dH_2O, and treated with Mayer's hematoxylin for 30 min at room temperature, followed by 5 washes with dH_2O. Sections were immediately

immersed in aqueous Eosin Y for 30 min, followed by five washes with dH_2O, mounting with aqueous mounting medium, and attaching of a coverslip. Bright field images of H&E stained sections were acquired using a 1× objective attached to a Nikon microscope, equipped with a Nikon Coolpix digital camera (Nikon Instruments, Inc., Melville, NY).

6.3 Results and discussion

Breast cancer cells were exposed to physiological hypoxia (hypoxic chamber) as well as a hypoxia mimetic ($CoCl_2$) and proteome changes were monitored by quantitative analysis of hypoxic *versus* normoxic proteomes. Using this approach we identified and quantified more than 5000 proteins (figure 6.1A-B), many of which were up-regulated (figure 6.1C) or down-regulated (figure 6.1D) under hypoxic and hypoxia-mimetic conditions. Hypoxia up-regulated proteins involved in cellular processes such as energy metabolism, apoptosis, heme metabolism, and immune system modulation, while proteins involved in cellular division and cellular adhesion were down-regulated by hypoxia.
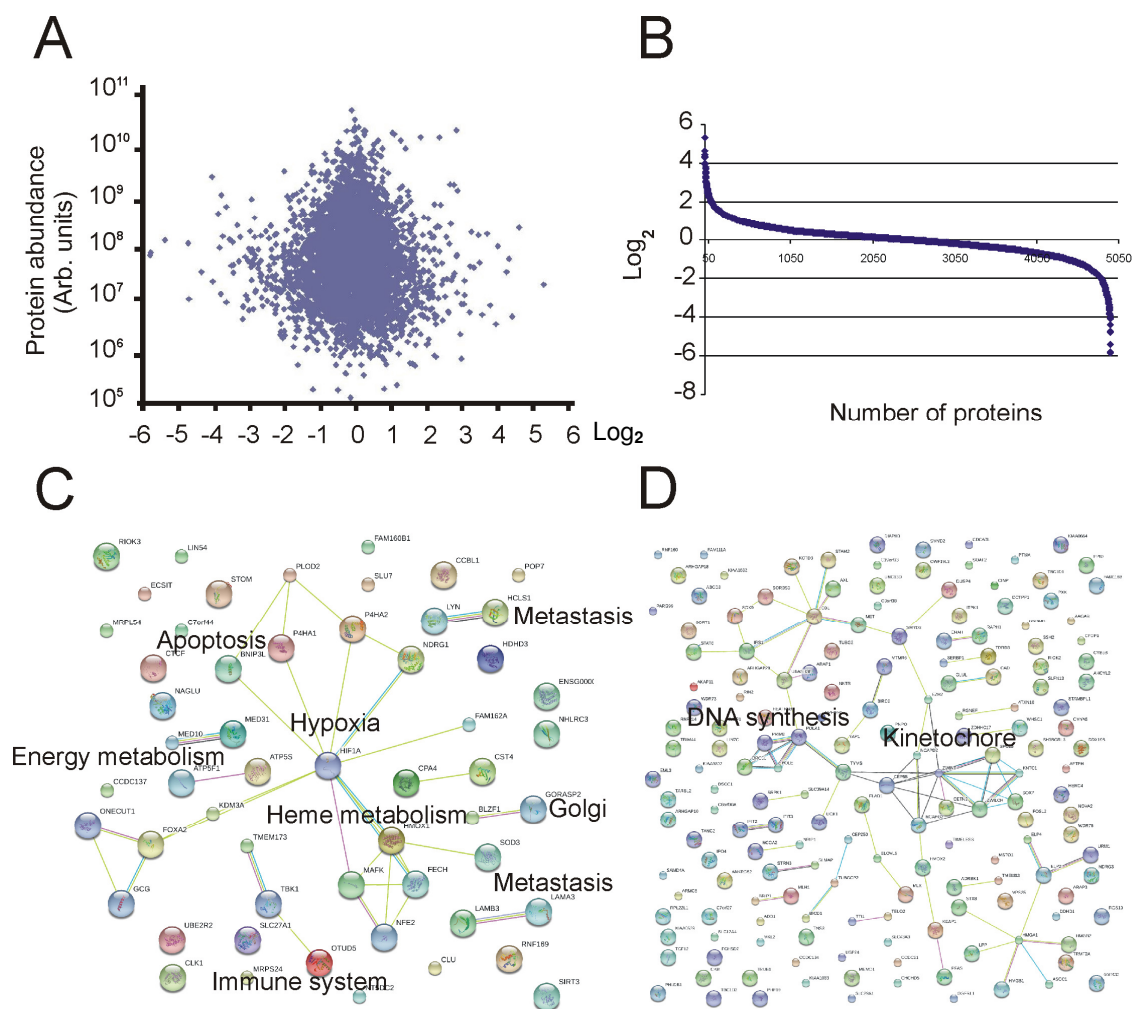
Figure 6.1 (A) Hypoxia-induced proteome changes in breast cancer. The x-axis represents the log$_2$ change in protein expression, while the y-axis shows the peak area of peaks identified by mass spectrometric analysis. (B) The x-axis shows the number of quantified proteins, while the y-axis represents the log$_2$ change in protein expression. (C) String analysis of up-regulated proteins[464]. (D) String analysis of down-regulated proteins.

Figure 6.2 presents hypoxia-induced proteome changes in the human MDA-MB-231-HRE-tdTomato breast cancer cell line. Figure 6.2A shows the response of the proteome to hypoxia induced by incubation of the cells inside a hypoxic chamber flushed with 0.5% O$_2$ for 3, 24 or 72 h. Figure 6.2B presents the changes in response to cobalt chloride treatment for 3, 24 or 72 h. The proteome changes observed after incubation inside the hypoxic chamber were gradually accumulating over time and the highest degree of change was observed in cells incubated for 72 h. On the other hand, the cobalt chloride treated samples showed a rapid up-

and down-regulation of multiple proteins just 3 h after treatment, proteome stabilization after 24 h, followed by accumulation of hypoxia-induced changes after 72 h.
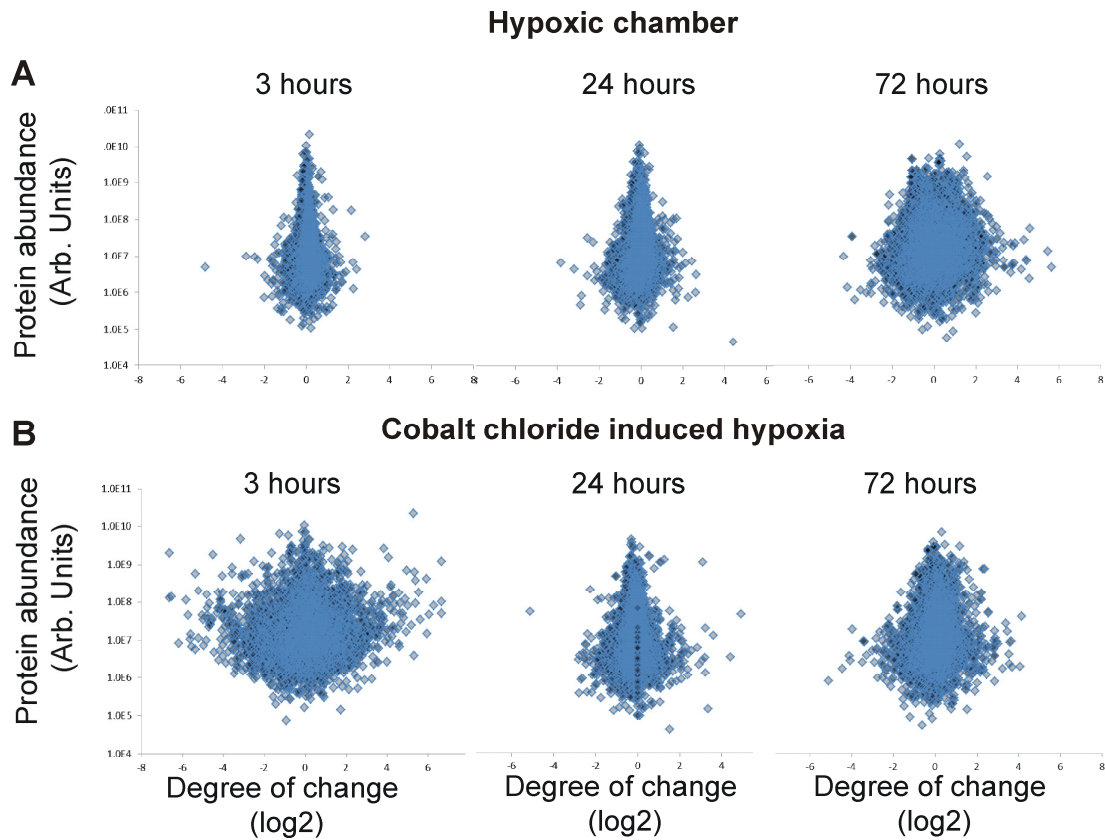
Figure 6.2 Hypoxia-induced proteome changes. (A) Changes induced in the proteome of breast cancer cells after exposure to 0.5% O$_2$ in a hypoxic chamber for 3, 24 and 72 h. (B) Proteome changes observed after cobalt chloride treatment for 3, 24 and 72 h.

As shown in figure 6.3 response to hypoxia triggered by incubation of cancer cells inside the hypoxic chamber resulted in rapid up- and down-regulation of more than 1300 proteins after 72 h, while in cobalt chloride treated cells expression of more than 1900 proteins was affected after 3 h.
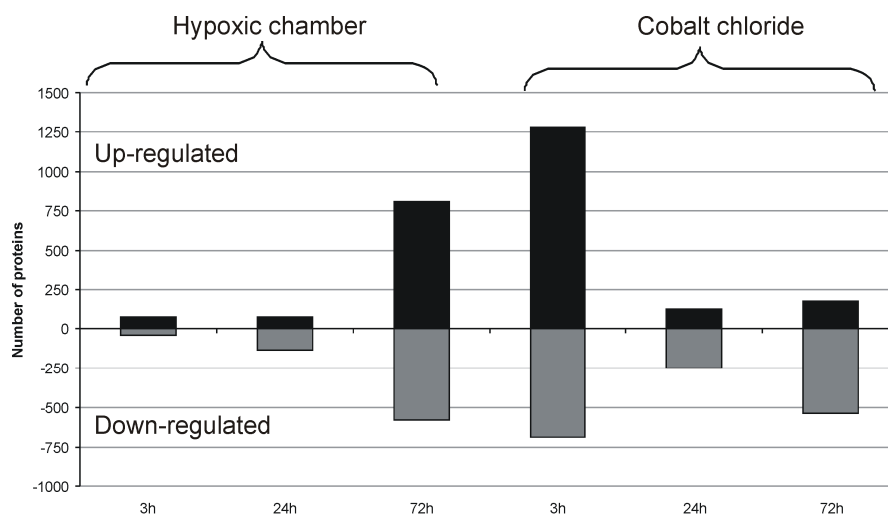
Figure 6.3 Number of up- and down-regulated proteins detected after 3, 24 and 72h from MDA-MB-231-HRE-tdTomato breast cancer cells incubated at 0.5% O$_2$ in a hypoxic chamber or treated with cobalt chloride.

Table 6.1 lists selected proteins whose expression was most significantly affected by hypoxia in MDA-MB-231-HRE-tdTomato cells. Heme oxygenase 1 was the most up-regulated protein under both hypoxic conditions in these breast cancer cells. Heme oxygenase 1 whose well known function is to dispose heme, also has a cyto-protective function against oxidative injury and cellular stress,[465] which may explain its up-regulation under hypoxia. It is a stress-inducible protein with potential anti-inflammatory effect.[456] Erythrocyte band 7 integral membrane protein and deoxyguanosine kinase were also up-regulated under hypoxia in MDA-MB-231-HRE-tdTomato cells. Deoxyguanosine kinase is required for the phosphorylation of several deoxyribonucleosides and certain nucleoside analogs widely employed as chemotherapeutic agents,[466] while Erythrocyte band 7 integral membrane protein was previously found among lysosomal integral membrane proteins.[467]

Loss of cell adhesion is one of the first steps leading to cancer metastasis. Integrin alpha-3, integrin beta-4 and syndecan-4 were down-regulated in our proteomics experiments (data not shown). Integrins are receptors that mediate cell-cell and cell-extracellular matrix attachment, play a role in cell signaling and regulate cellular shape, motility, and the cell cycle.[459,460] Integrin alpha-3 is a receptor for fibronectin, laminin, collagen 1 and thrombospondin.[468-471] Integrin beta-4 is a receptor for laminin and plays a critical structural role in the hemidesmosome of epithelial cells.[472] Syndecan-4 is a cell surface proteoglycan, which mediates cell–cell and cell–matrix interaction and plays a role in tumor metastasis.[473]

Table 6.1 The most significantly up-regulated proteins detected in the MDA-MB-231-HRE-tdTomato breast cancer cell line exposed to hypoxia (0.5% O$_2$) as well as a hypoxia mimetic (CoCl$_2$). The numbers in the treatment column represent the log$_2$ change in protein expression.

Accession	Description	Treatment	
		Chamber	CoCl$_2$
P09601	Heme oxygenase 1	4.6	3.8
P27105	Erythrocyte band 7 integral membrane protein	4.6	3.4
Q16854	Deoxyguanosine kinase, mitochondrial	2.9	3.3
Q9H1B7	Enhanced at puberty protein 1	2.2	2.7
P48723	Heat shock 70 kDa protein 13	2.8	2.6
Q9Y4C1	JmjC domain-containing histone demethylation protein 2A	2.5	2.6
O60675	Transcription factor MafK	3.9	2.5
Q8NE86	Coiled-coil domain-containing protein 109A	3.7	2.4
Q63HN8	RING finger protein 213	4.4	2.2
Q96G74	OTU domain-containing protein 5	2.3	2.2

A large number of proteins whose expression was altered under hypoxic conditions, was subjected to pathway analysis by REACTOME, which is an open-source, open access, manually curated and peer-reviewed pathway database.[474,475] Figure 6.4 presents the number of pathways that were up-regulated in breast cancer cells exposed to 0.5% O$_2$ in the hypoxic chamber or treated with cobalt chloride. In cobalt chloride treated cells the largest number of up-regulated pathways was observed after 3 h of treatment, followed by a gradual decrease of up-regulated pathways. Opposite to the cells treated with the hypoxia mimetic, the proteome of cells incubated inside the hypoxic chamber at 0.5% O$_2$ experienced a gradual increase in the number of up-regulated pathways, with the highest number observed after 72 h of hypoxic exposure.

Pathways up-regulated
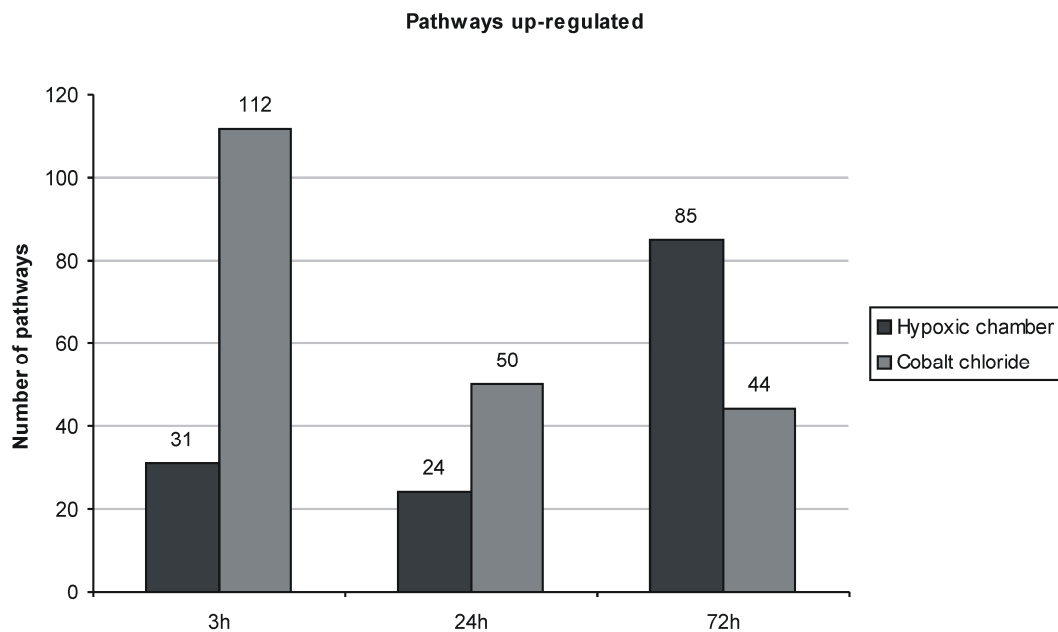
Figure 6.4 Number of up- or down-regulated pathways in human MDA-MB-231-HRE-tdTomato breast cancer cells incubated inside the hypoxic chamber at 0.5% O$_2$ or treated with cobalt chloride.

The data obtained from quantitative proteomics experiments was analyzed by bio-informatics tools such as STRAP.[476] Figure 6.5 shows the up-regulated proteins detected in MDA-MB-231-HRE-tdTomato breast cancer cells subjected to hypoxia by incubation in the hypoxic chamber for three different time points (3 h, 24 h and 72 h). The proteins involved in different biological functions such as binding, catalytic activity and translation regulation were significantly more up-regulated at 72 h, while proteins related to antioxidant activity were more up-regulated at 3 h and 24 h. On average, more biological functions were subject to up-regulation at 72 h as compared to 3 h and 24 h, which indicates a gradual increase in the up-regulation of the proteome due to hypoxia.
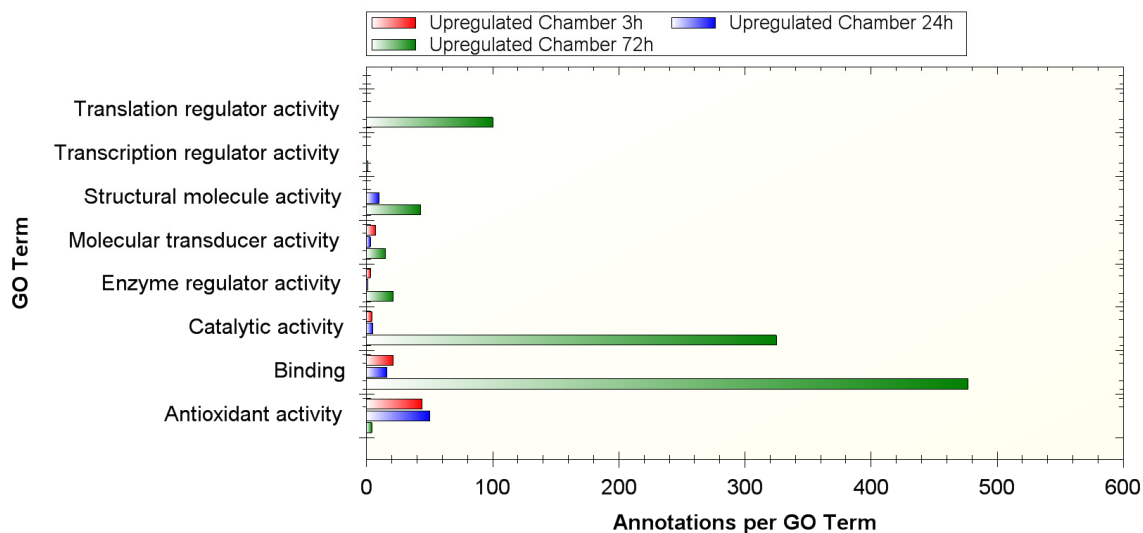
Figure 6.5 Comparison of up-regulated proteins detected in MDA-MB-231-HRE-tdTomato cells incubated inside the hypoxic chamber for three different time points. The x-axis represents the number of up-regulated proteins, while the y-axis shows their biological function. GO – gene ontology

The up-regulated proteins detected in MDA-MB-231-HRE-tdTomato breast cancer cells subjected to the hypoxia mimetic $CoCl_2$ for three different time points (3 h, 24 h and 72 h) are presented in figure 6.6. As compared to hypoxic chamber incubation, $CoCl_2$-induced hypoxia triggered the up-regulation of proteins involved in binding, transcription and catalytic activity after 3 h of treatment, while no significant up-regulation of proteins related to antioxidant activity was observed at any time point. The rapid hypoxic effect of $CoCl_2$ was observed with regard to different cell functions which lead to high catalytic activity and binding actions within the first 3 h of treatment.
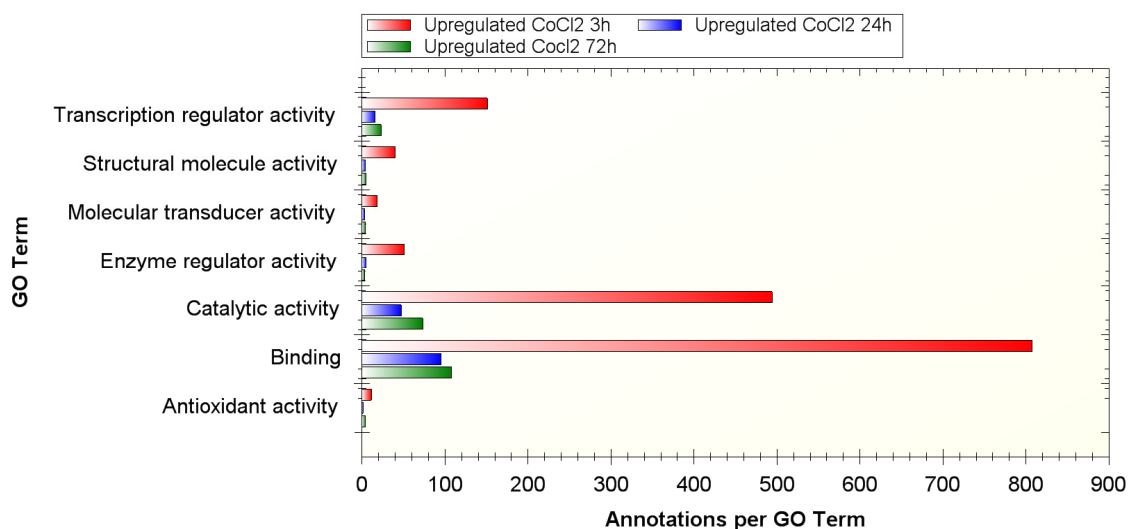
Figure 6.6 Comparison of up-regulated proteins detected in MDA-MB-231-HRE-tdTomato cells incubated with CoCl₂ for three different time points. The x-axis represents the number of up-regulated proteins, while the y-axis shows their biological function. GO – gene ontology

Table 6.2 presents up-regulated pathways in breast cancer cells that were incubated inside the hypoxic chamber or treated with cobalt chloride for 3, 24 and 72 h. Hypoxia up-regulated signaling by nerve growth factor (NGF), which is responsible for cell growth and survival,[477] and signaling by Rho GTPases and GPCRs, which are involved in metastasis.[478] Hypoxia also up-regulated energy metabolism, which manifested itself by an up-regulation of fatty acid, triacylglycerol, and ketone body metabolism pathway under hypoxia at all three time points tested.

Table 6.2 Pathways up-regulated by hypoxia in MDA-MB-231-tdTomato breast cancer cells.

Role	Pathways
Cell growth and survival	Signaling by NGF
Metastasis	Signaling by Rho GTPases
	GPCR downstream signaling
Energy metabolism	Fatty acid, triacylglycerol, and ketone body metabolism

These cell culture experiments provided information about hypoxia-induced proteome changes. However cancer cells grown in cell culture may respond differently to hypoxia as compared to cells grown in a native tumor environment. In our study, we performed multimodal imaging, which combined fluorescence imaging and MSI of breast tumor

xenograft models to visualize different tumor microenvironments such as normoxic, hypoxic and necrotic microenvironments. Accurate co-registration and alignment of different modalities was possible using fiducial markers compatible with all imaging techniques (figure 6.7). The tumor tissue boundary was imaged by bright field microscopy (figure 6.7A) while fluorescence microscopy revealed regions of tissue hypoxia marked by the presence of the tdTomato red fluorescent protein (figure 6.7B). Figure 6.7C presents H&E stained tumor tissue section obtained from the 2 mm thick tissue section presented in figure 6.7A. Adjacent tumor sections were analyzed by MSI to detect and identify small metabolites and proteins localized to normoxic, hypoxic and necrotic tumor regions. Detection of a tryptic peptide at *m/z* 2225.0 of the tdTomato fluorescent protein allowed mass spectrometric co-localization of tumor hypoxia with the corresponding fluorescence images (figure 6.7D).
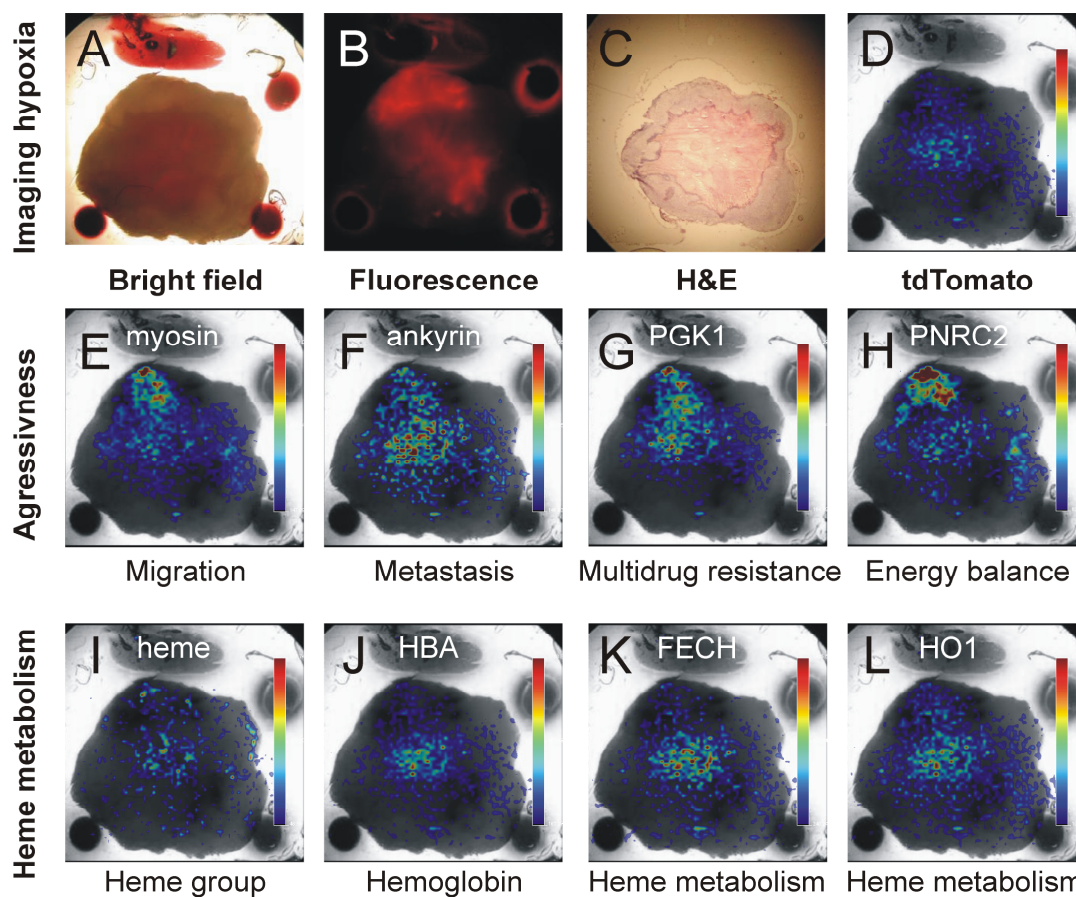
Figure 6.7 Multimodal imaging of MDA-MB-231-HRE-tdTomato breast tumor xenografts.
(A) Bright field and (B) fluorescence microscopy of a representative MDA-MB-231-HRE-
tdTomato breast tumor tissue section. (C) H&E stained tissue section obtained from the tumor
showin in (A). (D) tdTomato signal (m/z 2225.0) detected by MSI and overlaid with bright
field/fluorescence image. Imaging of molecules involved in tumor aggressiveness: (E) myosin

(m/z 833.5), (F) ankyrin (m/z 970.5), (G) phosphoglycerate kinase 1 (m/z 851.5) and (H) proline-rich nuclear receptor co- regulatory protein 2 (m/z 1279.8). Imaging of vasculature related molecules: (I) heme group (m/z 616.2), (J) hemoglobin subunit alpha (m/z 1529.7), (K) mitochondrial ferrochelatase (FECH) (m/z 1127.5) and (L) heme oxygenase 1 (HO1) (m/z 1248.6).

Metastasis is the most lethal aspect of cancer. A cancer cell's ability to metastasize depends on its loss of adhesion to the surrounding extracellular matrix, its migration into connective tissue, its intravasation, intravascular survival, extravasation and metastatic growth at a distant site. MSI images demonstrated that tryptic peptides from myosin (figure 6.7E) and ankyrin (figure 6.7F) co-localized with hypoxic tumor regions. Myosin heavy chain, non-muscle IIa is a cellular myosin that plays a role in cytokinesis, cell shape and migration.[479] A number of studies showed that myosins are involved in breast cancer cell spreading and migration.[479,480] Ankyrin, membrane-associated cytoskeletal protein, is involved in oncogenic signaling and metastatic progression of breast tumors.[481,482] The co-localization of myosin and ankyrin with hypoxic tumor regions indicates that enhanced cancer migration may occur from hypoxic regions in this breast tumor xenograft model.

The MSI images of tryptic peptides from human phosphoglycerate kinase 1 (PGK1, *m/z* 851.5, figure 6.7G) and proline-rich nuclear receptor co-regulatory protein 2 (PNRC2, *m/z* 1279.8, figure 6.7H) co-localized with the region of tumor hypoxia. Overexpression of PGK1 induces a multidrug resistance phenotype in an ovarian cancer cell line.[483] PGK1 is known to be involved in the onset of several malignancies, such as breast,[484] pancreatic,[485] gastric[486] and prostate cancer.[487] PGK1 is induced by exposure of cells to hypoxia,[488] which is in good agreement with our finding of PGK1 co-localization with hypoxic tumor regions. Multidrug resistance is a known indication of tumor aggressiveness and a significant barrier to the development of successful anti-cancer treatment. PNRC2 modulates the transcriptional activation of multiple nuclear receptors including estrogen related receptor alpha-1, PNRC2 also up-regulates the transcriptional activity of the progesterone receptor.[489,490] PNRC2 plays a role in controlling the energy balance between energy storage and energy expenditure,[491] targets the aberrant mRNA-containing RNPs into P bodies[492] and plays a role in activating aromatase, which is a key enzyme in estrogen synthesis in breast tumors.[493]

Exposure of cancer cells to hypoxia led to a rapid up-regulation of heme-related proteins such as heme oxygenase 1 (HO1) (100-fold after 72 h of chamber treatment) and mitochondrial ferrochelatase (FECH) (22-fold after 72 h of chamber treatment). MSI visualized tissue

regions with high heme and hemoglobin signal. The tryptic peptides of mitochondrial ferrochelatase (figure 6.7K) and heme oxygenase (figure 6.7L) from hypoxia up-regulated enzymes involved in heme metabolism co-localized with regions of high heme (figure 6.7I) and hemoglobin subunit alpha (figure 6.7J) signals.

6.4 Conclusions

Our combined proteomic and multimodal imaging approach resulted in the detection and visualization of multiple tryptic peptides obtained from proteins that are altered as a consequence of tumor hypoxia. Tumor hypoxia up-regulated proteins involved in pathways such as energy metabolism, metastasis, apoptosis, heme metabolism and immune system modulation. Tumor hypoxia down-regulated cell adhesion molecules such as integrin alpha-3, integrin beta-4 and syndecan-4. Interdisciplinary molecular techniques integrated with multimodal imaging methods revealed biological changes of hypoxia-regulated molecular signaling pathways inside heterogeneously distributed hypoxic tumor regions.

Abbreviations

2D-PAGE	2-dimensional polyacrylamide gel electrophoresis
ADP	adenosine diphosphate
AMP	adenosine monophosphate
amu	atomic mass unit
AP	atmospheric pressure
APCI	atmospheric pressure chemical ionization
AQ4N	anticancer drug banoxatrone
AQP0	Aquaporin-0
ASM	active shape model
ATCC	American Type Culture Collection
ATP	adenosine triphosphate
AuNP	gold nanoparticle
BB	bromophenol blue
BRPs	bradykinin related peptides
CAD	collisionally activated dissociation
CFP	cyan fluorescent protein
CHCA	alpha-cyano-4-hydroxycinnamic acid
CID	collision induced dissociation
CMC	carboxymethylcellulose
CNT	carbon nanotube
$CoCl_2$	cobalt chloride
CQ	clioquinol
CT	computed tomography
CV	cresyl violet
CVPS	cresyl violet-Ponceau S
Da	Dalton
DAG	diacylglycerol
DART	direct analysis in real time
DCE	Datacube Explorer
DESI	desorption electrospray ionization

dH$_2$O	distilled water
DHA	2,6-dihydroxyacetophenone
DHB	2.5-dihydroxy-benzoic acid
DI	desorption ionization
DIOS	desorption-ionization on silicon
DTT	dithiothreitol
EF1α	elongation factor 1α
EPPE	ethanol-preserved and paraffin embedded
ESI	electrospray ionization
ESI-MS	electrospray ionization mass spectrometry
EVA	ethylene vinyl acetate
F20TPP	meso-tetrakis (pentafluorophenyl) porphyrin
FAIMS	high-field asymmetric waveform ion mobility spectrometry
FDA	Food and Drug Administration
FECH	ferrochelatase
FFPE	formaldehyde fixed and paraffin embedded
FM	fiducial markers
FTICR	Fourier transform ion cyclotron resonance
FTMS	Fourier transform mass spectrometer
FWHM	full width at half maximum
GALDI	graphite-assisted laser desorption/ionization
GIMP	GNU Image Manipulation Program
GlcNAc	N-acetyl-D-glucosamine
GPChos	glycerophosphocholines
GPCR	G protein-coupled receptors
GPL	glycerophospholipid
Grp78	glucose regulated protein 78 kDa
H&E	hematoxylin and eosin
HDI	high definition imaging
HDMS	high definition mass spectrometry
HIF-1	hypoxia inducible factor 1
HIV	human immunodeficiency virus
HO1	heme oxygenase 1

HPLC	high performance liquid chromatography
HRE	hypoxia response element
HUPO-PSI	Human Proteome Organization-Proteomics Standards Initiative
HV	high vacuum
Hz	hertz
IAA	iodoacetamide
ICA	in-cell ion accumulation
ICR	ion cyclotron resonance
IHC	immunohistochemistry
IMS	ion mobility separation
IR-MALDI	infrared MALDI
ITO	indium tin oxide
IZ	interface zones
LAESI	laser ablation electrospray ionization
LA-ICP	laser ablation inductively coupled plasma
LC	liquid chromatography
LCM	laser capture microdissection
LDI	laser desorption ionization
Lipid MAPS	Lipid Metabolites and Pathways Strategy database
LIT	linear ion traps
LMIG	liquid metal ion gun
LPC	lysophosphatidylcholine
LPI	lysophosphatidylinositol
LTP	lipid transfer protein
LTQ	linear trap quadrupole
m/z	mass over charge ratio
m/Δm	resolving power
MALDESI	matrix assisted laser desorption electrospray ionization
MALDI	matrix-assisted laser desorption/ionization
MBP	myelin basic protein
ME-SALDI	matrix-enhanced surface-assisted laser desorption/ionization
ME-SIMS	matrix enhanced-SIMS
MetA-SIMS	metal assisted-SIMS

MITICS	MALDI Imaging Team Imaging Computing System
MMA	mass measurement accuracy
mmHg	millimetre of mercury
MPTP	1-methyl-4-phenyl-1,2,3,6-tetrahydropyridin
MRI	magnetic resonance imaging
MRM	multiple reaction monitoring
MRSI	magnetic resonance spectrometric imaging
MS	mass spectrometry
MS/MS	tandem mass spectrometry
MSI	mass spectrometric imaging
Mw	molecular weight
NAFLD	nonalcoholic fatty liver disease
nano-PALDI	nano-particle-assisted laser desorption/ionization
Nd:YAG	neodymium-doped yttrium aluminum garnet
NGF	nerve growth factor
NIMS	nanostructure initiator mass spectrometry
NIRF	near-infrared fluorescence
NL	neutral loss
NMR	nuclear magnetic resonance
oa-TOF	orthogonal acceleration-TOF
OBP-9	odorant binding protein 9
OCT	optimal cutting temperature
OGR1	ovarian cancer G protein-coupled receptor 1
OsO_4	osmium oxide
PA	phosphatidic acid
PBS	phosphate buffered saline
PC	phosphatidylcholine
PCA	principal component analysis
PE	phosphatidylethanolamine
PEG	polyethylene glycol
PET	positron emission tomography
PG	phosphatidylglycerol
PGK1	phosphoglycerate kinase 1

PHS	Public Health Service
PI	phosphatidylinositol
pL	picoliter
PLA	phospholipase A
PlsEtn	plasmenylethanolamine
PMI	post-mortem interval
PNA	p-nitroaniline
PNG	Portable Network Graphics
PNRC2	proline-rich nuclear receptor co regulatory protein
pO_2	pressure of oxygen
PPS	3-[3-(1,1-bisalkyloxyethyl)pyridin-1-yl]propane-1-sulfonate
PRDX 1	peroxiredoxin 1
PS	phosphatidylserine
PS	Ponceau S
PTM	post-translational modification
PUFA	polyunsaturated fatty acid
PVDF	polyvinylidene fluoride
q	quadrupole
QqQLIT	triple quadrupole linear ion trap
rcf	relative centrifugal force
RF	radio frequency
ROI	region of interest
RT	room temperature
SA	sinapinic acid
SCR-KO	Scrapper-knockout
SELDI	surface enhanced laser desorption
SIMS	secondary ion mass spectrometry
SM	sphingomyelin
SRM	single reaction monitoring
ST	sulfatide
TAG	triacylglycerol
td	tandem dimer
TFA	trifluoroacetic acid

TLC	thin-layer chromatography
TOF	time of flight
UDP	uridine diphosphate
UHV	ultra high vacuum
UV	ultraviolet
vol/vol	volume/volume
VTK	Visualisation Toolkit
WBA	whole-body autoradiography
wt/vol	weight/volume
z	charge state

Summary

Understanding the molecular composition of tumors is crucial for the development of successful cancer treatment strategies. Knowing "what" and "where" brings us closer to "how". In the case of disease related molecules mass spectrometry imaging (MSI) can not only detect and identify a broad range of substances but also provides their spatial distribution as images. In a single measurement MSI is able to deliver multiple molecular maps of complex biological samples. The combination of different imaging methods to visualize multiple molecular processes occurring inside breast tumors allowed us to explore the role of different tumor microenvironments in breast cancer in a more holistic approach.

In the present study, we combined bright field/fluorescence microscopy, MSI (reviewed in **chapter 2**) and histological tissue staining to visualize and explore the molecular consequences of tumor hypoxia and necrosis. Microscopy provided information about the localization of hypoxic and necrotic tumor regions, while MSI revealed the distribution of important biomolecules in these regions within heterogeneous tumor tissue. Additionally, the broad range of biological information acquired during mass spectrometric analysis makes MSI a modality that provides extremely rich data sets. Among all other imaging techniques, MSI has the capability of localizing the broadest range of biomolecules in a single experiment.

A novel fiducial marker system, presented in **chapter 3**, was developed for the alignment of images acquired by different imaging modalities. We used fiducial markers such as cresyl violet, Ponceau S, and bromophenol blue that possess a combination of optical and molecular properties that result in a clear mass spectrometric signature. This system allowed not only the precise overlay of images by providing a reference point but also proved to be a powerful tool for 3D volume reconstruction of different breast tumor microenvironments imaged in parallel by all three imaging methods. Fiducial markers were also used for 3D volume reconstruction of lipid and peptide distributions from multiple breast tumors imaged solely by MSI. Such reconstructions enabled the analysis of biomolecular distributions in all three dimensions with high molecular specificity. MSI proved to be a versatile tool capable of detecting biomolecules exclusively present in different tumor microenvironments as well as fiducial markers externally incorporated into the system under investigation.

One of the major goals of the project was to localize and investigate effects of hypoxia in breast tumor xenografts. In order to meet the first milestone of detecting hypoxia in this study, we used a genetically modified breast cancer cell line that expresses tdTomato red fluorescent protein under hypoxic conditions to generate breast tumor xenografts. **Chapter 4** presents a novel approach aimed at MSI visualization and MS investigation of this red fluorescent protein, which has traditionally only been imaged by fluorescence microscopy. To combine these two approaches, we performed targeted MS analysis and MSI visualization of tdTomato red fluorescent protein, which was expressed in the hypoxic regions of a breast tumor xenograft model. For the first time, a fluorescent protein has been visualized by both optical microscopy and MSI. While microscopy detected this protein's intrinsic feature of fluorescence, MSI detected its unique primary structure, in other words its unique amino acid sequence.

Samples of breast tumor tissue labeled with fiducial makers and containing the tdTomato red fluorescent protein provide great opportunities for detecting and visualizing biomolecules present in different tumor microenvironments, making MSI a great discovery tool.

Multimodal imaging incorporating MSI has been employed for investigating metabolites and lipids present in breast tumor xenograft mouse models. The identification of selected biomolecules was facilitated by ion mobility separation, which is a gas-phase separation method of ions implemented by mass spectrometry. This additional separation tool was useful during the MS analysis of complex tumor tissue. The multimodal imaging results of metabolites and lipids are presented in **chapter 5**. Ion images were overlaid with optical images of normoxic, hypoxic and necrotic tumor regions to identify molecules of interest in these regions and tandem mass spectrometry was employed for the identification of biomolecules. Our focus was on phosphocholine containing lipids, which could not be imaged *in vivo* by magnetic resonance spectroscopy imaging (MRSI) or *ex vivo* by secondary ion mass spectrometry (SIMS) imaging. While those imaging methods are capable of detecting free phosphocholine and total choline, MALDI-MSI proved to be a good method for imaging intact phospholipids and generated an atlas of multiple phosphatidylcholine distributions, which were assigned to three different tumor microenvironments, namely normoxic, hypoxic, and necrotic tumor regions. The spatial resolution of MALDI-MSI (150 µm) was well suited

to image different tumor microenvironments and revealed the molecular heterogeneity of these tumors.

Analyzing the tumor metabolome, lipidome and proteome is crucial for understanding tumor growth, angiogenesis, hypoxia, metastasis, drug- and radio-resistance, apoptosis and necrosis. All these processes contribute to tumor aggressiveness and challenge our understanding of tumor expansion and treatment strategies. In this study, we have integrated state of the art quantitative proteomics, which provided global as well as detailed information about hypoxia-induced proteome changes in breast cancer cells. **Chapter 6** presents results from the analysis of hypoxia-induced proteome changes in breast cancer cells performed by a classical bottom-up approach utilizing peptide labeling. We investigated changes occurring in breast cancer cells exposed to hypoxic conditions, which mimicked the state of tissue hypoxia frequently present inside growing tumors. We also exposed breast cancer cells to cobalt chloride, which is a well-established hypoxia mimetic, and discovered that in addition to its hypoxia-mimicking effects, it also exerts proapoptotic activity. Our results indicated that hypoxia triggers the expression of multiple proteins involved in heme metabolism, cell proliferation and survival as well as cancer metastasis.

We deem the current effort will bring us nearer to comprehend the molecular biology of breast cancer and ultimately facilitate the development of new strategies for breast cancer treatment.

Samenvatting

Het begrijpen van de moleculaire samenstelling van tumoren is één van de cruciale stappen in de ontwikkeling van succesvolle behandelingsstrategieën tegen kanker. Kennis van het "wat"en "waar" brengt ons dichter bij het "hoe". In het geval we te maken hebben met ziektegerelateerde moleculen, kan massaspectrometrie imaging (MSI) niet alleen een grote verscheidenheid van stoffen detecteren maar kan het ook informatie over hun ruimtelijke verdeling verschaffen. MSI kan in één enkele meting ruimtelijke verdelingen van meerdere moleculen genereren voor complexe biologische monsters. De combinatie van verschillende imaging methoden voor de gerichte visualisatie van meerdere specifieke processen die in borstkankertumoren plaatsvinden, gaf ons de mogelijkheid om het verschijnsel van tumorgroei op een meer holistische wijze te bestuderen.

In deze studie combineren we lichtveld/fluorescentie microscopie, MSI (besproken in hoofdstuk 2) en histologische weefselkleuring, voor het visualiseren en onderzoeken van de samenstelling van tumorhypoxie en -necrose. Microscopie leverde informatie over de lokalisatie van de hypoxisische en necrotische tumorgebieden, terwijl MSI de bio-moleculaire verdeling van heterogeen tumorweefsel toonde. De diepgang in biologische kennis die werd opgedaan gedurende de analyse met massaspectrometrie maakt bovendien van MSI, van alle modaliteiten, de meest waardevolle modaliteit. Van alle afbeeldingstechnieken, heeft MSI het vermogen om de grootste diversiteit van biomoleculen in een enkel experiment af te beelden.

Een baanbrekend referentie-markeer-systeem, beschreven in hoofdstuk 3, is ontwikkeld ten behoeve van de uitlijning van afbeeldingen die verworven zijn met verschillende imaging modaliteiten. We hebben referentiemarkeringen zoals cresyl violet, Ponceau S, en bromophenol blue gebruikt, die een combinatie van optische en moleculaire eigenschappen hebben die een een uitgesproken massaspectrometrische signatuur geven. Dit referentie-markeer-systeem was niet alleen in staat om verschillende afbeeldingen exact over elkaar heen te kunnen leggen door middel van de referentiepunten, maar bewees ook een krachtig instrument te zijn voor 3D ruimtelijke reconstructie van verschillende borsttumor micro-milieus, die parallel gemeten zijn met de drie imaging methoden. De referentiemarkeringen zijn ook gebruikt voor de 3D ruimtelijke reconstructie van lipide- en peptide-verdelingen in meerdere borsttumoren, die alleen met MSI gemeten zijn. Deze reconstructies gaven de

mogelijkheid om biomoleculaire verdelingen te analyseren in drie dimensies met een grote moleculaire specificiteit. MSI heeft bewezen een veelzijdig instrument te zijn om onafhankelijke waarnemingen te doen van zowel biomoleculen die enkel in verschillende micro-milieus van tumoren voorkomen, als van referentiemarkeringen die later zijn toegevoegd aan het te bestuderen systeem.

Eén van de belangrijkste doelen van het project was het opsporen en onderzoeken van de effecten van hypoxie in borsttumoren. Om deze eerste mijlpaal in de hypoxie-studie van borstkanker te bereiken, werd er gebruik gemaakt van een genetisch gemodificeerde borstkanker cellijn die het fluorescerende eiwit tdTomato onder hypoxie tot expressie brengt om zo xenograft borstkankermodellen te genereren. Hoofdstuk 4 beschrijft de aanpak gericht op MSI-visualisatie en MS-onderzoek van een rood-fluorescent eiwit dat traditioneel alleen met fluorescentie microscopie bekeken kon worden. Om deze twee aanpakken te combineren, hebben we gerichte MS-analyse en MSI-visualisatie op een rood-fluorescent tdTomato eiwit uitgevoerd, waarbij het eiwit tot expressie gebracht was in de hypoxie regio's van een xenograft model van een borsttumor. Voor de eerste maal is een fluorescent eiwit gevisualiseerd met zowel optische microscopie als MSI. Hoewel microscopie gebruikt maakt van de intrinsieke eigenschap van fluorescentie van een eiwit, kan MSI een meer fundamentele eigenschap bepalen, namelijk de unieke structuur van het eiwit, in andere woorden de unieke aminozuursequentie. Het specifieke biochemische karakter van MSI opent de weg naar de detectie van elk biomolecuul, dat aanwezig is in een weefselmonster.

Monsters van borsttumorweefsel die gelabeld zijn met referentiemarkeringen en het rood-fluorescente tdTomato eiwit, kunnen interessant studiemateriaal zijn voor aanvullende detectie en visualisatie van biomoleculen die aanwezig zijn in verschillende micro-milieus in een tumor. Dit leidt ons naar tot nu toe onverkende wetenschappelijke gebieden en maakt van MSI een geweldig instrument om nieuwe ontdekkingen te doen.

Multi-modale imaging met MSI als één van de modaliteiten, is gebruikt voor de studie van metabolieten en peptiden die aanwezig zijn in borsttumor xenograft muismodellen.
De identificatie van geselecteerde biomoleculen werd ondersteund door gebruik te maken van ion mobility separation, een massaspectrometrische scheidingsmethode van ionen in de gasfase. Deze extra scheidingsstap was noodzakelijk voor de MS-analyse van de extreem complexe tumorweefsels. De resultaten van de multi-modale imaging van metabolieten en

lipiden staan in hoofdstuk 5. Ionenafbeeldingen zijn gebruikt als leidraad op zoek naar weefselregio's die interessante moleculen bevatten, en tandem massaspectrometie werd gebruikt voor de identificatie van de biomoleculen.

Onze focus was gericht op fosfor bevattende lipiden, welke in vivo niet zichtbaar gemaakt kunnen worden met magnetic resonance spectroscopy imaging (MRSI) en ook ex vivo niet met SIMS-imaging (secondary ion mass spectrometry imaging). Terwijl deze twee imaging methoden in staat zijn om vrije fosfocholine en totaal choline te detecteren, heeft MALDI-MSI (matrix-assisted laser desorption/ionization MSI) bewezen een ideale methode te zijn voor het afbeelden van intacte fosfolipiden. MALDI-MSI heeft een altas van meerdere fosfatidylcholine-verdelingen voortgebracht die aan drie verschillende tumor-micro-milieus toegekend werden, namelijk de hypoxie-regio, de necrotische kern en het levend weefsel. De ruimtelijke resolutie van MALDI-MSI (150 µm) was toereikend om verschillende micro-milieus af te beelden die aanwezig zijn in tumoren en de biochemische heterogeniteit van weefsel te ontrafelen.

Hoewel MSI een zeer effectief ex vivo instrument is voor het detecteren en visualiseren van biomoleculen, zijn de methoden voor MSI nog in ontwikkeling, en blijft het een uitdaging om biomoleculen af te beelden die in minder grote hoeveelheden aanwezig zijn. De analyse van tumormetaboloom, -lipodoom en -proteoom is cruciaal voor het begrijpen van tumorgroei, hypoxie, metastase, medicijnresistentie en radiotherapie, apoptose en necrose. Al deze processen dragen bij aan de tumor-agressiviteit en vormen een uitdaging voor het begrijpen van tumorgroei en behandelingsstrategieën. In deze studie hebben we state-of-the-art kwantitatieve proteomics geïntegreerd, dat zowel globale als gedetailleerde informatie opleverde over hypoxie-geïnduceerde proteome veranderingen in borstkankercellen. Hoofdstuk 6 toont de resultaten van de analyse van hypoxie-geïnduceerde veranderingen in borstkanker, die uitgevoerd zijn met een klassieke bottom-up aanpak met peptide-labeling. We onderzochten veranderingen die optraden in borstkankercellen onder invloed van het zuurstoftekort dat de toestand van weefselhypoxie nabootste die plaatsvindt in groeiende tumoren. We hebben de kankercellen ook blootgesteld aan kobaltchloride, een gevestigde hypoxie-nabootsing, en vonden naast de hypoxia-nabootsingseffecten een aanvullende pro-apoptotische activiteit. Resultaten gaven aan dat hypoxia de expressie van meerdere eiwitten induceert die betrokken zijn bij heem metabolisme, celproliferatie, het overleven van de cellen en tevens kankermetastase.

Bibliography

(1)   Chaurand, P.; Cornett, D.S.; Angel, P.M.; Caprioli, R.M. From whole-body sections down to cellular level, multiscale imaging of phospholipids by MALDI mass spectrometry. *Mol Cell Proteomics* **2011**, *10*, O110 004259.

(2)   Giaccia, A.; Siim, B.G.; Johnson, R.S. HIF-1 as a target for drug development. *Nat Rev Drug Discov* **2003**, *2*, 803-811.

(3)   Epstein, A.C.; Gleadle, J.M.; McNeill, L.A.; Hewitson, K.S.; O'Rourke, J.; Mole, D.R.; Mukherji, M.; Metzen, E.; Wilson, M.I.; Dhanda, A.; Tian, Y.M.; Masson, N.; Hamilton, D.L.; Jaakkola, P.; Barstead, R.; Hodgkin, J.; Maxwell, P.H.; Pugh, C.W.; Schofield, C.J.; Ratcliffe, P.J. C. elegans EGL-9 and mammalian homologs define a family of dioxygenases that regulate HIF by prolyl hydroxylation. *Cell* **2001**, *107*, 43-54.

(4)   Berra, E.; Ginouves, A.; Pouyssegur, J. The hypoxia-inducible-factor hydroxylases bring fresh air into hypoxia signalling. *EMBO Rep* **2006**, *7*, 41-45.

(5)   Jaakkola, P.; Mole, D.R.; Tian, Y.M.; Wilson, M.I.; Gielbert, J.; Gaskell, S.J.; Kriegsheim, A.; Hebestreit, H.F.; Mukherji, M.; Schofield, C.J.; Maxwell, P.H.; Pugh, C.W.; Ratcliffe, P.J. Targeting of HIF-alpha to the von Hippel-Lindau ubiquitylation complex by O2-regulated prolyl hydroxylation. *Science* **2001**, *292*, 468-472.

(6)   Jewell, U.R.; Kvietikova, I.; Scheid, A.; Bauer, C.; Wenger, R.H.; Gassmann, M. Induction of HIF-1alpha in response to hypoxia is instantaneous. *FASEB J* **2001**, *15*, 1312-1314.

(7)   Vaupel, P.; Kallinowski, F.; Okunieff, P. Blood flow, oxygen and nutrient supply, and metabolic microenvironment of human tumors: a review. *Cancer Res* **1989**, *49*, 6449-6465.

(8)   Siuzdak, G. *The Expanding Role of Mass Spectrometry in Biotechnology*, Second ed.; MCC Press: San Diego, CA, 2006

(9)   Fenn, J.B.; Mann, M.; Meng, C.K.; Wong, S.F.; Whitehouse, C.M. Electrospray Ionization for Mass Spectrometry of Large Biomolecules. *Science* **1989**, *246*, 64.

(10)   Karas, M.; Bachmann, D.; Hillenkamp, F. Influence of the Wavelength in High Irradiance Ultraviolet Laser Desorption Mass Spectrometry of Organic Molecules. *Anal. Chem.* **1985**, *57*, 2935-2939.

(11)   Leinweber, B.D.; Tsaprailis, G.; Monks, T.J.; Lau, S.S. Improved MALDI-TOF imaging yields increased protein signals at high molecular mass. *J. Am. Soc. Mass Spectrom.* **2009**, *20*, 89-95.

(12)   Caprioli, R.M.; Farmer, T.B.; Gile, J. Molecular imaging of biological samples: localization of peptides and proteins using MALDI-TOF MS. *Anal. Chem.* **1997**, *69*, 4751-4760.

(13)   Stoeckli, M.; Chaurand, P.; Hallahan, D.E.; Caprioli, R.M. Imaging mass spectrometry: a new technology for the analysis of protein expression in mammalian tissues. *Nat. Med.* **2001**, *7*, 493-496.

(14)   Colliver, T.L.; Brummel, C.L.; Pacholski, M.L.; Swanek, F.D.; Ewing, A.G.; Winograd, N. Atomic and molecular imaging at the single-cell level with TOF-SIMS. *Anal. Chem.* **1997**, *69*, 2225-2231.

(15)   Clerc, J.; Fourre, C.; Fragu, P. SIMS microscopy: methodology, problems and perspectives in mapping drugs and nuclear medicine compounds. *Cell Biol. Int.* **1997**, *21*, 619-633.

(16)   Heeren, R.M.A.; McDonnell, L.A.; Amstalden, E.; Luxembourg, S.L.; Altelaar, A.F.M.; Piersma, S.R. Why don't biologists use SIMS?: A critical evaluation of imaging MS *Appl. Surf. Sci.* **2006**, *252*, 6827-6835.

(17)   Takats, Z.; Wiseman, J.M.; Gologan, B.; Cooks, R.G. Mass spectrometry sampling under ambient conditions with desorption electrospray ionization. *Science* **2004**, *306*, 471-473.

(18)   Woods, A.S.; Jackson, S.N. Brain tissue lipidomics: direct probing using matrix-assisted laser desorption/ionization mass spectrometry. *AAPS J.* **2006**, *8*, 391-395.

(19)   Tanaka, K.; Ido, Y.; Akita, S.; Yoshida, Y.; Yoshida, T. Detection of High Mass Molecules by Laser Desorption Time-Of-Flight Mass Spectrometry. *Proc. Japan-China Joint Symp. Mass Spectrom., 2nd* **1987**, 185-188

(20)   Karas, M.; Hillenkamp, F. Laser desorption ionization of proteins with molecular masses exceeding 10,000 daltons. *Anal. Chem.* **1988**, *60*, 2299-2301.

(21)   McDonnell, L.A.; Heeren, R.M. Imaging mass spectrometry. *Mass Spectrom. Rev.* **2007**, *26*, 606-643.

(22)   Todd, P.J.; Schaaff, T.G.; Chaurand, P.; Caprioli, R.M. Organic ion imaging of biological tissue with secondary ion mass spectrometry and matrix-assisted laser desorption/ionization. *J. Mass Spectrom.* **2001**, *36*, 355-369.

(23)   Spengler, B.; Hubert, M. Scanning microprobe matrix-assisted laser desorption ionization (SMALDI) mass spectrometry: instrumentation for sub-micrometer resolved LDI and MALDI surface analysis. *J. Am. Soc. Mass Spectrom.* **2002**, *13*, 735-748.

(24)   Chaurand, P.; Schriver, K.E.; Caprioli, R.M. Instrument design and characterization for high resolution MALDI-MS imaging of tissue sections. *J. Mass Spectrom.* **2007**, *42*, 476-489.

(25)   Holle, A.; Haase, A.; Kayser, M.; Hohndorf, J. Optimizing UV laser focus profiles for improved MALDI performance. *J. Mass Spectrom.* **2006**, *41*, 705-716.

(26)   Khatib-Shahidi, S.; Andersson, M.; Herman, J.L.; Gillespie, T.A.; Caprioli, R.M. Direct molecular analysis of whole-body animal tissue sections by imaging MALDI mass spectrometry. *Anal. Chem.* **2006**, *78*, 6448-6456.

(27)   Slaveykova, V.I.; Guignard, C.; Eybe, T.; Migeon, H.N.; Hoffmann, L. Dynamic NanoSIMS ion imaging of unicellular freshwater algae exposed to copper. *Anal. Bioanal. Chem.* **2009**, *393*, 583-589.

(28)   Pacholski, M.L.; Winograd, N. Imaging with Mass Spectrometry. *Chem. Rev.* **1999**, *99* 2977-3005

(29)   Kaletas, B.K.; van der Wiel, I.M.; Stauber, J.; Guzel, C.; Kros, J.M.; Luider, T.M.; Heeren, R.M. Sample preparation issues for tissue imaging by imaging MS. *Proteomics* **2009**, *9*, 2622-2633.

(30)   Weibel, D.; Wong, S.; Lockyer, N.; Blenkinsopp, P.; Hill, R.; Vickerman, J.C. A C60 primary ion beam system for time of flight secondary ion mass spectrometry: its development and secondary ion yield characteristics. *Anal. Chem.* **2003**, *75*, 1754-1764.

(31)   Klerk, L.A.; Lockyer, N.P.; Kharchenko, A.; MacAleese, L.P.; Dankers, P.Y.W.; Vickerman, J.C.; Heeren, R.M.A. C60+ Secondary Ion Microscopy Using a Delay Line Detector. *Anal. Chem.* **2010**, *82*, 801-807.

(32)   Altelaar, A.F.; Luxembourg, S.L.; McDonnell, L.A.; Piersma, S.R.; Heeren, R.M. Imaging mass spectrometry at cellular length scales. *Nat. Protoc.* **2007**, *2*, 1185-1196.

(33)   McDonnell, L.A.; Piersma, S.R.; Altelaar, A.F.M.; Mize, T.H.; Luxembourg, S.L.; Verhaert, P.D.; van Minnen, J.; Heeren, R.M. Subcellular imaging mass spectrometry of brain tissue. *J. Mass Spectrom.* **2005**, *40*, 160-168.

(34)   Altelaar, A.F.; Klinkert, I.; Jalink, K.; de Lange, R.P.; Adan, R.A.; Heeren, R.M.; Piersma, S.R. Gold-enhanced biomolecular surface imaging of cells and tissue by SIMS and MALDI mass spectrometry. *Anal. Chem.* **2006**, *78*, 734-742.

(35)   Delcorte, A.; Bour, J.; Aubriet, F.; Muller, J.-F.; Bertrand, P., 75, . Sample Metallization for Performance Improvement in Desorption/Ionization of Kilodalton Molecules: Quantitative Evaluation, Imaging Secondary Ion MS, and Laser Ablation *Anal. Chem.* **2003**, *75*, 6875.

(36)   Wu, K.J.; Odom, R.W. Matrix-Enhanced Secondary Ion Mass Spectrometry: A Method for Molecular Analysis of Solid Surfaces. *Anal. Chem.* **1996**, *68*, 873-882.

(37)   Francese, S.; Dani, F.R.; Traldi, P.; Mastrobuoni, G.; Pieraccini, G.; Moneti, G. MALDI mass spectrometry imaging, from its origins up to today: the state of the art. *Comb. Chem. High Throughput Screening* **2009**, *12*, 156-174.

(38)   Nakata, Y.; Honda, Y.; Ninomiya, S.; Seki, T.; Aoki, T.; Matsuo, J. Matrix-free high-resolution imaging mass spectrometry with high-energy ion projectiles. *J. Mass Spectrom.* **2009**, *44*, 128-136.

(39)   Nygren, H.; Malmberg, P. High resolution imaging by organic secondary ion mass spectrometry. *Trends Biotechnol.* **2007**, *25*, 499-504.

(40)   Pumphrey, G.M.; Hanson, B.T.; Chandra, S.; Madsen, E.L. Dynamic secondary ion mass spectrometry imaging of microbial populations utilizing C-labelled substrates in pure culture and in soil. *Environ. Microbiol.* **2009**, *11*, 220-229.

(41)   Finzi-Hart, J.A.; Pett-Ridge, J.; Weber, P.K.; Popa, R.; Fallon, S.J.; Gunderson, T.; Hutcheon, I.D.; Nealson, K.H.; Capone, D.G. Fixation and fate of C and N in the cyanobacterium Trichodesmium using nanometer-scale secondary ion mass spectrometry. *Proc. Natl. Acad. Sci. U. S. A.* **2009**, *106*, 6345-6350.

(42)   Ostrowski, S.G.; Kurczy, M.E.; Roddy, T.P.; Winograd, N.; Ewing, A.G. Secondary ion MS imaging to relatively quantify cholesterol in the membranes of individual cells from differentially treated populations. *Anal. Chem.* **2007**, *79*, 3554-3560.

(43)   Chandra, S. 3D subcellular SIMS imaging in cryogenically prepared single cells. *Appl. Surf. Sci.* **2004**, *231-232*, 467-469.

(44)   Kabalka, G.W.; Yao, M.L.; Marepally, S.R.; Chandra, S. Biological evaluation of boronated unnatural amino acids as new boron carriers. *Appl. Radiat. Isot.* **2009**, *67*, S374-S379.

(45)   Chandra, S.; Morrison, G.H. Imaging ion and molecular transport at subcellular resolution by secondary ion mass spectrometry. *Int. J. Mass Spectrom.* **1995**, *143*, 161- 176.

(46)   Pacholski, M.L.; Cannon, D.M., Jr.; Ewing, A.G.; Winograd, N. Static time-of-flight secondary ion mass spectrometry imaging of freeze-fractured, frozen-hydrated biological membranes. *Rapid Commun. Mass Spectrom.* **1998**, *12*, 1232-1235.

(47)   Strick, R.; Strissel, P.L.; Gavrilov, K.; Levi-Setti, R. Cation-chromatin binding as shown by ion microscopy is essential for the structural integrity of chromosomes. *J. Cell Biol.* **2001**, *155*, 899-910.

(48)   Wu, L.; Lu, X.; Kulp, K.S.; Knize, M.G.; Berman, E.S.; Nelson, E.J.; Felton, J.S.; Wu, K.J. Imaging and differentiation of mouse embryo tissues by ToF-SIMS. *Int. J. Mass Spectrom.* **2007**, *260*, 137-145.

(49)   Nygren, H.; Borner, K.; Malmberg, P.; Tallarek, E.; Hagenhoff, B. Imaging TOF-SIMS of rat kidney prepared by high-pressure freezing. *Microsc. Res. Tech.* **2005**, *68*, 329-334.

(50)   Nygren, H.; Malmberg, P.; Kriegeskotte, C.; Arlinghaus, H.F. Bioimaging TOF-SIMS: localization of cholesterol in rat kidney sections. *FEBS Lett.* **2004**, *566*, 291-293.

(51)   Nygren, H.; Johansson, B.R.; Malmberg, P. Bioimaging TOF-SIMS of tissues by gold ion bombardment of a silver-coated thin section. *Microsc. Res. Tech.* **2004**, *65*, 282-286.

(52)   Jones, E.A.; Lockyera, N.P.; Vickerman, J.C. Mass spectral analysis and imaging of tissue by ToF-SIMS—The role of buckminsterfullerene, C60+, primary ions *Int. J. Mass Spectrom.* **2007**, *260*, 146-157

(53)   McCandlish, C.A.; McMahon, J.M.; Todd, P.J. Secondary ion images of the rodent brain. *J. Am. Soc. Mass Spectrom.* **2000**, *11*, 191-199.

(54)   Touboul, D.; Halgand, F.; Brunelle, A.; Kersting, R.; Tallarek, E.; Hagenhoff, B.; Laprevote, O. Tissue molecular ion imaging by gold cluster ion bombardment. *Anal. Chem.* **2004**, *76*, 1550-1559.

(55)   Sjovall, P.; Lausmaa, J.; Johansson, B. Mass spectrometric imaging of lipids in brain tissue. *Anal. Chem.* **2004**, *76*, 4271-4278.

(56)   Todd, P.J.; McMahon, J.M.; McCandlish, C.A., Jr. Secondary ion images of the developing rat brain. *J. Am. Soc. Mass Spectrom.* **2004**, *15*, 1116-1122.

(57)   Malmberg, P.; Nygren, H.; Richter, K.; Chen, Y.; Dangardt, F.; Friberg, P.; Magnusson, Y. Imaging of lipids in human adipose tissue by cluster ion TOF-SIMS. *Microsc. Res. Tech.* **2007**, *70*, 828-835.

(58)   Belazi, D.; Sole-Domenech, S.; Johansson, B.; Schalling, M.; Sjovall, P. Chemical analysis of osmium tetroxide staining in adipose tissue using imaging ToF-SIMS. *Histochem. Cell Biol.* **2009**, *132*, 105-115.

(59)   Perkins, M.C.; Bell, G.; Briggs, D.; Davies, M.C.; Friedman, A.; Hart, C.A.; Roberts, C.J.; Rutten, F.J. The application of ToF-SIMS to the analysis of herbicide formulation penetration into and through leaf cuticles. *Colloids Surf., B* **2008**, *67*, 1-13.

(60)   Ameen, A.P.; Short, R.D.; Johns, R.; Schwach, G. The surface analysis of implant materials. 1. The surface composition of a titanium dental implant material. *Clin. Oral Implants Res.* **1993**, *4*, 144-150.

(61)   Touboul, D.; Brunelle, A.; Halgand, F.; De La Porte, S.; Laprevote, O. Lipid imaging by gold cluster time-of-flight secondary ion mass spectrometry: application to Duchenne muscular dystrophy. *J. Lipid Res.* **2005**, *46*, 1388-1395.

(62)   Tahallah, N.; Brunelle, A.; De La Porte, S.; Laprevote, O. Lipid mapping in human dystrophic muscle by cluster-time-of-flight secondary ion mass spectrometry imaging. *J. Lipid Res.* **2008**, *49*, 438-454.

(63)   Kishikawa, Y.; Gong, H.; Kitaoka, T.; Amemiya, T.; Takaya, K.; Tozu, M.; Hoshi, T.; Ohashi, Y. Elements and organic substances in epiretinal proliferative tissue excised during vitreous surgery: analysis by time-of-flight secondary-ion mass spectrometry. *J. Electron Microsc.* **2003**, *52*, 349-354.

(64)   Gong, H.; Takami, Y.; Amemiya, T.; Tozu, M.; Ohashi, Y. Ocular surface in Zn-deficient rats. *Ophthalmic Res.* **2004**, *36*, 129-138.

(65)   Malmberg, P.; Borner, K.; Chen, Y.; Friberg, P.; Hagenhoff, B.; Mansson, J.E.; Nygren, H. Localization of lipids in the aortic wall with imaging TOF-SIMS. *Biochim. Biophys. Acta* **2007**, *1771*, 185-195.

(66)   Mas, S.; Touboul, D.; Brunelle, A.; Aragoncillo, P.; Egido, J.; Laprevote, O.; Vivanco, F. Lipid cartography of atherosclerotic plaque by cluster-TOF-SIMS imaging. *Analyst* **2007**, *132*, 24-26.

(67)   Kulp, K.S.; Berman, E.S.; Knize, M.G.; Shattuck, D.L.; Nelson, E.J.; Wu, L.; Montgomery, J.L.; Felton, J.S.; Wu, K.J. Chemical and biological differentiation of three human breast cancer cell types using time-of-flight secondary ion mass spectrometry. *Anal. Chem.* **2006**, *78*, 3651-3658.

(68)   Nygren, H.; Hagenhoff, B.; Malmberg, P.; Nilsson, M.; Richter, K. Bioimaging TOF-SIMS: High resolution 3D imaging of single cells. *Microsc. Res. Tech.* **2007**, *70*, 969-974.

(69)   Fletcher, J.S.; Lockyer, N.P.; Vaidyanathan, S.; Vickerman, J.C. TOF-SIMS 3D biomolecular imaging of Xenopus laevis oocytes using buckminsterfullerene (C60) primary ions. *Anal. Chem.* **2007**, *79*, 2199-2206.

(70)   Smith, D.R.; Chandra, S.; Barth, R.F.; Yang, W.; Joel, D.D.; Coderre, J.A. Quantitative imaging and microlocalization of boron-10 in brain tumors and infiltrating tumor cells by SIMS ion microscopy: relevance to neutron capture therapy. *Cancer Res.* **2001**, *61*, 8179-8187.

(71)   Chandra, S.; Kabalka, G.W.; Lorey, D.R., 2nd; Smith, D.R.; Coderre, J.A. Imaging of fluorine and boron from fluorinated boronophenylalanine in the same cell at organelle resolution by correlative ion microscopy and confocal laser scanning microscopy. *Clin. Cancer Res.* **2002**, *8*, 2675-2683.

(72)   Monroe, E.B.; Jurchen, J.C.; Lee, J.; Rubakhin, S.S.; Sweedler, J.V. Vitamin E imaging and localization in the neuronal membrane. *J. Am. Chem. Soc.* **2005**, *127*, 12152-12153.

(73)   Kempson, I.M.; Skinner, W.M.; Kirkbride, P.K.; Nelson, A.J.; Martin, R.R. Time-of-flight secondary ion mass spectrometry analysis of hair from archaeological remains. *Eur. J. Mass Spectrom.* **2003**, *9*, 589-597.

(74)   Mazel, V.; Richardin, P.; Debois, D.; Touboul, D.; Cotte, M.; Brunelle, A.; Walter, P.; Laprevote, O. Identification of ritual blood in African artifacts using TOF-SIMS and synchrotron radiation microspectroscopies. *Anal. Chem.* **2007**, *79*, 9253-9260.

(75)   Brunelle, A.; Laprevote, O. Lipid imaging with cluster time-of-flight secondary ion mass spectrometry. *Anal. Bioanal. Chem.* **2009**, *393*, 31-35.

(76)   Ifa, D.R.; Wiseman, J.M.; Song, Q.; Cooks, R.G. Development of capabilities for imaging mass spectrometry under ambient conditions with desorption electrospray ionization (DESI). *Int. J. Mass Spectrom.* **2007**, *259*, 8-15.

(77)   Dole, M.; Mack, L.L.; Hines, R.L.; Mobley, R.C.; Ferguson, L.D.; Alice, M.B. Molecular beams of macroions. *J. Chem. Phys.* **1968**, *49*, 2240.

(78)   Iribarne, J.V.; Thomson, B.A. On the evaporation of small ions from charged droplets. *J. Chem. Phys.* **1976**, *64*, 2287.

(79)   Dill, A.L.; Ifa, D.R.; Manicke, N.E.; Ouyang, Z.; Cooks, R.G. Mass spectrometric imaging of lipids using desorption electrospray ionization. *J. Chromatogr., B: Anal. Technol. Biomed. Life Sci.* **2009**, *877*, 2883-2889

(80)   Wiseman, J.M.; Puolitaival, S.M.; Takats, Z.; Cooks, R.G.; Caprioli, R.M. Mass spectrometric profiling of intact biological tissue by using desorption electrospray ionization. *Angew. Chem., Int. Ed. Engl.* **2005**, *44*, 7094-7097.

(81)   Talaty, N.; Takats, Z.; Cooks, R.G. Rapid in situ detection of alkaloids in plant tissue under ambient conditions using desorption electrospray ionization. *Analyst* **2005**, *130*, 1624-1633.

(82)   Kertesz, V.; Van Berkel, G.J. Improved imaging resolution in desorption electrospray ionization mass spectrometry. *Rapid Commun. Mass Spectrom.* **2008**, *22*, 2639-2644.

(83)   Wiseman, J.M.; Ifa, D.R.; Zhu, Y.; Kissinger, C.B.; Manicke, N.E.; Kissinger, P.T.; Cooks, R.G. Desorption electrospray ionization mass spectrometry: Imaging drugs and metabolites in tissues. *Proc. Natl. Acad. Sci. U. S. A.* **2008**, *105*, 18120-18125.

(84)   Esquenazi, E.; Dorrestein, P.C.; Gerwick, W.H. Probing marine natural product defenses with DESI-imaging mass spectrometry. *Proc. Natl. Acad. Sci. U. S. A.* **2009**, *106*, 7269-7270.

(85)   Lane, A.L.; Nyadong, L.; Galhena, A.S.; Shearer, T.L.; Stout, E.P.; Parry, R.M.;
        Kwasnik, M.; Wang, M.D.; Hay, M.E.; Fernandez, F.M.; Kubanek, J. Desorption
        electrospray ionization mass spectrometry reveals surface-mediated antifungal
        chemical defense of a tropical seaweed. *Proc. Natl. Acad. Sci. U. S. A.* **2009**, *106*,
        7314-7319.

(86)   Myung, S.; Wiseman, J.M.; Valentine, S.J.; Takats, Z.; Cooks, R.G.; Clemmer, D.E.
        Coupling desorption electrospray ionization with ion mobility/mass spectrometry for
        analysis of protein structure: evidence for desorption of folded and denatured States. *J.
        Phys. Chem. B* **2006**, *110*, 5045-5051.

(87)   Berry, J.I.; Sun, S.; Dou, Y.; Wucher, A.; Winograd, N. Laser desorption and imaging
        of proteins from ice via UV femtosecond laser pulses. *Anal. Chem.* **2003**, *75*, 5146-
        5151.

(88)   Bouamrani, A.; Ternier, J.; Ratel, D.; Benabid, A.L.; Issartel, J.P.; Brambilla, E.;
        Berger, F. Direct-tissue SELDI-TOF mass spectrometry analysis: a new application
        for clinical proteomics. *Clin. Chem.* **2006**, *52*, 2103-2106.

(89)   Ageta, H.; Asai, S.; Sugiura, Y.; Goto-Inoue, N.; Zaima, N.; Setou, M. Layer-specific
        sulfatide localization in rat hippocampus middle molecular layer is revealed by
        nanoparticle-assisted laser desorption/ionization imaging mass spectrometry. *Med.
        Mol. Morphol.* **2009**, *42*, 16-23.

(90)   Liu, Q.; Xiao, Y.; Pagan-Miranda, C.; Chiu, Y.M.; He, L. Metabolite Imaging Using
        Matrix-Enhanced Surface-Assisted Laser Desorption/Ionization Mass Spectrometry
        (ME-SALDI-MS). *J. Am. Soc. Mass Spectrom.* **2009**, *20*, 80-88.

(91)   Yanes, O.; Woo, H.K.; Northen, T.R.; Oppenheimer, S.R.; Shriver, L.; Apon, J.;
        Estrada, M.N.; Potchoiba, M.J.; Steenwyk, R.; Manchester, M.; Siuzdak, G.
        Nanostructure initiator mass spectrometry: tissue imaging and direct biofluid analysis.
        Anal. Chem. **2009**, *81*, 2969-2975.

(92)   Becker, J.S.; Zoriy, M.; Matusch, A.; Wu, B.; Salber, D.; Palm, C.; Becker, J.S.
        Bioimaging of metals by laser ablation inductively coupled plasma mass spectrometry
        (LA-ICP-MS). *Mass Spectrom Rev* **2009**, *29*, 156-175.

(93)   Sampson, J.S.; Hawkridge, A.M.; Muddiman, D.C. Generation and detection of
        multiply-charged peptides and proteins by matrix-assisted laser desorption
        electrospray ionization (MALDESI) Fourier transform ion cyclotron resonance mass
        spectrometry. *J Am Soc Mass Spectrom* **2006**, *17*, 1712-1716.

(94)   Nemes, P.; Woods, A.S.; Vertes, A. Simultaneous imaging of small metabolites and
        lipids in rat brain tissues at atmospheric pressure by laser ablation electrospray
        ionization mass spectrometry. *Anal Chem* **2010**, *82*, 982-988.

(95)   Li, Y.; Shrestha, B.; Vertes, A. Atmospheric pressure infrared MALDI imaging mass
        spectrometry for plant metabolomics. *Anal. Chem.* **2008**, *80*, 407-420.

(96)   Goodwin, R.J.; Pennington, S.R.; Pitt, A.R. Protein and peptides in pictures: imaging
        with MALDI mass spectrometry. *Proteomics* **2008**, *8*, 3785-3800.

(97)   Taban, I.M.; Altelaar, A.F.; van der Burgt, Y.E.; McDonnell, L.A.; Heeren, R.M.;
        Fuchser, J.; Baykut, G. Imaging of peptides in the rat brain using MALDI-FTICR
        mass spectrometry. *J. Am. Soc. Mass Spectrom.* **2007**, *18*, 145-151.

(98)   Trim, P.J.; Henson, C.M.; Avery, J.L.; McEwen, A.; Snel, M.F.; Claude, E.; Marshall,
        P.S.; West, A.; Princivalle, A.P.; Clench, M.R. Matrix-assisted laser
        desorption/ionization-ion mobility separation-mass spectrometry imaging of
        vinblastine in whole body tissue sections. *Anal. Chem.* **2008**, *80*, 8628-8634.

(99)   Northen, T.R.; Yanes, O.; Northen, M.T.; Marrinucci, D.; Uritboonthai, W.; Apon, J.;
        Golledge, S.L.; Nordstrom, A.; Siuzdak, G. Clathrate nanostructures for mass
        spectrometry. *Nature* **2007**, *449*, 1033-1036.

(100)   Sanchez, J.C.; Corthals, G.L.; Hochstrasser, D.F. *Biomedical Applications of Proteomics*; Wiley-vch Verlag Gmbh Weinheim, 2004.

(101)   Aerni, H.R.; Cornett, D.S.; Caprioli, R.M. Automated acoustic matrix deposition for MALDI sample preparation. *Anal. Chem.* **2006**, *78*, 827-834.

(102)   Schwartz, S.A.; Reyzer, M.L.; Caprioli, R.M. Direct tissue analysis using matrix-assisted laser desorption/ionization mass spectrometry: practical aspects of sample preparation. *J. Mass Spectrom.* **2003**, *38*, 699-708.

(103)   Kim, J.S.; Kim, J.Y.; Kim, H.J. Suppression of matrix clusters and enhancement of peptide signals in MALDI-TOF mass spectrometry using nitrilotriacetic acid. *Anal. Chem.* **2005**, *77*, 7483-7488.

(104)   Mas, S.; Perez, R.; Martinez-Pinna, R.; Egido, J.; Vivanco, F. Cluster TOF-SIMS imaging: a new light for in situ metabolomics? *Proteomics* **2008**, *8*, 3735-3745.

(105)   Stoeckli, M.; Staab, D.; Schweitzer, A. Compound and metabolite distribution measured by MALDI mass spectrometric imaging in whole-body tissue sections. *Int. J. Mass Spectrom.* **2007**, *260*, 195-202

(106)   MacAleese, L.; Stauber, J.; Heeren, R.M. Perspectives for imaging mass spectrometry in the proteomics landscape. *Proteomics* **2009**, *9*, 819-834.

(107)   Chaurand, P.; Norris, J.L.; Cornett, D.S.; Mobley, J.A.; Caprioli, R.M. New developments in profiling and imaging of proteins from tissue sections by MALDI mass spectrometry. *J. Proteome Res.* **2006**, *5*, 2889-2900.

(108)   Ayorinde, F.O.; Hambright, P.; Porter, T.N.; Keith, Q.L., Jr. Use of meso-tetrakis(pentafluorophenyl)porphyrin as a matrix for low molecular weight alkylphenol ethoxylates in laser desorption/ ionization time-of-flight mass spectrometry. *Rapid Commun. Mass Spectrom.* **1999**, *13*, 2474-2479.

(109)   Wisztorski, M.; Croix, D.; Macagno, E.; Fournier, I.; Salzet, M. Molecular MALDI imaging: an emerging technology for neuroscience studies. *Dev. Neurobiol.* **2008**, *68*, 845-858.

(110)   Reyzer, M.L.; Caprioli, R.M. MALDI-MS-based imaging of small molecules and proteins in tissues. *Curr. Opin. Chem. Biol.* **2007**, *11*, 29-35.

(111)   Rubakhin, S.S.; Greenough, W.T.; Sweedler, J.V. Spatial profiling with MALDI MS: distribution of neuropeptides within single neurons. *Anal. Chem.* **2003**, *75*, 5374-5380.

(112)   Hopfgartner, G.; Varesio, E.; Stoeckli, M. Matrix-assisted laser desorption/ionization mass spectrometric imaging of complete rat sections using a triple quadrupole linear ion trap. *Rapid Commun. Mass Spectrom.* **2009**, *23*, 733-736.

(113)   Stoeckli, M.; Staab, D.; Schweitzer, A.; Gardiner, J.; Seebach, D. Imaging of a beta-peptide distribution in whole-body mice sections by MALDI mass spectrometry. *J. Am. Soc. Mass Spectrom.* **2007**, *18*, 1921-1924.

(114)   Sugiura, Y.; Konishi, Y.; Zaima, N.; Kajihara, S.; Nakanishi, H.; Taguchi, R.; Setou, M. Visualization of the cell-selective distribution of PUFA-containing phosphatidylcholines in mouse brain by imaging mass spectrometry. *J. Lipid Res.* **2009**, *50*, 1776-1788.

(115)   Murphy, R.C.; Hankin, J.A.; Barkley, R.M. Imaging of lipid species by MALDI mass spectrometry. *J. Lipid Res.* **2008**, in press.

(116)   Monroe, E.B.; Annangudi, S.P.; Hatcher, N.G.; Gutstein, H.B.; Rubakhin, S.S.; Sweedler, J.V. SIMS and MALDI MS imaging of the spinal cord. *Proteomics* **2008**, *8*, 3746-3754.

(117)   Skold, K.; Svensson, M.; Nilsson, A.; Zhang, X.; Nydahl, K.; Caprioli, R.M.; Svenningsson, P.; Andren, P.E. Decreased striatal levels of PEP-19 following MPTP lesion in the mouse. *J. Proteome Res.* **2006**, *5*, 262-269.

(118) Minerva, L.; Clerens, S.; Baggerman, G.; Arckens, L. Direct profiling and identification of peptide expression differences in the pancreas of control and ob/ob mice by imaging mass spectrometry. *Proteomics* **2008**, *8*, 3763-3774.

(119) Schwamborn, K.; Krieg, R.C.; Reska, M.; Jakse, G.; Knuechel, R.; Wellmann, A. Identifying prostate carcinoma by MALDI-Imaging. *Int. J. Mol. Med.* **2007**, *20*, 155-159.

(120) Burnum, K.E.; Tranguch, S.; Mi, D.; Daikoku, T.; Dey, S.K.; Caprioli, R.M. Imaging mass spectrometry reveals unique protein profiles during embryo implantation. *Endocrinology* **2008**, *149*, 3274-3278.

(121) Mikawa, S.; Suzuki, M.; Fujimoto, C.; Sato, K. Imaging of phosphatidylcholines in the adult rat brain using MALDI-TOF MS. *Neurosci. Lett.* **2009**, *451*, 45-49.

(122) Fletcher, J.S. Cellular imaging with secondary ion mass spectrometry. *Analyst* **2009**, *134*, 2204-2215.

(123) Debois, D.; Hamze, K.; Guerineau, V.; Le Caer, J.P.; Holland, I.B.; Lopes, P.; Ouazzani, J.; Seror, S.J.; Brunelle, A.; Laprevote, O. In situ localisation and quantification of surfactins in a Bacillus subtilis swarming community by imaging mass spectrometry. *Proteomics* **2008**, *8*, 3682-3691.

(124) Yang, Y.L.; Xu, Y.; Straight, P.; Dorrestein, P.C. Translating metabolic exchange with imaging mass spectrometry. *Nat. Chem. Biol.* **2009**, *5*, 885-887.

(125) Esquenazi, E.; Coates, C.; Simmons, L.; Gonzalez, D.; Gerwick, W.H.; Dorrestein, P.C. Visualizing the spatial distribution of secondary metabolites produced by marine cyanobacteria and sponges via MALDI-TOF imaging. *Mol. BioSyst.* **2008**, *4*, 562-570.

(126) Cha, S.; Zhang, H.; Ilarslan, H.I.; Wurtele, E.S.; Brachova, L.; Nikolau, B.J.; Yeung, E.S. Direct profiling and imaging of plant metabolites in intact tissues by using colloidal graphite-assisted laser desorption ionization mass spectrometry. *Plant J.* **2008**, *55*, 348-360.

(127) Chaurand, P.; Fouchecourt, S.; DaGue, B.B.; Xu, B.J.; Reyzer, M.L.; Orgebin-Crist, M.C.; Caprioli, R.M. Profiling and imaging proteins in the mouse epididymis by imaging mass spectrometry. *Proteomics* **2003**, *3*, 2221-2239.

(128) Chaurand, P.; Rahman, M.A.; Hunt, T.; Mobley, J.A.; Gu, G.; Latham, J.C.; Caprioli, R.M.; Kasper, S. Monitoring mouse prostate development by profiling and imaging mass spectrometry. *Mol. Cell. Proteomics* **2008**, *7*, 411-423.

(129) Yanagisawa, K.; Shyr, Y.; Xu, B.J.; Massion, P.P.; Larsen, P.H.; White, B.C.; Roberts, J.R.; Edgerton, M.; Gonzalez, A.; Nadaf, S.; Moore, J.H.; Caprioli, R.M.; Carbone, D.P. Proteomic patterns of tumour subsets in non-small-cell lung cancer. *Lancet* **2003**, *362*, 433-439.

(130) Chaurand, P.; Latham, J.C.; Lane, K.B.; Mobley, J.A.; Polosukhin, V.V.; Wirth, P.S.; Nanney, L.B.; Caprioli, R.M. Imaging mass spectrometry of intact proteins from alcohol-preserved tissue specimens: bypassing formalin fixation. *J. Proteome Res.* **2008**, *7*, 3543-3555.

(131) Groseclose, M.R.; Massion, P.P.; Chaurand, P.; Caprioli, R.M. High-throughput proteomic analysis of formalin-fixed paraffin-embedded tissue microarrays using MALDI imaging mass spectrometry. *Proteomics* **2008**, *8*, 3715-3724.

(132) Ronci, M.; Bonanno, E.; Colantoni, A.; Pieroni, L.; Di Ilio, C.; Spagnoli, L.G.; Federici, G.; Urbani, A. Protein unlocking procedures of formalin-fixed paraffin-embedded tissues: application to MALDI-TOF imaging MS investigations. *Proteomics* **2008**, *8*, 3702-3714.

(133) Stauber, J.; Lemaire, R.; Franck, J.; Bonnel, D.; Croix, D.; Day, R.; Wisztorski, M.; Fournier, I.; Salzet, M. MALDI imaging of formalin-fixed paraffin-embedded tissues:

application to model animals of Parkinson disease for biomarker hunting. *J. Proteome Res.* **2008**, *7*, 969-978.

(134)   Lemaire, R.; Desmons, A.; Tabet, J.C.; Day, R.; Salzet, M.; Fournier, I. Direct analysis and MALDI imaging of formalin-fixed, paraffin-embedded tissue sections. *J. Proteome Res.* **2007**, *6*, 1295-1305.

(135)   Djidja, M.C.; Francese, S.; Loadman, P.M.; Sutton, C.W.; Scriven, P.; Claude, E.; Snel, M.F.; Franck, J.; Salzet, M.; Clench, M.R. Detergent addition to tryptic digests and ion mobility separation prior to MS/MS improves peptide yield and protein identification for in situ proteomic investigation of frozen and formalin-fixed paraffin-embedded adenocarcinoma tissue sections. *Proteomics* **2009**, *9*, 2750-2763.

(136)   Djidja, M.C.; Claude, E.; Snel, M.F.; Scriven, P.; Francese, S.; Carolan, V.; Clench, M.R. MALDI-ion mobility separation-mass spectrometry imaging of glucose-regulated protein 78 kDa (Grp78) in human formalin-fixed, paraffin-embedded pancreatic adenocarcinoma tissue sections. *J. Proteome Res.* **2009**, *8*, 4876-4884.

(137)   Stauber, J.; Macaleese, L.; Franck, J.; Claude, E.; Snel, M.; Kukrer Kaletas, B.; Wiel, I.M.; Wisztorski, M.; Fournier, I.; Heeren, R.M. On-Tissue Protein Identification and Imaging by MALDI-Ion Mobility Mass Spectrometry. *J. Am. Soc. Mass Spectrom.* **2010**, *21*, 338-347.

(138)   Crecelius, A.C.; Cornett, D.S.; Caprioli, R.M.; Williams, B.; Dawant, B.M.; Bodenheimer, B. Three-dimensional visualization of protein expression in mouse brain structures using imaging mass spectrometry. *J. Am. Soc. Mass Spectrom.* **2005**, *16*, 1093-1099.

(139)   Liu, Q.; Xiao, Y.; Pagan-Miranda, C.; Chiu, Y.M.; He, L. Metabolite imaging using matrix-enhanced surface-assisted laser desorption/ionization mass spectrometry (ME-SALDI-MS). *J Am Soc Mass Spectrom* **2009**, *20*, 80-88.

(140)   Schwartz, S.A.; Weil, R.J.; Thompson, R.C.; Shyr, Y.; Moore, J.H.; Toms, S.A.; Johnson, M.D.; Caprioli, R.M. Proteomic-based prognosis of brain tumor patients using direct-tissue matrix-assisted laser desorption ionization mass spectrometry. *Cancer Res.* **2005**, *65*, 7674-7681.

(141)   Seeley, E.H.; Caprioli, R.M. Molecular imaging of proteins in tissues by mass spectrometry. *Proc. Natl. Acad. Sci. U. S. A.* **2008**, *105*, 18126-18131.

(142)   Cornett, D.S.; Mobley, J.A.; Dias, E.C.; Andersson, M.; Arteaga, C.L.; Sanders, M.E.; Caprioli, R.M. A novel histology-directed strategy for MALDI-MS tissue profiling that improves throughput and cellular specificity in human breast cancer. *Mol. Cell. Proteomics* **2006**, *5*, 1975-1983.

(143)   Lemaire, R.; Menguellet, S.A.; Stauber, J.; Marchaudon, V.; Lucot, J.P.; Collinet, P.; Farine, M.O.; Vinatier, D.; Day, R.; Ducoroy, P.; Salzet, M.; Fournier, I. Specific MALDI imaging and profiling for biomarker hunting and validation: fragment of the 11S proteasome activator complex, Reg alpha fragment, is a new potential ovary cancer biomarker. *J. Proteome Res.* **2007**, *6*, 4127-4134.

(144)   Roy, S.; Touboul, D.; Brunelle, A.; Germain, D.P.; Prognon, P.; Laprevote, O.; Chaminade, P. Imaging mass spectrometry: a new tool for the analysis of skin biopsy. Application in Fabry's disease. *Ann. Pharm. Fr.* **2006**, *64*, 328-334.

(145)   Berman, E.S.; Fortson, S.L.; Checchi, K.D.; Wu, L.; Felton, J.S.; Wu, K.J.; Kulp, K.S. Preparation of single cells for imaging/profiling mass spectrometry. *J. Am. Soc. Mass Spectrom.* **2008**, *19*, 1230-1236.

(146)   Guo, J.; Colgan, T.J.; DeSouza, L.V.; Rodrigues, M.J.; Romaschin, A.D.; Siu, K.W. Direct analysis of laser capture microdissected endometrial carcinoma and epithelium by matrix-assisted laser desorption/ionization mass spectrometry. *Rapid Commun. Mass Spectrom.* **2005**, *19*, 2762-2766.

(147) Chaurand, P.; Sanders, M.E.; Jensen, R.A.; Caprioli, R.M. Proteomics in diagnostic pathology: profiling and imaging proteins directly in tissue sections. *Am. J. Pathol.* **2004**, *165*, 1057-1068.

(148) Lemaire, R.; Wisztorski, M.; Desmons, A.; Tabet, J.C.; Day, R.; Salzet, M.; Fournier, I. MALDI-MS direct tissue analysis of proteins: Improving signal sensitivity using organic treatments. *Anal. Chem.* **2006**, *78*, 7145-7153.

(149) Crecelius, A.; Gotz, A.; Arzberger, T.; Frohlich, T.; Arnold, G.J.; Ferrer, I.; Kretzschmar, H.A. Assessing quantitative post-mortem changes in the gray matter of the human frontal cortex proteome by 2-D DIGE. *Proteomics* **2008**, *8*, 1276-1291.

(150) Svensson, M.; Skold, K.; Nilsson, A.; Falth, M.; Nydahl, K.; Svenningsson, P.; Andren, P.E. Neuropeptidomics: MS applied to the discovery of novel peptides from the brain. *Anal. Chem.* **2007**, *79*, 15-16, 18-21.

(151) Jia, X.; Hollung, K.; Therkildsen, M.; Hildrum, K.I.; Bendixen, E. Proteome analysis of early post-mortem changes in two bovine muscle types: M. longissimus dorsi and M. semitendinosis. *Proteomics* **2006**, *6*, 936-944.

(152) Svensson, M.S., K.; Svenningsson, P.; Andren, P. E. Peptidomics-Based Discovery of Novel Neuropeptides. *J. Proteome Res.* **2003**, *2*, 213-219.

(153) O'Callaghan, J.P.; Sriram, K. Focused microwave irradiation of the brain preserves in vivo protein phosphorylation: comparison with other methods of sacrifice and analysis of multiple phosphoproteins. *J. Neurosci. Methods* **2004**, *135*, 159-168.

(154) Ferrer, I.; Santpere, G.; Arzberger, T.; Bell, J.; Blanco, R.; Boluda, S.; Budka, H.; Carmona, M.; Giaccone, G.; Krebs, B.; Limido, L.; Parchi, P.; Puig, B.; Strammiello, R.; Strobel, T.; Kretzschmar, H. Brain protein preservation largely depends on the postmortem storage temperature: implications for study of proteins in human neurologic diseases and management of brain banks: a BrainNet Europe Study. *J. Neuropathol. Exp. Neurol.* **2007**, *66*, 35-46.

(155) Fountoulakis, M.; Hardmeier, R.; Hoger, H.; Lubec, G. Postmortem changes in the level of brain proteins. *Exp. Neurol.* **2001**, *167*, 86-94.

(156) Franzen, B.; Yang, Y.; Sunnemark, D.; Wickman, M.; Ottervald, J.; Oppermann, M.; Sandberg, K. Dihydropyrimidinase related protein-2 as a biomarker for temperature and time dependent post mortem changes in the mouse brain proteome. *Proteomics* **2003**, *3*, 1920-1929.

(157) Goodwin, R.J.; Dungworth, J.C.; Cobb, S.R.; Pitt, A.R. Time-dependent evolution of tissue markers by MALDI-MS imaging. *Proteomics* **2008**, *8*, 3801-3808.

(158) Skold, K.; Svensson, M.; Norrman, M.; Sjogren, B.; Svenningsson, P.; Andren, P.E. The significance of biochemical and molecular sample integrity in brain proteomics and peptidomics: stathmin 2-20 and peptides as sample quality indicators. *Proteomics* **2007**, *7*, 4445-4456.

(159) O'Callaghan, J.P.; Sriram, K. Focused microwave irradiation of the brain preserves in vivo protein phosphorylation: comparison with other methods of sacrifice and analysis of multiple phosphoproteins. *J Neurosci Methods* **2004**, *135*, 159-168.

(160) Svensson, M.; Skold, K.; Svenningsson, P.; Andren, P.E. Peptidomics-based discovery of novel neuropeptides. *J Proteome Res* **2003**, *2*, 213-219.

(161) Svensson, M.; Boren, M.; Skold, K.; Falth, M.; Sjogren, B.; Andersson, M.; Svenningsson, P.; Andren, P.E. Heat stabilization of the tissue proteome: a new technology for improved proteomics. *J. Proteome Res.* **2009**, *8*, 974-981.

(162) Mange, A.; Chaurand, P.; Perrochia, H.; Roger, P.; Caprioli, R.M.; Solassol, J. Liquid Chromatography-Tandem and MALDI imaging mass spectrometry analyses of RCL2/SC100-fixed paraffin embedded tissues: proteomics evaluation of an alternate fixative for biomarker discovery. *J. Proteome Res.* **2009**, *8*, 5619-5628.

(163) Chen, R.; Hui, L.; Sturm, R.M.; Li, L. Three dimensional mapping of neuropeptides and lipids in crustacean brain by mass spectral imaging. *J. Am. Soc. Mass Spectrom.* **2009**, *20*, 1068-1077.

(164) Sugiura, Y.; Shimma, S.; Setou, M. Thin Sectioning Improves the Peak Intensity and Signal-to-Noise Ratio in Direct Tissue Mass Spectrometry *J. Mass Spectrom. Soc. Jpn.* **2006**, *54*, 45-48.

(165) Caldwell, R.L.; Caprioli, R.M. Tissue profiling by mass spectrometry: a review of methodology and applications. *Mol. Cell. Proteomics* **2005**, *4*, 394-401.

(166) Chaurand, P.; Schwartz, S.A.; Crecelius, A.; Caprioli, R.M., Montreal, Canada, June 8-12, 2003 **2003**; ASMS.

(167) Chaurand, P.; Schwartz, S.A.; Billheimer, D.; Xu, B.J.; Crecelius, A.; Caprioli, R.M. Integrating histology and imaging mass spectrometry. *Anal. Chem.* **2004**, *76*, 1145-1155.

(168) Groseclose, M.R.; Andersson, M.; Hardesty, W.M.; Caprioli, R.M. Identification of proteins directly from tissue: in situ tryptic digestions coupled with imaging mass spectrometry. *J. Mass Spectrom.* **2007**, *42*, 254-262.

(169) Andersson, M.; Groseclose, M.R.; Deutch, A.Y.; Caprioli, R.M. Imaging mass spectrometry of proteins and peptides: 3D volume reconstruction. *Nat. Methods* **2008**, *5*, 101-108.

(170) Brocchieri, L.; Karlin, S. Protein length in eukaryotic and prokaryotic proteomes. *Nucleic Acids Res.* **2005**, *33*, 3390-3400.

(171) Duncan, R.; McConkey, E.H. How many proteins are there in a typical mammalian cell? *Clin. Chem.* **1982**, *28*, 749-755.

(172) Rohner, T.C.; Staab, D.; Stoeckli, M. MALDI mass spectrometric imaging of biological tissue sections. *Mech. Ageing Dev.* **2005**, *126*, 177-185.

(173) Binz, P.A.; Muller, M.; Hoogland, C.; Zimmermann, C.; Pasquarello, C.; Corthals, G.; Sanchez, J.C.; Hochstrasser, D.F.; Appel, R.D. The molecular scanner: concept and developments. *Curr. Opin. Biotechnol.* **2004**, *15*, 17-23.

(174) Stauber, J.; Macaleese, L.; Franck, J.; Claude, E.; Snel, M.; Kukrer Kaletas, B.; Wiel, I.M.; Wisztorski, M.; Fournier, I.; Heeren, R.M. On-Tissue Protein Identification and Imaging by MALDI-Ion Mobility Mass Spectrometry. *J. Am. Soc. Mass Spectrom.* **2009**.

(175) Gluckmann, M.; Pfenninger, A.; Kruger, R.; Thierolf, M.; Karas, M.; Horneffer, V.; Hillenkamp, F.; Strupat, K. Mechanisms in MALDI analysis: surface interaction or incorporation of analytes? *Int. J. Mass Spectrom.* **2001**, *210/211*, 121-132.

(176) Zenobi, R.; Knochenmuss., R. Ion formation in MALDI mass spectrometry. *Mass Spec. Rev.* **1998**, *17*, 227.

(177) Beavis, R.C.; Chait, B.T. Cinnamic acid derivatives as matrices for ultraviolet laser desorption mass spectrometry of proteins. *Rapid Commun. Mass Spectrom.* **1989**, *3*, 432-435.

(178) Beavis, R.C.; Chait, B.T. Matrix-assisted laser-desorption mass spectrometry using 355 nm radiation. *Rapid Commun. Mass Spectrom.* **1989**, *3*, 436-439.

(179) Tang, K.; Taranenko, N.I.; Allman, S.L.; Chang, L.Y.; Chen, C.H. Detection of 500-nucleotide DNA by laser desorption mass spectrometry. *Rapid Commun. Mass Spectrom.* **1994**, *8*, 727-730.

(180) Wu, K.J.; Steding, A.; Becker, C.H. Matrix-assisted laser desorption time-of-flight mass spectrometry of oligonucleotides using 3-hydroxypicolinic acid as an ultraviolet-sensitive matrix. *Rapid Commun. Mass Spectrom.* **1993**, *7*, 142-146.

(181) Herring, K.D.; Oppenheimer, S.R.; Caprioli, R.M. Direct tissue analysis by matrix-assisted laser desorption ionization mass spectrometry: application to kidney biology. *Semin. Nephrol.* **2007**, *27*, 597-608.

(182) Puolitaival, S.M.; Burnum, K.E.; Cornett, D.S.; Caprioli, R.M. Solvent-free matrix dry-coating for MALDI imaging of phospholipids. *J. Am. Soc. Mass Spectrom.* **2008**, *19*, 882-886.

(183) Heeren, R.M.A.; Smith, D.F.; Stauber, J.; Kükrer-Kaletas, B.; Macaleese, L.A. Imaging Mass Spectrometry: Hype or Hope? *J Am Soc Mass Spectrom* **2009**, *20*, 1006-1014.

(184) Lemaire, R.; Tabet, J.C.; Ducoroy, P.; Hendra, J.B.; Salzet, M.; Fournier, I. Solid ionic matrixes for direct tissue analysis and MALDI imaging. *Anal. Chem.* **2006**, *78*, 809-819.

(185) Dreisewerd, K. The desorption process in MALDI. *Chem. Rev.* **2003**, *103*, 395-426.

(186) Chen, Y.T.; Ling, Y.C. Detection of water-soluble vitamins by matrix-assisted laser desorption/ionization time-of-flight mass spectrometry using porphyrin matrices. *J. Mass Spectrom.* **2002**, *37*, 716-730.

(187) Ling, Y.C.; Lin, L.; Chen, Y.T. Quantitative analysis of antibiotics by matrix-assisted laser desorption/ionization time-of-flight mass spectrometry. *Rapid Commun. Mass Spectrom.* **1998**, *12*, 317-327.

(188) McLean, J.A.; Stumpo, K.A.; Russell, D.H. Size-selected (2-10 nm) gold nanoparticles for matrix assisted laser desorption ionization of peptides. *J. Am. Chem. Soc.* **2005**, *127*, 5304-5305.

(189) Su, C.L.; Tseng, W.L. Gold nanoparticles as assisted matrix for determining neutral small carbohydrates through laser desorption/ionization time-of-flight mass spectrometry. *Anal. Chem.* **2007**, *79*, 1626-1633.

(190) Feng, C.H.; Lu, C.Y. A new matrix for analyzing low molecular mass compounds and its application for determination of carcinogenic areca alkaloids by matrix-assisted laser desorption ionization time-of-flight mass spectrometry. *Anal. Chim. Acta* **2009**, *649*, 230-235.

(191) Bouslimani, A.; Bec, N.; Glueckmann, M.; Hirtz, C.; Larroque, C. Matrix-assisted laser desorption/ionization imaging mass spectrometry of oxaliplatin derivatives in heated intraoperative chemotherapy (HIPEC)-like treated rat kidney. *Rapid Commun. Mass Spectrom.* **2010**, *24*, 415-421.

(192) Norris, J.L.; Porter, N.A.; Caprioli, R.M. Mass spectrometry of intracellular and membrane proteins using cleavable detergents. *Anal. Chem.* **2003**, *75*, 6642-6647.

(193) Stoeckli, M.; Staab, D.; Staufenbiel, M.; Wiederhold, K.H.; Signor, L. Molecular imaging of amyloid beta peptides in mouse brain sections using mass spectrometry. *Anal. Biochem.* **2002**, *311*, 33-39.

(194) Luxembourg, S.L.; McDonnell, L.A.; Duursma, M.C.; Guo, X.; Heeren, R.M. Effect of local matrix crystal variations in matrix-assisted ionization techniques for mass spectrometry. *Anal. Chem.* **2003**, *75*, 2333-2341.

(195) Lipton, M.S.; Pasa-Tolic, L. *Mass Spectrometry of Proteins and Peptides: Methods and Protocols*, Second ed.; Humana Press: USA, 2009.

(196) Franck, J.; Arafah, K.; Barnes, A.; Wisztorski, M.; Salzet, M.; Fournier, I. Improving tissue preparation for matrix-assisted laser desorption ionization mass spectrometry imaging. Part 1: using microspotting. *Anal. Chem.* **2009**, *81*, 8193-8202.

(197) Cornett, D.S.; Reyzer, M.L.; Chaurand, P.; Caprioli, R.M. MALDI imaging mass spectrometry: molecular snapshots of biochemical systems. *Nat. Methods* **2007**, *4*, 828-833.

(198) Baluya, D.L.; Garrett, T.J.; Yost, R.A. Automated MALDI matrix deposition method with inkjet printing for imaging mass spectrometry. *Anal. Chem.* **2007**, *79*, 6862-6867.

(199) Hankin, J.A.; Barkley, R.M.; Murphy, R.C. Sublimation as a method of matrix application for mass spectrometric imaging. *J. Am. Soc. Mass Spectrom.* **2007**, *18*, 1646-1652.

(200) Dekker, L.J.; van Kampen, J.J.; Reedijk, M.L.; Burgers, P.C.; Gruters, R.A.; Osterhaus, A.D.; Luider, T.M. A mass spectrometry based imaging method developed for the intracellular detection of HIV protease inhibitors. *Rapid Commun. Mass Spectrom.* **2009**, *23*, 1183-1188.

(201) Liu, Q.; Guo, Z.; He, L. Mass spectrometry imaging of small molecules using desorption/ionization on silicon. *Anal. Chem.* **2007**, *79*, 3535-3541.

(202) Mengistu, T.Z.; DeSouza, L.; Morin, S. Probing proteins on functionalized silicon surfaces using matrix-assisted laser desorption/ionization mass spectrometry. *J. Chromatogr., A* **2006**, *1135*, 194-202.

(203) Wei, J.; Buriak, J.M.; Siuzdak, G. Desorption-ionization mass spectrometry on porous silicon. *Nature* **1999**, *399*, 243.

(204) Zhang, H.; Cha, S.; Yeung, E.S. Colloidal graphite-assisted laser desorption/ionization MS and MS(n) of small molecules. 2. Direct profiling and MS imaging of small metabolites from fruits. *Anal. Chem.* **2007**, *79*, 6575-6584.

(205) Pan, C.; Xu, S.; Zou, H.; Guo, Z.; Zhang, Y.; Guo, B. Carbon nanotubes as adsorbent of solid-phase extraction and matrix for laser desorption/ionization mass spectrometry. *J. Am. Soc. Mass Spectrom.* **2005**, *16*, 263-270.

(206) Pan, C.; Xu, S.; Hu, L.; Su, X.; Ou, J.; Zou, H.; Guo, Z.; Zhang, Y.; Guo, B. Using oxidized carbon nanotubes as matrix for analysis of small molecules by MALDI-TOF MS. *J. Am. Soc. Mass Spectrom.* **2005**, *16*, 883-892.

(207) Keller, B.O.; Sui, J.; Young, A.B.; Whittal, R.M. Interferences and contaminants encountered in modern mass spectrometry. *Anal. Chim. Acta* **2008**, *627*, 71-81.

(208) Aebersold, R.; Mann, M. Mass spectrometry-based proteomics. *Nature* **2003**, *422*, 198-207.

(209) Stephens, W.E.; Serin, B.; Meyerhof, W.E. *Phys. Rev.* **1946**, *69*, 42.

(210) Schwieters, J.; Cramer, H.G.; Heller, T.; Jurgens, U.; Niehuis, E.; Zehnpfenning, J.; Benninghoven, A. *J. Vac. Sci. Technol., A* **1991**, *9*, 2864.

(211) Kutz, K.K.; Schmidt, J.J.; Li, L. *Anal. Chem.* **2004**, *76*, 5630.

(212) Laiko, V.V.; Dodonov, A.F. *Rapid Commun. Mass Spectrom.* **1994**, *8*, 720.

(213) Dunn, W.B. Current trends and future requirements for the mass spectrometric investigation of microbial, mammalian and plant metabolomes. *Phys. Biol.* **2008**, *5*, 11001.

(214) Cornett, D.S.; Frappier, S.L.; Caprioli, R.M. MALDI-FTICR imaging mass spectrometry of drugs and metabolites in tissue. *Anal. Chem.* **2008**, *80*, 5648-5653.

(215) Wolters, D.A.; Washburn, M.P.; Yates, J.R. *Anal. Chem.* **2001**, *73*, 5683.

(216) Wiseman, J.M.; Ifa, D.R.; Song, Q.; Cooks, R.G. Tissue imaging at atmospheric pressure using desorption electrospray ionization (DESI) mass spectrometry. *Angew. Chem., Int. Ed. Engl.* **2006**, *45*, 7188-7192.

(217) Landgraf, R.R.; Prieto Conaway, M.C.; Garrett, T.J.; Stacpoole, P.W.; Yost, R.A. Imaging of lipids in spinal cord using intermediate pressure matrix-assisted laser desorption-linear ion trap/Orbitrap MS. *Anal. Chem.* **2009**, *81*, 8488-8495.

(218) Garrett, T.J.; Prieto-Conaway, M.C.; Kovtoun, V.; Bui, H.; Izgarian, N.; Stafford, G.; Yost, R.A. Imaging of small molecules in tissue sections with a new intermediate-pressure MALDI linear ion trap mass spectrometer. *Int. J. Mass Spectrom.* **2007**, *260*, 166-176.

(219) Panos, H.; Stephan, B.; Jay, C.; Peter, K.; Dietrich, A.V. *Rapid Commun. Mass Spectrom.* **2003**, *17*, 2303.

(220) Slodzian, G.; Daigne, B.; Girard, F.; Boust, F.; Hillion, F. *Biol. Cell* **1992**, *74*, 43.

(221) Jardin-Mathe, O.; Bonnel, D.; Franck, J.; Wisztorski, M.; Macagno, E.; Fournier, I.; Salzet, M. MITICS (MALDI Imaging Team Imaging Computing System): a new open source mass spectrometry imaging software. *J. Proteomics* **2008**, *71*, 332-345.

(222) Perkins, D.N.; Pappin, D.J.; Creasy, D.M.; Cottrell, J.S. Probability-based protein identification by searching sequence databases using mass spectrometry data. *Electrophoresis* **1999**, *20*, 3551-3567.

(223) Hanselmann, M.; Kothe, U.; Kirchner, M.; Renard, B.Y.; Amstalden, E.R.; Glunde, K.; Heeren, R.M.; Hamprecht, F.A. Toward Digital Staining using Imaging Mass Spectrometry and Random Forests. *J. Proteome Res.* **2009**, *8*, 3558-3567.

(224) Deininger, S.O.; Ebert, M.P.; Futterer, A.; Gerhard, M.; Rocken, C. MALDI Imaging Combined with Hierarchical Clustering as a New Tool for the Interpretation of Complex Human Cancers. *J. Proteome Res.* **2008**, *7*, 5230-5236

(225) Zaima, N.; Matsuyama, Y.; Setou, M. Principal component analysis of direct matrix-assisted laser desorption/ionization mass spectrometric data related to metabolites of fatty liver. *J. Oleo Sci.* **2009**, *58*, 267-273.

(226) Van de Plas, R.; Ojeda, F.; Dewil, M.; Van Den Bosch, L.; De Moor, B.; Waelkens, E. Prospective exploration of biochemical tissue composition via imaging mass spectrometry guided by principal component analysis. *Pac. Symp. Biocomput.* **2007**, 458-469.

(227) Verbeck, G.; Ruotolo, B.; Sawyer, H.; Gillig, K.; Russell, D. A fundamental introduction to ion mobility mass spectrometry applied to the analysis of biomolecules. *J. Biomol. Tech.* **2002**, *13*, 56-61.

(228) Jackson, S.N.; Ugarov, M.; Egan, T.; Post, J.D.; Langlais, D.; Albert Schultz, J.; Woods, A.S. MALDI-ion mobility-TOFMS imaging of lipids in rat brain tissue. *J. Mass Spectrom.* **2007**, *42*, 1093-1098.

(229) McLean, J.A.; Ridenour, W.B.; Caprioli, R.M. Profiling and imaging of tissues by imaging ion mobility-mass spectrometry. *J. Mass Spectrom.* **2007**, *42*, 1099-1105.

(230) van Duijn, E.; Barendregt, A.; Synowsky, S.; Versluis, C.; Heck, A.J. Chaperonin complexes monitored by ion mobility mass spectrometry. *J. Am. Chem. Soc.* **2009**, *131*, 1452-1459.

(231) Stauber, J.; van der Wiel, I.M.; Snel, M.; Claude, E.; Heeren, R.M.A. Ion Mobility Imaging Mass Spectrometry: A New Tool for In Situ Identification. *Proc. ASMS Conf., 56th* **2008**.

(232) Pringle, S.D.; Giles, K.; Wildgoose, J.L.; Williams, J.P.; Slade, S.E.; Thalassinos, K.; Bateman, R.H.; Bowers, M.T.; Scrivens, J.H. An investigation of the mobility separation of some peptide and protein ions using a new hybrid quadrupole/travelling wave IMS/oa-ToF instrument *Int. J. Mass Spectrom.* **2007**, *261*, 1-12

(233) Altelaar, M.A.; Taban, I.M.; McDonnell, L.A.; de Lange, R.P.; Adan, R.A.; Mooi, W.J.; Heeren, R.M.; Piersma, S.R. High-resolution MALDI imaging mass spectrometry allows localization of peptide distributions at cellular length scales in pituitary tissue sections *Int. J. Mass Spectrom.* **2006**, *260*, 203-211

(234) Xu, B.J.; Caprioli, R.M.; Sanders, M.E.; Jensen, R.A. Direct analysis of laser capture microdissected cells by MALDI mass spectrometry. *J. Am. Soc. Mass Spectrom.* **2002**, *13*, 1292-1297.

(235) Palmer-Toy, D.E.; Sarracino, D.A.; Sgroi, D.; LeVangie, R.; Leopold, P.E. Direct acquisition of matrix-assisted laser Desorption/Ionization time-of-flight mass spectra from laser capture microdissected tissues. *Clin. Chem.* **2000**, *46*, 1513-1516.

(236) Lemaire, R.; Stauber, J.; Wisztorski, M.; Van Camp, C.; Desmons, A.; Deschamps, M.; Proess, G.; Rudlof, I.; Woods, A.S.; Day, R.; Salzet, M.; Fournier, I. Tag-mass: specific molecular imaging of transcriptome and proteome by mass spectrometry based on photocleavable tag. *J. Proteome Res.* **2007**, *6*, 2057-2067.

(237) Thiery, G.; Shchepinov, M.S.; Southern, E.M.; Audebourg, A.; Audard, V.; Terris, B.; Gut, I.G. Multiplex target protein imaging in tissue sections by mass spectrometry-- TAMSIM. *Rapid Commun. Mass Spectrom.* **2007**, *21*, 823-829.

(238) Pierson, J.; Norris, J.L.; Aerni, H.R.; Svenningsson, P.; Caprioli, R.M.; Andren, P.E. Molecular profiling of experimental Parkinson's disease: direct analysis of peptides and proteins on brain tissue sections by MALDI mass spectrometry. *J. Proteome Res.* **2004**, *3*, 289-295.

(239) Grossi, C.; Francese, S.; Casini, A.; Rosi, M.C.; Luccarini, I.; Fiorentini, A.; Gabbiani, C.; Messori, L.; Moneti, G.; Casamenti, F. Clioquinol Decreases Amyloid-beta Burden and Reduces Working Memory Impairment in a Transgenic Mouse Model of Alzheimer's Disease. *J. Alzheimer's Dis.* **2009**, *17*, 423-440.

(240) Touboul, D.; Roy, S.; Germain, D.P.; Chaminade, P.; Brunelle, A.; Laprévote, O. MALDI-TOF and cluster-TOF-SIMS imaging of Fabry disease biomarkers *Int. J. Mass Spectrom.* **2007**, *260*, 158-165

(241) Touboul, D.; Piednoel, H.; Voisin, V.; De La Porte, S.; Brunelle, A.; Halgand, F.; Laprevote, O. Changes of phospholipid composition within the dystrophic muscle by matrix-assisted laser desorption/ionization mass spectrometry and mass spectrometry imaging. *Eur. J. Mass Spectrom.* **2004**, *10*, 657-664.

(242) Meistermann, H.; Norris, J.L.; Aerni, H.R.; Cornett, D.S.; Friedlein, A.; Erskine, A.R.; Augustin, A.; De Vera Mudry, M.C.; Ruepp, S.; Suter, L.; Langen, H.; Caprioli, R.M.; Ducret, A. Biomarker discovery by imaging mass spectrometry: transthyretin is a biomarker for gentamicin-induced nephrotoxicity in rat. *Mol. Cell. Proteomics* **2006**, *5*, 1876-1886.

(243) Xu, B.J.; Shyr, Y.; Liang, X.; Ma, L.J.; Donnert, E.M.; Roberts, J.D.; Zhang, X.; Kon, V.; Brown, N.J.; Caprioli, R.M.; Fogo, A.B. Proteomic patterns and prediction of glomerulosclerosis and its mechanisms. *J. Am. Soc. Nephrol.* **2005**, *16*, 2967-2975.

(244) Debois, D.; Bralet, M.P.; Le Naour, F.; Brunelle, A.; Laprevote, O. In situ lipidomic analysis of nonalcoholic fatty liver by cluster TOF-SIMS imaging. *Anal. Chem.* **2009**, *81*, 2823-2831.

(245) Chen, Y.; Allegood, J.; Liu, Y.; Wang, E.; Cachon-Gonzalez, B.; Cox, T.M.; Merrill, A.H., Jr.; Sullards, M.C. Imaging MALDI mass spectrometry using an oscillating capillary nebulizer matrix coating system and its application to analysis of lipids in brain from a mouse model of Tay-Sachs/Sandhoff disease. *Anal. Chem.* **2008**, *80*, 2780-2788.

(246) Quonga, J.N.; Knizeb, M.G.; Kulpb, K.S.; Wu, K.J. Molecule-specific imaging analysis of carcinogens in breast cancer cells using time-of-flight secondary ion mass spectrometry *Appl. Surf. Sci.* **2004**, *231/232*, 424-427.

(247) Cazares, L.H.; Troyer, D.; Mendrinos, S.; Lance, R.A.; Nyalwidhe, J.O.; Beydoun, H.A.; Clements, M.A.; Drake, R.R.; J., S. Imaging Mass Spectrometry of a Specific Fragment of Mitogen-Activated Protein Kinase/Extracellular Signal-Regulated Kinase Kinase Kinase 2 Discriminates Cancer from Uninvolved Prostate Tissue. *Clin. Cancer Res.* **2009**, *15*, 5541-5551.

(248) Shimma, S.; Sugiura, Y.; Hayasaka, T.; Hoshikawa, Y.; Noda, T.; Setou, M. MALDI-based imaging mass spectrometry revealed abnormal distribution of phospholipids in colon cancer liver metastasis. *J. Chromatogr., B: Anal. Technol. Biomed. Life Sci.* **2007**, *855*, 98-103.

(249) Schwartz, S.A.; Weil, R.J.; Johnson, M.D.; Toms, S.A.; Caprioli, R.M. Protein profiling in brain tumors using mass spectrometry: feasibility of a new technique for the analysis of protein expression. *Clin. Cancer Res.* **2004**, *10*, 981-987.

(250) Sanders, M.E.; Dias, E.C.; Xu, B.J.; Mobley, J.A.; Billheimer, D.; Roder, H.; Grigorieva, J.; Dowsett, M.; Arteaga, C.L.; Caprioli, R.M. Differentiating proteomic biomarkers in breast cancer by laser capture microdissection and MALDI MS. *J. Proteome Res.* **2008**, *7*, 1500-1507.

(251) Kang, S.; Shim, H.S.; Lee, J.S.; Kim, D.S.; Kim, H.Y.; Hong, S.H.; Kim, P.S.; Youn, J.H.; Cho, N.H. Molecular Proteomics Imaging of Tumor Interfaces by Mass Spectrometry. *J. Proteome Res.* **2010**, *9*, 1157-1164.

(252) Dill, A.L.; Ifa, D.R.; Manicke, N.E.; Costa, A.B.; Ramos-Vara, J.A.; Knapp, D.W.; Cooks, R.G. Lipid profiles of canine invasive transitional cell carcinoma of the urinary bladder and adjacent normal tissue by desorption electrospray ionization imaging mass spectrometry. *Anal. Chem.* **2009**, *81*, 8758-8764.

(253) Matusch, A.; Depboylu, C.; Palm, C.; Wu, B.; Hoglinger, G.U.; Schafer, M.K.; Becker, J.S. Cerebral Bioimaging of Cu, Fe, Zn, and Mn in the MPTP Mouse Model of Parkinson's Disease Using Laser Ablation Inductively Coupled Plasma Mass Spectrometry (LA-ICP-MS). *J. Am. Soc. Mass Spectrom.* **2009**, *21*, 161-171

(254) Yao, I.; Sugiura, Y.; Matsumoto, M.; Setou, M. In situ proteomics with imaging mass spectrometry and principal component analysis in the Scrapper-knockout mouse brain. *Proteomics* **2008**, *8*, 3692-3701.

(255) Le Naour, F.; Bralet, M.P.; Debois, D.; Sandt, C.; Guettier, C.; Dumas, P.; Brunelle, A.; Laprevote, O. Chemical imaging on liver steatosis using synchrotron infrared and ToF-SIMS microspectroscopies. *PLoS One* **2009**, *4*, 7408.

(256) Manicke, N.E.; Nefliu, M.; Wu, C.; Woods, J.W.; Reiser, V.; Hendrickson, R.C.; Cooks, R.G. Imaging of lipids in atheroma by desorption electrospray ionization mass spectrometry. *Anal. Chem.* **2009**, *81*, 8702-8707.

(257) Patel, S.A.; Barnes, A.; Loftus, N.; Martin, R.; Sloan, P.; Thakker, N.; Goodacre, R. Imaging mass spectrometry using chemical inkjet printing reveals differential protein expression in human oral squamous cell carcinoma. *Analyst* **2009**, *134*, 301-307.

(258) Kim, J.H.; Kim, J.H.; Ahn, B.J.; Park, J.H.; Shon, H.K.; Yu, Y.S.; Moon, D.W.; Lee, T.G.; Kim, K.W. Label-free calcium imaging in ischemic retinal tissue by TOF-SIMS. *Biophys. J.* **2008**, *94*, 4095-4102.

(259) McDonnell, L.A.; van Remoortere, A.; van Zeijl, R.J.; Dalebout, H.; Bladergroen, M.R.; Deelder, A.M. Automated Imaging MS: Toward High Throughput Imaging Mass Spectrometry. *J. Proteomics* **2009**, in press.

(260) Fournier, I.; Wisztorski, M.; Salzet, M. Tissue imaging using MALDI-MS: a new frontier of histopathology proteomics. *Expert Rev. Proteomics* **2008**, *5*, 413-424.

(261) Wisztorski, M.; Lemaire, R.; Stauber, J.; Menguelet, S.A.; Croix, D.; Mathe, O.J.; Day, R.; Salzet, M.; Fournier, I. New developments in MALDI imaging for pathology proteomic studies. *Curr. Pharm. Des.* **2007**, *13*, 3317-3324.

(262) Caprioli, R.M. Perspectives on imaging mass spectrometry in biology and medicine. *Proteomics* **2008**, *8*, 3679-3680.

(263) Cobb, S.R.; Pitt, A. Proteomics in the study of hippocampal plasticity. *Expert Rev. Proteomics* **2008**, *5*, 393-404.

(264) Jaffer, F.A.; Libby, P.; Weissleder, R. Optical and multimodality molecular imaging: insights into atherosclerosis. *Arterioscler., Thromb., Vasc. Biol.* **2009**, *29*, 1017-1024.

(265) Magalhaes, B.S.; Melo, J.A.; Leite, J.R.; Silva, L.P.; Prates, M.V.; Vinecky, F.; Barbosa, E.A.; Verly, R.M.; Mehta, A.; Nicoli, J.R.; Bemquerer, M.P.; Andrade, A.C.;

Bloch, C., Jr. Post-secretory events alter the peptide content of the skin secretion of Hypsiboas raniceps. *Biochem. Biophys. Res. Commun.* **2008**, *377*, 1057-1061.

(266) Brand, G.D.; Krause, F.C.; Silva, L.P.; Leite, J.R.; Melo, J.A.; Prates, M.V.; Pesquero, J.B.; Santos, E.L.; Nakaie, C.R.; Costa-Neto, C.M.; Bloch, C., Jr. Bradykinin-related peptides from Phyllomedusa hypochondrialis. *Peptides* **2006**, *27*, 2137-2146.

(267) Han, J.; Schey, K.L. MALDI tissue imaging of ocular lens alpha-crystallin. *Invest. Ophthalmol. Visual Sci.* **2006**, *47*, 2990-2996.

(268) Grey, A.C.; Schey, K.L. Age-related Changes in the Spatial Distribution of Human Lens {alpha}-Crystallin Products by MALDI Imaging Mass Spectrometry. *Invest. Ophthalmol. Visual Sci.* **2009**, *50*, 4319-4329.

(269) Grey, A.C.; Chaurand, P.; Caprioli, R.M.; Schey, K.L. MALDI Imaging Mass Spectrometry of Integral Membrane Proteins from Ocular Lens and Retinal Tissue. *J. Proteome Res.* **2009**, *8*, 3278-3283.

(270) Rujoi, M.; Estrada, R.; Yappert, M.C. In situ MALDI-TOF MS regional analysis of neutral phospholipids in lens tissue. *Anal. Chem.* **2004**, *76*, 1657-1663.

(271) Kutz, K.K.; Schmidt, J.J.; Li, L. In situ tissue analysis of neuropeptides by MALDI FTMS in-cell accumulation. *Anal. Chem.* **2004**, *76*, 5630-5640.

(272) Hummon, A.B.; Amare, A.; Sweedler, J.V. Discovering new invertebrate neuropeptides using mass spectrometry. *Mass Spectrom. Rev.* **2006**, *25*, 77-98.

(273) DeKeyser, S.S.; Kutz-Naber, K.K.; Schmidt, J.J.; Barrett-Wilt, G.A.; Li, L. Imaging mass spectrometry of neuropeptides in decapod crustacean neuronal tissues. *J. Proteome Res.* **2007**, *6*, 1782-1791.

(274) Verhaerta, P.D.; Prieto Conawaye M.C. ; Pekare, T.M.; Miller, K. Neuropeptide imaging on an LTQ with vMALDI source: The complete 'all-in-one' peptidome analysis. *Int. J. Mass Spectrom.* **2006**, *260*, 177-184.

(275) Sugiura, Y.; Shimma, S.; Konishi, Y.; Yamada, M.K.; Setou, M. Imaging mass spectrometry technology and application on ganglioside study; visualization of age-dependent accumulation of C20-ganglioside molecular species in the mouse hippocampus. *PLoS ONE* **2008**, *3*, 3232.

(276) Chan, K.; Lanthier, P.; Liu, X.; Sandhu, J.K.; Stanimirovic, D.; Li, J. MALDI mass spectrometry imaging of gangliosides in mouse brain using ionic liquid matrix. *Anal. Chim. Acta* **2009**, *639*, 57-61.

(277) Robinson, S.; Warburton, K.; Seymour, M.; Clench, M.; Thomas-Oates, J. Localization of water-soluble carbohydrates in wheat stems using imaging matrix-assisted laser desorption ionization mass spectrometry. *New Phytol.* **2007**, *173*, 438-444.

(278) Mullen, A.K.; Clench, M.R.; Crosland, S.; Sharples, K.R. Determination of agrochemical compounds in soya plants by imaging matrix-assisted laser desorption/ionisation mass spectrometry. *Rapid Commun. Mass Spectrom.* **2005**, *19*, 2507-2516.

(279) Anderson, D.M.; Carolan, V.A.; Crosland, S.; Sharples, K.R.; Clench, M.R. Examination of the distribution of nicosulfuron in sunflower plants by matrix-assisted laser desorption/ionisation mass spectrometry imaging. *Rapid Commun. Mass Spectrom.* **2009**, *23*, 1321-1327.

(280) Burrell, M.; Earnshaw, C.; Clench, M. Imaging Matrix Assisted Laser Desorption Ionization Mass Spectrometry: a technique to map plant metabolites within tissues at high spatial resolution. *J. Exp. Bot.* **2007**, *58*, 757-763.

(281) Cha, S.; Song, Z.; Nikolau, B.J.; Yeung, E.S. Direct profiling and imaging of epicuticular waxes on Arabidopsis thaliana by laser desorption/ionization mass spectrometry using silver colloid as a matrix. *Anal. Chem.* **2009**, *81*, 2991-3000.

(282) Cavatorta, V.; Sforza, S.; Mastrobuoni, G.; Pieraccini, G.; Francese, S.; Moneti, G.; Dossena, A.; Pastorello, E.A.; Marchelli, R. Unambiguous characterization and tissue localization of Pru P 3 peach allergen by electrospray mass spectrometry and MALDI imaging. *J. Mass Spectrom.* **2009**, *44*, 891-897.

(283) Genji, T.; Fukuzawa, S.; Tachibana, K. Distribution and Possible Function of the Marine Alkaloid, Norzoanthamine, in the Zoanthid Zoanthus sp. Using MALDI Imaging Mass Spectrometry. *Mar. Biotechnol.* **2010**, *12*, 81-87.

(284) Burnum, K.E.; Cornett, D.S.; Puolitaival, S.M.; Milne, S.B.; Myers, D.S.; Tranguch, S.; Brown, H.A.; Dey, S.K.; Caprioli, R.M. Spatial and temporal alterations of phospholipids determined by mass spectrometry during mouse embryo implantation. *J. Lipid Res.* **2009**, *50*, 2290-2298.

(285) Francese, S.; Lambardi, D.; Mastrobuoni, G.; la Marca, G.; Moneti, G.; Turillazzi, S. Detection of honeybee venom in envenomed tissues by direct MALDI MSI. *J. Am. Soc. Mass Spectrom.* **2009**, *20*, 112-123.

(286) Wysocki, V.H.; Resing, K.A.; Zhang, Q.; Cheng, G. Mass spectrometry of peptides and proteins. *Methods* **2005**, *35*, 211-222.

(287) Han, X.; Aslanian, A.; Yates, J.R., 3rd Mass spectrometry for proteomics. *Curr. Opin. Chem. Biol.* **2008**, *12*, 483-490.

(288) Chaurand, P.; Stoeckli, M.; Caprioli, R.M. Direct profiling of proteins in biological tissue sections by MALDI mass spectrometry. *Anal. Chem.* **1999**, *71*, 5263-5270.

(289) Bienvenut, W.V.; Sanchez, J.C.; Karmime, A.; Rouge, V.; Rose, K.; Binz, P.A.; Hochstrasser, D.F. Toward a clinical molecular scanner for proteome research: parallel protein chemical processing before and during western blot. *Anal. Chem.* **1999**, *71*, 4800-4807.

(290) Binz, P.A.; Muller, M.; Walther, D.; Bienvenut, W.V.; Gras, R.; Hoogland, C.; Bouchet, G.; Gasteiger, E.; Fabbretti, R.; Gay, S.; Palagi, P.; Wilkins, M.R.; Rouge, V.; Tonella, L.; Paesano, S.; Rossellat, G.; Karmime, A.; Bairoch, A.; Sanchez, J.C.; Appel, R.D.; Hochstrasser, D.F. A molecular scanner to automate proteomic research and to display proteome images. *Anal. Chem.* **1999**, *71*, 4981-4988.

(291) Muller, M.; Gras, R.; Appel, R.D.; Bienvenut, W.V.; Hochstrasser, D.F. Visualization and analysis of molecular scanner peptide mass spectra. *J. Am. Soc. Mass Spectrom.* **2002**, *13*, 221-231.

(292) Dani, F.R.; Francese, S.; Mastrobuoni, G.; Felicioli, A.; Caputo, B.; Simard, F.; Pieraccini, G.; Moneti, G.; Coluzzi, M.; della Torre, A.; Turillazzi, S. Exploring proteins in Anopheles gambiae male and female antennae through MALDI mass spectrometry profiling. *PLoS ONE* **2008**, *3*, 2822.

(293) Rubakhin, S.S.; Li, L.; Moroz, T.P.; Sweedler, J.V. Characterization of the Aplysia californica cerebral ganglion F cluster. *J. Neurophysiol.* **1999**, *81*, 1251-1260.

(294) Li, L.; Garden, R.W.; Sweedler, J.V. Single-cell MALDI: a new tool for direct peptide profiling. *Trends Biotechnol.* **2000**, *18*, 151-160.

(295) Masujima, T. Live single-cell mass spectrometry. *Anal. Sci.* **2009**, *25*, 953-960.

(296) van Veelen, P.A.; Jiménez , C.R.; Li, K.W.; Wildering, W.C.; M., G.W.P.; Tjaden, U.R.; van der Greef, J. Direct peptide profiling of single neurons by matrix-assisted laser desorption-ionization mass spectrometry. *Org. Mass Spectrom.* **1993**, *28* 1542 - 1546.

(297) Jimenez, C.R.; van Veelen, P.A.; Li, K.W.; Wildering, W.C.; Geraerts, W.P.; Tjaden, U.R.; van der Greef, J. Neuropeptide expression and processing as revealed by direct matrix-assisted laser desorption ionization mass spectrometry of single neurons. *J. Neurochem.* **1994**, *62*, 404-407.

198

(298) Hsieh, S.; Dreisewerd, K.; van der Schors, R.C.; Jimenez, C.R.; Stahl-Zeng, J.; Hillenkamp, F.; Jorgenson, J.W.; Geraerts, W.P.; Li, K.W. Separation and identification of peptides in single neurons by microcolumn liquid chromatography-matrix-assisted laser desorption/ionization time-of-flight mass spectrometry and postsource decay analysis. *Anal. Chem.* **1998**, *70*, 1847-1852.

(299) Redeker, V.; Toullec, J.Y.; Vinh, J.; Rossier, J.; Soyez, D. Combination of peptide profiling by matrix-assisted laser desorption/ionization time-of-flight mass spectrometry and immunodetection on single glands or cells. *Anal. Chem.* **1998**, *70*, 1805-1811.

(300) Ma, P.W.; Garden, R.W.; Niermann, J.T.; M, O.C.; Sweedler, J.V.; Roelofs, W.L. Characterizing the Hez-PBAN gene products in neuronal clusters with immunocytochemistry and MALDI MS. *J. Insect Physiol.* **2000**, *46*, 221-230.

(301) Whittal, R.M.; Keller, B.O.; Li, L. Nanoliter chemistry combined with mass spectrometry for peptide mapping of proteins from single mammalian cell lysates. *Anal. Chem.* **1998**, *70*, 5344-5347.

(302) Shimizu, M.; Levi-Schaffer, F.; Ojima, N.; Shingaki, T.; Masujima, T. A single-cell matrix-assisted laser desorption/ionization time-of-flight mass-spectroscopic assay of the cell-maturation process. *Anal. Sci.* **2002**, *18*, 107-108.

(303) Rubakhin, S.S.; Sweedler, J.V. Characterizing peptides in individual mammalian cells using mass spectrometry. *Nat. Protoc.* **2007**, *2*, 1987-1997.

(304) Altelaar, A.F.M.; van Minnen, J.; Jimenez, C.R.; Heeren, R.M.A.; Piersma, S.R. Direct Molecular Imaging of Lymnaea stagnalis Nervous Tissue at Subcellular Spatial Resolution by Mass Spectrometry. *Analytical Chemistry* **2005**, *77*, 735-741.

(305) Li, K.W.; Hoek, R.M.; Smith, F.; Jimenez, C.R.; van der Schors, R.C.; van Veelen, P.A.; Chen, S.; van der Greef, J.; Parish, D.C.; Benjamin, P.R.; et al. Direct peptide profiling by mass spectrometry of single identified neurons reveals complex neuropeptide-processing pattern. *J. Biol. Chem.* **1994**, *269*, 30288-30292.

(306) Garden, R.W.; Moroz, L.L.; Moroz, T.P.; Shippy, S.A.; Sweedler, J.V. Excess salt removal with matrix rinsing: direct peptide profiling of neurons from marine invertebrates using matrix-assisted laser desorption/ionization time-of-flight mass spectrometry. *J. Mass Spectrom.* **1996**, *31*, 1126-1130.

(307) Wong, S.C.; Chan, C.M.; Ma, B.B.; Lam, M.Y.; Choi, G.C.; Au, T.C.; Chan, A.S.; Chan, A.T. Advanced proteomic technologies for cancer biomarker discovery. *Expert Rev. Proteomics* **2009**, *6*, 123-134.

(308) Miura, D.; Fujimura, Y.; Tachibana, H.; Wariishi, H. Highly sensitive matrix-assisted laser desorption ionization-mass spectrometry for high-throughput metabolic profiling. *Anal Chem* **2010**, *82*, 498-504.

(309) Forster, J.; Famili, I.; Fu, P.; Palsson, B.O.; Nielsen, J. Genome-scale reconstruction of the Saccharomyces cerevisiae metabolic network. *Genome Res.* **2003**, *13*, 244-253.

(310) Sugiura, Y.; Setou, M. Imaging Mass Spectrometry for Visualization of Drug and Endogenous Metabolite Distribution: Toward In Situ Pharmacometabolomes. *J. Neuroimmune Pharmacol.* **2009**.

(311) Benabdellah, F.; Touboul, D.; Brunelle, A.; Laprevote, O. In situ primary metabolites localization on a rat brain section by chemical mass spectrometry imaging. *Anal. Chem.* **2009**, *81*, 5557-5560.

(312) Lee, S.H.; Williams, M.V.; DuBois, R.N.; Blair, I.A. Targeted lipidomics using electron capture atmospheric pressure chemical ionization mass spectrometry. *Rapid Commun. Mass Spectrom.* **2003**, *17*, 2168-2176.

(313) Jones, J.J.; Borgmann, S.; Wilkins, C.L.; O'Brien, R.M. Characterizing the phospholipid profiles in mammalian tissues by MALDI FTMS. *Anal. Chem.* **2006**, *78*, 3062-3071.

(314) Nakanishi, H.; Shindou, H.; Hishikawa, D.; Harayama, T.; Ogasawara, R.; Suwabe, A.; Taguchi, R.; Shimizu, T. Cloning and characterization of mouse lung-type acyl-CoA:lysophosphatidylcholine acyltransferase 1 (LPCAT1). Expression in alveolar type II cells and possible involvement in surfactant production. *J. Biol. Chem.* **2006**, *281*, 20140-20147.

(315) O'Brien, J.S.; Sampson, E.L.; Stern, M.B. Lipid composition of myelin from the peripheral nervous system. Intradural spinal roots. *J. Neurochem.* **1967**, *14*, 357-365.

(316) Woollett, L.A. The origins and roles of cholesterol and fatty acids in the fetus. *Curr. Opin. Lipidol.* **2001**, *12*, 305-312.

(317) Woollett, L.A. Where does fetal and embryonic cholesterol originate and what does it do? *Annu. Rev. Nutr.* **2008**, *28*, 97-114.

(318) Fahy, E.; Sud, M.; Cotter, D.; Subramaniam, S. LIPID MAPS online tools for lipid research. *Nucleic Acids Res* **2007**, *35*, W606-612.

(319) Schiller, J.; Suss, R.; Arnhold, J.; Fuchs, B.; Lessig, J.; Muller, M.; Petkovic, M.; Spalteholz, H.; Zschornig, O.; Arnold, K. Matrix-assisted laser desorption and ionization time-of-flight (MALDI-TOF) mass spectrometry in lipid and phospholipid research. *Prog. Lipid Res.* **2004**, *43*, 449-488.

(320) Dill, A.L.; Ifa, D.R.; Manicke, N.E.; Ouyang, Z.; Cooks, R.G. Mass spectrometric imaging of lipids using desorption electrospray ionization. *J. Chromatogr., B: Anal. Technol. Biomed. Life Sci.* **2008**.

(321) Pulfer, M.; Murphy, R.C. Electrospray mass spectrometry of phospholipids. *Mass Spectrom. Rev.* **2003**, *22*, 332-364.

(322) Malmberg, P.; Nygren, H.; Sjövall, P.; Lausmaa, J. Subcellular localisation of cholesterol and phosphocholine with pattern-recognition-imaging-TOF-SIMS. *Spectroscopy* **2004**, *18*, 503-511.

(323) Hsu, F.F.; Turk, J.; Zhang, K.; Beverley, S.M. Characterization of inositol phosphorylceramides from Leishmania major by tandem mass spectrometry with electrospray ionization. *J. Am. Soc. Mass Spectrom.* **2007**, *18*, 1591-1604.

(324) Li, C.; Yergey, J.A. Continuous Flow Liquid Secondary Ion MassSpectrometric Characterization of Phospholipid Molecular Species. *J. Mass Spectrom.* **1997**, *32*, 314-322.

(325) Kim, Y.; Shanta, S.R.; Zhou, L.H.; Kim, K.P. Mass spectrometry based cellular phosphoinositides profiling and phospholipid analysis: a brief review. *Exp. Mol. Med.* **2009**, *42*, 1-11.

(326) Jackson, S.N.; Wang, H.Y.; Woods, A.S. In situ structural characterization of phosphatidylcholines in brain tissue using MALDI-MS/MS. *J. Am. Soc. Mass Spectrom.* **2005**, *16*, 2052-2056.

(327) Sugiura, Y.; Setou, M. Selective imaging of positively charged polar and nonpolar lipids by optimizing matrix solution composition. *Rapid Commun. Mass Spectrom.* **2009**, *23*, 3269-3278.

(328) Sugiura, Y.; Shimma, S.; Setou, M. Two-step matrix application technique to improve ionization efficiency for matrix-assisted laser desorption/ionization in imaging mass spectrometry. *Anal. Chem.* **2006**, *78*, 8227-8235.

(329) Isaac, G.; Jeannotte, R.; Esch, S.W.; Welti, R. New mass-spectrometry-based strategies for lipids. *Genet. Eng.* **2007**, *28*, 129-157.

(330) Hayasaka, T.; Goto-Inoue, N.; Sugiura, Y.; Zaima, N.; Nakanishi, H.; Ohishi, K.; Nakanishi, S.; Naito, T.; Taguchi, R.; Setou, M. Matrix-assisted laser

desorption/ionization quadrupole ion trap time-of-flight (MALDI-QIT-TOF)-based imaging mass spectrometry reveals a layered distribution of phospholipid molecular species in the mouse retina. *Rapid Commun. Mass Spectrom.* **2008**, *22*, 3415-3426.

(331) Garrett, T.J.; Dawson, W.W. Lipid geographical analysis of the primate macula by imaging mass spectrometry. *Methods Mol. Biol.* **2009**, *579*, 247-260.

(332) Patti, G.J.; Woo, H.K.; Yanes, O.; Shriver, L.; Thomas, D.; Uritboonthai, W.; Apon, J.V.; Steenwyk, R.; Manchester, M.; Siuzdak, G. Detection of carbohydrates and steroids by cation-enhanced nanostructure-initiator mass spectrometry (NIMS) for biofluid analysis and tissue imaging. *Anal. Chem.* **2010**, *82*, 121-128.

(333) Solon, E.G.; Schweitzer, A.; Stoeckli, M.; Prideaux, B. Autoradiography, MALDI-MS, and SIMS-MS imaging in pharmaceutical discovery and development. *AAPS J.* **2010**, *12*, 11-26.

(334) Troendle, F.J.; Reddick, C.D.; Yost, R.A. Detection of pharmaceutical compounds in tissue by matrix-assisted laser desorption/ionization and laser desorption/chemical ionization tandem mass spectrometry with a quadrupole ion trap *J. Am. Soc. Mass Spectrom.* **1999**, *10*, 1315-1321.

(335) Reyzer, M.L.; Hsieh, Y.; Ng, K.; Korfmacher, W.A.; Caprioli, R.M. Direct analysis of drug candidates in tissue by matrix-assisted laser desorption/ionization mass spectrometry. *J. Mass Spectrom.* **2003**, *38*, 1081-1092.

(336) Hsieh, Y.; Casale, R.; Fukuda, E.; Chen, J.; Knemeyer, I.; Wingate, J.; Morrison, R.; Korfmacher, W. Matrix-assisted laser desorption/ionization imaging mass spectrometry for direct measurement of clozapine in rat brain tissue. *Rapid Commun. Mass Spectrom.* **2006**, *20*, 965-972.

(337) Rubakhin, S.S.; Jurchen, J.C.; Monroe, E.B.; Sweedler, J.V. Imaging mass spectrometry: fundamentals and applications to drug discovery. *Drug Discovery Today* **2005**, *10*, 823-837.

(338) Bunch, J.; Clench, M.R.; Richards, D.S. Determination of pharmaceutical compounds in skin by imaging matrix-assisted laser desorption/ionisation mass spectrometry. *Rapid Commun. Mass Spectrom.* **2004**, *18*, 3051-3060.

(339) Wang, H.Y.; Jackson, S.N.; McEuen, J.; Woods, A.S. Localization and analyses of small drug molecules in rat brain tissue sections. *Anal. Chem.* **2005**, *77*, 6682-6686.

(340) Atkinson, S.J.; Loadman, P.M.; Sutton, C.; Patterson, L.H.; Clench, M.R. Examination of the distribution of the bioreductive drug AQ4N and its active metabolite AQ4 in solid tumours by imaging matrix-assisted laser desorption/ionisation mass spectrometry. *Rapid Commun. Mass Spectrom.* **2007**, *21*, 1271-1276.

(341) Zhigaltsev, I.V.; Maurer, N.; Akhong, Q.F.; Leone, R.; Leng, E.; Wang, J.; Semple, S.C.; Cullis, P.R. Liposome-encapsulated vincristine, vinblastine and vinorelbine: a comparative study of drug loading and retention. *J. Controlled Release* **2005**, *104*, 103-111.

(342)

(343) Eberlin, L.S.; Ifa, D.R.; Wu, C.; Cooks, R.G. Three-Dimensional Vizualization of Mouse Brain by Lipid Analysis Using Ambient Ionization Mass Spectrometry. *Angew. Chem., Int. Ed. Engl.* **2009**, *49*, 873-876.

(344) Sinha, T.K.; Khatib-Shahidi, S.; Yankeelov, T.E.; Mapara, K.; Ehtesham, M.; Cornett, D.S.; Dawant, B.M.; Caprioli, R.M.; Gore, J.C. Integrating spatially resolved three-dimensional MALDI IMS with in vivo magnetic resonance imaging. *Nat. Methods* **2008**, *5*, 57-59.

(345) Amstalden van Hove, E.R.; Blackwell, T.R.; Klinkert, I.; Eijkel, G.B.; Heeren, R.M.; Glunde, K. Multimodal mass spectrometric imaging of small molecules reveals

distinct spatio-molecular signatures in differentially metastatic breast tumor models. *Cancer Res* **2010**, *70*, 9012-9021.

(346) Sinha, T.K.; Khatib-Shahidi, S.; Yankeelov, T.E.; Mapara, K.; Ehtesham, M.; Cornett, D.S.; Dawant, B.M.; Caprioli, R.M.; Gore, J.C. Integrating spatially resolved three-dimensional MALDI IMS with in vivo magnetic resonance imaging. *Nat Methods* **2008**, *5*, 57-59.

(347) Altelaar, A.F.; Luxembourg, S.L.; McDonnell, L.A.; Piersma, S.R.; Heeren, R.M.A. Imaging mass spectrometry at cellular length scales. *Nat Protoc* **2007**, *2*, 1185-1196.

(348) Djidja, M.C.; Claude, E.; Snel, M.F.; Scriven, P.; Francese, S.; Carolan, V.; Clench, M.R. MALDI-ion mobility separation-mass spectrometry imaging of glucose-regulated protein 78 kDa (Grp78) in human formalin-fixed, paraffin-embedded pancreatic adenocarcinoma tissue sections. *J Proteome Res* **2009**, *8*, 4876-4884.

(349) Khatib-Shahidi, S.; Andersson, M.; Herman, J.L.; Gillespie, T.A.; Caprioli, R.M. Direct molecular analysis of whole-body animal tissue sections by imaging MALDI mass spectrometry. *Anal Chem* **2006**, *78*, 6448-6456.

(350) Chughtai, K.; Heeren, R.M.A. Mass spectrometric imaging for biomedical tissue analysis. *Chem Rev* **2010**, *110*, 3237-3277.

(351) Shaner, N.C.; Campbell, R.E.; Steinbach, P.A.; Giepmans, B.N.; Palmer, A.E.; Tsien, R.Y. Improved monomeric red, orange and yellow fluorescent proteins derived from Discosoma sp. red fluorescent protein. *Nat Biotechnol* **2004**, *22*, 1567-1572.

(352) Winnard, P.T., Jr.; Kluth, J.B.; Raman, V. Noninvasive optical tracking of red fluorescent protein-expressing cancer cells in a model of metastatic breast cancer. *Neoplasia* **2006**, *8*, 796-806.

(353) Kakkad, S.M.; Solaiyappan, M.; O'Rourke, B.; Stasinopoulos, I.; Ackerstaff, E.; Raman, V.; Bhujwalla, Z.M.; Glunde, K. Hypoxic tumor microenvironments reduce collagen I fiber density. *Neoplasia* **2010**, *12*, 608-617.

(354) Eberlin, L.S.; Ifa, D.R.; Wu, C.; Cooks, R.G. Three-dimensional vizualization of mouse brain by lipid analysis using ambient ionization mass spectrometry. *Angew Chem Int Ed Engl* **2010**, *49*, 873-876.

(355) Chen, R.; Hui, L.; Sturm, R.M.; Li, L. Three dimensional mapping of neuropeptides and lipids in crustacean brain by mass spectral imaging. *J Am Soc Mass Spectrom* **2009**, *20*, 1068-1077.

(356) Andersson, M.; Groseclose, M.R.; Deutch, A.Y.; Caprioli, R.M. Imaging mass spectrometry of proteins and peptides: 3D volume reconstruction. *Nat Methods* **2008**, *5*, 101-108.

(357) Lazebnik, R.S.; Lancaster, T.L.; Breen, M.S.; Lewin, J.S.; Wilson, D.L. Volume registration using needle paths and point landmarks for evaluation of interventional MRI treatments. *IEEE Trans Med Imaging* **2003**, *22*, 653-660.

(358) Breen, M.S.; Lazebnik, R.S.; Wilson, D.L. Three-dimensional registration of magnetic resonance image data to histological sections with model-based evaluation. *Ann Biomed Eng* **2005**, *33*, 1100-1112.

(359) Humm, J.L.; Ballon, D.; Hu, Y.C.; Ruan, S.; Chui, C.; Tulipano, P.K.; Erdi, A.; Koutcher, J.; Zakian, K.; Urano, M.; Zanzonico, P.; Mattis, C.; Dyke, J.; Chen, Y.; Harrington, P.; O'Donoghue, J.A.; Ling, C.C. A stereotactic method for the three-dimensional registration of multi-modality biologic images in animals: NMR, PET, histology, and autoradiography. *Med Phys* **2003**, *30*, 2303-2314.

(360) Breen, M.S.; Lancaster, T.L.; Wilson, D.L. Correcting spatial distortion in histological images. *Comput Med Imaging Graph* **2005**, *29*, 405-417.

(361) McGrath, D.M.; Vlad, R.M.; Foltz, W.D.; Brock, K.K. Technical note: fiducial markers for correlation of whole-specimen histopathology with MR imaging at 7 tesla. *Med Phys* **2010**, *37*, 2321-2328.

(362) Rouviere, O.; Reynolds, C.; Le, Y.; Lai, J.; Roberts, L.R.; Felmlee, J.P.; Ehman, R.L. Fiducial markers for MR histological correlation in ex vivo or short-term in vivo animal experiments: a screening study. *J Magn Reson Imaging* **2006**, *23*, 50-59.

(363) Raman, V.; Artemov, D.; Pathak, A.P.; Winnard, P.T., Jr.; McNutt, S.; Yudina, A.; Bogdanov, A., Jr.; Bhujwalla, Z.M. Characterizing vascular parameters in hypoxic regions: a combined magnetic resonance and optical imaging study of a human prostate cancer model. *Cancer Res* **2006**, *66*, 9929-9936.

(364) Glunde, K.; Shah, T.; Winnard, P.T., Jr.; Raman, V.; Takagi, T.; Vesuna, F.; Artemov, D.; Bhujwalla, Z.M. Hypoxia regulates choline kinase expression through hypoxia-inducible factor-1 alpha signaling in a human prostate cancer model. *Cancer Res* **2008**, *68*, 172-180.

(365) Jiang, L.; Greenwood, T.R.; Amstalden van Hove, E.R.; Chughtai, K.; Raman, V.; Winnard Jr., P.; Heeren, R.M.A.; Artemov, D.; Glunde, K. Combined magnetic resonance, fluorescence, and histology imaging strategy in a human breast tumor xenograft model. *NMR in Biomedicine* **in Press**.

(366) Chughtai, K.; Jiang, L.; Greenwood, T.R.; Klinkert, I.; Amstalden van Hove, E.R.; Heeren, R.M.; Glunde, K. Fiducial Markers for Combined 3-Dimensional Mass Spectrometric and Optical Tissue Imaging. *Anal Chem* **2012**, *84* 1817−1823.

(367) Xu, C.; Prince, J.L. Snakes, shapes, and gradient vector flow. *IEEE Trans Image Process* **1998**, *7*, 359-369.

(368) Morrison, P.R.; Jolesz, F.A.; Charous, D.; Mulkern, R.V.; Hushek, S.G.; Margolis, R.; Fried, M.P. MRI of laser-induced interstitial thermal injury in an in vivo animal liver model with histologic correlation. *J Magn Reson Imaging* **1998**, *8*, 57-63.

(369) Breen, M.S.; Lancaster, T.L.; Lazebnik, R.S.; Nour, S.G.; Lewin, J.S.; Wilson, D.L. Three-dimensional method for comparing in vivo interventional MR images of thermally ablated tissue with tissue response. *J Magn Reson Imaging* **2003**, *18*, 90-102.

(370) Hazle, J.D.; Diederich, C.J.; Kangasniemi, M.; Price, R.E.; Olsson, L.E.; Stafford, R.J. MRI-guided thermal therapy of transplanted tumors in the canine prostate using a directional transurethral ultrasound applicator. *J Magn Reson Imaging* **2002**, *15*, 409-417.

(371) Chughtai, K.; Heeren, R.M. Mass spectrometric imaging for biomedical tissue analysis. *Chem Rev* **2010**, *110*, 3237-3277.

(372) Campbell, R.E.; Tour, O.; Palmer, A.E.; Steinbach, P.A.; Baird, G.S.; Zacharias, D.A.; Tsien, R.Y. A monomeric red fluorescent protein. *Proc Natl Acad Sci U S A* **2002**, *99*, 7877-7882.

(373) Matz, M.V.; Fradkov, A.F.; Labas, Y.A.; Savitsky, A.P.; Zaraisky, A.G.; Markelov, M.L.; Lukyanov, S.A. Fluorescent proteins from nonbioluminescent Anthozoa species. *Nat Biotechnol* **1999**, *17*, 969-973.

(374) Gross, L.A.; Baird, G.S.; Hoffman, R.C.; Baldridge, K.K.; Tsien, R.Y. The structure of the chromophore within DsRed, a red fluorescent protein from coral. *Proc Natl Acad Sci U S A* **2000**, *97*, 11990-11995.

(375) Baird, G.S.; Zacharias, D.A.; Tsien, R.Y. Biochemistry, mutagenesis, and oligomerization of DsRed, a red fluorescent protein from coral. *Proc Natl Acad Sci U S A* **2000**, *97*, 11984-11989.

(376) Morris, L.M.; Klanke, C.A.; Lang, S.A.; Lim, F.Y.; Crombleholme, T.M. TdTomato and EGFP identification in histological sections: insight and alternatives. *Biotech Histochem.* **2010**, *85*, 379-387.

(377) Deliolanis, N.C.; Kasmieh, R.; Wurdinger, T.; Tannous, B.A.; Shah, K.; Ntziachristos, V. Performance of the red-shifted fluorescent proteins in deep-tissue molecular imaging applications. *J Biomed Opt* **2008**, *13*, 044008.

(378) Krishnamachary, B.; Penet, M.F.; Nimmagadda, S.; Mironchik, Y.; Raman, V.; Solaiyappan, M.; Semenza, G.L.; Pomper, M.G.; Bhujwalla, Z.M. Hypoxia regulates CD44 and its variant isoforms through HIF-1α in triple negative breast cancer. *PLoS ONE* **2012 in press**.

(379) Chughtai, K.; Jiang, L.; Greenwood, T.R.; Klinkert, I.; Amstalden van Hove, E.R.; Heeren, R.M.; Glunde, K. Fiducial markers for combined 3-dimensional mass spectrometric and optical tissue imaging. *Anal Chem* **2012**, *84*, 1817-1823.

(380) Jiang, L.; Greenwood, T.R.; Artemov, D.; Raman, V.; Winnard Jr., P.T.; Heeren, R.M.; Bhujwalla, Z.M.; Glunde, K. Localized Hypoxia Results in Spatially Heterogeneous Metabolic Signatures in Breast Tumor Models. *Neoplasia* **2012 (in press)**.

(381) Jiang, L.; Greenwood, T.R.; Amstalden van Hove, E.R.; Chughtai, K.; Raman, V.; Winnard Jr., P.T.; Heeren, R.M.A.; Artemov, D.; Glunde, K. Combined magnetic resonance, fluorescence, and histology imaging strategy in a human breast tumor xenograft model. *NMR Biomed* **2012 (in press)**.

(382) Stoeckli, M.; Staab, D.; Schweitzer, A. Compound and metabolite distribution measured by MALDI mass spectrometric imaging in whole-body tissue sections. *International Journal of Mass Spectrometry* **2007**, *260*, 195-202.

(383) Surrey, T.; Jahnig, F. Refolding and oriented insertion of a membrane protein into a lipid bilayer. *Proc Natl Acad Sci U S A* **1992**, *89*, 7457-7461.

(384) Cheley, S.; Malghani, M.S.; Song, L.; Hobaugh, M.; Gouaux, J.E.; Yang, J.; Bayley, H. Spontaneous oligomerization of a staphylococcal alpha-hemolysin conformationally constrained by removal of residues that form the transmembrane beta-barrel. *Protein Eng* **1997**, *10*, 1433-1443.

(385) Chiang, C.F.; Okou, D.T.; Griffin, T.B.; Verret, C.R.; Williams, M.N. Green fluorescent protein rendered susceptible to proteolysis: positions for protease-sensitive insertions. *Arch Biochem Biophys* **2001**, *394*, 229-235.

(386) Alvarez, L.A.; Merola, F.; Erard, M.; Rusconi, F. Mass spectrometry-based structural dissection of fluorescent proteins. *Biochemistry* **2009**, *48*, 3810-3812.

(387) Vaupel, P.; Mayer, A.; Briest, S.; Hockel, M. Oxygenation gain factor: a novel parameter characterizing the association between hemoglobin level and the oxygenation status of breast cancers. *Cancer Res* **2003**, *63*, 7634-7637.

(388) Hoogsteen, I.J.; Marres, H.A.; van den Hoogen, F.J.; Rijken, P.F.; Lok, J.; Bussink, J.; Kaanders, J.H. Expression of EGFR Under Tumor Hypoxia: Identification of a Subpopulation of Tumor Cells Responsible for Aggressiveness and Treatment Resistance. *Int J Radiat Oncol Biol Phys* **2012**.

(389) Vaupel, P.; Mayer, A. Hypoxia in cancer: significance and impact on clinical outcome. *Cancer Metastasis Rev* **2007**, *26*, 225-239.

(390) Morton, C.L.; Houghton, P.J. Establishment of human tumor xenografts in immunodeficient mice. *Nat Protoc* **2007**, *2*, 247-250.

(391) Penet, M.F.; Pathak, A.P.; Raman, V.; Ballesteros, P.; Artemov, D.; Bhujwalla, Z.M. Noninvasive multiparametric imaging of metastasis-permissive microenvironments in a human prostate cancer xenograft. *Cancer Res* **2009**, *69*, 8822-8829.

(392) Hart, P.J.; Francese, S.; Claude, E.; Woodroofe, M.N.; Clench, M.R. MALDI-MS imaging of lipids in ex vivo human skin. *Anal Bioanal Chem* **2011**, *401*, 115-125.

(393) Tanaka, H.; Zaima, N.; Yamamoto, N.; Sagara, D.; Suzuki, M.; Nishiyama, M.; Mano, Y.; Sano, M.; Hayasaka, T.; Goto-Inoue, N.; Sasaki, T.; Konno, H.; Unno, N.; Setou, M. Imaging mass spectrometry reveals unique lipid distribution in primary varicose veins. *Eur J Vasc Endovasc Surg* **2010**, *40*, 657-663.

(394) Meriaux, C.; Franck, J.; Wisztorski, M.; Salzet, M.; Fournier, I. Liquid ionic matrixes for MALDI mass spectrometry imaging of lipids. *J Proteomics* **2010**, *73*, 1204-1218.

(395) Burnum, K.E.; Cornett, D.S.; Puolitaival, S.M.; Milne, S.B.; Myers, D.S.; Tranguch, S.; Brown, H.A.; Dey, S.K.; Caprioli, R.M. Spatial and temporal alterations of phospholipids determined by mass spectrometry during mouse embryo implantation. *J Lipid Res* **2009**, *50*, 2290-2298.

(396) Touboul, D.; Piednoel, H.; Voisin, V.; De La Porte, S.; Brunelle, A.; Halgand, F.; Laprevote, O. Changes of phospholipid composition within the dystrophic muscle by matrix-assisted laser desorption/ionization mass spectrometry and mass spectrometry imaging. *Eur J Mass Spectrom (Chichester, Eng)* **2004**, *10*, 657-664.

(397) Enomoto, H.; Sugiura, Y.; Setou, M.; Zaima, N. Visualization of phosphatidylcholine, lysophosphatidylcholine and sphingomyelin in mouse tongue body by matrix-assisted laser desorption/ionization imaging mass spectrometry. *Anal Bioanal Chem* **2011**, *400*, 1913-1921.

(398) Landgraf, R.R.; Prieto Conaway, M.C.; Garrett, T.J.; Stacpoole, P.W.; Yost, R.A. Imaging of lipids in spinal cord using intermediate pressure matrix-assisted laser desorption-linear ion trap/Orbitrap MS. *Anal Chem* **2009**, *81*, 8488-8495.

(399) Menger, R.F.; Stutts, W.L.; Anbukumar, D.S.; Bowden, J.A.; Ford, D.A.; Yost, R.A. MALDI mass spectrometric imaging of cardiac tissue following myocardial infarction in a rat coronary artery ligation model. *Anal Chem* **2012**, *84*, 1117-1125.

(400) Astigarraga, E.; Barreda-Gomez, G.; Lombardero, L.; Fresnedo, O.; Castano, F.; Giralt, M.T.; Ochoa, B.; Rodriguez-Puertas, R.; Fernandez, J.A. Profiling and imaging of lipids on brain and liver tissue by matrix-assisted laser desorption/ ionization mass spectrometry using 2-mercaptobenzothiazole as a matrix. *Anal Chem* **2008**, *80*, 9105-9114.

(401) Cha, S.; Yeung, E.S. Colloidal graphite-assisted laser desorption/ionization mass spectrometry and MSn of small molecules. 1. Imaging of cerebrosides directly from rat brain tissue. *Anal Chem* **2007**, *79*, 2373-2385.

(402) Koizumi, S.; Yamamoto, S.; Hayasaka, T.; Konishi, Y.; Yamaguchi-Okada, M.; Goto-Inoue, N.; Sugiura, Y.; Setou, M.; Namba, H. Imaging mass spectrometry revealed the production of lyso-phosphatidylcholine in the injured ischemic rat brain. *Neuroscience* **2010**, *168*, 219-225.

(403) Puolitaival, S.M.; Burnum, K.E.; Cornett, D.S.; Caprioli, R.M. Solvent-free matrix dry-coating for MALDI imaging of phospholipids. *J Am Soc Mass Spectrom* **2008**, *19*, 882-886.

(404) Trim, P.J.; Atkinson, S.J.; Princivalle, A.P.; Marshall, P.S.; West, A.; Clench, M.R. Matrix-assisted laser desorption/ionisation mass spectrometry imaging of lipids in rat brain tissue with integrated unsupervised and supervised multivariant statistical analysis. *Rapid Commun Mass Spectrom* **2008**, *22*, 1503-1509.

(405) Wang, H.Y.; Jackson, S.N.; Post, J.; Woods, A.S. A Minimalist Approach to MALDI Imaging of Glycerophospholipids and Sphingolipids in Rat Brain Sections. *Int J Mass Spectrom* **2008**, *278*, 143-149.

(406) Chen, Y.; Allegood, J.; Liu, Y.; Wang, E.; Cachon-Gonzalez, B.; Cox, T.M.; Merrill, A.H., Jr.; Sullards, M.C. Imaging MALDI mass spectrometry using an oscillating

capillary nebulizer matrix coating system and its application to analysis of lipids in brain from a mouse model of Tay-Sachs/Sandhoff disease. *Anal Chem* **2008**, *80*, 2780-2788.

(407) Murphy, R.C.; Hankin, J.A.; Barkley, R.M. Imaging of lipid species by MALDI mass spectrometry. *J Lipid Res* **2009**, *50 Suppl*, S317-322.

(408) Veloso, A.; Astigarraga, E.; Barreda-Gomez, G.; Manuel, I.; Ferrer, I.; Giralt, M.T.; Ochoa, B.; Fresnedo, O.; Rodriguez-Puertas, R.; Fernandez, J.A. Anatomical distribution of lipids in human brain cortex by imaging mass spectrometry. *J Am Soc Mass Spectrom* **2011**, *22*, 329-338.

(409) Veloso, A.; Fernandez, R.; Astigarraga, E.; Barreda-Gomez, G.; Manuel, I.; Giralt, M.T.; Ferrer, I.; Ochoa, B.; Rodriguez-Puertas, R.; Fernandez, J.A. Distribution of lipids in human brain. *Anal Bioanal Chem* **2011**, *401*, 89-101.

(410) Eberlin, L.S.; Norton, I.; Dill, A.L.; Golby, A.J.; Ligon, K.L.; Santagata, S.; Cooks, R.G.; Agar, N.Y. Classifying human brain tumors by lipid imaging with mass spectrometry. *Cancer Res* **2012**, *72*, 645-654.

(411) Masterson, T.A.; Dill, A.L.; Eberlin, L.S.; Mattarozzi, M.; Cheng, L.; Beck, S.D.; Bianchi, F.; Cooks, R.G. Distinctive glycerophospholipid profiles of human seminoma and adjacent normal tissues by desorption electrospray ionization imaging mass spectrometry. *J Am Soc Mass Spectrom* **2011**, *22*, 1326-1333.

(412) Gustafsson, J.O.; Oehler, M.K.; Ruszkiewicz, A.; McColl, S.R.; Hoffmann, P. MALDI Imaging Mass Spectrometry (MALDI-IMS)-Application of Spatial Proteomics for Ovarian Cancer Classification and Diagnosis. *Int J Mol Sci* **2011**, *12*, 773-794.

(413) Liu, Y.; Chen, Y.; Momin, A.; Shaner, R.; Wang, E.; Bowen, N.J.; Matyunina, L.V.; Walker, L.D.; McDonald, J.F.; Sullards, M.C.; Merrill, A.H., Jr. Elevation of sulfatides in ovarian cancer: an integrated transcriptomic and lipidomic analysis including tissue-imaging mass spectrometry. *Mol Cancer* **2010**, *9*, 186.

(414) Willems, S.M.; van Remoortere, A.; van Zeijl, R.; Deelder, A.M.; McDonnell, L.A.; Hogendoorn, P.C. Imaging mass spectrometry of myxoid sarcomas identifies proteins and lipids specific to tumour type and grade, and reveals biochemical intratumour heterogeneity. *J Pathol* **2010**, *222*, 400-409.

(415) Eberlin, L.S.; Dill, A.L.; Golby, A.J.; Ligon, K.L.; Wiseman, J.M.; Cooks, R.G.; Agar, N.Y. Discrimination of human astrocytoma subtypes by lipid analysis using desorption electrospray ionization imaging mass spectrometry. *Angew Chem Int Ed Engl* **2010**, *49*, 5953-5956.

(416) Eberlin, L.S.; Dill, A.L.; Costa, A.B.; Ifa, D.R.; Cheng, L.; Masterson, T.; Koch, M.; Ratliff, T.L.; Cooks, R.G. Cholesterol sulfate imaging in human prostate cancer tissue by desorption electrospray ionization mass spectrometry. *Anal Chem* **2010**, *82*, 3430-3434.

(417) Shimma, S.; Sugiura, Y.; Hayasaka, T.; Hoshikawa, Y.; Noda, T.; Setou, M. MALDI-based imaging mass spectrometry revealed abnormal distribution of phospholipids in colon cancer liver metastasis. *J Chromatogr B Analyt Technol Biomed Life Sci* **2007**, *855*, 98-103.

(418) Dill, A.L.; Ifa, D.R.; Manicke, N.E.; Ouyang, Z.; Cooks, R.G. Mass spectrometric imaging of lipids using desorption electrospray ionization. *J Chromatogr B Analyt Technol Biomed Life Sci* **2009**, *877*, 2883-2889.

(419) Le, T.T.; Huff, T.B.; Cheng, J.X. Coherent anti-Stokes Raman scattering imaging of lipids in cancer metastasis. *BMC Cancer* **2009**, *9*, 42.

(420) Ramos, C.V.; Taylor, H.B. Lipid-rich carcinoma of the breast. A clinicopathologic analysis of 13 examples. *Cancer* **1974**, *33*, 812-819.

(421) Sijens, P.E.; Levendag, P.C.; Vecht, C.J.; van Dijk, P.; Oudkerk, M. 1H MR spectroscopy detection of lipids and lactate in metastatic brain tumors. *NMR Biomed* **1996**, *9*, 65-71.

(422) Folick, A.; Min, W.; Wang, M.C. Label-free imaging of lipid dynamics using Coherent Anti-stokes Raman Scattering (CARS) and Stimulated Raman Scattering (SRS) microscopy. *Curr Opin Genet Dev* **2011**, *21*, 585-590.

(423) Le, T.T.; Yue, S.; Cheng, J.X. Shedding new light on lipid biology with coherent anti-Stokes Raman scattering microscopy. *J Lipid Res* **2010**, *51*, 3091-3102.

(424) Maier, O.; Oberle, V.; Hoekstra, D. Fluorescent lipid probes: some properties and applications (a review). *Chem Phys Lipids* **2002**, *116*, 3-18.

(425) Krishnamachary, B.; Penet, M.F.; Nimmagadda, S.; Mironchik, Y.; Raman, V.; Solaiyappan, M.; Semenza, G.L.; Pomper, M.G.; Bhujwalla, Z.M. Hypoxia regulates CD44 and its variant isoforms through HIF-1α in triple negative breast cancer. *PLoS ONE* **2012 (in press)**.

(426) Jiang, L.; Greenwood, T.R.; Artemov, D.; Raman, V.; Winnard Jr., P.T.; Heeren, R.M.A.; Bhujwalla, Z.M.; Glunde, K. Localized Hypoxia Results in Spatially Heterogeneous Metabolic Signatures in Breast Tumor Models. . *Neoplasia* **2012 (in press)**.

(427) Jiang, L.; Greenwood, T.R.; Amstalden van Hove, E.R.; Chughtai, K.; Raman, V.; Winnard Jr., P.T.; Heeren, R.M.A.; Artemov, D.; Glunde, K. Combined magnetic resonance, fluorescence, and histology imaging strategy in a human breast tumor xenograft model. *NMR Biomed.* **2012 (in press)**.

(428) Fahy, E.; Subramaniam, S.; Murphy, R.C.; Nishijima, M.; Raetz, C.R.; Shimizu, T.; Spener, F.; van Meer, G.; Wakelam, M.J.; Dennis, E.A. Update of the LIPID MAPS comprehensive classification system for lipids. *J Lipid Res* **2009**, *50 Suppl*, S9-14.

(429) Cootes, T.F.; Taylor, C.J.; Cooper, D.H.; Graham, J. Active Shape Models-Their Training and Application. *Computer Vision and Image Understanding* **1995**, *61*, 38-59.

(430) Peterson, B.L.; Cummings, B.S. A review of chromatographic methods for the assessment of phospholipids in biological samples. *Biomed Chromatogr* **2006**, *20*, 227-243.

(431) Watson, A.D. Thematic review series: systems biology approaches to metabolic and cardiovascular disorders. Lipidomics: a global approach to lipid analysis in biological systems. *J Lipid Res* **2006**, *47*, 2101-2111.

(432) Jackson, S.N.; Ugarov, M.; Post, J.D.; Egan, T.; Langlais, D.; Schultz, J.A.; Woods, A.S. A study of phospholipids by ion mobility TOFMS. *J Am Soc Mass Spectrom* **2008**, *19*, 1655-1662.

(433) Jackson, S.N.; Ugarov, M.; Egan, T.; Post, J.D.; Langlais, D.; Albert Schultz, J.; Woods, A.S. MALDI-ion mobility-TOFMS imaging of lipids in rat brain tissue. *J Mass Spectrom* **2007**, *42*, 1093-1098.

(434) Snel, M.F.; Fuller, M. High-Spatial Resolution Matrix-Assisted Laser Desorption Ionization Imaging Analysis of Glucosylceramide in Spleen Sections from a Mouse Model of Gaucher Disease. *Analytical Chemistry* **2010**, *82*, 3664-3670.

(435) Petkovic, M.; Schiller, J.; Muller, M.; Benard, S.; Reichl, S.; Arnold, K.; Arnhold, J. Detection of individual phospholipids in lipid mixtures by matrix-assisted laser desorption/ionization time-of-flight mass spectrometry: phosphatidylcholine prevents the detection of further species. *Anal Biochem* **2001**, *289*, 202-216.

(436) Estrada, R.; Yappert, M.C. Alternative approaches for the detection of various phospholipid classes by matrix-assisted laser desorption/ionization time-of-flight mass spectrometry. *J Mass Spectrom* **2004**, *39*, 412-422.

(437)   Arnhold, J.; Osipov, A.N.; Spalteholz, H.; Panasenko, O.M.; Schiller, J. Formation of lysophospholipids from unsaturated phosphatidylcholines under the influence of hypochlorous acid. *Biochim Biophys Acta* **2002**, *1572*, 91-100.

(438)   Wang, H.Y.; Liu, C.B.; Wu, H.W.; Kuo, J.S. Direct profiling of phospholipids and lysophospholipids in rat brain sections after ischemic stroke. *Rapid Commun Mass Spectrom* **2010**, *24*, 2057-2064.

(439)   Goetzl, E.J.; Dolezalova, H.; Kong, Y.; Zeng, L. Dual mechanisms for lysophospholipid induction of proliferation of human breast carcinoma cells. *Cancer Res* **1999**, *59*, 4732-4737.

(440)   Imai, A.; Furui, T.; Tamaya, T.; Mills, G.B. A gonadotropin-releasing hormone-responsive phosphatase hydrolyses lysophosphatidic acid within the plasma membrane of ovarian cancer cells. *J Clin Endocrinol Metab* **2000**, *85*, 3370-3375.

(441)   Spiegelberg, B.D.; Hamm, H.E. Roles of G-protein-coupled receptor signaling in cancer biology and gene transcription. *Curr Opin Genet Dev* **2007**, *17*, 40-44.

(442)   Umezu-Goto, M.; Tanyi, J.; Lahad, J.; Liu, S.; Yu, S.; Lapushin, R.; Hasegawa, Y.; Lu, Y.; Trost, R.; Bevers, T.; Jonasch, E.; Aldape, K.; Liu, J.; James, R.D.; Ferguson, C.G.; Xu, Y.; Prestwich, G.D.; Mills, G.B. Lysophosphatidic acid production and action: validated targets in cancer? *J Cell Biochem* **2004**, *92*, 1115-1140.

(443)   Modrak, D.E.; Gold, D.V.; Goldenberg, D.M. Sphingolipid targets in cancer therapy. *Mol Cancer Ther* **2006**, *5*, 200-208.

(444)   Auge, N.; Maupas-Schwalm, F.; Elbaz, M.; Thiers, J.C.; Waysbort, A.; Itohara, S.; Krell, H.W.; Salvayre, R.; Negre-Salvayre, A. Role for matrix metalloproteinase-2 in oxidized low-density lipoprotein-induced activation of the sphingomyelin/ceramide pathway and smooth muscle cell proliferation. *Circulation* **2004**, *110*, 571-578.

(445)   Zeidan, Y.H.; Hannun, Y.A. The acid sphingomyelinase/ceramide pathway: biomedical significance and mechanisms of regulation. *Curr Mol Med* **2010**, *10*, 454-466.

(446)   Signorelli, P.; Ghidoni, R. Breast cancer and sphingolipid signalling. *J Dairy Res* **2005**, *72 Spec No*, 5-13.

(447)   Momin, A.A.; Park, H.; Portz, B.J.; Haynes, C.A.; Shaner, R.L.; Kelly, S.L.; Jordan, I.K.; Merrill, A.H., Jr. A method for visualization of "omic" datasets for sphingolipid metabolism to predict potentially interesting differences. *J Lipid Res* **2011**, *52*, 1073-1083.

(448)   Chalfant, C.E.; Spiegel, S. Sphingosine 1-phosphate and ceramide 1-phosphate: expanding roles in cell signaling. *J Cell Sci* **2005**, *118*, 4605-4612.

(449)   Pettus, B.J.; Bielawska, A.; Subramanian, P.; Wijesinghe, D.S.; Maceyka, M.; Leslie, C.C.; Evans, J.H.; Freiberg, J.; Roddy, P.; Hannun, Y.A.; Chalfant, C.E. Ceramide 1-phosphate is a direct activator of cytosolic phospholipase A2. *J Biol Chem* **2004**, *279*, 11320-11326.

(450)   Kerner, J.; Hoppel, C. Fatty acid import into mitochondria. *Biochim Biophys Acta* **2000**, *1486*, 1-17.

(451)   Das, D.K.; Ayromlooi, J.; Neogi, A. Effect of ischemia on fatty acid metabolism in fetal lung. *Life Sci* **1983**, *33*, 569-576.

(452)   Yamada, K.A.; McHowat, J.; Yan, G.X.; Donahue, K.; Peirick, J.; Kleber, A.G.; Corr, P.B. Cellular uncoupling induced by accumulation of long-chain acylcarnitine during ischemia. *Circ Res* **1994**, *74*, 83-95.

(453)   Bruder, E.D.; Raff, H. Cardiac and plasma lipid profiles in response to acute hypoxia in neonatal and young adult rats. *Lipids Health Dis* **2010**, *9*, 3.

(454)   Hutter, J.F.; Alves, C.; Soboll, S. Effects of hypoxia and fatty acids on the distribution of metabolites in rat heart. *Biochim Biophys Acta* **1990**, *1016*, 244-252.

(455)   Whitmer, J.T.; Idell-Wenger, J.A.; Rovetto, M.J.; Neely, J.R. Control of fatty acid metabolism in ischemic and hypoxic hearts. *J Biol Chem* **1978**, *253*, 4305-4309.

(456)   Wainwright, M.S.; Kohli, R.; Whitington, P.F.; Chace, D.H. Carnitine treatment inhibits increases in cerebral carnitine esters and glutamate detected by mass spectrometry after hypoxia-ischemia in newborn rats. *Stroke* **2006**, *37*, 524-530.

(457)   McHowat, J.; Yamada, K.A.; Saffitz, J.E.; Corr, P.B. Subcellular distribution of endogenous long chain acylcarnitines during hypoxia in adult canine myocytes. *Cardiovasc Res* **1993**, *27*, 1237-1243.

(458)   Meyburg, J.; Schulze, A.; Kohlmueller, D.; Linderkamp, O.; Mayatepek, E. Postnatal changes in neonatal acylcarnitine profile. *Pediatr Res* **2001**, *49*, 125-129.

(459)   Hockel, M.; Vaupel, P. Biological consequences of tumor hypoxia. *Semin Oncol* **2001**, *28*, 36-41.

(460)   Wang, G.L.; Jiang, B.H.; Rue, E.A.; Semenza, G.L. Hypoxia-inducible factor 1 is a basic-helix-loop-helix-PAS heterodimer regulated by cellular O2 tension. *Proc Natl Acad Sci U S A* **1995**, *92*, 5510-5514.

(461)   Boersema, P.J.; Raijmakers, R.; Lemeer, S.; Mohammed, S.; Heck, A.J. Multiplex peptide stable isotope dimethyl labeling for quantitative proteomics. *Nat Protoc* **2009**, *4*, 484-494.

(462)   Krishnamachary, B.; Penet, M.F.; Nimmagadda, S.; Mironchik, Y.; Venu Raman; Solaiyappan, M.; Semenza, G.L.; Pomper, M.G.; Bhujwalla, Z.M. Hypoxia regulates CD44 and its variant isoforms through HIF-1α in MDA-MB-231 human breast cancer cells and tumors. **in Press**.

(463)   Bradford, M.M. A rapid and sensitive method for the quantitation of microgram quantities of protein utilizing the principle of protein-dye binding. *Anal Biochem* **1976**, *72*, 248-254.

(464)   Szklarczyk, D.; Franceschini, A.; Kuhn, M.; Simonovic, M.; Roth, A.; Minguez, P.; Doerks, T.; Stark, M.; Muller, J.; Bork, P.; Jensen, L.J.; von Mering, C. The STRING database in 2011: functional interaction networks of proteins, globally integrated and scored. *Nucleic Acids Res* **2011**, *39*, D561-568.

(465)   Morse, D.; Choi, A.M. Heme oxygenase-1: from bench to bedside. *Am J Respir Crit Care Med* **2005**, *172*, 660-670.

(466)   Zhu, C.; Johansson, M.; Permert, J.; Karlsson, A. Enhanced cytotoxicity of nucleoside analogs by overexpression of mitochondrial deoxyguanosine kinase in cancer cell lines. *J Biol Chem* **1998**, *273*, 14707-14711.

(467)   Bagshaw, R.D.; Mahuran, D.J.; Callahan, J.W. A proteomic analysis of lysosomal integral membrane proteins reveals the diverse composition of the organelle. *Mol Cell Proteomics* **2005**, *4*, 133-143.

(468)   Truong, H.; Danen, E.H. Integrin switching modulates adhesion dynamics and cell migration. *Cell Adh Migr* **2009**, *3*, 179-181.

(469)   de Melker, A.A.; Sterk, L.M.; Delwel, G.O.; Fles, D.L.; Daams, H.; Weening, J.J.; Sonnenberg, A. The A and B variants of the alpha 3 integrin subunit: tissue distribution and functional characterization. *Lab Invest* **1997**, *76*, 547-563.

(470)   Ahmed, N.; Riley, C.; Rice, G.; Quinn, M. Role of integrin receptors for fibronectin, collagen and laminin in the regulation of ovarian carcinoma functions in response to a matrix microenvironment. *Clin Exp Metastasis* **2005**, *22*, 391-402.

(471)   DeFreitas, M.F.; Yoshida, C.K.; Frazier, W.A.; Mendrick, D.L.; Kypta, R.M.; Reichardt, L.F. Identification of integrin alpha 3 beta 1 as a neuronal thrombospondin receptor mediating neurite outgrowth. *Neuron* **1995**, *15*, 333-343.

(472) Nagle, R.B.; Hao, J.; Knox, J.D.; Dalkin, B.L.; Clark, V.; Cress, A.E. Expression of hemidesmosomal and extracellular matrix proteins by normal and malignant human prostate tissue. *Am J Pathol* **1995**, *146*, 1498-1507.

(473) O'Connell, M.P.; Fiori, J.L.; Kershner, E.K.; Frank, B.P.; Indig, F.E.; Taub, D.D.; Hoek, K.S.; Weeraratna, A.T. Heparan sulfate proteoglycan modulation of Wnt5A signal transduction in metastatic melanoma cells. *J Biol Chem* **2009**, *284*, 28704-28712.

(474) D'Eustachio, P. Reactome knowledgebase of human biological pathways and processes. *Methods Mol Biol* **2011**, *694*, 49-61.

(475) Croft, D.; O'Kelly, G.; Wu, G.; Haw, R.; Gillespie, M.; Matthews, L.; Caudy, M.; Garapati, P.; Gopinath, G.; Jassal, B.; Jupe, S.; Kalatskaya, I.; Mahajan, S.; May, B.; Ndegwa, N.; Schmidt, E.; Shamovsky, V.; Yung, C.; Birney, E.; Hermjakob, H.; D'Eustachio, P.; Stein, L. Reactome: a database of reactions, pathways and biological processes. *Nucleic Acids Res* **2011**, *39*, D691-697.

(476) Bhatia, V.N.; Perlman, D.H.; Costello, C.E.; McComb, M.E. Software tool for researching annotations of proteins: open-source protein annotation software with data visualization. *Anal Chem* **2009**, *81*, 9819-9823.

(477) Molloy, N.H.; Read, D.E.; Gorman, A.M. Nerve Growth Factor in Cancer Cell Death and Survival. *Cancers* **2011**, *3*, 510-530.

(478) Burbelo, P.; Wellstein, A.; Pestell, R.G. Altered Rho GTPase signaling pathways in breast cancer cells. *Breast Cancer Res Treat* **2004**, *84*, 43-48.

(479) Bastian, P.; Lang, K.; Niggemann, B.; Zaenker, K.S.; Entschladen, F. Myosin regulation in the migration of tumor cells and leukocytes within a three-dimensional collagen matrix. *Cell Mol Life Sci* **2005**, *62*, 65-76.

(480) Betapudi, V.; Licate, L.S.; Egelhoff, T.T. Distinct roles of nonmuscle myosin II isoforms in the regulation of MDA-MB-231 breast cancer cell spreading and migration. *Cancer Res* **2006**, *66*, 4725-4733.

(481) O'Driscoll, L.; McMorrow, J.; Doolan, P.; McKiernan, E.; Mehta, J.P.; Ryan, E.; Gammell, P.; Joyce, H.; O'Donovan, N.; Walsh, N.; Clynes, M. Investigation of the molecular profile of basal cell carcinoma using whole genome microarrays. *Mol Cancer* **2006**, *5*, 74.

(482) Bourguignon, L.Y.; Zhu, H.; Shao, L.; Chen, Y.W. Ankyrin-Tiam1 interaction promotes Rac1 signaling and metastatic breast tumor cell invasion and migration. *J Cell Biol* **2000**, *150*, 177-191.

(483) Duan, Z.; Lamendola, D.E.; Yusuf, R.Z.; Penson, R.T.; Preffer, F.I.; Seiden, M.V. Overexpression of human phosphoglycerate kinase 1 (PGK1) induces a multidrug resistance phenotype. *Anticancer Res* **2002**, *22*, 1933-1941.

(484) Zhang, D.; Tai, L.K.; Wong, L.L.; Chiu, L.L.; Sethi, S.K.; Koay, E.S. Proteomic study reveals that proteins involved in metabolic and detoxification pathways are highly expressed in HER-2/neu-positive breast cancer. *Mol Cell Proteomics* **2005**, *4*, 1686-1696.

(485) Hwang, T.L.; Liang, Y.; Chien, K.Y.; Yu, J.S. Overexpression and elevated serum levels of phosphoglycerate kinase 1 in pancreatic ductal adenocarcinoma. *Proteomics* **2006**, *6*, 2259-2272.

(486) Zieker, D.; Konigsrainer, I.; Tritschler, I.; Loffler, M.; Beckert, S.; Traub, F.; Nieselt, K.; Buhler, S.; Weller, M.; Gaedcke, J.; Taichman, R.S.; Northoff, H.; Brucher, B.L.; Konigsrainer, A. Phosphoglycerate kinase 1 a promoting enzyme for peritoneal dissemination in gastric cancer. *Int J Cancer* **2010**, *126*, 1513-1520.

(487) Wang, J.; Dai, J.; Jung, Y.; Wei, C.L.; Wang, Y.; Havens, A.M.; Hogg, P.J.; Keller, E.T.; Pienta, K.J.; Nor, J.E.; Wang, C.Y.; Taichman, R.S. A glycolytic mechanism regulating an angiogenic switch in prostate cancer. *Cancer Res* **2007**, *67*, 149-159.

(488) Semenza, G.L.; Roth, P.H.; Fang, H.M.; Wang, G.L. Transcriptional regulation of genes encoding glycolytic enzymes by hypoxia-inducible factor 1. *J Biol Chem* **1994**, *269*, 23757-23763.

(489) Gao, X.; Nawaz, Z. Progesterone receptors - animal models and cell signaling in breast cancer: Role of steroid receptor coactivators and corepressors of progesterone receptors in breast cancer. *Breast Cancer Res* **2002**, *4*, 182-186.

(490) Zhou, D.; Quach, K.M.; Yang, C.; Lee, S.Y.; Pohajdak, B.; Chen, S. PNRC: a proline-rich nuclear receptor coregulatory protein that modulates transcriptional activation of multiple nuclear receptors including orphan receptors SF1 (steroidogenic factor 1) and ERRalpha1 (estrogen related receptor alpha-1). *Mol Endocrinol* **2000**, *14*, 986-998.

(491) Zhou, D.; Shen, R.; Ye, J.J.; Li, Y.; Tsark, W.; Isbell, D.; Tso, P.; Chen, S. Nuclear receptor coactivator PNRC2 regulates energy expenditure and adiposity. *J Biol Chem* **2008**, *283*, 541-553.

(492) Cho, H.; Kim, K.M.; Kim, Y.K. Human proline-rich nuclear receptor coregulatory protein 2 mediates an interaction between mRNA surveillance machinery and decapping complex. *Mol Cell* **2009**, *33*, 75-86.

(493) Rajhans, R.; Nair, H.B.; Nair, S.S.; Cortez, V.; Ikuko, K.; Kirma, N.B.; Zhou, D.; Holden, A.E.; Brann, D.W.; Chen, S.; Tekmal, R.R.; Vadlamudi, R.K. Modulation of in situ estrogen synthesis by proline-, glutamic acid-, and leucine-rich protein-1: potential estrogen receptor autocrine signaling loop in breast cancer cells. *Mol Endocrinol* **2008**, *22*, 649-664.

Publications

K. Chughtai and R.M.A. Heeren. Mass spectrometric imaging for biomedical tissue analysis. Chem. Rev. 2010, 110, 3237–3277. (**Chapter 2**)

K. Chughtai, L. Jiang, T.R. Greenwood, I. Klinkert, E.R. Amstalden van Hove, R.M.A. Heeren and K. Glunde. Fiducial Markers for Combined 3-Dimensional Mass Spectrometric and Optical Tissue Imaging. Anal Chem. 2012, 21;84(4):1817-23. (**Chapter 3**)

K. Chughtai, L. Jiang, H. Post, P.T. Winnard Jr., T.R. Greenwood, V. Raman, Z.M. Bhujwalla, R.M.A. Heeren and K. Glunde. Mass Spectrometric Imaging of Red Fluorescent Protein in Breast Tumor Xenografts. Manuscript accepted for publication in JASMS. (**Chapter 4**)

K. Chughtai, L. Jiang, T.R. Greenwood, K. Glunde and R.M.A. Heeren. Mass Spectrometry Images Acylcarnitines, Phosphatidylcholines and Sphingomyelin in MDA-MB-231 Breast Tumor Models. J. Lipid Res. 2012, doi:10.1194/jlr.M027961 (**Chapter 5**)

K. Chughtai, H. Post, A.F.M. Altelaar, L. Jiang, A.J.R. Heck, K. Glunde and R.M.A. Heeren. A Survival Strategy of Hypoxic Breast Tumors. Manuscript to be submitted. (**Chapter 6**)

Other publications

L. Jiang, T.R. Greenwood, E.R. Amstalden van Hove, K. Chughtai, V. Raman, P.T. Winnard Jr., R.M.A. Heeren, D. Artemov, K. Glunde. Combined magnetic resonance, fluorescence, and histology imaging strategy in a human breast tumor xenograft model. NMR Biomed. 2012 (in press).

S. Chughtai, K. Chughtai, B. Cillero-Pastor, A. Kiss, P. Agrawal, L. MacAleese, R.M.A. Heeren. A multimodal mass spectrometry imaging approach for the study of musculoskeletal tissues. IJMS. 2012, 325–327:150-160.

A. Bodzon-Kulakowska, A. Kiss, <u>K. Chughtai</u>, R.M.A. Heeren. Distribution of cholesterol in the brain tissue as an example of TOF-SIMS analysis. Biomacromolecular Mass Spectrometry. Tips from the Bench. NOVA Science Publishers, Haupauge, NJ, USA. 2012, 3(1):1-10.

E. Ciara, D. Piekutowska-Abramczuk, E. Popowska, W. Grajkowska, S. Barszcz, D. Perek, B. Dembowska-Bagińska, M. Perek-Polnik, E. Kowalewska, A. Czajńska, M. Syczewska, <u>K. Czornak</u>, M. Krajewska-Walasek, M. Roszkowski, KH. Chrzanowska. Heterozygous germ-line mutations in the NBN gene predispose to medulloblastoma in pediatric patients. Acta Neuropathol. 2010, Mar 119(3):325-334.

<u>K. Czornak</u>, S. Chughtai, K.H. Chrzanowska. Mystery of DNA repair: the role of the MRN complex and ATM kinase in DNA damage repair. J Appl Genet. 2008, 49(4):383-96.

M.H. Luo, K. Rosenke, <u>K. Czornak</u>, E.A. Fortunato. Human cytomegalovirus disrupts both ATM and ATR-mediated DNA damage responses during lytic infection. J. Virol. 2007, 81:1934-50.

Conferences – Poster presentations

<u>K. Chughtai</u>, L. Jiang, T.R. Greenwood, K. Glunde and R.M.A. Heeren. Mass Spectrometry Images the Lipidome of Breast Tumor Xenograft Tissue. **I-International Conference in Imaging Mass Spectrometry 2012** Ourense, Spain (best poster prize)

L. Fornai, A. Angelini, A. Kiss, G. Eijkel, <u>K. Chughtai</u>, M. Fedrigo, ML. Valente, G. Thiene and R.M.A. Heeren. A new image of the heart failure. **I-International Conference in Imaging Mass Spectrometry 2012** Ourense, Spain

<u>K. Chughtai</u>, L. Jiang, T.R. Greenwood, K. Glunde and R.M.A. Heeren. Mass Spectrometric Imaging of Lipidome in Breast Tumor Xenograft Models. **60th Annual ASMS Conference on Mass Spectrometry and Allied Topics** Vancouver, BC, Canada

K. Chughtai, L. Jiang, T.R. Greenwood, K. Glunde and R.M.A. Heeren. Mass Spectrometric Imaging of Lipidome in Breast Tumor Xenograft Models. **NVMS/BSMS International Congress on Mass Spectrometry 2012** Kerkrade, The Netherlands

S. Chughtai, K. Chughtai, A. Kiss, B.C. Pastor, L. MacAleese, R.M.A. Heeren. Imaging Rheumatoid Arthritis: Novel MS Investigation of an Old Disease. **59th ASMS Conference On Mass Spectrometry and Allied Topics** Denver, USA

K. Chughtai, L. Jiang, H. Post, T. Blackwell, A.F.M. Altelaar, A.J.R. Heck, K. Glunde, R.M.A. Heeren. Breast Tumors Inside Out: Exploring the Breast Tumor Microenvironment by MSI. **Netherlands Proteomic Center Progress Meeting 2011** Utrecht, The Netherlands

K. Chughtai, L. Jiang, T.R. Blackwell, K. Glunde, R.M.A. Heeren. Mass Spectrometry Images Breast Cancer. **NVMS International Congress on Mass Spectrometry 2010** Amsterdam, The Netherlands

S. Chughtai, K. Chughtai, L.MacAleese, R.M.A. Heeren. Imaging rheumatoid arthritis: A multimodal mass spectrometric investigation. **NVMS International Congress on Mass Spectrometry 2010** Amsterdam, The Netherlands

K. Czornak, T. R. Blackwell, Lu Jiang, K. Glunde, R.M.A. Heeren. Mass Spectrometric Imaging of Glycosphingolipids from Breast Cancer Tissue Sections in Ion Mobility Separation Mode. **58th ASMS Conference On Mass Spectrometry and Allied Topics** Salt Lake City, Utah, USA

K. Czornak, T.R. Blackwell, L. Jiang, K. Glunde, R.M.A. Heeren. Ion Mobility Separation images cancer. **Netherlands Proteomic Center Progress Meeting 2010** Utrecht, The Netherlands

K. Czornak, E.R. Amstalden, L. Fornai, T.R. Blackwell, I. Klinkert, L. Jiang, F. Giskes, D. Smith, K. Glunde, R.M.A. Heeren. Physics for molecular pathology: a multi-modal molecular imaging approach. **Physics@FOM, Veldhoven 2010** Veldhoven, The Netherlands

K. Czornak, T.R. Blackwell, A.F.M. Altelaar , K. Glunde, R.M.A. Heeren. Molecular Profiling and Imaging of trypsin digested biological samples using Ion Mobility Separation. **18th International Mass Spectrometry Conference** Bremen, Germany

K. Czornak, J. Stauber, L. MacAleese, S.Mohammed, A.J.R. Heck, R.M.A. Heeren, A.F. M. Altelaar. Improved on-tissue protein identification in MALDI imaging mass spectrometry (MSI) using the metalloendopeptidase Lys-N. **57th ASMS Conference on Mass Spectrometry and Allied Topics** Philadelphia, PA, USA

E.R. Amstalden, I. Klinkert, T.R. Greenwood, K. Czornak, K. Glunde, R.M.A. Heeren. 3D reconstruction of xenograft breast tumors with a combination of Mass Spectrometry Imaging. **57th ASMS Conference on Mass Spectrometry and Allied Topics** Philadelphia, PA, USA

K. Czornak, L. Fortunato. Defects of HCMV maturation and egress in p53KO cells. **31st Annual International Herpesvirus Workshop** Seattle, WA, USA

Conferences – Oral presentations

K. Chughtai. Exploring hypoxia-induced signaling networks in breast cancer. **Netherlands Proteomic Center Progress Meeting 2012** Utrecht, The Netherlands

K. Chughtai, L. Jiang, T.R. Greenwood, K. Glunde, R.M. A. Heeren. Mass Spectrometry Visualizes Hypoxia-driven Processes in Breast Tumors. **59th Annual ASMS Conference on Mass Spectrometry and Allied Topics** Denver, CO, USA

K. Chughtai. Mass spectrometric imaging of hypoxia-driven signaling pathways in breast cancer. **ICMIC seminar**
Johns Hopkins University School of Medicine, Baltimore, MD, USA

K. Chughtai. Suffocating tumors: Local protein changes under hypoxic conditions. **FOM-Institute AMOLF colloquium** Amsterdam, The Netherlands

K. Chughtai. Mass Spectrometry Images Breast Cancer. **Netherlands Proteomic Center Progress Meeting 2011** Utrecht, The Netherlands

K. Czornak. Ion Mobility Separation for Molecular Imaging of Breast Cancer. **ICMIC seminar** Johns Hopkins University School of Medicine, Baltimore, MD, USA

K. Czornak. Ion Mobility Separation for Molecular Imaging of Breast Cancer. **FOM-Institute AMOLF colloquium** Amsterdam, The Netherlands

K. Czornak. On-tissue protein digestion for Mass Spectrometric Imaging. **ICMIC seminar** Johns Hopkins University School of Medicine, Baltimore, MD, USA

Acknowledgements

Curriculum Vitae

Kamila Chughtai obtained her first M.Sc. degree in biotechnology at Maria Curie-Sklodowska University in Poland. In 2005 she joined Prof. Elizabeth Ann (Lee) Fortunato's research group at University of Idaho and in 2007 graduated as a M.Sc. in Microbiology, Molecular Biology, and Biochemistry. She returned to Poland to become a research assistant in the Department of Medical Genetics of the Children's Memorial Health Institute in Warsaw.

In January 2009 she started her Ph.D. project focused on multimodal imaging of breast tumors under the supervision of Prof. Ron M. A. Heeren from the FOM-Institute AMOLF in Amsterdam, The Netherlands and Prof. Kristine Glunde from the Johns Hopkins University School of Medicine in Baltimore, MD, USA. The major results of this Ph.D. project are presented in this thesis.